

Republic of Iraq
Ministry of Higher Education and
Scientific Research
University of Al- Qadisiyah
College of Science
Department of Chemistry



Synthesis and Characterization of Magnetic Molecular imprinted polymer and Using for Quantitation of Some Drugs in Human Urine and Blood

A Thesis

Submitted to the College of Science – University of Al- Qadisiyah in
Partial Fulfillment of the Requirements for the Degree of Doctorate of
Science in Chemistry

By

Rana Raheem Ali

(BSc. Chemistry, 2000) University of Al- Babylon
(M.Sc. Chemistry, 2021) University of Al- Qadisiyah

Supervised by

Prof. Dr. Faiq Fathallah Karam
prof. Dr. Zianab Tariq Ibrahim

1447 A.H.

2026A.D.

بِسْمِ اللَّهِ الرَّحْمَنِ الرَّحِيمِ

((مَا تَوْفِيقِي إِلَّا بِاللَّهِ عَلَيْهِ تَوَكَّلْتُ وَإِلَيْهِ أُنِيبُ))

صدق الله العظيم

(سورة هود، الآية 88)

Dedication

To the pure soul of my late father,
whose presence may have departed, but whose memory and values live on in my heart.

*This work is dedicated to him, with deep love and eternal gratitude.
May Allah have mercy on his soul and grant him the highest ranks in Paradise.*

To my beloved mother,
*the source of endless love and strength. Your prayers and unwavering support have been my guiding light.
May Allah protect you and bless you always.*

To my respected supervisors,
*Prof. Dr. Faiq Fathallah Karam and Prof. Dr. Zainab Tariq Ibrahim with sincere appreciation and gratitude for your invaluable guidance, knowledge, and support throughout this journey.
Your encouragement and insight have greatly enriched this work.*

To my dear husband,
*your patience, encouragement, and constant support have been my pillar through every challenge.
Thank you for standing by my side.*

To my precious children,
you are the light of my life and the greatest motivation behind my perseverance and achievements.

To my beloved siblings,
your support and love have meant the world to me. May Allah bless and preserve you all.

And to all my dear friends,
*your kindness, encouragement, and companionship have helped make this journey easier and more beautiful.
With all my appreciation and love, I dedicate this work to you*



Rana Raheem Ali

Acknowledgments

First and foremost, all praise is due to Almighty Allah for granting me the strength, patience, and perseverance to complete this work. This dissertation would not have been possible without the support, guidance, and encouragement of many individuals to whom I am sincerely grateful.

*I would like to express my deepest gratitude and appreciation to my supervisor, **Prof. Dr. Faiq Fathallah Karam**, for his invaluable guidance, continuous support, and insightful advice throughout every stage of this research. His patience, generosity with his time, and unwavering commitment to academic excellence have had a profound impact on my work and personal growth. I am especially grateful for his encouragement during difficult moments and for always believing in my potential.*

*My sincere thanks also go to my co-supervisor, **Prof. Dr. Zainab Tariq**, for her valuable input, constructive feedback, and kind support during the course of this study.*

*I am also pleased to extend my thanks and appreciation to the honorable professors in the Department of Chemistry, whose knowledge and guidance have been instrumental throughout my academic journey. I would like to express my special thanks to the Dean of the College of Science, **Prof. Dr. Salwan Ali Abed**, and the Head of the Chemistry Department, **Prof. Dr. Bassam Faron**, for their continued efforts in fostering an academic environment that inspires excellence, innovation, and the development of a conscious and capable generation.*

Finally, I extend my heartfelt thanks to all those who supported me throughout this journey family, friends, and colleagues—for their encouragement, patience, and motivation.

Summary

Part one :This thesis focused on the synthesis of a series of magnetic molecularly imprinted polymers (MMIPs) specifically designed for the selective recognition and efficient extraction of several pharmaceutical compounds from complex matrices. The preparation strategy was based on integrating molecular imprinting technology with a magnetic core (Fe_3O_4), where polymerization was carried out in the presence of an appropriate template molecule and functional monomer. The use of microwave-assisted polymerization was incorporated within the synthesis procedure, contributing to reduced reaction time and improved homogeneity of the polymeric structure.

Part two: A comprehensive characterization of the prepared polymers was performed using a set of complementary physicochemical techniques. These included X-ray diffraction (XRD), thermogravimetric analysis (TGA), vibrating sample magnetometry (VSM), and Fourier-transform infrared spectroscopy (FTIR), in addition to field emission scanning electron microscopy (FESEM) and Brunauer–Emmett–Teller (BET) surface area analysis. The obtained results confirmed the successful synthesis and molecular imprinting process and provided clear evidence of the structural, morphological, and magnetic properties of the prepared polymers.

Part three :The effects of various operational parameters on adsorption and extraction efficiency were systematically investigated, including contact time, polymer dosage, solution pH, temperature, and sample volume. Kinetic studies, adsorption isotherm models, and thermodynamic analyses were employed to elucidate the adsorption mechanisms. The results demonstrated the superior performance of the imprinted polymers compared to the non-imprinted counterparts, as reflected by higher imprinting factors and selectivity coefficients, indicating the formation of specific and efficient recognition sites.

The final part of the thesis involved the practical application of the synthesized MMIPs to real urine and blood samples. The results showed high extraction efficiency, good selectivity, and excellent reusability without significant loss of performance. These findings confirm the suitability of the prepared polymers for practical analytical applications involving complex biological matrices.

List of Contents

NO.	Subject	Page
	Abstract	I
	List of Contents	III
	List of Figures	IX
	List of Tables	XIV
	List of Abbreviations	XV
Chapter One Introduction		
1.1	General introduction	1
1.2	Drugs studied in the thesis	2
1.2.1	Heroin	2
1.2.2	Amphetamine	3
1.2.3	Artane	4
1.2.4	Lyrica	5
1.3	Magnetic molecularly imprinted polymers	6 – 8
1.3.1	Principle of molecular imprinting polymers	8 – 9
1.3.2	Key Variables Influencing the Molecular Imprinting process	10
1.3.2.1	Template	10 – 11
1.3.2.2	Functional monomers	11 – 14
1.3.2.3	Cross linkers	14 – 15
1.3.2.4	Progenic solvents	15 – 17
1.3.2.5	Initiators	17 – 19
1.4	Polymerization reaction	19
1.4.1	Free Radical polymerization(FRP)	19
1.4.1.1	Initiation reaction	20
1.4.1.2	Propagation reaction	20 – 21
1.4.1.3	Termination reaction	21
1.4.2	Controlled radical polymerization	22 – 23
1.5	Strategies for Synthesizing Molecularly Imprinted Polymers (MIPs)	23
1.5.1	Bulk polymerization	23 - 24
1.5.2	Suspension polymerization	24 – 25
1.5.3	Precipitation polymerization	25
1.5.4	Seed polymerization	26
1.5.5	Core-shell Emulsion polymerization	27
1.6	Applications of Molecularly imprinted polymers	27

1.6.1	Chromatographic Separations Using Molecularly imprinted polymers(MIPs)	28 - 29
1.6.2	Binding Assays	30 – 31
1.6.3	Chemical sensors	31 – 32
1.6.4	Drug delivery	32 – 33
1.6.5	Catalysis	33
1.6.6	Solid phase extraction	33 – 36
1.7	Extraction of drugs from human urine and blood using Molecularly imprinted polymers	36
1.7.1	Principle of MIP-based extraction	37
1.7.2	Drug extraction from human urine	37 – 38
1.7.3	Drug extraction from human blood	38
1.7.4	Factors affecting extraction efficiency	38
1.7.5	Quantitative and mechanistic Evaluation of drug binding on to MIPs	39
1.7.5.1	Adsorption capacity Q_e	39
1.7.5.2	Isotherm Models	40
1.	Langmuir isotherm	40
2.	Freundlich isotherm	40
3.	Timken isotherm	41
1.7.5.3	Kinetic Models	41
1.	Pseudo first –order model	41
2.	Pseudo second –order model	41
1.7.5.4	Thermodynamic studies	42
1.8	Literature review	43 – 45
1.9	Aims of the study	46
Chapter Two Experimental part		
2.	Experimental part	47
2.1	Chemicals materials	47
2.2	Instruments	48
2.3	Purification of heroin and amphetamin	50
2.4	Synthesis of MMIP and MNIP	50
2.4.1	Synthesis of non-imprinted magnetic polymer (MNIP) using 2-acetamidoacrylic acid	51
2.4.2	Synthesis of magnetic molecularly imprinted polymers MMIPs for heroin and amphetamine Using 2-acetamidoacrylic acid	51
2.4.2.1	Synthesis of $Fe_3O_4@SiO_2@Her$ -MMIP	51 – 52
2.4.2.2	Synthesis of $Fe_3O_4@SiO_2@AMP$ -MMIP	52
2.4.3	Synthesis of non-imprinted magnetic polymer (MNIP) using 3,4 Dihydroxy-1-butane	52

2.4.4	Synthesis of magnetic molecularly imprinted polymers MMIPs for Artane and Pregabalin Using 2-acetamidoacrylic acid	53
2.4.4.1	Synthesis of Fe ₃ O ₄ @SiO ₂ @ART-MMIP	53
2.4.4.2	Synthesis of Fe ₃ O ₄ @SiO ₂ @Pre-MMIP	53 – 54
2.5	Characterization of synthesized polymers	54
2.5.1	UV-visible Spectrophotometry(uv-vis)	54
2.5.2	Fourier transform infrared (FT-IR) analysis	54
2.5.3	Field Emission-Scanning Electron Microscopes(FE-SEM)	54
2.5.4	X-ray Diffraction Spectroscopy(XRD)	54 – 55
2.5.5	Analysis of the surface Area and Porosity Characterization of the surface(BET,BJH)	55
2.5.6	Thermogravimetric Analysis(TGA)	55
2.5.7	Magnetic properties measurement (VSM)	55
2.6	Preparation of standard solutions of heroin and amphetamine	56
2.7	Preparation of standard solutions of Artane and Pregabalin	56
2.8	Determination of the maximum wavelength of drugs (λ_{max})	56
2.9	Determination of Calibration curves of drugs	58
2.9.1	Determination of Calibration curves of drugs in aqueous solution	58
2.9.2	Determination of Calibration curves of heroin and amphetamine in urine sample	60 – 61
2.9.3	Determination of Calibration curves of Artane and Pregabalin in serum samples	61 – 62
2.10	Optimization of extraction conditions	63
2.10.1	Effect of contact time(Equilibrium time)	63
2.10.2	Effect of MMIP Dosage	63 – 64
2.10.3	Effect of pH	64
2.10.4	Effect of temperature	64
2.10.5	Effect of drug solution volume	64 – 65
2.11	Adsorption isotherm	65
2.12	Kinetic adsorption experiments	65
2.13	Static adsorption of the MMIP	65 - 66
2.14	Molecularly imprinted magnetic solid– phase extraction (MIMSPE) of heroin and amphetamine From urine samples	67
2.15	Molecularly imprinted magnetic solid– phase extraction (MIMSPE) of Artane and Pregabalin From serum samples	67
2.15.1	Serum collection	67
2.15.2	Serum pretreatment	68
2.15.3	Extraction procedure using MMIPs	68
2.16	Selectivity of MMIPs	69

2.17	Reusability and stability	69
2.18	Determination of Analytical Performance Parameters (LOD, LOQ, RSD, and Recovery)	69 – 70
Chapter Three (Results and Discussion)		
3.	Results and discussion	71
3.1	Synthesis of magnetic molecularly imprinted polymers (MMIPs)	71
3.1.1	MMIPs for heroin and amphetamine(Her-MMIP and AMP-MMIP)	71 – 73
3.1.2	MMIPs for Artane and Pregabalin (ART-MMIP and Pre-MMIP)	73 – 75
3.2	Characterization of MMIPs and MNIP	75
3.2.1	Analysis through the use of X-ray Diffraction(XRD)	75 – 77
3.2.2	Thermal gravimetric analysis(TGA)	77 – 79
3.2.3	Vibrating sample magnetmeter(VSM) Analysis	80 – 81
3.2.4	Fourier transform infrared spectroscopy analysis (FTIR)	82
3.2.4.1	FTIR spectra of Her-MMIP and MNIP	82 – 83
3.2.4.2	FTIR spectra of AMP-MMIP and MNIP	84 – 85
3.2.4.3	FTIR spectra of ART-MMIP and MNIP	86 – 87
3.2.4.4	FTIR spectra of Pre-MMIP and MNIP	88 – 89
3.2.5	Field emission scanning electron microscope (FESEM) Analysis	90
3.2.5.1	FESEM of Her-MMIP and MNIP	90 – 91
3.2.5.2	FESEM of AMP-MMIP and MNIP	91 – 92
3.2.5.3	FESEM of Art-MMIP and MNIP	93 – 94
3.2.5.4	FESEM of Pre-MMIP and MNIP	94 – 95
3.2.6	Nitrogen adsorption- desorption analysis	96
3.2.6.1	Surface area analyzer of MMIP and MNIP for heroin and amphetamine	96 – 97
3.2.6.2	Surface area analyzer of MMIP and MNIP for Artane and Pregabalin	97 – 99
3.3	Enhancement of the extraction parameters	100
3.3.1	Enhancement of the extraction parameters of Her-MMIP	100
3.3.1.1	Equilibrium time impact	100
3.3.1.2	Effect of the amount of Her-MMIP	101
3.3.1.3	Effect of pH	102 – 103
3.3.1.4	Effect of temperature	103 – 104
3.3.1.5	Effect of sample solution	104 – 105
3.3.2	Enhancement of the extraction parameters of AMP-MMIP	105 – 106
3.3.2.1	Equilibrium time impact	105 – 106
3.3.2.2	Effect of the amount of AMP-MMIP	106 – 107

3.3.2.3	Effect of pH	107 – 108
3.3.2.4	Effect of temperature	108 – 109
3.3.2.5	Effect of sample solution	109 – 110
3.3.3	Enhancement of the extraction parameters of ART-MMIP	110
3.3.3.1	Equilibrium time impact	110 – 111
3.3.3.2	Effect of the amount of ART-MMIP	111 – 112
3.3.3.3	Effect of pH	112 – 113
3.3.3.4	Effect of temperature	113 – 114
3.3.3.5	Effect of sample solution	114 – 115
3.3.4	Enhancement of the extraction parameters of Pre-MMIP	115
3.3.4.1	Equilibrium time impact	115 – 116
3.3.4.2	Effect of the amount of Pre-MMIP	116 – 117
3.3.4.3	Effect of pH	117 – 119
3.3.4.4	Effect of temperature	119 – 120
3.3.4.5	Effect of sample solution	120 – 121
3.4	Adsorption characteristics of MMIPs	121
3.4.1	Adsorption kinetic	121
3.4.1.1	Heroin adsorption kinetics	121 – 122
3.4.1.2	Amphetamine adsorption kinetics	122 – 123
3.4.1.3	Artane adsorption kinetics	123
3.4.1.4	Pregabalin adsorption kinetics	124
3.4.2	Adsorption isotherms	124
3.4.2.1	Adsorption isotherms of heroin and Amphetamine	125 – 127
3.4.2.2	Adsorption isotherms of Artane and Pregabalin	127 – 129
3.4.3	Thermodynamics studies of drugs adsorption	129 – 133
3.5	Selectivity and reusability of MMIPs	133
3.5.1	Selectivity of MMIPs toward target drugs	133 – 137
3.5.2	Reusability of MMIPs	137 – 140
3.6	Application of MMIPs for the selective extraction of target drugs from biological samples (urine and Serum)	140
3.6.1	Evaluation of Heroin extraction efficiency and method sensitivity in human urine	140 – 142
3.6.2	Evaluation of Amphetamine extraction efficiency and method sensitivity in human urine	142 – 143
3.6.3	Evaluation of Artane extraction efficiency and method sensitivity in human serum	143 – 145
3.6.4	Evaluation of Pregabalin extraction efficiency and method sensitivity in human serum	145 – 147

3.7	Comparsion with other studies	147 – 148
3.8	Conclusions	149 – 150
3.9	Recommendation	150
References		
	References	151 - 174

List of Figures

NO.	Subject	Page
Chapter One (Introduction)		
Figure [1.1]	Chemical structure of heroin	2
Figure [1.2]	Chemical structure of amphetamin	3
Figure [1.3]	Chemical structure of artane	4
Figure [1.4]	Chemical structure of pregabalin	5
Figure [1.5]	Principle of molecular imprinting process	9
Figure [1.6]	Functional monomers applied in the non-covalent imprinting approach	14
Figure [1.7]	Chemical structures of common cross-linkers used in MIP	15
Figure [1.8]	Chemical structuresChemical structure of widespread initiators applied in non-covalent molecular imprinting Chemical structures of selected chemical initiators: (a) 2,2'-azobis- isobutyronitrile; (AIBN) (b) benzoyl peroxide (BPO), (c) azo-bis-dimethylvaleronitrile; (ABDV) and (d) 4,4'- azo(4- cyanovaleric acid	19
Figure [1.9]	Principle of MIP utilized in chromatographic separation methodologies	29
Figure [1.10]	General principle of the MIP	30
Figure [1.11]	Principle of the three types of the MIP based sensors	32
Figure [1.12]	Principle of the MIP-SPE	34
Figure [1.13]	Drug extraction by MMIP	37
Chapter Two Experimental part		
Figure[2.1]	Synthesis process of Her-MMIP	56
Figure[2.2]	Synthesis process of AMP-MMIP	57
Figure[2.3]	Synthesis process of ART-MMIP	57
Figure[2.4]	Synthesis process of Pre-MMIP	57
Figure[2.5]	Calibration curve of heroin	58
Figure[2.6]	Calibration curve of amphetamin	59
Figure[2.7]	Calibration curve of Artane	59
Figure [2.8]	Calibration curve of Pregabalin	60
Figure [2.9]	Calibration curve of heroin in urine sample	61

Figure [2.10]	Calibration curve of Amphetamine in urine sample	61
Figure [2.11]	Calibration curve of Artane in serum sample	62
Figure [2.12]	Calibration curve of Pregabalin in serum sample	62
Figure [2.13]	Steps of serum pretreatment	68
Chapter Three (Results and Discussion)		
Figure [3.1]	XRD spectra of MNIP ₁	72
Figure [3.2]	XRD spectra of MNIP ₂	73
Figure [3.3]	TGA curve of MNIP ₁	74
Figure [3.4]	TGA curve of MNIP ₂	75
Figure [3.5]	Magnetization curve across magnetic field range from (-10000 to 10000) Q _e at 25C° of MNIP ₁	76
Figure [3.6]	Magnetization curve across magnetic field range from (-10000 to 10000) Q _e at 25C° of MNIP ₂	77
Figure [3.7]	FT-IR spectra of heroin (A) MNIP (B) unwashed MMIP (C) washed MMIP	79
Figure [3.8]	FT-IR spectra of Amphetamine (A) MNIP (B) unwashed MMIP (C) washed MMIP	79
Figure [3.9]	FT-IR spectra of Artane (A) MNIP (B) unwashed MMIP (C) washed MMIP	81
Figure [3.10]	FT-IR spectra of Pregabalin (A) MNIP (B) unwashed MMIP (C) washed MMIP	81
Figure [3.11]	FESEM image of heroin (A) MNIP (B) Her-MMIP (C) MMIP	83
Figure [3.12]	FESEM image of Amphetamine (A) MNIP (B) AMP-MMIP (C) MMIP	85
Figure [3.13]	FESEM image of Artane (A) MNIP (B) ART-MMIP (C) MMIP	87
Figure [3.14]	FESEM image of Pregabalin (A) MNIP (B) Per-MMIP (C) MMIP	89
Figure [3.15]	N ₂ - adsorption – desorption isotherm of the Her-MMIP	91
Figure [3.16]	N ₂ - adsorption – desorption isotherm of the AMP-MMIP	92
Figure [3.17]	N ₂ - adsorption – desorption isotherm of the ART-MMIP	94
Figure [3.18]	N ₂ - adsorption – desorption isotherm of the Pre-MMIP	95
Figure [3.19]	Effect of contact time on the adsorption capacity of Heroin on to Her-MMIP	97
Figure [3.20]	Effect of weight of Her-MMIP on the adsorption capacity of heroin solution	97

Figure [3.21]	Effect of pH solution on the adsorption capacity of Heroin on to Her-MMIP	99
Figure [3.22]	Effect of temperature on the adsorption capacity of Heroin on to Her-MMIP	99
Figure [3.23]	Effect of sample volume on the Recovery percentage of heroin using Her-MMIP	100
Figure [3.24]	Effect of contact time on the adsorption capacity of Amphetamine on to AMP-MMIP	101
Figure [3.25]	Effect of weight of AMP-MMIP on the adsorption capacity of Amphetamine solution	103
Figure [3.26]	Effect of pH solution on the adsorption capacity of Amphetamine on to AMP-MMIP	104
Figure [3.27]	Effect of temperature on the adsorption capacity of Amphetamine on to AMP-MMIP	105
Figure [3.28]	Effect of sample volume on the Recovery percentage of Amphetamine using AMP-MMIP	106
Figure [3.29]	Effect of contact time on the adsorption capacity of Artane on to ART-MMIP	107
Figure [3.30]	Effect of weight of AMP-MMIP on the adsorption capacity of Artane solution	108
Figure [3.31]	Effect of pH solution on the adsorption capacity of Artane on to ART-MMIP	109
Figure [3.32]	Effect of temperature on the adsorption capacity of Artane on to ART-MMIP	110
Figure [3.33]	Effect of sample volume on the Recovery percentage of Artane using ART-MMIP	111
Figure [3.34]	Effect of contact time on the adsorption capacity of Pregabalin on to pre-MMIP	112
Figure [3.35]	Effect of weight of pre-MMIP on the adsorption capacity of pregabalin solution	113
Figure [3.36]	Effect of pH solution on the adsorption capacity of pregabalin on to pre-MMIP	114
Figure [3.37]	Effect of temperature on the adsorption capacity of pregabalin on to pre-MMIP	115
Figure [3.38]	Effect of sample volume on the Recovery percentage of pregabalin using pre-MMIP	116
Figure [3.39]	Pseudo –first order kinetics (B) (A) Pseudo – second order kinetics of heroin	117

Figure [3.40]	(A) Pseudo –first order kinetics (B) (A)Pseudo – second order kinetics of Amphetamine	119
Figure [3.41]	(A) Pseudo –first order kinetics (B) (A)Pseudo – second order kinetics of Artane	120
Figure [3.42]	(A) Pseudo –first order kinetics (B) (A)Pseudo – second order kinetics of Pregabalin	121
Figure [3.43]	adsorption isotherm (A) Freundlich isotherm (B) Langmuir isotherms(C) Timken isotherm of heroin	122
Figure [3.44]	adsorption isotherm (A) Freundlich isotherm (B) Langmuir isotherms(C) Timken isotherm of amphetamine	123
Figure [3.45]	adsorption isotherm (A)Freundlich isotherm(B) Langmuir isotherms(C) Timken isotherm of Artane	123
Figure [3.46]	adsorption isotherm (A) Freundlich isotherm (B) Langmuir isotherms(C) Timken isotherm of pregabalin	124
Figure [3.47]	adsorption of heroin on the surface of the MMIP	126
Figure [3.48]	adsorption of Amphetamine on the surface of the MMIP	127
Figure [3.49]	adsorption of Artane on the surface of the MMIP	129
Figure [3.50]	adsorption of pergabaline on the surface of the MMIP	129
Figure [3.51]	Selectivity of Her-MMIP toward Heroin and three drugs	131
Figure [3.52]	Selectivity of AMP-MMIP toward Amphetamine and three drugs	132
Figure [3.53]	Selectivity of ART-MMIP toward Artane and three drugs	132
Figure [3.54]	Selectivity of Pre-MMIP toward pregabaline and three drugs	133
Figure [3.55]	Reusability of the Heroin-MMIP	135
Figure [3.56]	Reusability of the AMP-MMIP	136
Figure [3.57]	Reusability of the ART-MMIP	136

Figure [3.58]	Reusability of the Pre -MMIP	137
----------------------	------------------------------	------------

List of Tables

NO.	Subject	Page
Chapter One (Introduction)		
Table [1-1]	General overview of the specific characteristics of different types of SPE sorbents	36
Chapter Two (Experimental part)		
Table [2-1]	Chemicals used manufacturers, chemical composition and purity	47
Table [2-2]	Devices used in this study, including their manufacturers, construction, model and worksite	48
Table [2-3]	the contact time for drugs	63
Chapter Three (Results and Discussion)		
Table [3-1]	Thermodynamic parameters for drugs adsorption on to MMIPs	131
Table [3-2]	Selectivity binding activities of MMIPs and MNIPs	134
Table [3-3]	Results of extraction of heroin in human urine	141
Table [3-4]	Accuracy of the method for sample solution spiked at different concentration	141
Table [3-5]	Results of extraction of Amphetamine in human urine	142
Table [3-6]	Accuracy of the method for sample solution spiked at different concentration	143
Table [3-7]	Results of extraction of Artane in human serum	144
Table [3-8]	Accuracy of the method for sample solution spiked at different concentration	145
Table [3-9]	Results of extraction of Pregabalin in human serum	145
Table[3-10]	Accuracy of the method for sample solution spiked at different concentration	146

List of Abbreviations

Abbreviations	Full Name
ADHD	attention deficit hyperactivity disorder
AC	2-Acetamidoacrylic acid
AMP-MMIP	Amphetamine-magnetic molecularly imprinted polymer
AIBN	azobisisobutyronitrile
AA	acrylamide
Ar	Argon
A	Absorbance
ABDV	azo-bis-dimethylvaleronitrile
APTES	3-Aminopropyltriethoxysilane
AMP	Amphetamine
ART	Artane
BET	Surface Area Analysis
BPO	benzoyl peroxide
B	Temkin Isotherm Constant
β	specific factor
CRP	controlled radical polymerization
CEC	capillary electro chromatography
C_e	Equilibrium concentration of adsorbate
C_0	Initial concentration of adsorbate
CLF	clofazimine
DVB	Divinyl benzene
EGDMA	Ethyleneglyoldimethacrylate
FRP	Free Radical Polymerization
FT-IR	Fourier Transform Infrared
FE-SEM	Field Emission Scanning Electron Microscopy
HEMA	2-hydroxyethyl methacrylate
Her-MMIP	Heroin-magnetic molecularly imprinted polymer
HMMIP	hydrophilic magnetic molecularly imprinted polymers
MIPs	Molecularly Imprinted Polymers
MNPs	Magnetic nanoparticles
MPs	Magnetic particals
MAA	methacrylic acid
MNIP	magnetic molecularly non-imprinted polymer
MIMs	molecularly imprinted monoliths
MIA	molecularly imprinted assay

MIP-SPE or MISPE	molecularly imprinted solid-phase extraction
NIP	non-imprinted polymer
NMP	Nitroxide-Mediated Polymerization
N₂	Nitrogen
N	Freundlich isotherm constant
4-VP	4-vinylpyridine
Q_e	Amount of adsorbate adsorbed per unit
PMMA	poly methyl methacrylate
V	Volume
K_{eq}	The equilibrium constant
K_F	Empirical Freundlich constant or capacity factor
K_L	Langmuir Isotherm Constant
K_T	The equilibrium Binding Constant
ΔG	Change Gibbs free energy
ΔH	Change of enthalpy of adsorption
RA	rosmarinic acid
λ_{max}	The wavelength of maximum absorbance
ΔS	Change of entropy of adsorption
R	Gas constant
R²	Correlation coefficient
X_m	The maximum adsorbed quantity at a certain equilibrium concentration
LOD	Limit of detection
LOQ	Limit of Quantitation
OA	Oleic acid
XRD	X-ray diffraction
UV-Vis	Ultraviolet-Visible
VSM	Vibrating sample magnetometer
TGA	Thermo gravimetric Analysis
pH	Acidic function
TEOS	tetraethyl orthosilicate
Her	Heroin
Pre	Pregabalin
DHB	3,4-dihydroxy -1- butene
JCPDS	Joint Committee on Powder Diffraction Standards
RSD	relative standard deviation
GABA	gamma-amino butyric acid
MMIP	Magnetic molecularly imprinted polymers

GC	gas chromatography
LC	liquid chromatography
MS	mass spectrometry
Pre-MMIP	Pregabalin-magnetic molecularly imprinted polymer
IF	imprinting factor
2-VP	2-vinylpyridine
Wt	Weight
TMDA	Tetramethylenedimethacrylate
SPE	Solid phase extraction
PEG	polyethylene glycol
PVA	polyvinyl alcohol
PLA	polylactic acid
TFMAA	trifluoromethyl acrylic acid

Chapter One

Introduction

1.1. General introduction

Substance misuse continues to be a significant concern for modern cultures, endangering public health, social stability, and economic progress. In recent decades, there has been a significant rise in the consumption and accessibility of illegal substances, encompassing both conventional narcotics and synthetic drugs.. This rise is driven by a complex interplay of factors, including psychological stress, social instability, ease of access to drugs, weak regulatory frameworks, and insufficient awareness of the associated health risks [1] The negative consequences of drug abuse are profound and multidimensional. On an individual level, chronic use often leads to severe physical and psychological deterioration, impaired behavioral functioning, addiction, and ultimately the erosion of personal productivity and social integration. Common outcomes include increased susceptibility to infectious diseases, neurocognitive decline, depression, and social withdrawal [2] from a societal perspective, the repercussions are equally severe. Drug abuse has been directly linked to rising crime rates, unemployment, and the overburdening of healthcare and law enforcement systems. These consequences place a significant strain on national resources and hinder sustainable development goals, particularly in low- and middle-income countries [3]. In response to this growing threat, scientific research has increasingly focused on the detection and quantification of drugs in biological matrices such as blood and urine. This line of investigation is particularly critical in forensic science, clinical diagnostics, and public health surveillance. Analytical methods capable of accurately identifying trace levels of narcotic substances are essential for legal investigations, treatment monitoring, and the development of evidence-based drug control policies

1.2. Drugs studied in the thesis

In this thesis, four drugs that are among the most abused substances in local and regional environments have been selected: heroin, amphetamine, Artane, and Pregabalin. These substances were chosen due to their widespread illicit use, their dangerous impact on individuals and society, and the difficulty of extracting them from biological samples such as urine and blood. Below is a detailed presentation of each substance:

1.2.1. Heroin (Diacetylmorphine)

- scientific (IUPAC) name: (5 α ,6 α)-7,8-didehydro-4,5-epoxy-17-methylmorphinan-3,6-diyl diacetate
- Chemical formula: C₂₁H₂₃NO₅
- Molecular weight: 369.4 g.mol⁻¹
- Melting point: ~173°C
- Solubility: Soluble in water, alcohol, and chloroform
- Commercial names: Not legally marketed; known on the street as "Brown Sugar", "Smack", or "Black Tar"
- Structural Formula as shown in Figure [1.1].

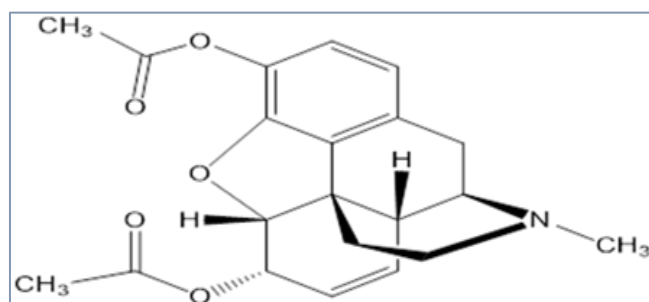


Figure [1.1] chemical structure of Heroin[4]

Heroin is a semi-synthetic opioid derived from morphine. Due to its lipophilic nature, it crosses the blood-brain barrier rapidly, producing an intense euphoric effect. Although originally synthesized for therapeutic purposes, it is now

classified as an illegal narcotic in most countries due to its high addiction potential.

- Negative effects: Physiological: Respiratory depression, chronic infections (e.g., HIV, hepatitis C), collapsed veins, malnutrition.
- Psychological: Severe dependence, depression, emotional blunting.
- Behavioral: Social withdrawal, criminal behavior, loss of occupational function[4].

1.2.2. Amphetamine

Scientific (IUPAC) name: 1-phenylpropan-2-amine

- Chemical formula: $C_9H_{13}N$
- Molecular weight: 135.2 g.mol^{-1}
- Boiling point: $\sim 203^\circ\text{C}$
- Solubility: Soluble in water and ethanol
- Commercial names: Adderall, Dexedrine (when prescribed)
- Structural Formula as shown in figure [1.2]

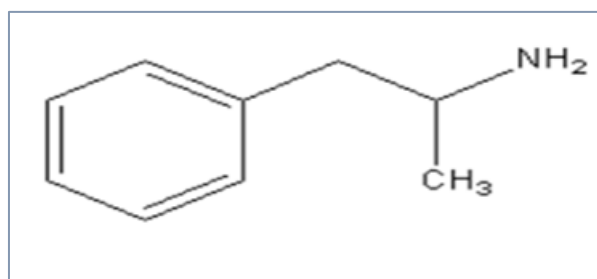


Figure [1.2] chemical structure of Amphetamine[5]

Amphetamine is a powerful central nervous system stimulant frequently taken for attention deficit hyperactivity disorder (ADHD) and narcolepsy. It exerts its effects by augmenting the synaptic levels of dopamine and norepinephrine.

- Negative effects: Physiological: Elevated heart rate and blood pressure, insomnia, appetite suppression.
- Psychological: Anxiety, paranoia, hallucinations.
- Behavioral: Aggression, compulsive behavior, social impairment[5]

1.2.3. Artane

- Scientific (IUPAC) Name: Trihexyphenidyl
- Chemical Formula: $C_{20}H_{31}NO \cdot HCl$
- Molecular Weight: $301.48 \text{ g} \cdot \text{mol}^{-1}$
- Melting Point: $\sim 247^{\circ}\text{C}$ (decomposes)
- Solubility: Slightly soluble in water; soluble in alcohol and chloroform
- Commercial Names: Artane, Pacitane and Cyclodol
- Structural Formula as shown in figure [1.3].

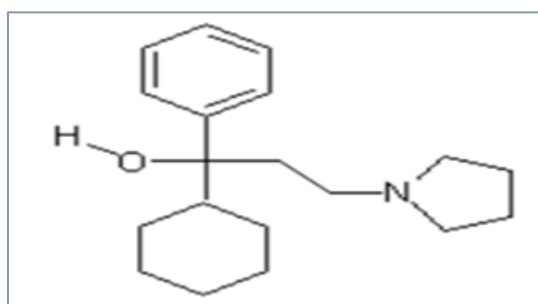


Figure [1.3] chemical structure of Artane[6]

Artane is an anticholinergic medication used in the treatment of Parkinson's disease and extrapyramidal symptoms caused by antipsychotic drugs. Abuse occurs due to its hallucinogenic effects at high doses, particularly among psychiatric populations.

- **Negative Effects:** Physiological: Dry mouth, blurred vision, and constipation.
- Psychological: Hallucinations, confusion, impaired cognition.

- Behavioral: Disorientation, social detachment, erratic behavior[6]

1.2.4. Lyrica (Pregabalin)

- Scientific(IUPAC) Name: (S)-3-(amino methyl)-5-methylhexanoic acid)
- Chemical Formula: $C_8H_{17}NO_2$
- Molecular Weight: $159.23 \text{ g.mol}^{-1}$
- Melting Point: $186\text{--}188^\circ\text{C}$
- Solubility: Highly soluble in water
- Commercial Names: Lyrica
- Structural Formula as shown in figure [1.4]

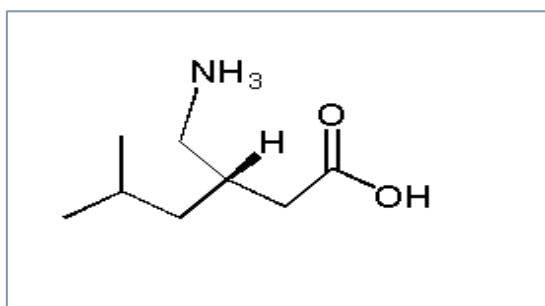


Figure [1.4] chemical structure of Pregabalin[7]

Pregabalin is a structural analog of gamma-amino butyric acid (GABA) used in the treatment of neuropathic pain, epilepsy, and anxiety disorders. While effective therapeutically, it has gained popularity as a drug of abuse due to its euphoric and sedative effects.

Negative Effects:

- **Physiological:** Drowsiness, dizziness, ataxia. **Psychological:** Mood swings, cognitive slowing, depression. **Behavioral:** Apathy, reduced productivity, isolation [7].

1.3. Magnetic molecularly imprinted polymers (MMIPs)

To effectively address drug use and enable timely intervention, it is essential to develop reliable analytical methods for the detection and quantification of drugs in biological fluids, including blood and urine. These analyses are fundamental in various settings, including forensic investigations, workplace testing, clinical diagnostics, and rehabilitation monitoring programs. Traditional techniques, including gas chromatography (GC) and liquid chromatography (LC) combined with mass spectrometry (MS) or UV detection, are well-established in toxicology., they are often limited by complex sample preparation procedures, long analysis times, and insufficient selectivity when dealing with trace-level analytes in complex biological matrices. These challenges have underscored the need for more selective, efficient, and streamlined extraction techniques that can enhance sensitivity and reduce analysis time, especially for routine screening and real-time diagnostics. Recent advancements in materials science and analytical chemistry have resulted in the development of Molecularly Imprinted Polymers (MIPs) as an effective method for the selective extraction and quantification of pharmaceuticals in intricate biological matrices. MMIPs are synthetic polymers designed with precise recognition sites that match the form, size, and functional group orientation of the target analyte. These recognition sites are created through a templating process during polymerization, resulting in a high degree of selectivity and binding affinity. One promising approach lies in the development of Molecularly Imprinted Polymers (MIPs), especially when combined with magnetic nanoparticles to form Magnetic Molecularly Imprinted Polymers (MMIPs). Magnetic micro- and nanoparticles (MNPs) have garnered significant interest in analytical chemistry due to their unique physicochemical properties, such as high surface area, rapid magnetic responsiveness, and ease of separation. Nevertheless, bare MNPs often suffer from drawbacks including aggregation, poor stability,

and susceptibility to oxidation, which can result in diminished magnetic properties and reduced dispersibility. To address these limitations, surface modification strategies such as coating with polymers, silica, or other inert materials are essential. These modifications not only improve colloidal stability and prevent oxidation but also provide functional groups for further chemical conjugation, enhancing their performance in analytical and bioanalytical applications [8]. To overcome the inherent limitations of magnetic particles (MPs), various surface modification strategies have been developed to enhance their stability and reduce undesired behaviors such as aggregation or oxidation. These surface engineering approaches typically yield core-shell structured particles, where the magnetic core is enveloped by a protective shell that acts as a barrier against environmental degradation. Generally, two main methodologies are employed for this purpose. The first involves post-synthetic coating, wherein a stabilizing layer often composed of polymers, silica, or other inert materials is applied onto pre-formed MPs. The second approach consists of in situ encapsulation, in which MPs are integrated directly into a matrix during synthesis, resulting in simultaneous formation of the core and the protective shell. Both strategies enhance the physicochemical stability and functional versatility of MPs, making them more suitable for advanced applications in sensing, separation, and catalysis [9,10]. The protective shells applied to magnetic particles (MPs) can be composed of a wide range of inorganic or organic materials. Inorganic coatings typically include silica, carbon, noble metals, or metal oxides that form through controlled oxidation or are directly deposited onto the particle surface. On the other hand, organic coatings often involve natural polymers such as chitosan, dextran, starch, or gelatin, as well as synthetic polymers like polyethylene glycol (PEG), polyvinyl alcohol (PVA), polylactic acid (PLA), polypyrrole, polyaniline, polyesters, alginate, and polyacrylic acid. In addition to polymers, surface stabilization can also be achieved using surfactants and low-molecular-weight compounds such as carboxylic acids (e.g., oleic acid, citric

acid, and di mercapto succinic acid), phosphates, and sulfates. These coating materials not only prevent aggregation and improve colloidal stability, but they also introduce functional groups such as carboxyl ($-\text{COOH}$), amino ($-\text{NH}_2$), hydroxyl ($-\text{OH}$), and amide ($-\text{CONH}_2$) on the particle surface. These groups serve as reactive sites for subsequent surface modification and facilitate binding with various analytes or biomolecules, which is particularly advantageous in analytical and biomedical applications [11].

1.3.1 Principle of Molecularly Imprinted Polymers (MIPs)

Surface molecular imprinting represents an advanced technique for designing polymeric materials with high molecular recognition capabilities. In this approach, specific recognition sites often referred to as “molecular cavities” are constructed on the polymer surface to complement the geometry and chemical functionality of a particular target molecule. These surface cavities enable selective binding, making the material highly suitable for use in analytical sensing, pharmaceutical separation, and environmental remediation.

The general process of MIP synthesis Figure[1.5] begins with the formation of a pre-polymerization complex, where a target analyte (template) or its structural analogue is mixed with functional monomers in a porogenic solvent. These monomers interact with the template via specific chemical or physical forces. Following this, cross-linking agents and initiators (thermal or photo-initiated) are introduced to initiate polymerization, resulting in a stable three-dimensional polymer network. After polymerization, the template molecule is extracted using appropriate solvents, leaving behind recognition sites that are complementary in size, shape, and functionality to the original template, thus preserving its "molecular memory" [12, 13]. The interactions between the monomers and the template during MIP formation can occur through three main strategies: covalent, non-covalent, and semi-covalent imprinting. In the covalent method, the template forms reversible covalent bonds with the monomers prior

to polymerization. These bonds are cleaved chemically during template removal but can reform upon re-binding. This technique yields highly uniform and well-defined binding sites; however, it often involves complex synthetic steps and slower binding kinetics [14]. The semi-covalent method combines the structural integrity of covalent imprinting with the binding dynamics of non-covalent interactions. Here, covalent bonds are used during polymer formation, while recognition of the target molecule during re-binding relies on non-covalent forces. This hybrid approach aims to balance selectivity and binding efficiency [15]. The non-covalent imprinting approach is the most widely employed due to its versatility and relatively simple preparation. It involves weak and reversible interactions such as hydrogen bonding, π - π stacking, van der Waals forces, and electrostatic attractions between the template and monomers in a low-polarity solvent. This flexibility allows for a wide selection of templates and monomers to be used. However, one drawback of this method is its reliance on equilibrium-based interactions, which necessitates an excess of functional monomers to favor complex formation. As a result, the distribution of binding sites may become heterogeneous, potentially affecting the specificity and affinity of the polymer for the target molecule [16, 17].

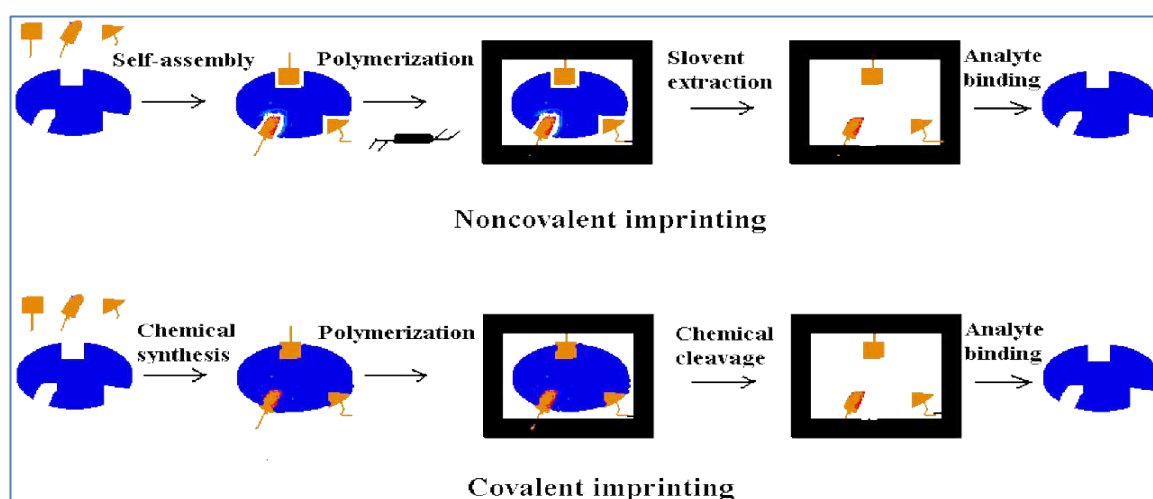


Figure [1.5] Principle of molecular imprinting[17]

1.3.2. Key Variables Influencing the Molecular Imprinting Process

The concept of molecular imprinting is relatively simple in theory. However, the practical design of (MIPs) is quite complex due to the numerous experimental factors involved. These include the choice of template molecule, selection of functional monomers, the ratio between the monomers and template, type and amount of cross-linkers, as well as the ratio of monomers to cross-linkers. Other important variables include the nature of pre-polymerization interactions, the solvent system, the type of initiator used, and various thermodynamic and polymerization conditions such as temperature and pressure. The orientation, stability, and accessibility of the binding sites—key elements for molecular recognition are largely influenced by the structural features of the polymer matrix. Therefore, careful evaluation and optimization of these parameters are critical for enhancing the recognition capabilities of MIPs [18].

1.3.2.1. Template:

The structural properties, molecular size, and chemical functionality of the template molecule are essential determinants in selecting a suitable molecular imprinting strategy. (MIPs) have been developed for a wide array of template molecules, encompassing various sizes, shapes, and functional groups. When choosing a template, important factors to consider include its solubility in organic solvents, the presence of electrostatic or polar functionalities, and its chemical inertness under free radical polymerization conditions. The imprinting of large biomolecules can be particularly challenging due to the difficulty in creating precise and selective recognition sites. Ultimately, despite the involvement of multiple variables, the physicochemical features of the template remain the most influential factor in the success of the imprinting process [19]. Molecular imprinting using a specific template is considered one of the most structurally restrictive approaches for targeting specific species. Upon removal of the template from the polymer matrix, highly selective cavities are formed that

precisely match the shape and chemical functionalities of the template molecule. Consequently, even minor structural deviations between the target molecule and the original template can lead to a significant decrease in selectivity. The impact of exceedingly high monomer-to-template ratios has been examined, revealing notable imprinting effects at minimal template concentrations. The influence of template size on the selectivity of molecularly imprinted polymers (MIPs) has been investigated. The quantities of template and porogen employed were adjusted to selectively extract a diverse array of phenylurea herbicides with similar structural characteristics. The findings indicated that the dimensions and configuration of the template, regarding the contact strength, were crucial to the efficacy of the imprinted polymer [20].

1.3.2.2 Functional Monomers

Functional monomers play a pivotal role in establishing selective binding interactions within the recognition sites of molecularly imprinted polymers (MIPs). The success of the imprinting process is largely determined by selecting monomers whose functional groups are capable of forming stable and specific interactions with the target template during the formation of the pre-polymerization complex. The compatibility between the chemical functionalities of the monomer and the template molecule is essential for ensuring effective molecular recognition. Functional monomers are typically classified into three categories: acidic, basic, and neutral. Among these, acidic monomers particularly those bearing carboxylic acid groups are extensively utilized due to their ability to engage in multiple forms of non-covalent interactions, including hydrogen bonding (acting both as proton donors and acceptors), ion-pair formation, and dipole-dipole interactions. Commonly employed examples include methacrylic acid (MAA) and trifluoromethyl acrylic acid (TFMAA), which have demonstrated high efficacy in recognizing and interacting with template molecules [21, 22]. However, certain limitations are associated with the use of

acidic monomers, especially under non-polar solvent conditions typically employed in non-covalent imprinting techniques. Under such conditions, carboxyl groups may undergo self-association, leading to the formation of anhydrides. This self-association reduces the number of reactive sites available for interacting with the template, potentially compromising imprinting efficiency. Moreover, the formation of anhydrides can disrupt the stoichiometric balance of the polymerization mixture, increasing the requirement for cross-linking agents and consequently influencing the structural and functional characteristics of the final polymer. On the other hand, basic monomers such as 4-vinylpyridine (4-VP) and 2-vinylpyridine (2-VP) are widely employed for their ability to form strong interactions with acidic moieties present on the template molecule. These interactions not only enhance the specificity of binding but also improve the stability and robustness of the resulting MIP network. [23].

Aromatic systems rich in π -electrons are notable for their capacity to act as hydrogen bond acceptors and engage in acid-base interactions, as well as π - π stacking with electron-deficient aromatic rings. These interactions are fundamental in the formation of molecularly imprinted polymers (MIPs), where functional monomers assemble around a template molecule to create specific binding sites. However, in aqueous environments, the strong π - π interactions can lead to significant non-specific binding. This phenomenon may result in non-imprinted polymers exhibiting binding affinities comparable to their imprinted counterparts, potentially compromising the selectivity of the MIPs [24]. Therefore, careful consideration of the polymerization mixture is essential to mitigate these effects. In low-polarity conditions, the use of neutral monomers such as acrylamide (AA) and 2-hydroxyethyl methacrylate (HEMA) has proven effective. These monomers can form stable interactions with the template molecule without contributing to non-specific binding. Additionally, employing a combination of functional monomers, known as "cocktail polymerization," can

enhance the specificity and affinity of the resulting MIPs. For instance, combinations like meth acrylic acid (MAA) with 2-vinylpyridine (2-VP), or AA with 2-VP, have been successfully utilized to tailor the binding characteristics of MIPs [25, 26]. While commercially available monomers are commonly used in MIP synthesis, designing custom monomers with structural features complementary to the target template can offer significant advantages. These tailor-made monomers can enhance the specificity and binding affinity of MIPs, particularly for complex or unique target molecules. Recent advancements in computational modeling have facilitated the design of such monomers, enabling the development of highly selective MIPs for various applications Figure [1.6]. In summary, the selection of appropriate monomers whether neutral, combined, or custom-designed is crucial in the synthesis of effective MIPs. Understanding the interactions between monomers and template molecules, as well as the influence of environmental conditions, can significantly impact the performance of the resulting polymers [27, 28]. In non-covalent molecular imprinting techniques, a surplus of functional monomers relative to the template molecule is typically employed to enhance the stability and formation of the pre-polymerization complex. This excess facilitates stronger non-covalent interactions, thereby improving the overall imprinting efficiency. Consequently, template-to-monomer molar ratios of 1:4 or higher are commonly adopted to ensure sufficient interaction during complex formation. Recent studies have emphasized the effectiveness of this approach in achieving high selectivity and binding capacity in molecularly imprinted polymers [29]

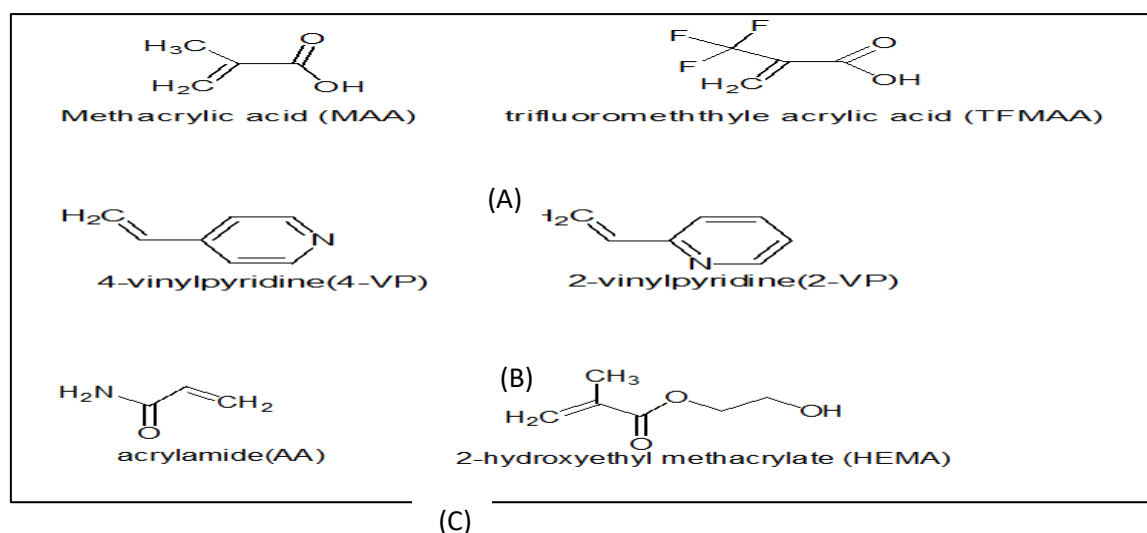


Figure [1.6] A .acid functional monomers, B. basic functional monomers and C. neutral functional monomers applied in the non-covalent imprinting approach[30].

1.3.2.3 Cross-Linkers

The effectiveness and selectivity of molecularly imprinted polymers (MIPs) are profoundly influenced by the type and concentration of the cross-linking agents used during their synthesis. Cross-linkers are pivotal in determining the structural architecture of the polymer matrix, which may range from gel-like to macroporous or microgel formations, as illustrated in Figure [1.7] [31]. In addition to dictating morphology, cross-linkers help maintain the stability of the imprinted cavities and reinforce the mechanical robustness of the polymer network [32]. From a polymer design standpoint, the use of high ratios of cross-linking agents is generally preferred, as it promotes the creation of robust, porous frameworks. These networks are essential for preserving the spatial distribution of functional groups within the imprinted sites following the removal of the template molecule. The maintenance of this three-dimensional cavity conformation ensures high selectivity by allowing the polymer to selectively rebind the target molecule based on both geometric and chemical functionality to the template. Moreover, while cross-linkers are indispensable, the selection of a suitable functional monomer remains equally important. Functional monomers

must possess the capacity to form strong, selective interactions such as hydrogen bonds or ionic forces with the template, thereby enabling the formation of highly specific binding sites. In most MIP formulations, the degree of cross-linking exceeds 80%, a factor that contributes significantly to the mechanical rigidity and shape fidelity of the polymer matrix [33] interestingly; certain cross-linking agents are known to perform dual roles. In addition to providing structural support, these agents may also participate in specific interactions with the template molecules. As a result, such cross-linkers can partially function as active components in the imprinting process, thereby enhancing the recognition properties of the final polymer.

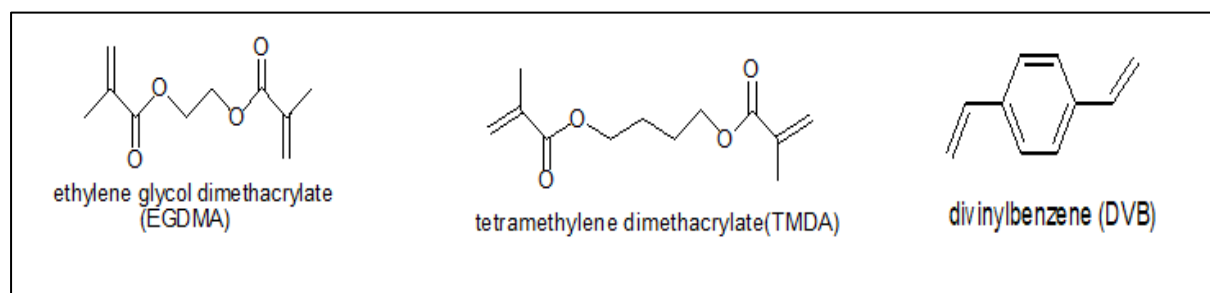


Figure [1.7] Chemical structures of common cross-linkers used in MIP[33]

1.3.2.4. Porogenic solvents:

Porogenic solvents play a pivotal role in determining the porous structure of molecularly imprinted polymers (MIPs). The type and concentration of the porogenic solvent directly influence the morphological and functional characteristics of the resulting polymer. Specifically, the solvent impacts the strength and stability of non-covalent interactions between the template molecule and the functional monomer during the pre-polymerization phase, which consequently determines the specificity and performance of the binding sites. Low-polarity solvents are often preferred, as they tend to promote the formation of micro- or mesoporous structures that enhance mass transfer and improve accessibility to recognition sites. In contrast, highly polar solvents may interfere with the establishment of stable pre-polymerization complexes, thus reducing the

selectivity of the final polymer [34]. The control over pore size and distribution is particularly important in analytical applications, such as the detection of heavy metal ions or pharmaceutical compounds. For instance, porogenic systems composed of mixed solvents like ethanol and toluene have been employed to produce MIPs capable of selectively binding lead and mercury ions due to the favorable formation of well-defined recognition sites [35]. Similarly, MIPs have been used in the development of sensors for psychoactive drugs such as ketamine and benzodiazepines, where the choice of porogen played a key role in stabilizing the imprinting sites [36]. Therefore, the selection of the porogenic solvent must be strategically aligned with the chemical nature of the template, monomer, and cross-linker to ensure the formation of an effective and selective recognition system. The imprinting efficiency and the resulting physical characteristics of molecularly imprinted polymers (MIPs) including their morphology, pore structure, pore size distribution, swell ability, and mechanical strength are highly dependent on both the type and volume of the porogenic solvent selected during polymer synthesis. As highlighted in recent literature, the polymerization solvent serves several critical functions throughout the imprinting process [37]. It facilitates the dissolution of all components in the pre-polymerization mixture, including the template, functional monomers, cross-linker, and initiator.

- It is essential for preserving the stability of the non-covalent interactions between the template molecule and the functional monomer, thereby facilitating the reliable formation of pre-polymerization complexes.
- It functions as a porogen, regulating the internal structure and porosity of the final polymer matrix, which directly affects the polymer's accessibility and performance in target molecule recognition. The rational selection of porogenic solvents is, therefore, essential not only for optimizing the imprinting process but also for tailoring the material properties of MIPs to suit specific applications in separation, sensing, or drug delivery. The

choice of porogenic solvent plays a crucial role in determining the porosity and surface area of molecularly imprinted polymers (MIPs). When solvents with favorable thermodynamic compatibility are employed, they often result in polymers with well-developed pore structures and high specific surface areas. Conversely, the use of thermodynamically poor solvents tends to yield polymers with less-defined porosity and reduced surface area [38]. Interestingly, the efficiency of selective binding in MIPs does not solely depend on pore size or volume. In many cases, enhanced molecular recognition has been observed even in polar porogenic solvents. This suggests that strong interactions between the template and monomer can still be achieved in such environments, as seen with solvent systems like methanol–water mixtures [39]. Moreover, increasing the volume of the porogenic solvent generally leads to an increase in pore size, which may benefit analyte diffusion but could also affect binding site fidelity. Porogenic solvents serve dual functions not only do they act as the medium for polymerization, but they also influence the morphology of the resulting polymer network. Therefore, careful selection of the solvent is necessary to promote effective non-covalent interactions between the template and the functional monomer. Typically, non-polar aprotic solvents such as toluene are favored due to their ability to stabilize hydrogen bonding during complex formation. However, in cases where hydrophobic interactions dominate the imprinting process, polar solvents like water may become more suitable [40].

1.3.2.5. Initiators:

Are essential components in the synthesis of (MIPs) via free radical polymerization. These compounds are responsible for generating free radicals that initiate the polymerization process. Depending on their chemical structure, initiators can decompose thermally, photo chemically, or electrochemically to

produce active radical species. Although used in relatively small amounts typically around 1 wt. % or 1 mol.% relative to the total moles of polymerizable double bonds they have a significant influence on the polymerization kinetics and the final properties of the polymer network [41]. One of the most commonly employed thermal and photochemical initiators is azobisisobutyronitrile (AIBN). Upon exposure to UV light or heat, AIBN decomposes to yield nitrogen gas and two stable carbon-centered radicals. These radicals are sufficiently reactive to initiate the polymerization of various vinyl monomers, including methacrylates and acrylates, which are frequently used in MIP fabrication [42]. The selection of an appropriate initiator must consider several factors, including the desired polymerization method (thermal vs. photochemical), reaction temperature, and compatibility with other components in the pre-polymerization mixture. For instance, photoinitiators such as benzoin ethyl ether are often used in UV-initiated systems, offering better spatial and temporal control, especially in surface imprinting or micro fabrication applications [43]. Azo-initiators such as azobisisobutyronitrile (AIBN) are widely used in the polymerization of vinyl monomers due to their ability to generate free radicals upon thermal decomposition. AIBN is particularly effective for initiating the polymerization of methyl methacrylate (MMA), resulting in the formation of poly (methyl methacrylate) (PMMA) under both thermal and photochemical conditions [44]. However, the presence of oxygen significantly hinders the efficiency of free radical polymerization by scavenging active radicals and delaying polymer chain propagation. To achieve consistent polymerization and maximize monomer conversion, it is crucial to eliminate dissolved oxygen from the reaction medium prior to initiation. Common deoxygenation techniques include purging the monomer solution with inert gases such as N₂ or Ar, or applying ultra-sonication to displace dissolved oxygen [45, 46]. These steps ensure a stable radical environment and enhance the reproducibility and control of the polymerization process, which is especially important in batch reactions involving sensitive

monomer-template complexes. Figure [1.8] illustrates the molecular structures of commonly employed initiators used in non-covalent molecular imprinting processes.

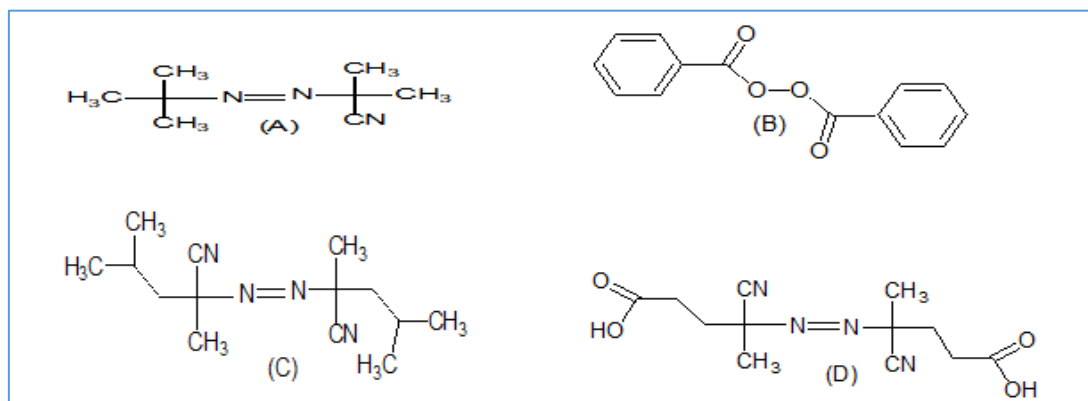


Figure [1.8] Chemical structure of widespread initiators applied in non-covalent molecular imprinting Chemical structures of selected chemical initiators: (a) 2,2'-azobis- isobutyronitrile; (AIBN) (b) benzoyl peroxide (BPO), (c) azo-bis-dimethylvaleronitrile; (ABDV) and (d) 4,4'-azo(4- cyanovaleric acid)[46]

1.4. Polymerization reactions

1.4.1. Free Radical Polymerization (FRP)

Polymerization refers to a chemical transformation in which individual monomer units or mixtures thereof are converted into a macromolecular polymer structure. The introduction of cross-linking agents enables the formation of three-dimensional polymeric networks. Among the various polymerization mechanisms, free radical polymerization (FRP) remains the most extensively utilized approach, owing to its high tolerance toward diverse functional groups, system impurities, and compatibility with mild reaction conditions. These advantages have made FRP a preferred method in the synthesis of molecularly imprinted polymers (MIPs). The FRP mechanism typically proceeds through three fundamental steps: initiation, propagation, and termination [47].

1.4.1.1. Initiation reaction

The initiation stage of free radical polymerization begins with the generation of reactive radical species, which can occur through various mechanisms such as thermal decomposition, photolytic cleavage of covalent bonds, or redox reactions. Among the wide range of initiators available, azobisisobutyronitrile (AIBN) is frequently employed due to its dual activation capability either thermally or via ultraviolet (UV) irradiation. The rate of radical formation and the concentration of generated radicals over time are strongly influenced by temperature. For instance, AIBN exhibits a temperature-dependent half-life: approximately 74 hours at 50 °C, 4.8 hours at 70 °C, and just 7.2 minutes at 100 °C. When UV light is used to initiate cleavage, factors such as light intensity, distance from the UV source, and penetration depth into the reaction medium significantly affect the efficiency and kinetics of radical formation. The initiation process not only involves the generation of the initial radical, but also encompasses its subsequent interaction with the first monomer molecule. During this step, the radical reacts with the monomer's π -bond, incorporating itself into the growing polymer chain and forming a new radical species at one of the chain termini. This newly formed reactive center serves as the starting point for the propagation phase [48, 49]

1.4.1.2. Propagation reaction

In the propagation step, the active radical center generated during initiation reacts sequentially with multiple monomer units, leading to the stepwise growth of the polymer chain. Each addition of a monomer results in the formation of a new radical site at the chain terminus, which maintains the chain's reactivity and allows further propagation. This repetitive chain-growth process continues efficiently as long as reactive monomers are available, and the resulting intermediate radicals maintain sufficient stability to sustain the polymerization reaction [50, 51] The propagation phase advances rapidly, with the polymer chain

elongating through successive monomer additions, and it persists until two radical species encounter each other and combine to form a stable, non-reactive covalent bond.

1.4.1.3. Termination reaction

The termination phase in free radical polymerization occurs when two radical species interact, leading to the cessation of chain growth. This interaction can involve either two growing polymer chain ends or a growing chain and a radical derived from the initiator. Termination may proceed via combination (coupling), where the two radicals form a stable covalent bond, or through disproportionation, a process in which a hydrogen atom is abstracted from one radical to another, resulting in two non-radical products. The dominant termination pathway depends on several factors, including the rate constants of each mechanism, temperature, and steric hindrance within the system. However, coupling is generally considered the more frequent route [53, 54]. Despite its simplicity and versatility, free radical polymerization (FRP) offers limited control over polymer architecture and molecular weight distribution. This limitation arises from the stochastic nature of the initiation, propagation, and termination steps, which occur simultaneously and compete with each other throughout the process. Consequently, terminated polymers often exhibit broad molecular weight distributions and variable chain lengths. To address these challenges and enhance control over polymer growth, controlled radical polymerization (CRP) techniques have been developed, enabling more uniform polymer structures with predictable molecular weights [55].

1.4.2. Controlled radical polymerization

Controlled radical polymerization (CRP) offers a powerful route to synthesize polymers with defined molecular weights, narrow dispersity, and tailored architectures. Unlike conventional free radical polymerization, CRP significantly minimizes termination and chain transfer events. As a result, the polymer chains retain their active chain ends, enabling further extension upon the addition of more monomer, a property that underlies the concept of "living" polymerization [56]. In recent years, CRP strategies have gained substantial attention in the design and synthesis of molecularly imprinted polymers (MIPs). The use of CRP allows for improved control over the structural uniformity and size distribution of the imprinted polymer particles two key factors that influence the specificity and binding efficiency of the resulting materials. Moreover, CRP facilitates post-synthesis modifications by allowing controlled grafting of functional monomers onto the MIP surface, thereby enhancing water compatibility and broadening application potential in aqueous environments [57]. Despite these advantages, CRP techniques demand precise control over reaction conditions. The presence of oxygen and moisture must be completely avoided, and the polymerization often needs to be conducted at relatively low temperatures to prevent undesirable side reactions. Furthermore, the selection of monomers is somewhat restricted, as certain functional groups may interfere with the controlled polymerization mechanism [58]. Iniferter polymerization is a technique that utilizes a multifunctional compound known as an iniferter that simultaneously acts as an initiator, chain transfer agent, and terminator during the polymerization process. Typically, dithiocarbamate-based iniferters are employed. Upon exposure to thermal or UV stimuli, these compounds undergo homolytic cleavage, generating a reactive alkyl radical capable of initiating polymerization, along with a stable dithiocarbamate radical that does not initiate new chains. Once the external energy source is removed, the two radicals

recombine, effectively halting the reaction. However, the polymerization can be reactivated by supplying fresh monomer into the system [59, 60]. On the other hand, Nitroxide-Mediated Polymerization (NMP) relies on nitroxide radicals to regulate the growth of polymer chains. In this approach, an alkoxyamine compound decomposes via homolytic cleavage of its carbon–oxygen bond, yielding an initiating carbon-centered radical and a nitroxide radical. The carbon radical reacts with a monomer to start chain propagation, while the nitroxide reversibly binds to the growing chain ends. This reversible binding significantly reduces the risk of irreversible termination reactions, allowing better control over molecular weight and polymer architecture. The polymerization continues as long as monomers remain in the reaction medium and terminates upon their depletion [61].

1.5. Strategies for Synthesizing (MIPs)

A range of techniques has been developed for the synthesis of molecularly imprinted polymer particles, driven by the growing need for MIPs tailored to specific applications and performance requirements. Each synthetic route offers distinct advantages and influences the final polymer characteristics differently, due to variations in reaction conditions, monomer-template interactions, and formulation parameters employed during the process (e.g. polymerization method, solvent system, and cross-linker type) .

1.5.1. Bulk Polymerization

Bulk polymerization is widely utilized for the synthesis of molecularly imprinted polymers (MIPs), owing to its straightforward procedure and broad adaptability. In this approach, the functional monomer, cross-linking agent, template molecule, and initiator are mixed together, often with little to no porogenic solvent, facilitating a simple yet effective polymerization process. The polymerization yields a rigid monolithic polymer block, which is subsequently

subjected to mechanical grinding and sieving processes to produce particles typically ranging in size from 20 to 50 μm . Despite its widespread use, bulk polymerization presents several limitations. These include labor-intensive post-polymerization steps such as grinding and sieving, low material yield (often only 30–40% of the total polymer is usable), and the production of particles with heterogeneous morphology and irregular shapes. Additionally, the resulting polymer matrix may exhibit non-uniform distribution of binding sites, which can compromise the recognition performance of the MIP [62].

1.5.2. Suspension polymerization

During suspension polymerization, the polymerizable organic phase is finely dispersed within a continuous immiscible medium commonly water or perfluorinated solvents through mechanical agitation such as stirring. To maintain droplet stability and prevent coalescence during polymer growth, stabilizers or surfactants are typically incorporated into the system. Each droplet serves as an individual microreactor where polymerization proceeds, ultimately forming uniform spherical beads, generally ranging in size from 5 to 50 μm . Following polymerization, the microspheres are isolated through successive washing and drying steps [63]. This method offers several advantages, including a relatively short reaction time often completed within 3 hours and reproducible control over particle size, which can be modulated by adjusting the stirring rate and the concentration of the stabilizing agent. Compared to bulk polymerization, suspension polymerization tends to yield particles with enhanced morphology and superior chromatographic performance, which is particularly beneficial for molecularly imprinted polymers (MIPs). Nevertheless, this approach is not as widely adopted as bulk or precipitation polymerization. This limited application is primarily due to the challenges associated with selecting an appropriate dispersion medium: aqueous systems are often unsuitable for non-covalent

imprinting due to their polarity, while fluorinated solvents, although effective, are costly [64].

1.5.3. Precipitation Polymerization

Precipitation polymerization is a widely used technique for the synthesis of (MIPs), particularly when aiming to obtain uniform particles in the submicron range. In this method, all the polymerization components including monomers, crosslinkers, template molecules, and initiators are dispersed within a large volume of porogenic solvent to form a homogeneous solution. As the polymer chains grow during the reaction, they eventually lose solubility in the continuous organic phase and precipitate out of the solution as solid particles. Once polymerization is complete, the resulting MIP particles are recovered by filtration, followed by thorough washing and drying. A notable advantage of this method is that it eliminates the need for a stabilizer. The presence of a high degree of cross-linking prevents particle coalescence during polymer growth. This approach typically yields high amounts of polymer (often exceeding 85%) and produces MIPs with narrow particle size distributions, enhanced binding affinities, and increased template-loading capacities compared to bulk polymerization. Nevertheless, the particles obtained tend to exhibit slightly irregular morphologies, which can be attributed to The impact of the template molecule on the polymerization process, sometimes hindering the formation of spherical shapes [65]. However, precipitation polymerization does have limitations. The use of a large volume of porogen results in lower template concentrations, which can negatively impact the mass transfer efficiency and may require a higher template quantity to maintain effective imprinting despite this, the method remains advantageous for preparing uniformly sized MIP particles with desirable recognition properties, especially when particle uniformity is a critical factor [66].

1.5.4. Seed polymerization: An advanced approach employed to achieve precise control over both the particle size distribution and morphology of molecularly imprinted polymers (MIPs) is the multi-step swelling polymerization technique. Initially, uniform polystyrene seed particles typically around 1 μm in diameter are synthesized in an aqueous continuous phase containing a stabilizing agent. These seeds act as templates for subsequent polymer growth stages. The process begins with an activation and swelling phase, where the seeds are exposed to a water-immiscible solvent such as dibutyl phthalate or chlorodecane, in addition to a free-radical initiator. These components are absorbed into the seed particles, facilitating their expansion. Subsequently, a polymerization mixture comprising the template molecule, a functional monomer, and a cross-linking agent is introduced. Under constant agitation, the monomers and template are adsorbed onto the swollen particles, initiating a controlled polymerization process that typically proceeds for approximately 24 hours. The resultant MIP microspheres are monodisperse, with diameters generally ranging from 2 to 50 μm . These particles are then isolated through sequential washing steps using organic solvents to remove unreacted species and template residues. This method has demonstrated reproducibility and scalability, making it suitable for applications requiring uniform MIP morphology, such as sensor development and chromatographic separations [67]. One of the main advantages of this method lies in its ability to precisely control the final particle size and yield by adjusting the concentration of the initiating solvent and the volumetric ratio of the dispersed phases. Additionally, the technique offers high reaction efficiency, often exceeding 88%, with minimal loss of material due to the formation of fine particles. This approach is time-consuming, complex, and does not appear to diminish the variety of the binding sites [68].

1.5.5. Core–Shell Emulsion Polymerization: Core–shell emulsion polymerization represents an advanced form of seed polymerization, specifically

designed to produce monodisperse colloidal particles with diameters typically ranging from 0.05 to 2 μm . These particles feature a well-defined architecture, consisting of an inner core encapsulated by an outer polymeric shell, enabling precise control over their structural and functional properties. The entire process occurs in an aqueous medium, similar to conventional seed polymerization [69]. Initially, the core particles are synthesized through a batch emulsion polymerization method. Subsequently, the shell is formed by introducing additional monomer components and template molecules into the aqueous phase containing the pre-formed cores. This step leads to the formation of a shell layer that encapsulates the core, enabling molecular imprinting localized to the particle surface or outer matrix. The final particles are typically recovered using ultrafiltration or centrifugation techniques [70]. One of the major advantages of this method is the ability to incorporate functional properties such as fluorescence, magnetism, or catalytic activity into the core without interfering with the binding characteristics of the outer shell. This makes core shell MIPs particularly attractive for applications in sensing, drug delivery, and selective separation. Furthermore, despite the complexity and time-intensive nature of this process, it does not appear to significantly affect the heterogeneity or accessibility of the imprinting sites [71].

1.6. Applications of Molecularly imprinted polymers

Molecularly imprinted polymers (MIPs) exhibit a wide spectrum of potential applications across various disciplines. They are commonly employed as stationary phases in chromatographic separation techniques, as selective sorbents in solid-phase extraction (SPE), in binding assays, and as functional films within membranes and sensor devices. In the biomedical and pharmaceutical sectors, MIPs have garnered attention for their utility in targeted drug delivery systems and their capacity to function as catalytic agents that enhance specific chemical reactions.

1.6.1. Chromatographic Separations Using Molecularly Imprinted Polymers (MIPs)

Due to their remarkable selectivity and strong affinity toward specific analytes, molecularly imprinted polymers (MIPs) are extensively utilized as stationary phases in liquid chromatography (LC). Traditionally, MIPs are synthesized through bulk polymerization, followed by mechanical grinding and sieving processes to obtain particles with suitable size and morphology for chromatographic column packing. However, this method often results in irregular particle sizes and shapes, leading to heterogeneous binding sites and reduced reproducibility in chromatographic performance. To address these limitations, in situ polymerization techniques have been developed, allowing the formation of molecularly imprinted monoliths (MIMs) Figure [1.9] directly within chromatographic columns. This approach produces continuous, porous structures with uniformly distributed binding sites, enhancing mass transfer and providing higher column efficiency. The monolithic format also eliminates the need for post-polymerization processing, simplifying the preparation process and improving reproducibility [73]. Recent studies have demonstrated the advantages of MIMs over traditional MIP particles in chromatographic applications. For instance, the monolithic structure offers increased permeability and reduced backpressure, facilitating faster analyses without compromising selectivity. Additionally, the uniform pore structure of MIMs contributes to improved binding site accessibility, resulting in better analytical performance. Molecularly imprinted monoliths (MIMs) have been effectively employed in capillary electrochromatography (CEC), a hybrid technique that merges the stationary phase principles of liquid chromatography (LC) with electroosmotic flow-driven mobile phases from capillary electrophoresis. Despite this advancement, challenges such as peak broadening and tailing persist, often resulting from heterogeneous binding sites, slow mass transfer, and variable association–

dissociation kinetics. To mitigate these drawbacks, novel polymerization methods such as precipitation polymerization have been introduced to generate more uniform, spherical particles that offer improved homogeneity and reproducibility. Furthermore, covalent imprinting strategies have been explored to enhance structural stability; however, chromatographic performance has only partially improved [74]. CEC offers advantages including reduced solvent consumption thanks to the development of micro-columns and shorter analysis times due to the ability to apply high voltages, given the mechanical and thermal resilience of MIPs used as stationary phases. Nonetheless, CEC remains predominantly confined to academic research and has yet to gain widespread adoption in routine analytical procedures. MIPs are prominently utilized in chromatographic separations as chiral stationary phases to resolve mixtures of enantiomers or structurally similar compounds, including amino acids, peptides, nucleotide bases, pharmaceuticals, sugars, and steroids.

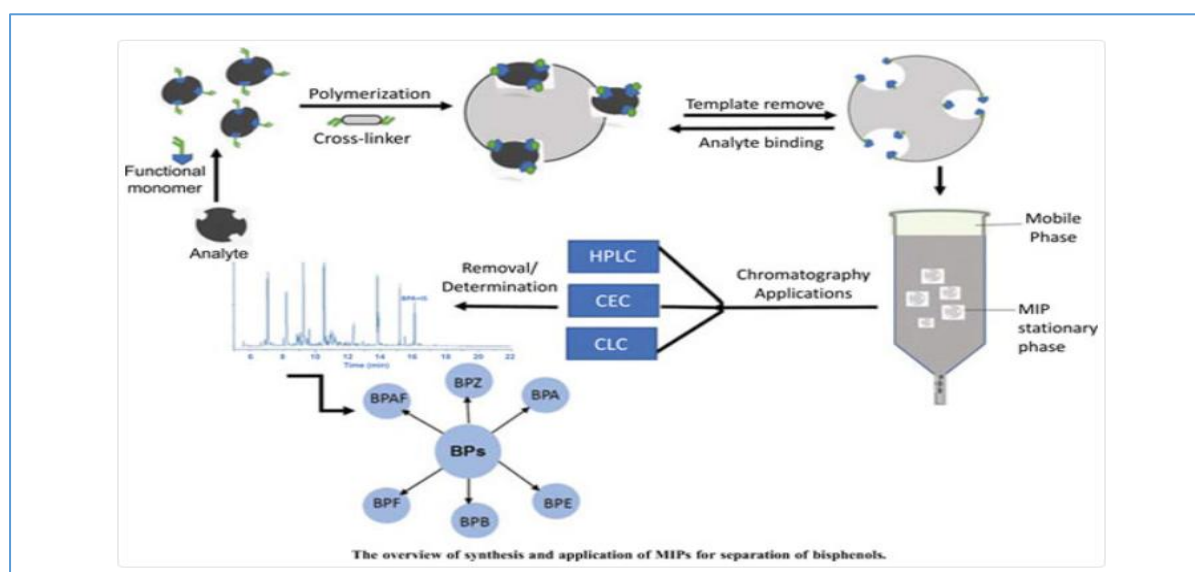


Figure [1.9] principle of MIP utilized in chromatographic separation methodologies [75, 76]

1.6.2. Binding Assays

Molecularly imprinted polymer (MIP) technology has been increasingly adopted as a synthetic alternative to antibodies in binding assays, owing to its high selectivity and sensitivity that closely emulate biological recognition systems. In addition to their biomimetic capabilities, MIPs offer distinct advantages derived from their polymeric nature, including extended shelf life, resistance to humidity, chemical stability, and improved tolerance to thermal and mechanical stress.

One of the prominent applications of MIPs in this context is the molecularly imprinted assay (MIA), particularly in the form of competitive radiolabeled tests. In such assays, the analyte of interest and a labeled analog compete for a limited number of specific binding sites on the MIP surface. The amount of bound labeled marker, which inversely correlates with the analyte concentration, is measured to produce a sigmoidal dose-response curve. This competitive binding model provides a quantitative framework for analyte detection, as illustrated in Figure [1.10] [77].

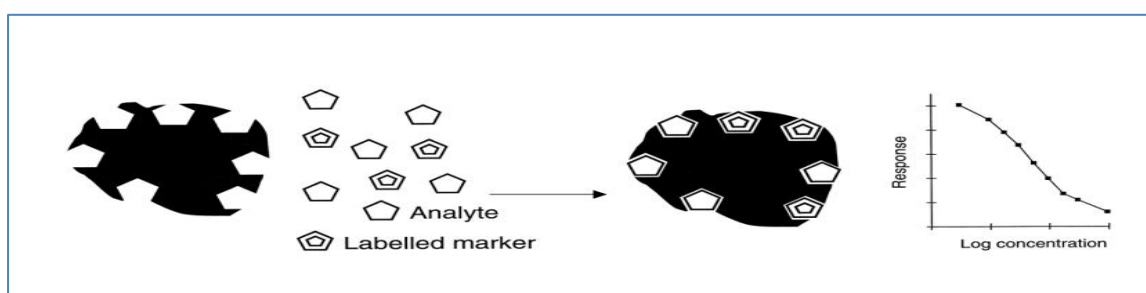


Figure [1.10] General principle of the MIA

Despite its promising potential, the practical application of molecularly imprinted assay (MIA) techniques remains constrained by concerns related to the handling and disposal of radioactive waste. To address this limitation, alternative MIA formats utilizing fluorescently labeled analogues have been proposed. However, these substitutions often result in reduced sensitivity and selectivity,

primarily due to structural disparities between the native analyte and its fluorescently tagged counterpart, including the presence of additional fluorophore groups. Furthermore, the overall sensitivity of the MIA platform still requires enhancement, and its application in complex biological matrices remains limited. Nevertheless, when applied under appropriate conditions, MIA systems continue to demonstrate notable efficacy, owing to their practical advantages and robust recognition performance in targeted analytical contexts [78].

1.6.3. Chemical Sensors

Molecularly imprinted polymers (MIPs) have been successfully integrated with transducer elements through in situ polymerization, forming a thin and selective recognition layer on the transducer surface, thereby enabling their function as chemical sensors. The role of the transducer is to detect the specific interaction between the template molecule and the imprinted binding sites, and convert this recognition event into a measurable signal—commonly using devices such as ammeters or potentiometers. The operational mechanisms of MIP-based sensors are generally categorized into three main types:

1. **Affinity Sensors:** These sensors rely on the specific binding of the target analyte to the imprinted sites, producing a detectable signal based on changes in properties such as fluorescence intensity or optical absorbance.
2. **Receptor Sensors:** In this type, the interaction with an inert or structurally passive template results in modifications to the polymer's surface characteristics—such as conformation or surface potential which are then transduced into a measurable response.
3. **Enzyme-Mimicking Sensors:** These sensors simulate enzymatic behavior by responding to environmental changes triggered by a reaction catalyzed at the MIP surface. The generated response reflects the occurrence of a specific catalytic interaction. A schematic representation of the working

principles of these three categories of MIP-based sensors is presented in Figure [1.11]

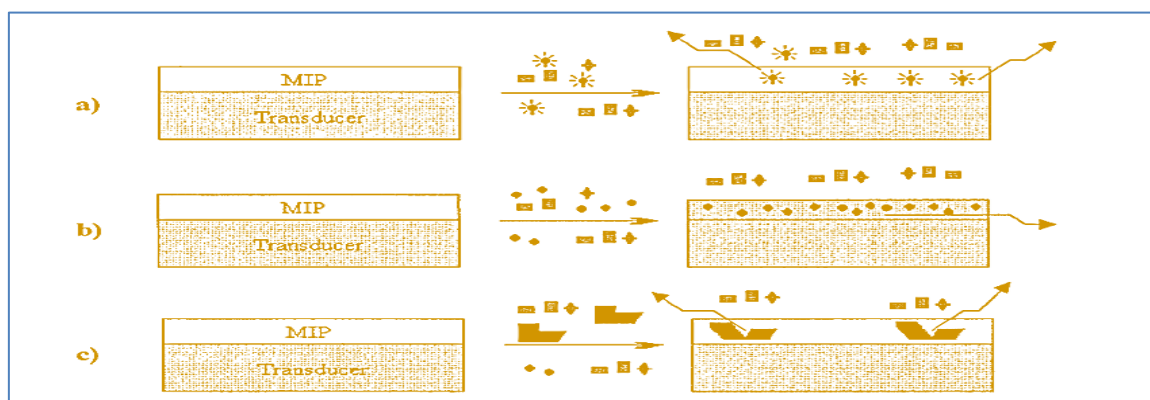


Figure [1.11] Principle of the three types of MIP based sensors: (a) affinity sensor (b) receptor sensor and (c) Catalytic sensor

1.6.4. Drug delivery

Molecularly imprinted polymers (MIPs) have shown great potential in the field of drug delivery, owing to their high selectivity, molecular memory, and efficient rebinding capabilities. These unique properties enable MIPs to serve as effective platforms for controlled and sustained drug release. For instance, theophylline-imprinted polymeric beads have been successfully utilized to achieve prolonged release profiles. Additionally, MIPs have been incorporated into soft contact lenses to facilitate localized and controlled drug administration. In another application, MIP-based tablets formulated with propranolol and cyclodextrin demonstrated selective and tunable drug release characteristics. Furthermore, composite MIP membranes have been engineered to enable the selective rebinding and delivery of compounds such as uric acid and propranolol. The integration of MIPs into targeted drug delivery and controlled release systems represents a rapidly advancing area in pharmaceutical sciences, offering significant therapeutic advantages and precision in drug administration [79].

1.6.5. Catalysis

Molecularly imprinted polymers (MIPs) have found promising applications in catalytic systems, particularly in the design and synthesis of zeolite-like structures for use in the processing and refinement of petroleum and gas, as well as in stereoselective catalysis and enzyme mimetics. By imprinting acid-base catalysts, metal complexes, or reactive intermediates, MIPs can function as synthetic analogues of natural enzymes, facilitating highly specific catalytic transformations. Ongoing research continues to explore novel MIP-based materials such as polymeric beads, monolithic structures, and ultrathin films to enhance molecular recognition and catalytic performance across diverse platforms. In addition, advanced imprinting methodologies, including monomolecular imprinting within dendritic architectures, have shown considerable promise in improving precision and reproducibility. These innovations are paving the way for the systematic and rational development of next-generation MIPs with tailored catalytic functionalities

1.6.6 Solid Phase Extraction

The use of molecularly imprinted polymers (MIPs) as selective sorbents in solid-phase extraction (SPE) has led to the development of molecularly imprinted solid-phase extraction (MIP-SPE or MISPE) techniques, which are widely employed for the isolation and enrichment of target compounds from complex matrices. Within this application domain, a distinction is made between offline and online formats. In the offline configuration, MIPs are packed into cartridges placed between two frits. After conditioning the sorbent, the sample is introduced, allowing target analytes to bind selectively to the imprinted sites. Non-specifically retained interferents are removed during the washing step, followed by elution of the bound target molecules for subsequent analysis. The eluate can then be subjected to analytical techniques such as LC-UV, fluorescence detection,

or LC-MS/MS. A simplified representation of this procedure is shown in Figure [1.12]. Conversely, in the online configuration, MIPs are integrated directly into a pre-column connected to the chromatographic and detection system, such as HPLC-UV or LC-MS/MS. Although offline methods are often preferred due to their operational flexibility and the ability to use diverse solvents without interfering with downstream detection, online approaches offer clear advantages—including reduced sample handling, minimized analyte loss, and lower contamination risk. A notable limitation of MISPE lies in its conventional reliance on organic solvents to maintain the specificity of interactions. This poses a challenge for biological applications, where aqueous environments tend to favor nonspecific or hydrophobic interactions. However, careful optimization of solvent systems particularly during the washing steps can significantly improve the performance of MIP-SPE protocols for use in biological sample preparation [81].

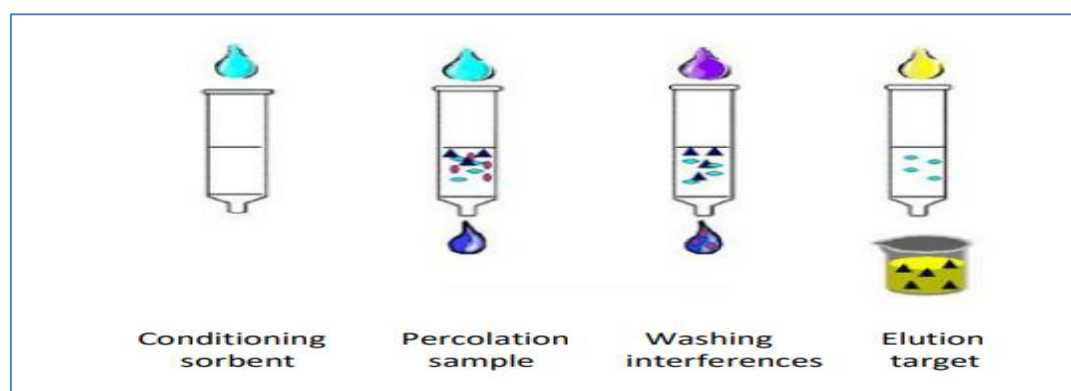


Figure [1.12] Principle of the MIP-SPE

The selection of solvents used in the molecularly imprinted solid-phase extraction (MIP-SPE) protocol is a critical factor influencing the specificity and efficiency of the extraction process. Sorbent conditioning, a preliminary step designed to remove residual analytes and activate binding sites, typically involves the sequential application of the elution solvent followed by the loading solvent. During the sample loading phase, solvents with polarity profiles comparable to

those used during polymerization, as the interactions between the target and the specific binding sites of the MIP sorbent must be tuned. In cases where electrostatic interactions such as hydrogen bonding govern the binding mechanism, non-polar solvents are preferable in the washing phase to preserve the stability of specific interactions between the target analyte and the imprinted sites. Conversely, the elution step requires solvents capable of disrupting these specific interactions, necessitating the use of more polar solvents to efficiently release the retained analyte [82]. To accurately evaluate the imprinting efficiency and specificity of the MIP, a non-imprinted polymer (NIP) is synthesized using identical reagents and polymerization conditions, but without the template molecule. This yields a chemically equivalent polymer devoid of specific recognition cavities. NIPs are routinely employed in parallel with MIPs to assess the level of selective binding achieved by the imprinted system. Currently, MISPE techniques are applied across a wide range of analytical fields, enabling the extraction of target compounds from diverse and complex sample matrices. These include biological fluids such as urine, serum, and plasma; environmental samples like groundwater, soil, and sediment; and food matrices including milk, fruits, honey, and animal tissues. Given the broad applicability of SPE techniques, the careful selection of sorbents is essential. Different sorbent materials exhibit distinct chemical and physical characteristics, and the optimal choice depends on the specific analytical requirements such as sensitivity, selectivity, matrix complexity, and cost. A detailed comparison of various SPE sorbents and their corresponding attributes is provided in Table 1.1.

Table 1.1: Comparison of SPE Sorbents

Characteristic	Immunoaffinity Sorbents	Molecularly Imprinted Polymers (MIPs)	Conventional SPE Sorbents
Affinity	Homogeneous	Heterogeneous (high- and low-affinity binding sites)	Homogeneous
Selectivity	Excellent	High	Low
Stability and Robustness	Limited (extreme pH and temperature)	Medium to high, dependent on the chemistry of the polymer	Medium to high (modified silicas not resistant to extreme pH)
Production	Laborious, time-consuming, small scale	Easy, short processing time, scalable	Easy, short processing time, scalable
Cost	Expensive	Inexpensive	Low cost
Applicability	Functions well in aqueous media; established for complex matrices; mostly single-use	Optimal in organic solvents; suitable for small compounds; fast method development; issues in template removal and reusability	Broad range of sorbent types; very easy to use; single-use
Availability	Must be developed for each analyte	Must be developed for each new class of analytes	Available commercially off-the-shelf

1.7. Extraction of Drugs from Human Urine and Blood Using Molecularly Imprinted Polymers (MIPs)

Molecularly imprinted polymers (MIPs) have emerged as powerful materials in analytical chemistry due to their exceptional selectivity, chemical stability, and ability to identify target molecules within complex biological matrices. Urine and human blood are common biological samples used in clinical diagnostics and drug monitoring; however, their complex composition poses challenges in drug extraction and analysis. MIPs provide a targeted and efficient method for extracting and concentrating drugs before automated analysis.

1.7.1. Principle of MIP-Based Extraction

Molecularly imprinted polymers (MIPs) are produced through the polymerization of functional monomers and cross linkers in the presence of a target molecule, known as the template. Following polymerization, the template is eliminated, resulting in distinct holes that are comparable in form, dimensions, and functional groups to the target analyte Figure [1.13]. These recognition sites facilitate the selective re-binding of the target molecule from complicated mixes, like urine or blood [83].

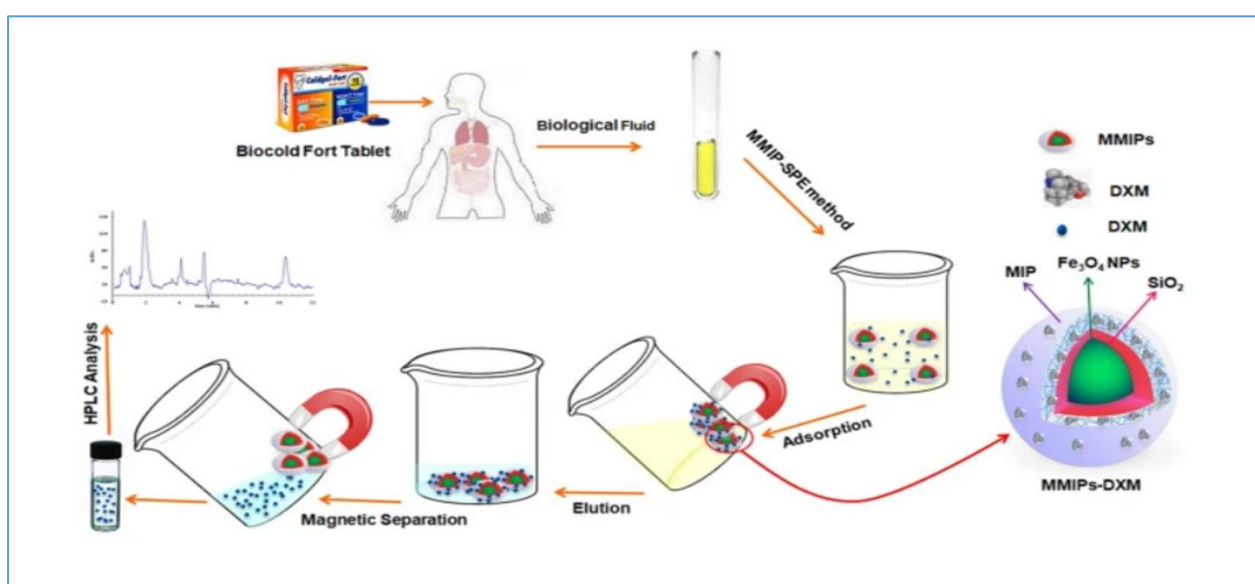


Figure [1.13] drug extraction by MMIP

1.7.2. Drug Extraction from Human Urine

Urine is a widely used diagnostic fluid due to its non-invasive collection and the presence of drug metabolites. MIPs are particularly advantageous in urine analysis because they reduce interference from matrix components and offer high recovery rates. The general steps for drug extraction from urine using MIPs include:

1. Sample collection and pre-treatment (e.g. filtration or dilution).
2. Addition of the MIP sorbent.

3. Incubation or shaking to facilitate interaction between the target drug and MIP binding sites.
4. Separation of the MIP (e.g., by centrifugation or magnetic separation).
5. Washing to remove non-specifically bound substances.
6. Elution of the drug for subsequent analysis

Recent studies have demonstrated the successful application of MIPs for the selective extraction of opioids such as morphine, codeine, and tramadol from urine, with recovery rates often exceeding 90% [84].

1.7.3. Drug Extraction from Human Blood

Blood and plasma samples are more complex than urine, as they contain proteins, lipids, and other interfering substances. Therefore, sample pre-treatment (e.g. protein precipitation or filtration) is often necessary before applying MIP extraction. MIPs have been employed for the extraction of several drugs from plasma, including:

- Methotrexate, using magnetic MIPs with HPLC-UV detection, achieving over 95% recovery [85].
- Carbamazepine and lamotrigine, using dual-template MIPs for selective enrichment and subsequent quantification via HPLC .

1.7.4. Factors Affecting Extraction Efficiency

Several parameters significantly influence the efficiency of MIP-based extraction from biological matrices:

- 1- MIP mass: Increasing the amount of MIP sorbent enhances the number of available binding sites, improving the extraction capacity. However, excessive polymer can cause aggregation and reduce extraction efficiency.
- 2- pH of the medium: The pH affects the ionization state of both the drug and the functional groups in the MIP. Optimal pH ensures stronger interactions

such as hydrogen bonding or electrostatic attraction. Each drug–MIP system has a specific optimal pH, often ranging between 5.0 and 7.5.

- 3- Temperature: Moderate increases in temperature can enhance diffusion and facilitate binding. However, very high temperatures may disrupt non-covalent interactions, reducing selectivity.
- 4- Equilibrium time: Sufficient incubation time allows the analyte to fully interact with the recognition sites. Most MIPs reach binding equilibrium within 15–60 minutes, depending on particle size and stirring conditions.

Optimization of these factors is essential to achieve high recovery rates, low detection limits, and reproducible results [86].

1.7.5. Quantitative and Mechanistic Evaluation of Drug Binding onto MIPs: Adsorption Capacity, Isotherm Models, Kinetics and thermodynamic studies

1.7.5.1. Adsorption capacity Q_e ($\text{mg}\cdot\text{g}^{-1}$) of MIPs is a critical parameter that reflects the amount of drug bound per unit mass of polymer. It is calculated using the following equation:

$$Q_e = (C_0 - C_e) \times V / W \dots\dots\dots 1.1$$

Where:

Q_e : Adsorption capacity ($\text{mg}\cdot\text{g}^{-1}$)

C_0 : Initial concentration of the drug in solution ($\text{mg}\cdot\text{L}^{-1}$)

C_e : Equilibrium concentration of the drug ($\text{mg}\cdot\text{L}^{-1}$)

V : Volume of the solution (L)

W : weight of the MIP (g)

To further understand the nature of drug binding to MIPs, isotherm and kinetic models are applied to the experimental data

1.7.5.2. Isotherm Models[87]:

1- Langmuir Isotherm: Assumes monolayer adsorption on a homogeneous

surface with finite identical sites.

Equation:

$$\frac{C_e}{Q_e} = \frac{1}{Q_m} + \frac{1}{Q_m K_L} \dots\dots\dots 1.2$$

Where:

C_e : is the equilibrium concentration of the adsorbate mg. L⁻¹

K_L : is the Langmuir constant, which is related to the adsorption capacity L.mg⁻¹ and can be related to the differences in the suitable surface area and porosity of the adsorbent, meaning that adsorbents with large surface area have high adsorption capacity.

Q_e : (mg. g⁻¹) refers to the equilibrium adsorption capacity

Q_m : (mg. g⁻¹) refers to the maximum adsorption capacity

2- Freundlich Isotherm: Assumes heterogeneous adsorption surfaces with sites of varied affinities. The linear form of the Freundlich equation is:

$$Q_e = K_f + C_e^{\frac{1}{n}} \dots\dots\dots 1.3$$

Where:

Q_e : The amount of drug at equilibrium in mg. g⁻¹.

C_e : The concentration of drug at equilibrium in mg. L⁻¹.

K_f, n : Are Freundlich constants

3. Timken Isotherm:

The Timken isotherm model assumes that the heat of adsorption of molecules decreases linearly with increasing surface coverage due to adsorbent–adsorbate interactions. It is particularly useful when the adsorption process involves a

uniform distribution of binding energies up to a certain point. The linear form of the Timken equation is:

$$Q_e = \frac{RT}{b} \ln K_T + \frac{RT}{b} \ln C_e \dots\dots\dots 1.4$$

K_T : is the equilibrium temperature enabling constant $L.g^{-1}$.

R : is the universal gas constant $8.314 J. K^{-1}. mol^{-1}$.

T : is the temperature at 298 K.

b : is the constant associated with the heat of adsorption ($J.mol^{-1}$)

1.7.5.3.Kinetic Models: Adsorption kinetics refers to the transfer of molecules from a solution to an adsorbent material until equilibrium is attained within a given timeframe, which varies based on the nature of the adsorbed molecules and the adsorbent surface. The outcome is contingent upon the temperature, catalyst, active sites, and concentration of the adsorbed molecules. The adsorption kinetics can be articulated by the subsequent kinetic models [88].

1- Pseudo-first-order model:

$$\text{Equation: } \ln(Q_e - Q_t) = \ln(Q_e) - k_1 \times t \dots\dots\dots 1.5$$

2- Pseudo-second-order model:

$$\text{Equation: } t/Q_t = 1/(k_2 \times Q_e^2) + t/Q_e \dots\dots\dots 1.6$$

Where: Q_t : Adsorption capacity at time t ($mg.g^{-1}$)

Q_e : Adsorption capacity at equilibrium ($mg.g^{-1}$)

k_1, k_2 : Rate constants

t : Time (min)

1.7.5.4. Thermodynamic Studies

Thermodynamic studies provide crucial insight into the nature of the adsorption process between the target drug and the molecularly imprinted polymer (MIP).

By evaluating thermodynamic parameters such as the Gibbs free energy change (ΔG°), enthalpy change (ΔH°), and entropy change (ΔS°), one can determine whether the adsorption is spontaneous, endothermic or exothermic, and whether disorder increases at the solid–solution interface.

The parameters are typically calculated using the Van't Hoff equation [89]:

$$\ln K = -\frac{\Delta H}{RT} + \frac{\Delta S}{R} \dots\dots\dots 1.7$$

Where:

K: is the equilibrium constant,

R: is the universal gas constant (8.314 J/mol·K),

T: is the temperature in Kelvin.

ΔH : is enthalpy change

ΔS : is entropy change, the change in Gibbs free energy (ΔG°) is calculated as:

$$\Delta G^\circ = -RT \ln K \dots\dots\dots 1.8$$

1.8. Literature review

Molecularly imprinted polymers (MIPs) are highly selective industrial materials designed to mimic the binding sites of biological receptors. By forming specific cavities that complement the template molecule during the polymerization process, these polymers provide excellent selectivity towards target molecules, especially small molecules such as narcotic drugs. The incorporation of magnetic nanoparticles (such as Fe_3O_4) into these polymers has led to the development of magnetic molecularly imprinted polymers (MMIPs),

which combine superior molecular recognition capability with the ability for rapid separation using an external magnetic field. Magnetized printed polymers have shown promising effectiveness in the typical preparation of samples, especially in the extraction and concentration of drugs at low concentrations from complex biological matrices such as urine and blood. While traditional preparation techniques such as solid-phase extraction (SPE) suffer from limited selectivity and high solvent consumption, MMIPs are a more efficient and environmentally friendly alternative, characterized by their high binding capacity and reusability. Many recent studies have used printed magnetic polymers to extract specific narcotic drugs such as opioids, amphetamines, and benzodiazepines. For example: Namrata Laskar et al. studied the synthesis of magnetic molecularly imprinted polymer (MMIP) based on chitosan and Fe_3O_4 to selectively target the fungicide tricyclazole. The polymer exhibited well-defined nanostructures and high selectivity, with a maximum binding capacity of $4579.9 \mu\text{g}\cdot\text{g}^{-1}$. The results showed that the adsorption followed a pseudo-second-order model and that the process was exothermic and spontaneous, achieving recovery rates exceeding 89% from fortified rice and water samples [90]. The study conducted by Marco Mora and Daived Gonzalize et al. aimed to develop a molecularly imprinted polymer (MIP) using 4-hydroxyphenyl acetic acid as a template to extract low molecular weight phenolic compounds from human urine samples. The results showed a high ability to selectively recognize the template molecule and its analogs. The method was validated over a concentration range of 0.25–40 mg/L with precision ($R^2 > 0.995$), and the recovery rate was 94%, with $\text{LOD} = 1.22 \text{ mg}\cdot\text{L}^{-1}$ and $\text{LOQ} = 3.69 \text{ mg}\cdot\text{L}^{-1}$ [91]. Junyu Li et al. discussed the methods of manufacturing MMIPs and showcased their innovative applications in separating antibiotics from complex environmental and food samples, demonstrating their ability to improve the efficiency and speed of analysis [92]. Takeshi Kumazawa et al. They conducted a study to extract methamphetamine, amphetamine, and their derivatives from whole blood using

the solid-phase extraction technique based on molecularly imprinted polymers (MIP-SPE). The method demonstrated high efficiency in removing impurities, with a recovery rate ranging from 89.1% to 102%, and low detection limits reaching 0.25 nanograms. The results demonstrated the reliability of the method for quantitative analysis using gas chromatography coupled with mass spectrometry [93]. "Radfar R. et al. They conducted a study on the fabrication and characterization of magnetically imprinted polymers (MMIPs) with a core-shell structure and fluorescent properties, for the selective detection of interleukin-6 (IL-6), an important biomarker for many pathological conditions. These materials were developed through three stages: modification of magnetic particles, polymerization, and template removal. The physical and chemical analyses showed successful synthesis and distinctive properties, and the MMIPs-based electrochemical sensor achieved a very low detection limit of 0.38 Pico mol.L⁻¹, with high selectivity (printing factor = 4). These polymers show great potential in sensing and bioimaging applications [94]. Nur Masyithah Zamruddin et al. conducted a study aimed to develop magnetic molecularly imprinted polymers (MMIPs) for the detection of clofazimine (CLF) in human blood plasma using two surface modifiers: APTES and oleic acid (OA). The MMIP modified with APTES showed superior physical properties and high selectivity, achieving a recovery rate of 92.3% for CLF even in the presence of other TB drugs. These results suggest that APTES-modified MMIPs can be effectively used for therapeutic drug monitoring in rifampicin-resistant tuberculosis patients [95]. Yanhui Wang et al. conducted a study aimed to develop novel hydrophilic magnetic molecularly imprinted polymers (HMMIPs) using rosmarinic acid (RA) as the template. The synthesized HMMIPs exhibited high selectivity (imprinting factor = 3.64), good adsorption capacity (8.012 mg/g), and efficient magnetic separation. When applied to plant extracts of *Perilla frutescens* and *Rosmarinus officinalis*, the polymers achieved high recovery rates (88.2–107.3%), confirming their suitability for rapid and selective RA extraction from complex samples [96].

1.9. Aims of the Study

The primary objective of this study is to:

- Synthesize novel magnetic molecularly imprinted polymers (MMIPs) designed for the selective recognition and binding of specific drugs compounds.
- These polymers were selected due to their distinct advantages, including high selectivity, chemical stability, and the ability to be rapidly and efficiently separated using an external magnetic field.
- Following synthesis, the study focuses on the comprehensive characterization of the synthesized polymers. This includes the use of various analytical techniques to evaluate their structural, physical, and chemical properties, as well as to confirm their suitability for the intended applications.
- Furthermore, the study aims to apply the synthesized MMIPs in the extraction and quantitative determination of selected pharmaceutical drugs from biological matrices, specifically human urine and blood.
- To optimize the extraction efficiency, the influence of key operational parameters such as pH, temperature, the amount of MMIP, and contact time will be systematically investigated to establish the most favorable conditions for accurate and efficient drug recovery.
- Evaluation of the extraction efficiency of magnetic molecularly imprinted polymers through the investigation of influencing factors.

Chapter Two
Experimental Part

2. Experimental Part

2.1. Chemicals Materials

Chemicals with a high degree of purity and from different companies were used as shown in the table [2-1].

Table [2-1] Chemicals used manufacturers, chemical composition and purity.

NO	Substance	Structure Formula	Company	M.wt	Purity
1	2-Acetamido acrylic acid	$C_5H_7NO_3$	Thermo Fisher Scientific (India)	129.11	97%
2	Benzoyl Peroxide	$(C_6H_5.CO)_2O_2$	General Drug House, Daryaganj New Delhi(India)	242.23	98%
3	Tetraethyl orthosilicate	$Si(OC_2H_5)_4$	Sigma-Aldrich	208.33	99%
4	3,4 Dihydroxy-1-butene	$CH_2=CHCH(OH)CH_2OH$	Sigma-Aldrich	88.11	99%
5	Methanol	CH_3OH	Sigma-Aldrich	32.04	99.9%
6	Hydrochloric acid	HCl	India	36.5	99%
7	Glacial acetic acid	CH_3CO_2H	Sigma-Aldrich	60.05	99%
8	Sodium Hydroxide	NaOH	Pancreac Spain	40	99.9
9	Diacetylmorphine (Heroin)	$C_{21}H_{23}NO_5$	/	369.41	/
10	(α -methylphenethylamine Amphetamine	$C_9H_{13}N$	/	135.21	/
11	Trihexyphenidyl (Artane)	$C_{20}H_{31}NO$	State Company for Drugs and Medical	301.47	/

			Appliances Industry / Samarra (SDI)		
12	Pregabalin (Lyrica)	C ₈ H ₁₇ NO ₂	Torrent Pharmaceuticals (India)	159.23	98%
13	Chlorophorm	CHCl ₃	Sigma-Aldrich	120.38	99.8%
14	Ammonium hydroxide solution	NH ₄ OH	Sigma-Aldrich	35.05	28- 30%

2.2. Instruments

"Various instruments employed in this study are listed in Table [2-2]."

Table [2-2] Devices used in this study, including their manufacturers, construction, model and worksite.

NO	Instrument	Model	Source & Company	Workplace
1	Fourier Transform Infrared (FTIR) Spectrophotometer	TENSOR27, Thermo- Nicolet avatar	BRUKER, USA	College of Science/ University of Al-Qadisiyah,
2	X-ray diffraction (XRD)	X'PertPro	Holland	University of Kashan/ Iran
3	Vibrating sample magnetometer(VSM)	LDJ9600-1	USA	University of Kashan/ Iran
4	Field emission Scanning Electron Microscope (FESEM)	JSM- 6700F, TESC AN CO. Ltd, Czech	Korea	University of Kashan/ Iran
5	UV-Visible Spectrophotometer Double Beam	UV-1900i	SHIMADZ U, Japan	College of Science/ University of Al-Qadisiyah,

6	Thermo gravimetric Analysis(TGA)	TGA-4000	Perkin Elmer,USA	University of Kashan/ Iran
7	BET Surface Area Analysis	NOVA 2200e	Qunta chrome,USA	University of Kashan/ Iran
8	Microwave	LG MH8265DIS	Korea	College of Science/ University of Al-Qadisiyah
9	Ultrasound device	405 power	Korea	College of Science/ University of Al-Qadisiyah
10	Oven	DO-81	Korea	College of Science/ University of Al-Qadisiyah
11	Shaker	LSI-1	Korea	College of Science/ University of Al-Qadisiyah
12	Shaker Water bath	SW23	USA	College of Science/ University of Al-Qadisiyah
13	Centrifuge	EBA 20	Germany	College of Science/ University of Al-Qadisiyah
14	pH-meter	Meter 11863	China	College of Science/ University of Al-Qadisiyah
15	Hotplate with Stirrer	LMS-1003	Korea	College of Science/ University of Al-Qadisiyah
16	Digital Sensitive Balance	L420 B	Germany	College of Science/ University of Al-Qadisiyah

2.3. Purification of Heroin and Amphetamine.

1. **The powdered sample was dissolved** in distilled water acidified with hydrochloric acid (HCl, 2N) to form the water-soluble salt of the target compound (heroin or amphetamine).
2. **The solution was filtered** to remove insoluble impurities.
3. **The pH was adjusted** to a basic range (pH 9–10) by the dropwise addition of ammonium hydroxide (NH₄OH) or sodium hydroxide (NaOH), converting the compound to its free base form.
4. **The basic solution was transferred** to a separatory funnel and **extracted** with an organic solvent such as chloroform.
5. **The organic layer was separated**, and the extraction was **repeated** 2–3 times to ensure complete recovery.
6. **The organic layers were combined**, and the solvent was **evaporated** under reduced pressure or mild heating to obtain the purified compound.
7. **The isolated substance was characterized** using spectroscopic techniques to confirm its identity [97].

2.4. Synthesis of MMIP and MNIP

A total of 2.16 mmol of Fe₃O₄ nanoparticles was dispersed in 80 mL of a methanol–water mixture. Subsequently, 20 mL of distilled water and 4 mL of tetraethyl orthosilicate (TEOS) were added to the suspension, which was stirred continuously for 8 hours at ambient temperature. The resulting product was isolated, washed several times with distilled water to remove any unreacted residues, and then dried under vacuum at 45 °C to yield Fe₃O₄@SiO₂ nanoparticles [98].

2.4.1. Synthesis of Non-Imprinted Magnetic Polymer (MNIP₁) Using 2-Acetamidoacrylic Acid

A quantity of 0.8 g of Fe₃O₄@SiO₂ was dispersed in 100 mL of methanol, followed by the sequential addition of 16 mmol of 2-acetamidoacrylic acid (functional monomer), 8 mL of TEOS (cross-linker), and 0.7 mmol of benzoyl peroxide (BPO) as the initiator. The resulting mixture was stirred for 1 hour at room temperature, then transferred into a 150 mL round-bottom flask and placed inside a microwave reactor equipped with a rotor. Microwave-assisted polymerization was carried out at a power of 80 W and a stirring speed of 120 rpm for 30 minutes. Upon completion, the synthesized product was repeatedly washed with a 5:1 (v/v)(100/20) mL mixture of methanol and glacial acetic acid to remove unreacted species, and subsequently dried to yield the magnetic molecularly non-imprinted polymer (MNIP) [99].

2.4.2. Synthesis of Magnetic Molecularly Imprinted Polymers (MMIPs) for Heroin and Amphetamine Using 2-Acetamidoacrylic Acid

2.4.2.1. Synthesis of Fe₃O₄@SiO₂@ Her-MMIP

An amount of 0.8 g of Fe₃O₄@SiO₂ was dispersed in 100 mL of methanol, followed by the sequential addition of 4 mmol of heroin (template molecule), 16 mmol of 2-acetamidoacrylic acid (functional monomer), 8 mL of tetraethyl orthosilicate (TEOS) as the cross-linker, and 0.7 mmol of benzoyl peroxide (BPO) as the initiator. The resulting mixture was stirred for 1 hour at room temperature, then transferred into a 150 mL round-bottom flask and placed into a microwave reactor equipped with a rotor. Microwave-assisted polymerization was conducted at a power of 80 W and a stirring speed of 120 rpm for 30 minutes. To remove the template molecule, the resulting polymer was repeatedly washed with a 5:1 (v/v) (100/20 ml)mixture of methanol and glacial acetic acid, and

subsequently dried to obtain the magnetic molecularly imprinted polymer (MMIP) [99]. Figure [2.1] illustrates the synthesis process of Her-MMIP,

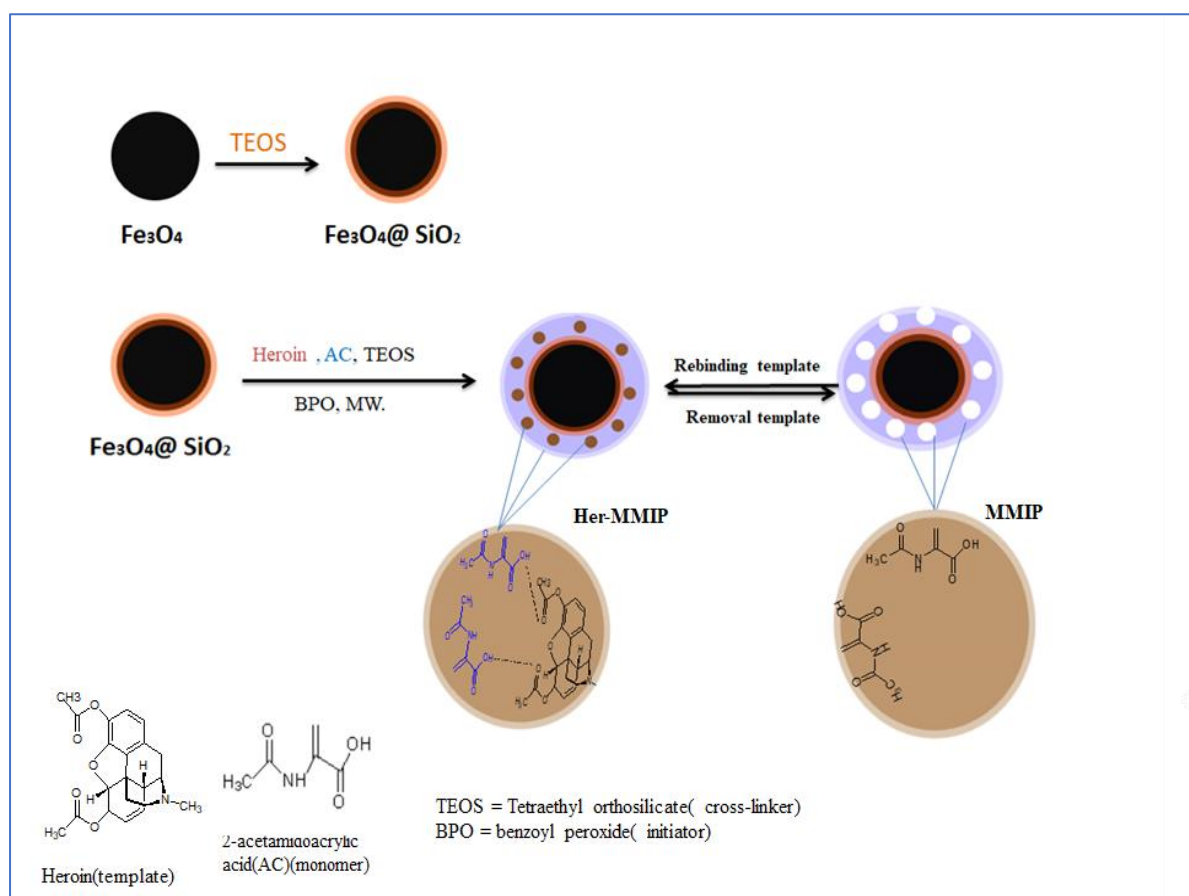


Figure [2.1] synthesis process of Her-MMIP

2.4.2.2. Synthesis of Fe₃O₄@SiO₂@ AMP-MMIP

A quantity of 0.8 g of Fe₃O₄@SiO₂ was dispersed in 100 mL of methanol, followed by the sequential addition of 4 mmol of amphetamine (template molecule), 16 mmol of 2-acetamidoacrylic acid (functional monomer), 8 mL of tetraethyl orthosilicate (TEOS) as the cross-linker, and 0.7 mmol of benzoyl peroxide (BPO) as the initiator. The resulting suspension was stirred for 1 hour at room temperature and then transferred to a 150 mL round-bottom flask, which was placed into a microwave reactor equipped with a rotor. Microwave-assisted polymerization was carried out at a power of 80 W and a stirring speed of 120

rpm for 15 minutes. Upon completion, the polymer was repeatedly washed with a 5:1 (v/v) mixture of methanol and glacial acetic acid to remove the template molecule, and then dried to yield the magnetic molecularly imprinted polymer (MMIP) [99]. Figure [2.2] represents the synthesis of AMP-MMIP.

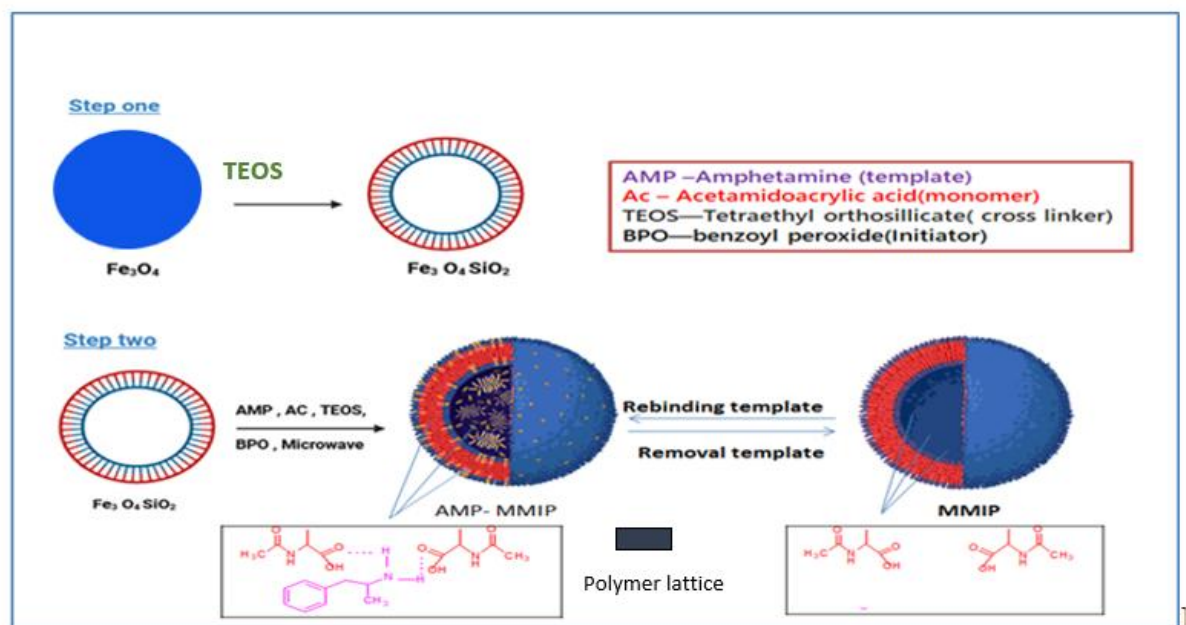


Figure [2.2] synthesis process of AMP-MMIP

2.4. 3. Synthesis of (MNIP₂) Using 3, 4-Dihydroxy-1-butene

A quantity of 0.2 g of $\text{Fe}_3\text{O}_4@\text{SiO}_2$ nanoparticles was dispersed in 25 mL of methanol under continuous stirring. Subsequently, 4 mmol of 3,4-dihydroxy-1-butene (functional monomer), 2 mmol of tetraethyl orthosilicate (TEOS) as a cross-linker, and 0.17 mmol of benzoyl peroxide (BPO) as an initiator were sequentially added. The resulting mixture was stirred for 1 hour to ensure homogeneity. The reaction mixture was then transferred to a 150 mL round-bottom flask and subjected to microwave-assisted polymerization for 30 minutes at 150 W and 120 rpm using a microwave reactor equipped with a rotor. Upon completion of the polymerization process, the product was repeatedly washed with a mixture of methanol and glacial acetic acid (5:1, v/v) to remove unreacted materials. Finally, the obtained solid was dried, resulting in the formation of the magnetic non-imprinted polymer (MNIP) [100].

2.4.4. Synthesis of Magnetic Molecularly Imprinted Polymers (MMIPs) for Artane and Pregabalin Using 3, 4-Dihydroxy-1-butene

2.4.4.1. Synthesis of Fe₃O₄@SiO₂@ ART-MMIP

A total of 0.2 g of Fe₃O₄@SiO₂ nanoparticles was dispersed in 25 mL of methanol under continuous stirring. Subsequently, 1 mmol of Artane (template molecule), 4 mmol of 3,4-dihydroxy-1-butene (functional monomer), 2 mmol of tetraethyl orthosilicate (TEOS, cross-linker), and 0.17 mmol of benzoyl peroxide (BPO, initiator) were added sequentially. The mixture was stirred for 1 hour to ensure complete homogenization. The reaction mixture was then transferred to a 150 mL round-bottom flask and subjected to microwave-assisted polymerization for 30 minutes at a power of 150 W and a stirring speed of 120 rpm using a microwave reactor equipped with a rotor. After polymerization, the resulting product was repeatedly washed with a 5:1 (v/v) mixture of methanol and glacial acetic acid to effectively remove the template molecule. The final product was dried to yield the magnetic molecularly imprinted polymer (MMIP) specific for Artane [100]. Figure [2.3] illustrates the synthesis process of ART-MMIP,

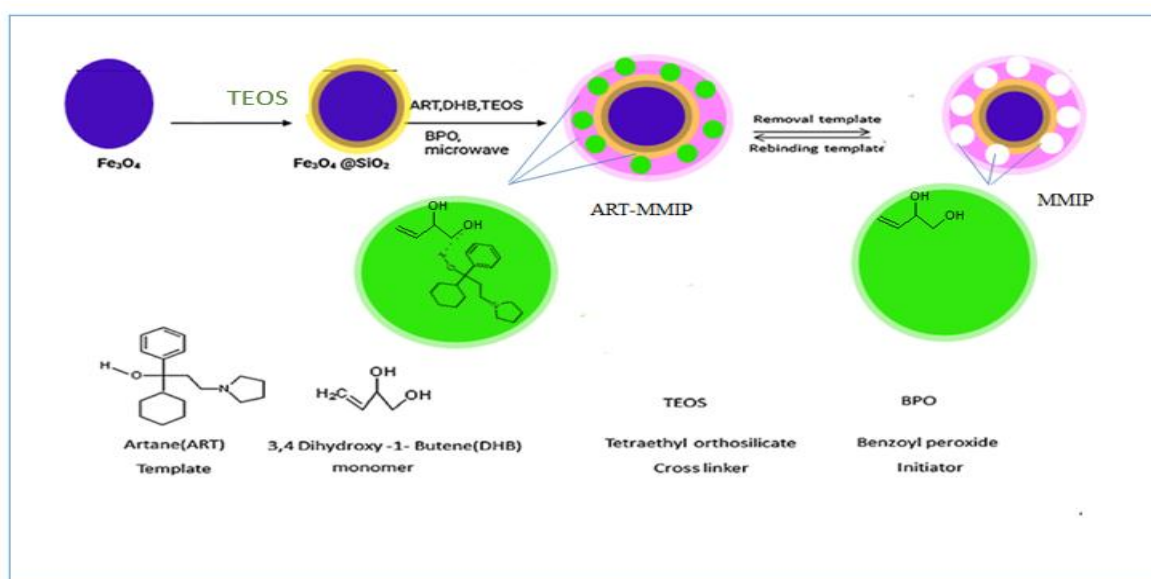


Figure [2.3] synthesis process of ART-MMIP

2.4.4.2. Synthesis of $\text{Fe}_3\text{O}_4@\text{SiO}_2@$ Pre-MMIP

A mass of 0.2 g of $\text{Fe}_3\text{O}_4@\text{SiO}_2$ nanoparticles was dispersed in 25 mL of methanol under constant magnetic stirring. Subsequently, 1 mmol of pregabalin (template molecule), 4 mmol of 3,4-dihydroxy-1-butene (functional monomer), 2 mmol of tetraethyl orthosilicate (TEOS, as cross-linker), and 0.17 mmol of benzoyl peroxide (BPO, initiator) were added sequentially. The mixture was stirred for 1 hour to ensure thorough mixing. The reaction solution was then transferred to a 150 mL round-bottom flask and subjected to microwave-assisted polymerization for 30 minutes at a power of 150 W and a stirring speed of 120 rpm using a microwave reactor with a rotor. After the polymerization process, the resulting solid was repeatedly washed with a 5:1 (v/v) methanol/glacial acetic acid solution to remove the template molecule. Finally, the material was dried to obtain the magnetic molecularly imprinted polymer (MMIP) for pregabalin [100]. Figure [2.4] represents the synthesis of Pre-MMIP.

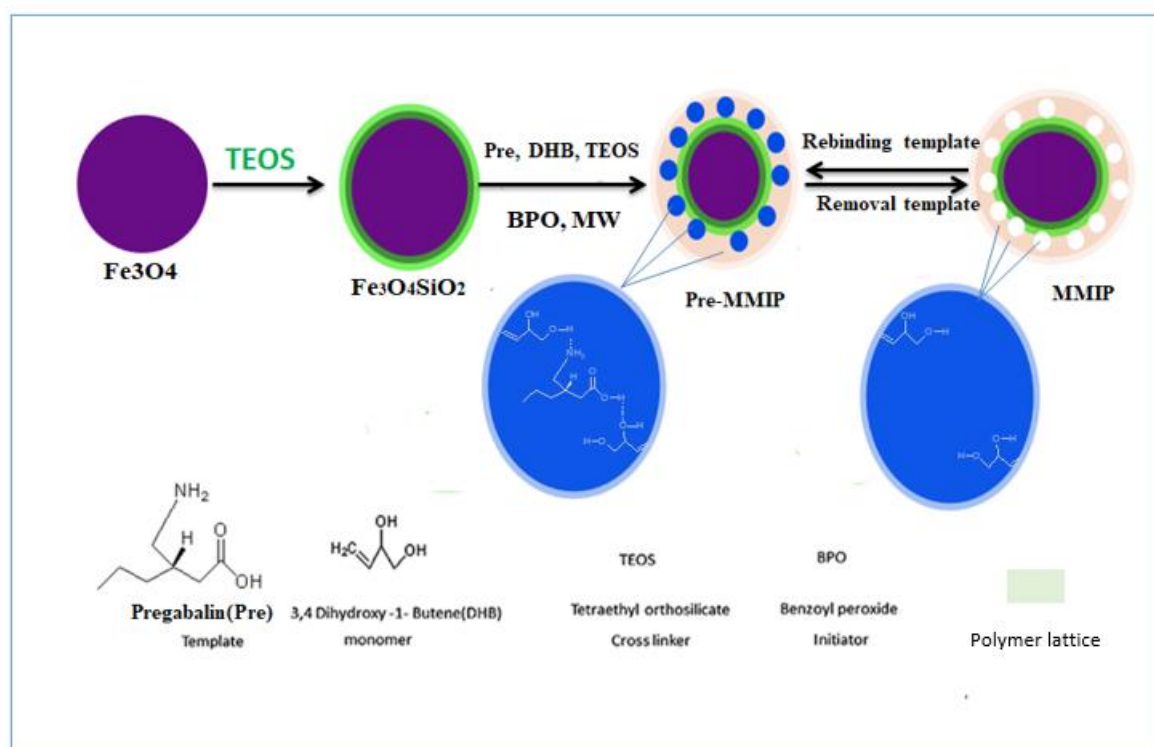


Figure [2.4] synthesis process of Pre-MMIP

2.5 Characterization of Synthesized Polymers

The synthesized polymers were characterized using the following techniques:

2.5.1. UV–Visible Spectrophotometry (UV–Vis)

The maximum absorption wavelength (λ_{max}) of each drug was determined using a UV–Vis spectrophotometer by scanning their corresponding standard solutions across the relevant spectral range. These wavelengths were then used to measure the absorbance of drug solutions after the adsorption process[101].

2.5.2. Fourier transform infrared (FT-IR) analysis

Using the potassium bromide (KBr) disk method to record the spectra of the prepared materials in their solid state within the wavenumber range (400-4000) cm^{-1} , infrared spectroscopy (FTIR) was used to characterize the active functional groups in the composition of the synthesized polymers[102].

2.5.3. Field Emission - Scanning Electron Microscopes (FE-SEM)

The FE-SEM facilitates high-resolution examination of samples using electron beam scanning in a vacuum, yielding comprehensive data on chemical composition and surface topography. Samples necessitate meticulous preparation, encompassing drying, metal layer deposition, and equipment mounting, alongside the calibration of parameters like as vacuum and accelerating voltage to provide precise and dependable photographs[103].

2.5.4. X-ray Diffraction Spectroscopy (XRD)

This non-destructive technology employs monochromatic light with a wavelength of 1.5104 Å from a copper source, utilizing nickel as a filter, to elucidate the crystal structure, chemical composition, and physical properties of materials and thin layers of crystalline substances. It can also disclose information regarding the dimensions of the crystals (in the context of

nanoparticles), the nature of the chemical bonding, and the lattice strain of the materials[104]. The range of diffraction angles (2Θ) extends from 10° to 80° .

2.5.5 . Analysis of the Surface Area and Porosity Characteristics of the Surface (BET, BJH)

In order to investigate the surface properties of the synthesized materials, including surface area, pore size distribution, and total pore volume, the BrunauerEmmett–Teller (BET) method was employed. Additionally, the Barrett–Joyner–Halenda (BJH) method was utilized to determine the pore size distribution. Nitrogen adsorption was conducted at a temperature of 77 K for a duration of approximately 2–3 hours[105].

2.5.6. Thermogravimetric Analysis (TGA)

Thermogravimetric analysis (TGA) was employed to evaluate the thermal stability of the synthesized materials, as well as to determine their decomposition behavior. This analysis was carried out by recording the change in mass as a function of temperature. The samples were subjected to thermal analysis by heating at a constant rate of $10^\circ\text{C}/\text{min}$ over a temperature range of 25 to 1000°C [106].

2.5.7. Magnetic Properties Measurement (VSM)

The magnetic characteristics of the synthesized materials were evaluated using a Vibrating Sample Magnetometer (VSM). All measurements were performed at room temperature to assess critical magnetic parameters, including saturation magnetization (M_s), coercivity (H_c), and remanent magnetization (M_r). The magnetic hysteresis loop was obtained by applying an external magnetic field ranging from $-10,000$ to $+10,000$ Oe. [107].

2.6. Preparation of a standard solutions of Heroin and Amphetamine

A standard solutions of 50 mg. L^{-1} were prepared by dissolving 0.01 g of Heroin and Amphetamine respectively in 200 mL(190mL distilled water + 10mL methanol) in a 250 mL volumetric flask.

2.7. Preparation of a standard solutions of Artane and Pregabalin

A standard solution of 50 mg. L^{-1} was prepared by dissolving 0.01 g of (Artane or Pregabalin) in 200 mL distilled water in a 250 mL volumetric flask.

2.8. Determination of the maximum wavelength of drugs (λ_{max})

A solution of defined concentration is created, and an ultraviolet/visible (U.V/Vis.) spectrometer is employed to document the adsorption spectra throughout the region of 200-1100 nm utilizing a 1.0 cm thick quartz cell. This facilitates the identification of the wavelength at which the medication exhibits maximum adsorption. The results showed distinct λ_{max} values for each drugs: heroin exhibited a maximum absorbance at 284 nm, amphetamine at 256 nm, Artane at 275 nm, and pregabalin at 207 nm. These wavelengths were subsequently used in all quantitative adsorption and extraction studies. As shown in Figures [2.5] , [2.6],[2.7] and [2.8]

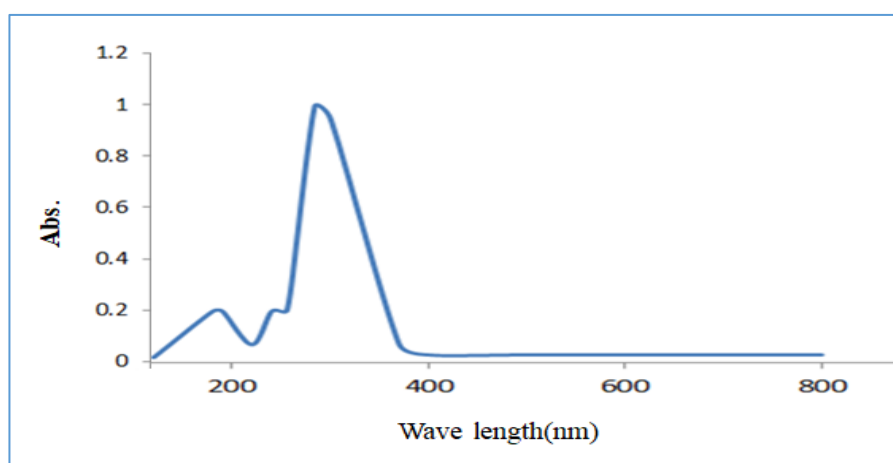


Figure [2.5] Maximum wavelength of Heroin (284nm)

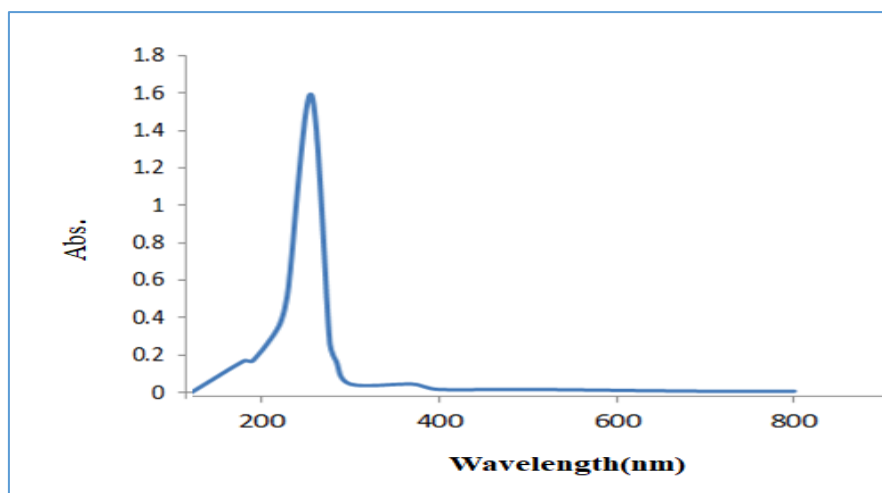


Figure [2.6] Maximum wavelength of Amphetamine (256nm)

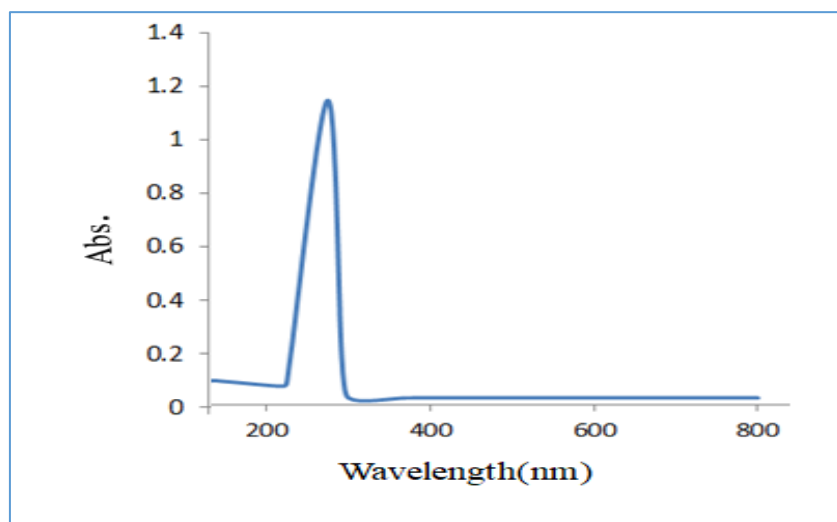


Figure [2.7] Maximum wavelength of Artane (275 nm)

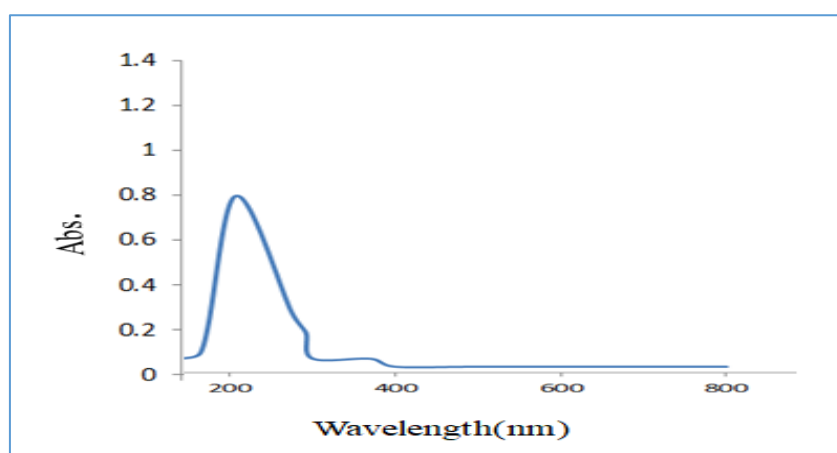


Figure [2.8] Maximum wavelength of Pregabalin (207 nm)

2.9. Determination of Calibration Curves of drugs

2.9.1. Determination of Calibration Curves of drugs in aqueous solution

A series of solutions with stepwise dilutions of the standard drugs solutions, covering concentrations in the range of 5 to 50 mg·L⁻¹, were prepared to construct the calibration curve for the drugs. The absorbance of these solutions were then measured at the λ_{max} for each drugs: heroin at 284 nm, amphetamine at 256 nm, Artane at 275 nm, and pregabalin at 207 nm As shown in Figures [2.9],[2.10],[2.11]and [2.12]. The calibration curve was constructed by plotting the relationship between absorbance and concentration and the equation can be expressed as follows:

$$y = aX - b \dots\dots\dots [2.1]$$

$$X = \frac{y + b}{a} \dots\dots\dots [2.2]$$

Where:

y – Absorbance of drug is measured by (UV-Vis)

X – Drug concentration remaining after adsorption, measured in units (mg.L⁻¹)

a – Slope, b – intercept

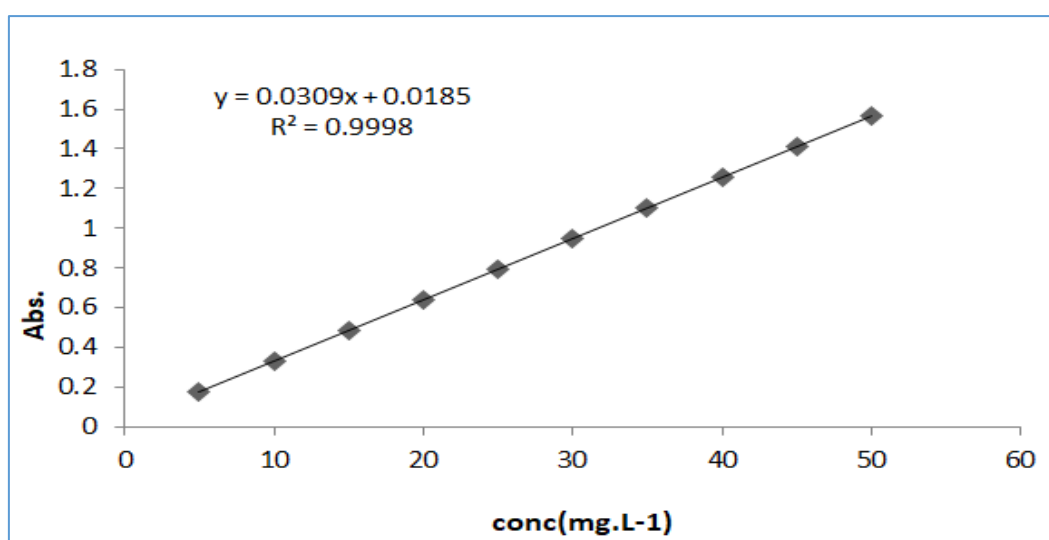


Figure [2.9] Calibration curve for Heroin

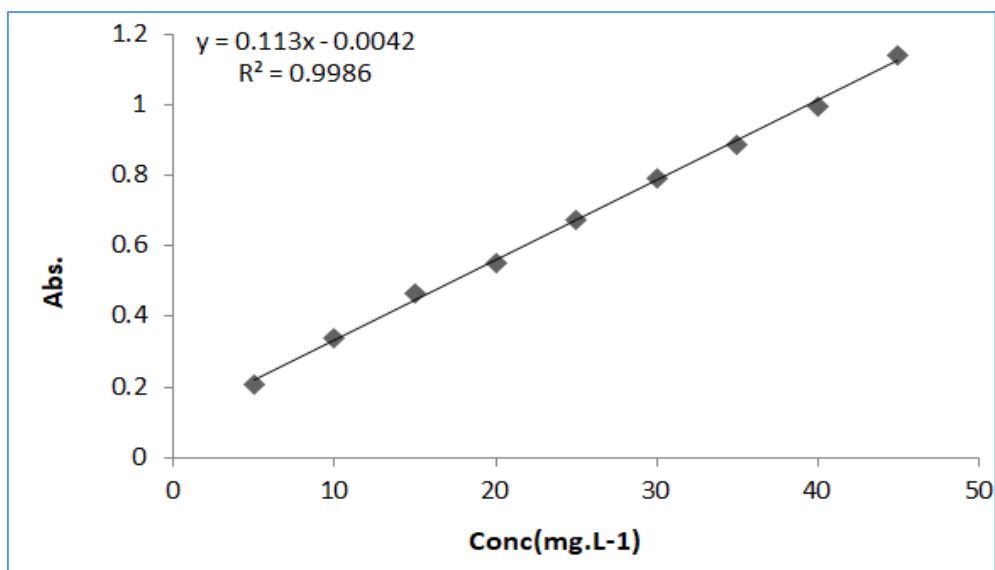


Figure [2.10] Calibration curve for Amphetamine

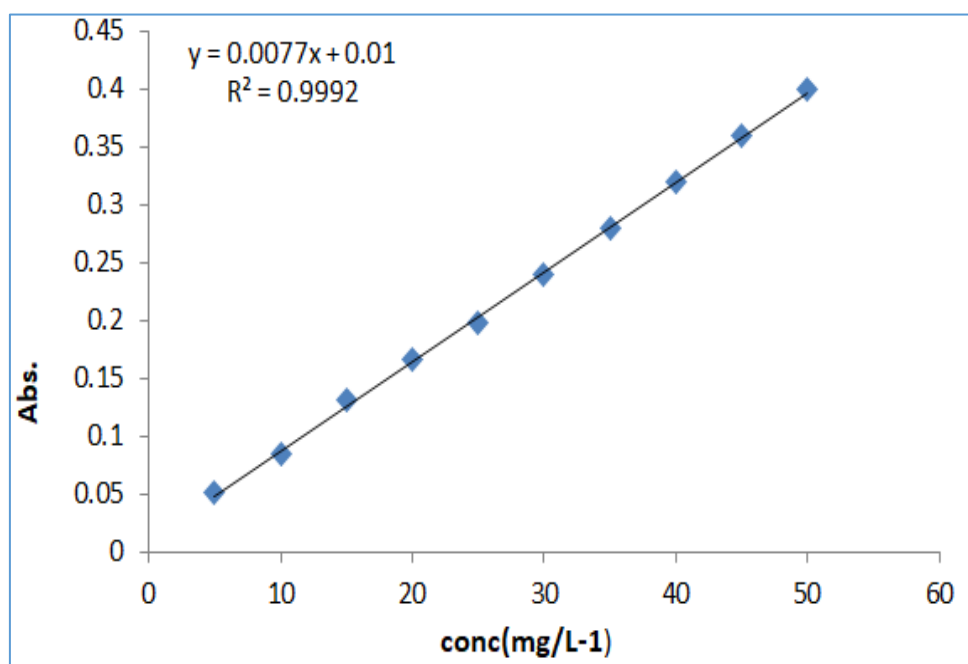


Figure [2.11] Calibration curve for Artane

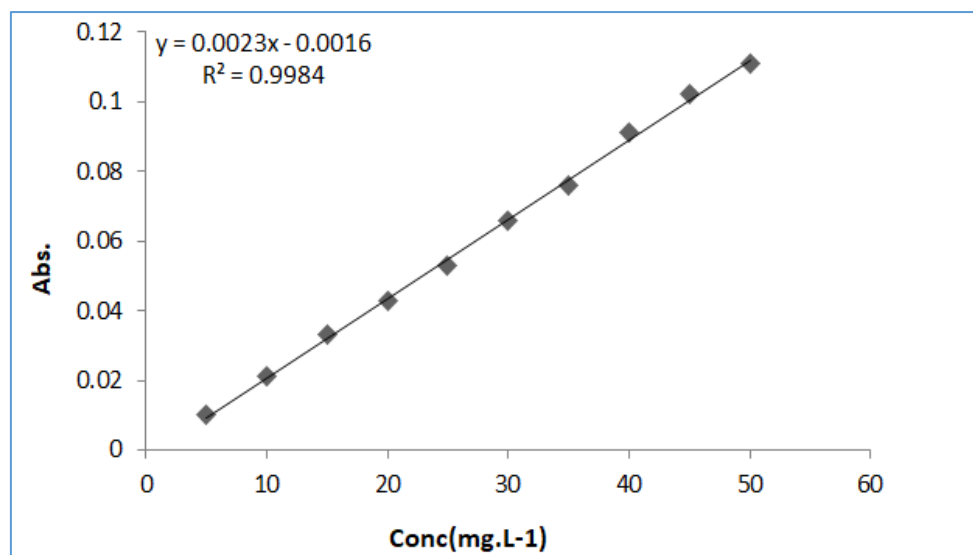


Figure [2.12] Calibration curve for Pregabaline

2.9.2. Determination of Calibration Curves of Heroin and Amphetamine in urine sample

stock standard solutions of drugs were prepared in water and methanol (9:1 v/v). with drug solution (40-180) mg. L⁻¹ for Heroin and (5-40) mg.L⁻¹ for Amphetamine to 10 mL volumetric flask and then the solution was diluted to the mark with urine. The absorbance of the prepared solutions was measured with a UV-Vis spectrophotometer at the specific wavelengths where each drug absorbs: 284 nm for Heroin and 256 nm for Amphetamine. The resulting calibration curves were used to determine the concentrations of the drugs extracted from the urine samples using the magnetic molecularly imprinted polymer (MMIP). Figures [2.13] and [2.14] shown the calibration curve of drugs(Heroin and Amphetamine) in urine sample[108].

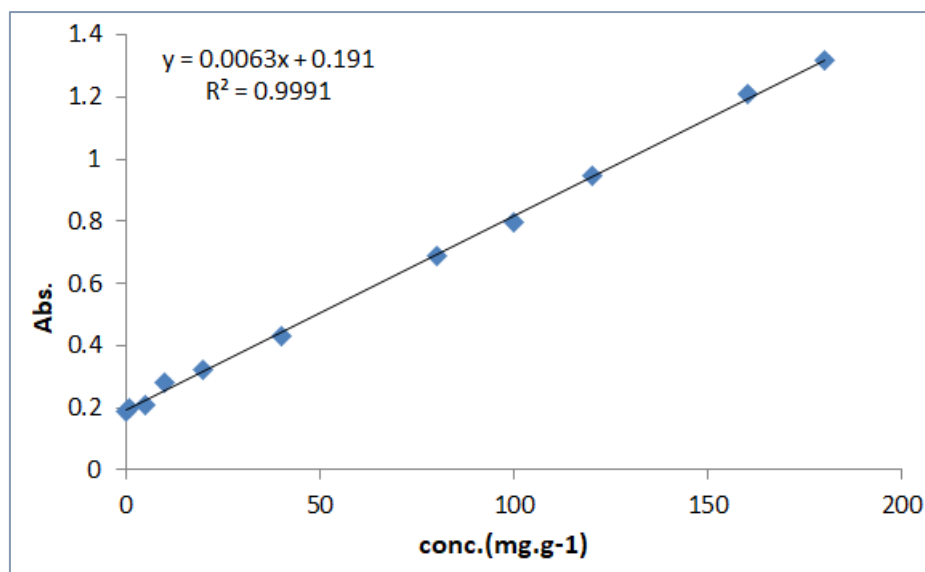


Figure [2.13] Calibration curve for Heroin in urine sample

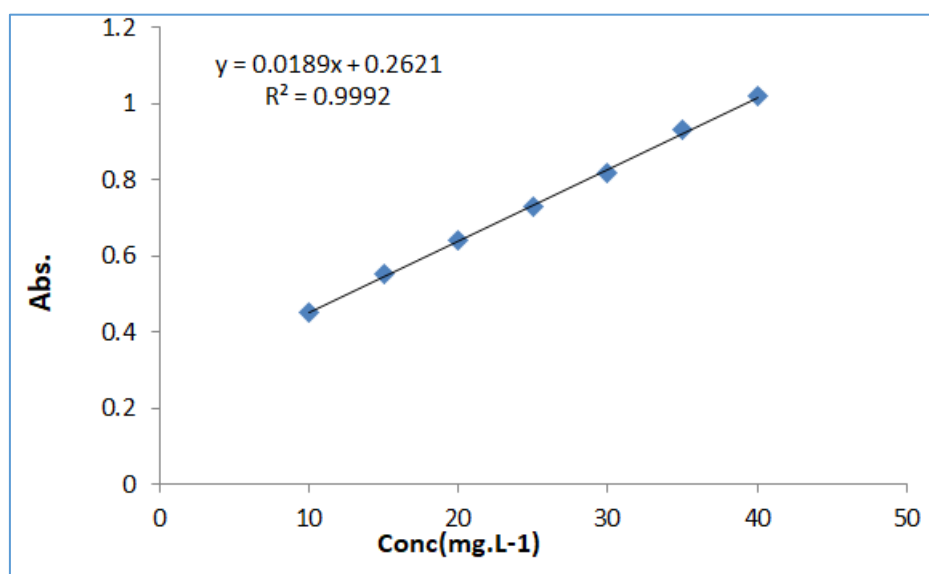


Figure [2.14] Calibration curve for Amphetamine in urine sample

2.9.3. Determination of Calibration Curves of Artane and Pregabalin in serum samples

A primary stock solution was prepared by mixing 5 mL of diluted human serum with 5 mL of drug solution (either Artane or Pregabalin) at a concentration of $25 \text{ mg}\cdot\text{L}^{-1}$. From this stock, a series of standard solutions were subsequently prepared: for Pregabalin (PRE), concentrations ranged from 5 to $40 \text{ mg}\cdot\text{L}^{-1}$, and

for Artane (ART), from 0.2 to 10 mg·L⁻¹. The corresponding calibration curves are illustrated in Figures [2.15] and [2.16]. The absorbance of the prepared solutions was measured with a UV-Vis spectrophotometer at the specific wavelengths where each drug absorbs: 207 nm for pregabalin and 275 nm for Artane. The resulting calibration curves were used to determine the concentrations of the drugs extracted from the serum samples using the magnetic molecularly imprinted polymer (MMIP)[109].

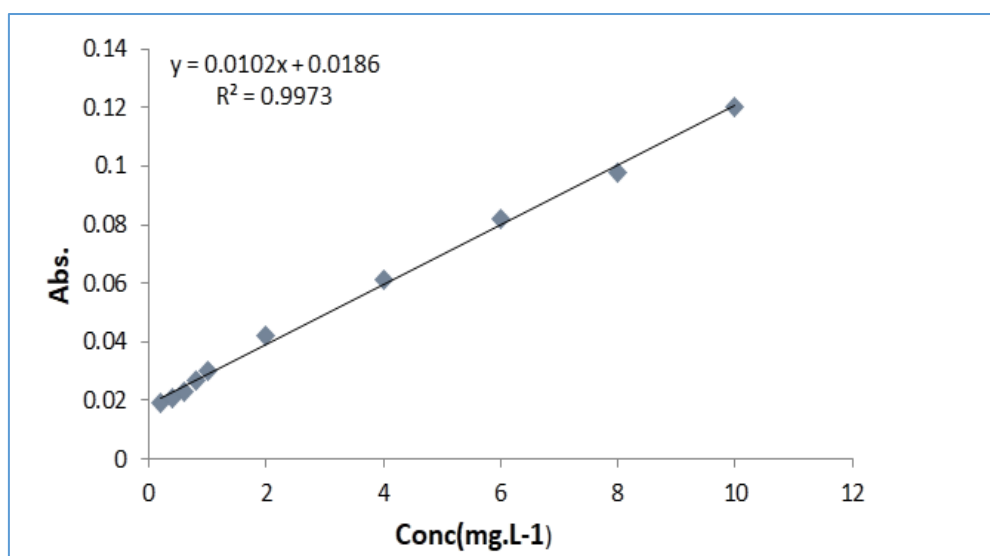


Figure [2.15] Calibration curve for Artane in serum sample

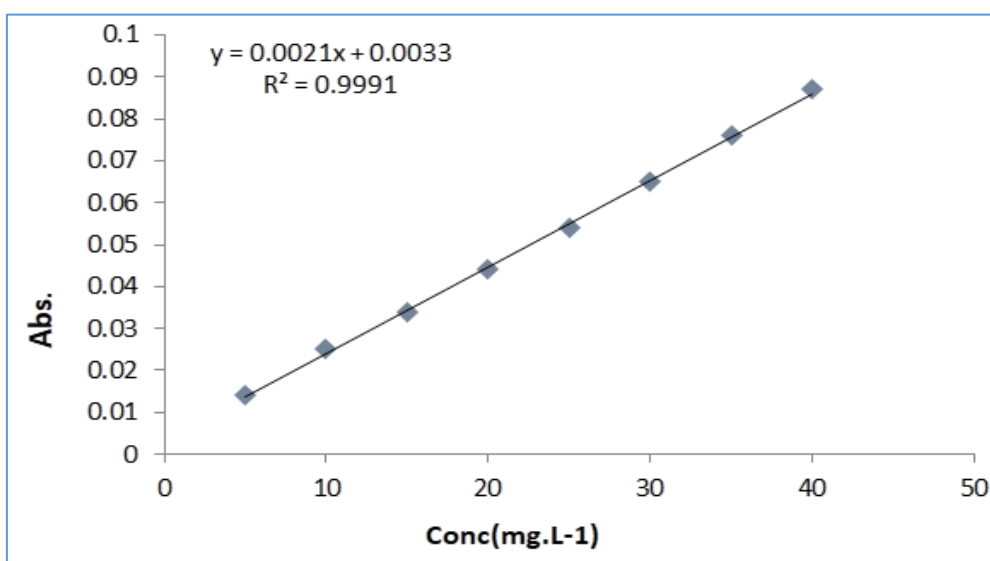


Figure [2.16] Calibration curve for Pregabalin in serum sample

2.10. Optimization of Extraction Conditions

This section presents the experimental evaluation of the parameters affecting the extraction performance of the polymers:

2.10.1. Effect of Contact Time (Equilibrium Time)

The equilibrium time of drugs on the surface of MMIP were calculated by changing the time factor and keeping the drugs concentration, surface weight, pH and temperature constant. MMIP was given 0.01 g (5 mL) of aqueous solutions (100 mg. L^{-1}) as the adsorbent surface. The solutions were separated by magnetic after being placed in the shaker for different time periods (10-120 min), and the equilibrium time was determined by measuring the absorbance of these solutions. The optimum adsorption time of drugs on the surface of the MMIP were shown in table [2.3].

Table [2.3] the contact time for drugs

No.	Drugs	Time(min)
1	Heroin	90 min
2	Amphetamine	120 min
3	Artane	60 min
4	Pregabaline	60 min

2.10.2. Effect of MMIP Dosage

By adding 5 mL of drugs at a concentration of 100 mg.L^{-1} to different weights of the prepared MMIP ranging from (0.01-0.05) g, and under ideal conditions in terms of temperature, pH, drug concentration and reaction time, and using a tightly sealed cup with a volume of (250 mL), the effect of changing the weight of the prepared MMIP was studied, then placed in a shaker whose temperature was controlled at $25 \text{ }^{\circ}\text{C}$ for (90 min(Her) , 120 min (AMP) , and 60 min for ART and Pre. at a speed of 150 rpm to reach equilibrium, and was separated by magnetic, and a graph was made between the weight and the amount

of the adsorbent material. Using the UV-visible spectrophotometer to measure the absorbance of solutions, and determine the appropriate weight in the extraction process.

2.10.3. Effect of pH

The role of pH on the extraction process was examined by preparing solutions with varying pH levels (3-9) to adsorb drugs onto the surface of the MMIP. Five milliliters of drug solution at a concentration of 100 mg.L⁻¹ were introduced to 0.01g of MMIP surface, while maintaining optimal conditions (temperature, drug concentration, MMIP weight, contact time). HCl and NaOH were employed to regulate the pH at a concentration of 0.1 M for both substances. Following the separation of the solutions via magnetic means, the absorbance was quantified, and subsequently, the pH was graphed against the quantity of adsorbent material to ascertain the impact of pH variation on drug adsorption.

2.10.4. Effect of temperature

Under optimal conditions (pH, contact time, and weight of the MMIP) . Subsequently, 5 mL of the drug solution was combined with 0.01 g of the MMIP. The solutions were then subjected to shaking for a specified duration (as detailed in section 2.10.1) for each drug and subsequently separated using magnetic methods. This procedure facilitated the examination of the impact of temperature variations on the extraction of the drug solution onto the surface of the MMIP at different temperatures (25- 45) C°. The data were analyzed by plotting temperature against the quantity of the adsorbent.

2.10.5. Effect of drug solution volume

To determine the optimal volume of the drug solution that allows for achieving the highest extraction efficiency without wasting materials or exceeding the adsorption capacity. By adding (3.0 ,4.0 , 5.0, 8.0 and 10.0) mL of drugs at a concentration of 100 mg.L⁻¹ to 0.01g of the prepared MMIP, and under ideal conditions in terms of temperature, pH, and reaction time, and using a tightly

sealed cup with a volume of (250 mL), then placed in a shaker whose temperature was controlled at 25 °C for 90 min(Her) , 120 min (AMP) , and 60 min for (ART) and(Pre) at a speed of 150 rpm to reach equilibrium, and was separated by magnetic, and a graph was made between the volume of drug solution and the recovery

2.11. Adsorption isotherms

The adsorption curves of pharmaceuticals were analyzed by altering the concentrations of the adsorbent within a certain range. 5 mL of the drug solution was applied to 0.01 g of the MMIP surface following the establishment of optimal conditions (temperature, contact time, MMIP surface weight, and pH) utilizing beakers of equivalent volume (250 mL). The solutions were agitated at 150 rpm and 25 °C for each medication, as detailed in section (2.10.1.) The solutions were segregated by magnetic. The adsorption of the drug solutions was assessed using UV-vis at the maximal wavelength of each drug.

2.12. Kinetic adsorption experiments

0.01 g of MMIP was added to a drug solution (5.0 mL) of various concentrations (5-50) mg. L⁻¹ and incubated at different times (0-130 min) for Her, (0-160 min) for AMP, and (0-90 min) for ART and Pre. The supernatant and imprinted polymers were separated by an external magnet, and the concentration of drug in the supernatants was measured using UV-Vis at the maximal wavelength of each drug.

2.13. Static adsorption of the MMIP

The static adsorption experiment for MMIP and MNIP was conducted as follows:

An amount of 0.01 g of MMIP or M NIP was placed into a beaker containing 5 mL of a 100 mg.L⁻¹ drug solution and shaken at 25°C for 90 min for Her, 120 min for AMP, and 60 min for ART and Pre. After the incubation period, the solutions were segregated magnetically. And analyzed using a UV-Vis

spectrophotometer at the maximal wavelength of each drug to determine the concentration of drugs. The binding capacity of the MMIP or MNIP was calculated using Equation [2.1]:

$$Q = (C_0 - C_e) \times V / M \dots \dots \dots [2.1]$$

Where:

- Q_e represents the adsorption capacity at equilibrium ($\text{mg} \cdot \text{g}^{-1}$),
- C_0 is the initial concentration of the drug in solution ($\text{mg} \cdot \text{L}^{-1}$),
- C_e denotes the equilibrium concentration of the drug ($\text{mg} \cdot \text{L}^{-1}$),
- V is the volume of the solution used (L),
- M is the mass of the adsorbent polymer (g).

The imprinting factor (IF) was then calculated using Equation [2.2]:

$$\text{IF} = Q_{\text{MMIP}} / Q_{\text{MNIP}} \dots \dots \dots [2.2]$$

Where Q_{MMIP} and Q_{MNIP} represent the adsorption capacities of the MMIP and MNIP, respectively

The selectivity of the magnetic molecularly imprinted polymer (MMIP) was evaluated using the specific selectivity factor (β), which is defined as the ratio of the difference in adsorption capacities between the MMIP and its corresponding non-imprinted polymer (MNIP) for a given interfering substance relative to the target drug. The value of β was calculated according to Equation [2.3].

$$\beta = Q_{\text{substrate}} / Q_{\text{drug}} \dots \dots \dots [2.3]$$

Where: $Q_{\text{substrate}} = (Q_{\text{MMIP}} - Q_{\text{MNIP}})_{\text{Substrate}}$

$$Q_{\text{drug}} = (Q_{\text{MMIP}} - Q_{\text{MNIP}})_{\text{drug}}$$

2.14. Molecularly imprinted magnetic solid-phase extraction of Heroin and Amphetamine from urine samples

Urine samples were collected from healthy male volunteers, approximately 25 years old. Stock standard solutions of the target drugs were prepared in a mixture of water and methanol (9:1, v/v). To prepare spiked urine samples,

varying volumes of the drug solution (2, 4, 5, 6, and 9 mL) were added to separate 10 mL volumetric flasks, followed by dilution to the mark with drug-free urine. The mixtures were vortexed for 3 minutes to ensure homogeneity.

The spiked urine samples were then centrifuged at 8000 rpm for 20 minutes, and the resulting supernatants were filtered using cellulose acetate filters (0.20 μm pore size). An aliquot of 5 mL of the filtered supernatant was mixed with 0.01 g of MMIP in a 10 mL centrifuge tube. The mixture was shaken on a platform shaker until adsorption equilibrium was reached. Subsequently, the MMIP particles were collected along the wall of the centrifuge tube using a magnet, and the supernatant was carefully removed.

To desorb the retained drug, 1.0 mL of elution solvent was added, and the mixture was vortexed for 2 minutes. The resulting eluate was filtered and subjected to final analysis [109]

2.15. Molecularly imprinted magnetic solid-phase extraction of Artane and Pregabalin from serum samples

2.15.1. Serum Collection

Fresh, drug-free human blood (10 mL) was collected into a clean glass tube and allowed to clot undisturbed at room temperature for 30 minutes. The clotted sample was then centrifuged at 5000 rpm for 15 minutes. The clear supernatant (serum) was carefully separated and stored for subsequent analysis [110].

2.15.2. Serum Pretreatment

A volume of 1.0 mL of human serum was diluted with 10 mL of deionized water. Subsequently, 1.0 mL of the diluted serum was transferred into a 10 mL volumetric flask, and methanol was added to reach the final volume. The resulting solution was heated in a water bath at a temperature not exceeding 60°C for 10–15 minutes until a transparent solution was obtained. Figure [2.17] shows the steps of serum pretreatment.

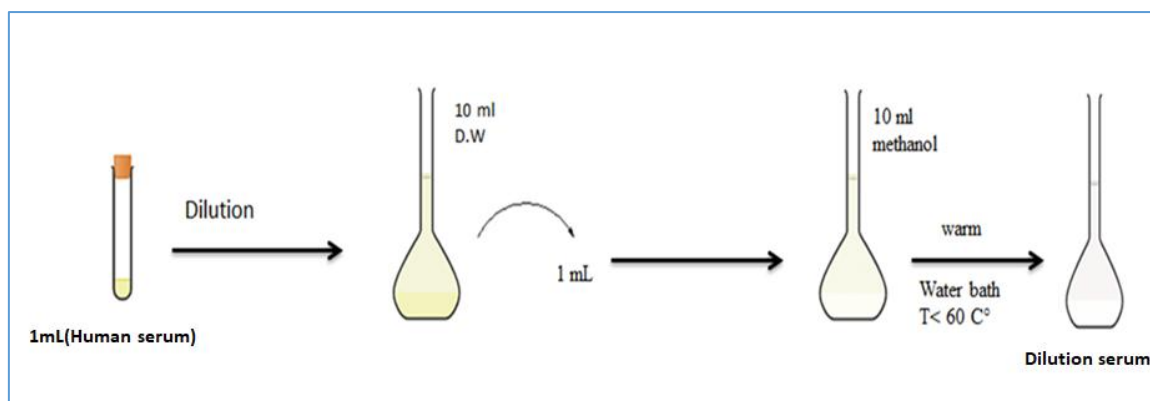


Figure [2.17] steps of Serum Pretreatment

2.15.3. Extraction Procedure Using MMIPs

Approximately 0.01g of the prepared magnetic molecularly imprinted polymer (MMIP) was added to conical flasks containing 10 mL of spiked serum samples. The flasks were placed on a mechanical shaker and agitated for 60 minutes to ensure adequate interaction between the polymer and target (drug). Following the extraction period, the magnetic polymer was separated from the solution using a strong flat permanent magnet. and the clear extract was collected for further analysis by UV-Vis spectrophotometry [111].

2.16. Selectivity of the MMIP

To assess the selectivity of the MMIP, several drugs, including Heroin (Her), Amphetamine (AMP), Artane (ART) and Pregabalin (pre), were evaluated. The experiment involved the addition of 0.01 g of the MMIP was distributed into four distinct conical flasks. Subsequently, 5 mL of Artane, Heroin, Pregabalin, and Amphetamine, each at a concentration of 35 mg.L⁻¹ were added accordingly. The flasks were agitated at ambient temperature for contact time. After the shaking period, the solutions were separated by using magnets. The concentration of the compounds were then determined using UV-VIS spectroscopy at a maximum wavelength of each drugs [112]

2.17. Reusability and stability

The reusability of the magnetic molecularly imprinted polymers (MMIPs) was evaluated under the same experimental conditions as described in Section 2.11. After each extraction cycle, the used MMIPs were regenerated by sequential washing with a mixture of methanol and acetic acid (5:1, v/v), followed by deionized water. The regenerated sorbents were then reused in subsequent extraction cycles to assess their stability and performance over repeated use [113].

2.18. Determination of Analytical Performance Parameters (LOD, LOQ, RSD, and Recovery)

To evaluate the analytical performance of the developed MMIP-based extraction method, several key validation parameters were calculated, including the limit of detection (LOD), limit of quantification (LOQ), relative standard deviation (RSD), and recovery percentage. The LOD and LOQ were determined in accordance with the ICH Q2(R1) guidelines by analyzing replicate blank samples and constructing calibration curves for each drug. The values were calculated using the following equations:

$$\text{LOD} = (3.3 \times \sigma) / S$$

$$\text{LOQ} = (10 \times \sigma) / S$$

Where:

- σ is the standard deviation
- S is the slope of the calibration curve.

The relative standard deviation (RSD) was calculated to assess the precision of the method using the equation:

$$\text{RSD} (\%) = (\text{Standard Deviation} / \text{Mean}) \times 100$$

The recovery percentage (Recovery %), which reflects the accuracy of the method, was computed by comparing the amount of drug extracted by MMIP to the known amount added (spiked) to the sample matrix

Chapter Three
Results and discussion

3. Results and discussion

3.1. Synthesis of Magnetic Molecularly Imprinted Polymers (MMIPs)

In the present investigation, four magnetic molecularly imprinted polymers (MMIPs) were synthesized to achieve selective recognition and extraction of heroin, amphetamine, Artane, and pregabalin. The synthesis employed two different functional monomers tailored to interact optimally with the respective target analytes.

3.1.1. MMIPs for Heroin and Amphetamine (Her-MMIP and Amp-MMIP)

Magnetic molecularly imprinted polymers (MMIPs) were successfully synthesized for the selective extraction of heroin and amphetamine through the use of 2-acetamidoacrylic acid as the functional monomer. This monomer possesses both amide and carboxylic acid groups, which facilitate the formation of hydrogen bonds and electrostatic interactions with the target analytes, thus enhancing molecular recognition and binding specificity. The synthesis process involved two main steps [112]:

Step one: Surface Modification of Magnetic Nanoparticles: Fe_3O_4 nanoparticles were coated with a silica layer through the use of tetraethyl orthosilicate (TEOS), providing a stable surface and reactive sites suitable for subsequent polymerization. This coating also enhances the colloidal stability and dispersibility of the magnetic core.

Step two: Polymerization and Template Imprinting: The functional monomer (2-acetamidoacrylic acid), cross-linker (TEOS), and the template molecule (either heroin or amphetamine) were dissolved in methanol. Polymerization was initiated by benzoyl peroxide (BPO) as a radical initiator, resulting in the formation of a polymer layer around the magnetic core. Following polymerization, the template molecules were removed through the use of (5:1) methanol: glacial acetic acid mixture to disrupt the non-covalent interactions and

generate recognition sites that are complementary in shape and functionality to the target molecules .

The resulting MMIPs exhibited significant binding affinity and selectivity toward heroin and amphetamine, confirming the suitability of 2-acetamidoacrylic acid as an effective functional monomer for imprinting these drug molecules.

3.1.2. MMIPs for Artane and Pregabalin (Art-MMIP and Pre-MMIP)

For the selective extraction of Artane and pregabalin, 3, 4-dihydroxy-1-butene was employed as the functional monomer due to its vicinal diol structure, which enables the formation of multiple hydrogen bonds with the target analytes, thereby enhancing molecular recognition. The synthesis of the magnetic molecularly imprinted polymers (MMIPs) was carried out in two main steps.

First step, Fe_3O_4 nanoparticles were surface-modified by coating with a silica layer, providing a stable and reactive platform for subsequent polymerization [113].

Second step, molecular imprinting was achieved by polymerizing a mixture comprising the functional monomer (3,4-dihydroxy-1-butene), tetraethyl orthosilicate (TEOS) as the cross-linker, and the template molecule (either Artane or pregabalin) in an appropriate solvent system (methanol) . Benzoyl peroxide (BPO) was used as the radical initiator to initiate the polymerization, resulting in the formation of an imprinted polymer shell around the magnetic core. Following polymerization, the template molecules were removed through the use of a methanol/ glacial acetic acid mixture (5:1, v/v), thereby generating specific recognition cavities complementary in shape and functionality to the target molecules. The resulting MMIPs exhibited significant binding affinity and selectivity toward Artane and pregabalin, confirming the suitability of 3,4-dihydroxy-1-butene as a functional monomer for the imprinting of these pharmaceutical compounds.

3.2. Characterization of MMIP and MNIP

3.2.1. Analysis through the use of X-ray Diffraction (XRD)

The crystalline nature of the synthesized magnetic non-imprinted polymers (MNIPs) was investigated through the use of X-ray diffraction (XRD) analysis. The XRD pattern of MNIP₁, presented in Figure [3.1] revealed distinct and sharp diffraction peaks at 2θ values of 35.5° , 43.0° , 54.0° , 57.0° , and 62.0° , corresponding primarily to the crystalline planes of magnetite (Fe_3O_4), in accordance with the Joint Committee on Powder Diffraction Standards (JCPDS card no. 88-0866). The intense and well-defined peaks confirm the successful formation of a highly crystalline Fe_3O_4 structure within the polymer matrix. Minor peaks at lower angles ($\sim 18^\circ$ and $\sim 32^\circ$) may be attributed to amorphous SiO_2 or trace impurities, while the peak at $\sim 76^\circ$ indicates higher-order reflections of Fe_3O_4 . The overall pattern reflects the structural stability and high ordering of the magnetic composite, which are crucial for its functional performance in targeted applications..

Similarly, the XRD pattern of MNIP₂ Figure [3.2] displayed multiple pronounced diffraction peaks in the 2θ range of 10° – 80° , consistent with a magnetite-based crystalline framework. Six major diffraction peaks were observed at 30.1° , 35.5° , 43.1° , 53.5° , 57.0° , and 62.6° , corresponding to the primarily to the crystalline planes of magnetite Fe_3O_4 , respectively. These reflections exhibit strong agreement with the standard diffraction data for magnetite, as referenced in JCPDS card no. 19-0629. [114].

The clear diffraction peaks observed in both MNIP₁ and MNIP₂ confirm the presence of a well-defined crystalline structure, suggesting significant phase purity and structural stability. Such crystallinity plays a pivotal role in enhancing the reproducibility and functional performance of the synthesized polymers,

particularly in their intended use for selective molecular recognition and magnetic separation processes.

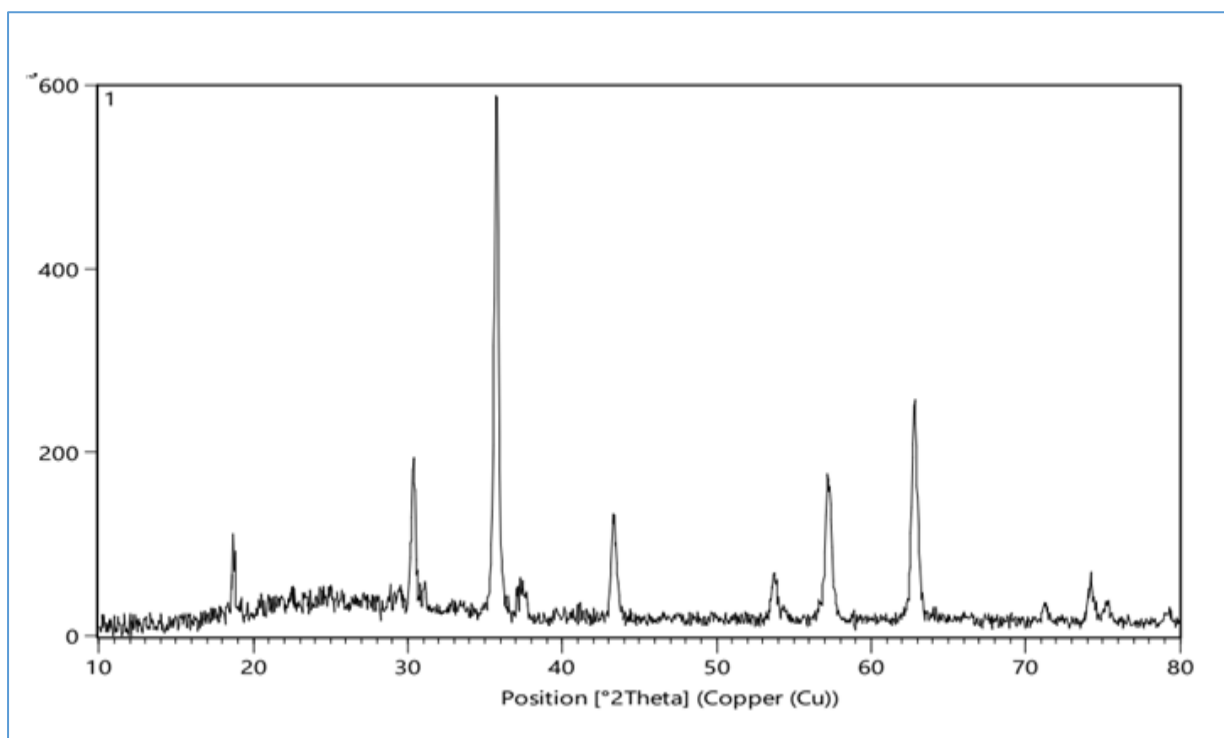


Figure [3.1] XRD Spectra of MNIP₁

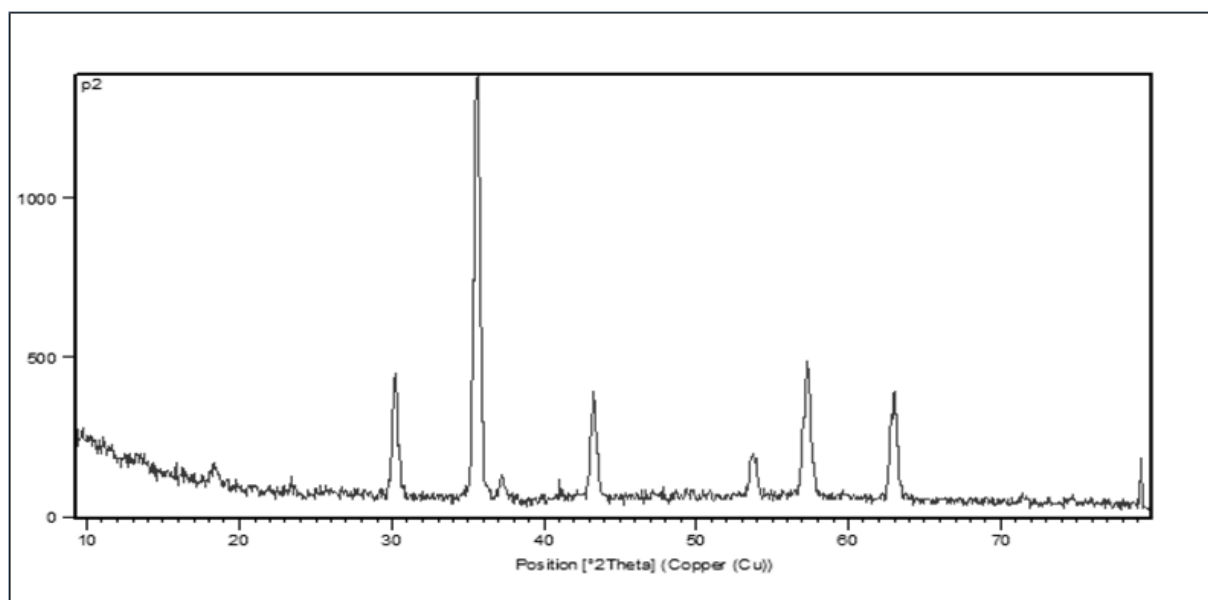


Figure [3.2] XRD Spectra of MNIP₂

3.2.2. Thermal gravimetric analysis:

Thermal gravimetric analysis (TGA) was carried out for the assessment of the thermal stability of the synthesized magnetic non-imprinted polymers (MNIPs). As illustrated in Figure [3.3], the TGA thermogram of the MNIP₁ sample reveals a multi-stage weight loss profile as the temperature increases up to 800°C. In the initial stage (0–200°C), a slight weight loss was observed, attributed to the evaporation of physically adsorbed water or residual volatile organic compounds. A substantial weight loss occurred in the range of 200–500°C, corresponding to the primary thermal decomposition of the organic polymer chains. Beyond this range, from 500 to 900°C, the rate of weight loss diminished significantly, suggesting the formation of thermally stable carbonaceous residues (char) or the absence of further degradable organic content. The total weight loss recorded was approximately 57.20%, indicating a significant presence of thermally degradable organic matter, while the remaining 42.80% may be attributed to inorganic or thermally resistant residues. This thermal behavior illustrates that MNIP₁ possesses moderate thermal stability, with a well-defined decomposition range.

For MNIP₂, the thermal decomposition profile Figure [3.4] also displayed a multi-step degradation process up to 1000°C. In the first stage, a minor weight loss of 1.713% occurred at lower temperatures, likely due to the evaporation of adsorbed moisture or low-molecular-weight volatiles. The second stage involved additional minor losses of 1.021% and 0.8401% within the 400–600°C range, possibly due to the breakdown of unstable side groups or small functional fragments. A third weight loss of 2.072% was observed around 800°C, potentially reflecting the decomposition of inorganic or carbonaceous species. The final and most significant mass loss of 6.453% occurred between 900 and 1000°C, indicating the degradation of residual components, oxidation of carbon, or decomposition of metal oxides. The total mass loss for MNIP₂ was approximately

12.10%, meaning the sample retained 87.9% of its original mass, demonstrating significantly higher thermal stability compared to MNIP₁. The comparative thermal behavior between the two polymers highlights the difference in their chemical composition and structure. MNIP₁ demonstrates a higher content of organic matter, resulting in a more pronounced decomposition, while MNIP₂ exhibits enhanced thermal resistance, likely due to the incorporation of thermally inert or inorganic components. These findings offer critical insights into the structural integrity and suitability of each material for significant-temperature or long-term applications [115].

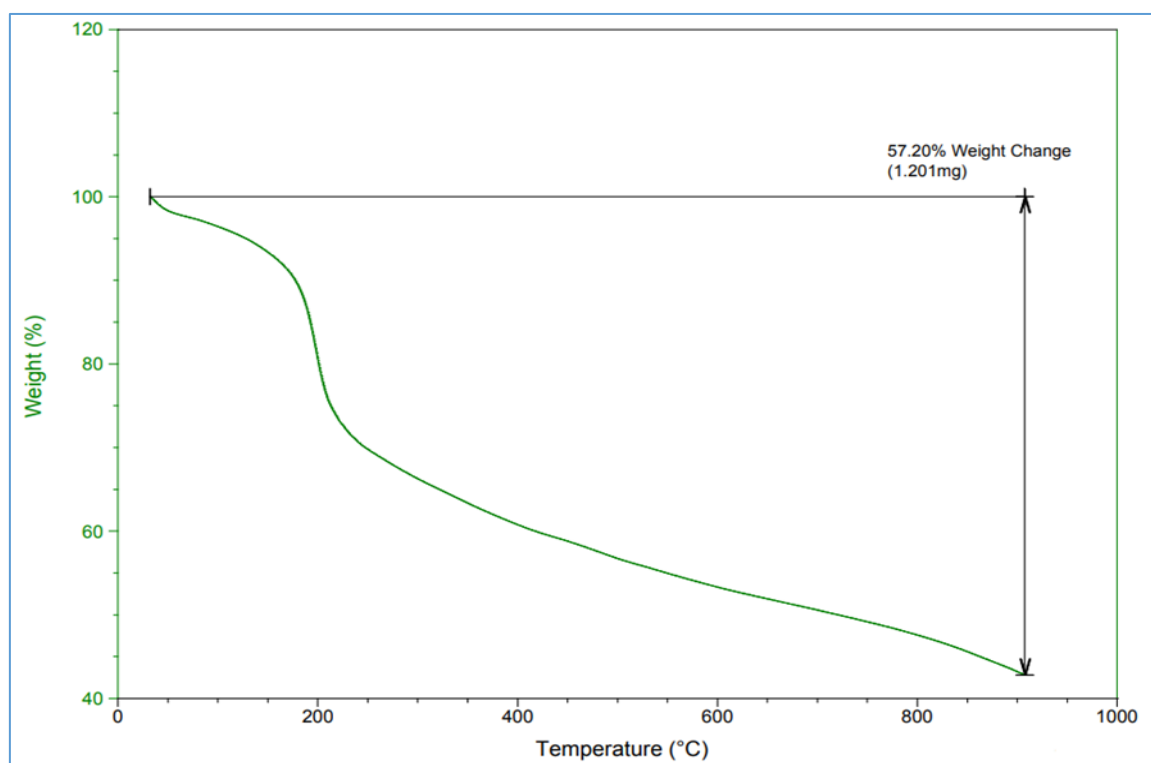


Figure [3.3] TGA curve of MNIP₁

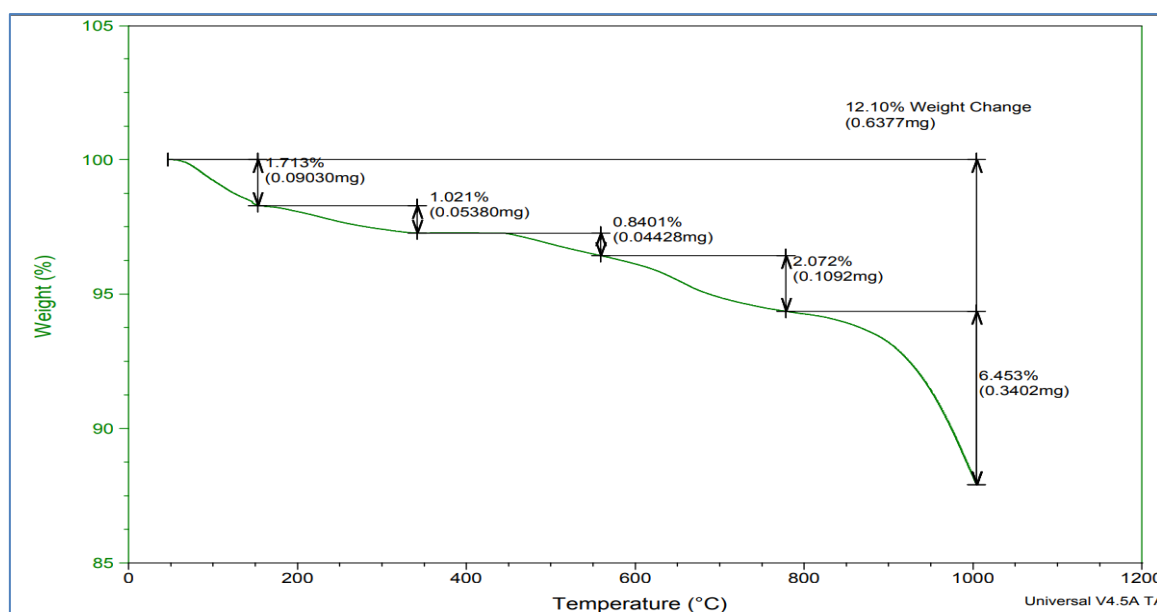


Figure [3.4] TGA curve of MNIP₂

3.2.3. Vibrating Sample Magnetometer (VSM) Analysis

The magnetization curves of the magnetic non-imprinted polymers MNIP₁ and MNIP₂, shown in Figures [3.5] and [3.6], exhibit similar magnetic behavior characterized by very narrow hysteresis loops at room temperature. The remanent magnetization (M_r) and coercive field (H_c) are close to zero, which clearly indicates that both samples possess superparamagnetic behavior[116].

It is observed that the saturation magnetization (M_s) value of MNIP₁ in Figure [3.5] is approximately 17.8 emu/g, whereas the M_s value of MNIP₂ in Figure [3.6] increases to about 20.1 emu/g. This difference can be attributed to variations in the degree of coating of Fe₃O₄ nanoparticles by the polymer layer in the two samples. A thicker polymer shell leads to a lower apparent magnetization due to dilution of the magnetic content, whereas a thinner coating allows a higher saturation magnetization to be expressed[117]. These values confirm that both polymers retain an effective magnetic response under an external magnetic field, with negligible remanent magnetization after removal of the field, which ensures rapid and easy magnetic separation during extraction procedures and practical applications. .

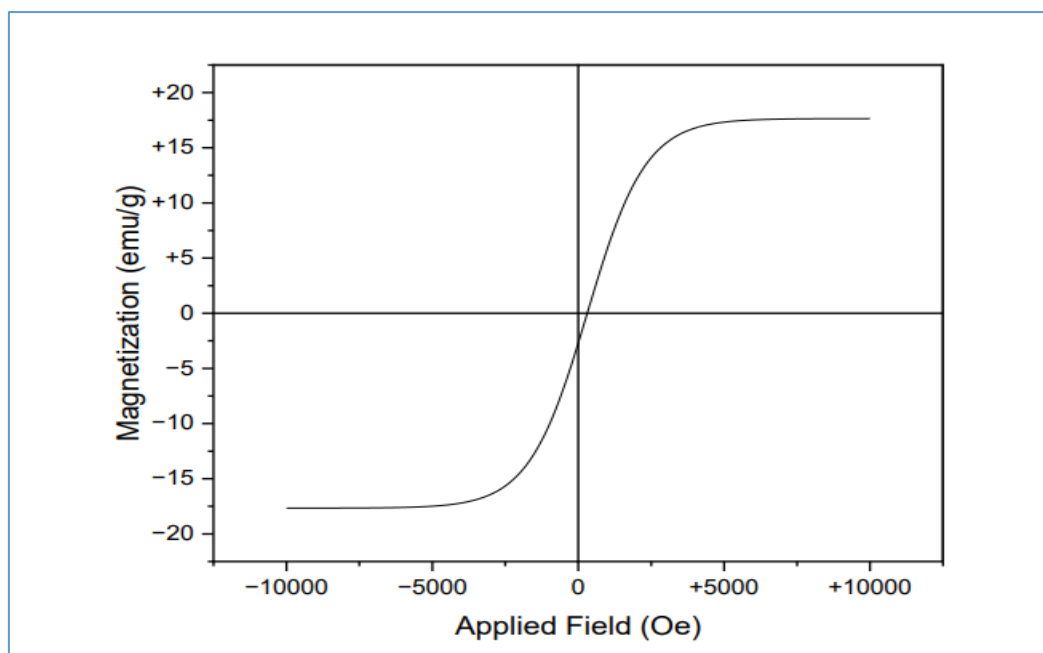


Figure [3.5] Magnetization curve across magnetic field range from (-10000 to 10000) Oe at 25C° of the MNIP₁

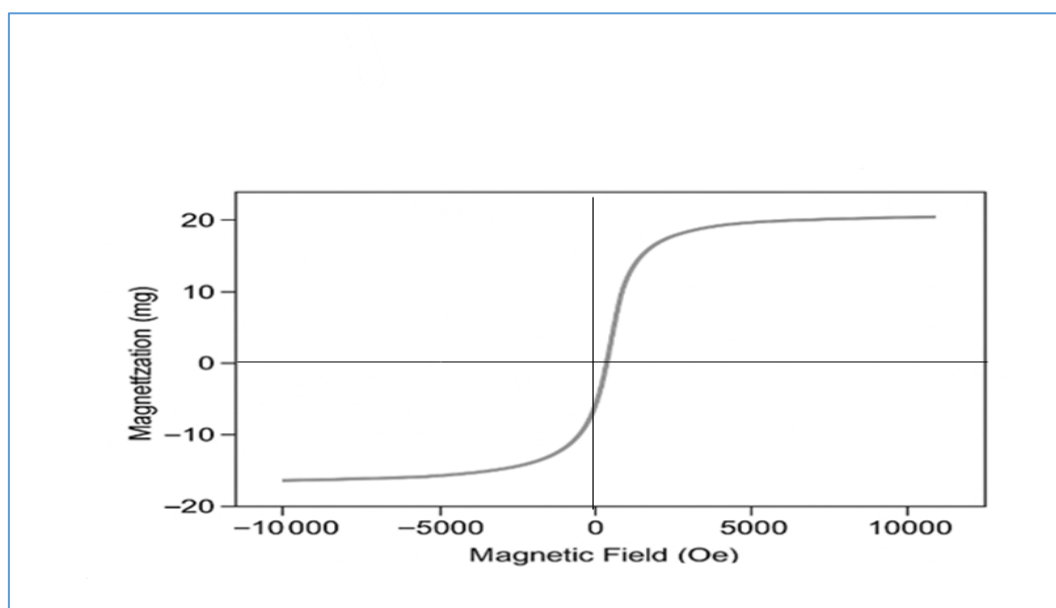


Figure [3.6] Magnetization curve across magnetic field range from (-10000 to 10000) Oe at 25C° of the MNIP₂

3.2.4. Fourier Transform Infrared Spectroscopy Analysis

3.2.4.1. FTIR Spectra of Her-MMIP and MNIP

FTIR Spectrum of (A) As shown in Figure [3.7] represents the fundamental structure of MNIP1 resulting from the interaction between 2-acetamidoacrylic acid with the $\text{Fe}_3\text{O}_4@\text{SiO}_2$ nanoparticles. The frequencies in the range of $1700\text{-}1600\text{ cm}^{-1}$ in an infrared (IR) spectrum correspond to the presence of carbonyl ($\text{C}=\text{O}$) bonds, which are characteristic of compounds containing amide ($-\text{CONH}_2$) or acrylic ($-\text{C}=\text{CH}_2$) groups. The range $3200\text{-}3500\text{ cm}^{-1}$ illustrates the presence of hydroxyl (O-H) or amine (N-H) bonds.[118] The frequencies in the range of $400\text{-}600\text{ cm}^{-1}$ may indicate the presence of vibrations associated with Si-O or Fe-O bonds, which could suggest the influence of a material like $\text{Fe}_3\text{O}_4@\text{SiO}_2$. These vibrations typically correspond to metal-oxygen bonds, such as those found in iron oxide (Fe_3O_4) and silica (SiO_2) composites.(B) demonstrates noticeable changes compared to the first one: The increase or appearance of new peaks in the range of $1500\text{-}1400\text{ cm}^{-1}$ may reflect the presence of aromatic ($\text{C}=\text{C}$) groups or additions resulting from heroin. Aromatic ($\text{C}=\text{C}$) stretches typically appear in this region and could indicate the presence of aromatic rings, such as in the case of aromatic compounds. In the case of heroin, the changes might suggest the presence of specific functional groups associated with the drug, such as additional modifications to the aromatic ring structure [119]. The peaks in the $1600\text{-}1700\text{ cm}^{-1}$ range may become more intense due to the additional carbonyl effect from heroin. The changes in the peaks between $1000\text{-}1200\text{ cm}^{-1}$ could be associated with ether bonds or interactions between heroin and the base compound. The addition of heroin may cause an enhancement in absorption at certain frequencies due to its complex chemical nature. The third spectrum (C) is similar to the first spectrum (A), but with some differences: The peaks associated with heroin (such as those in the $1500\text{-}1400\text{ cm}^{-1}$) disappear or weaken significantly. The reappearance of the basic structure with slight changes. The

changes in the low-frequency range ($400\text{-}600\text{ cm}^{-1}$) may indicate the stabilization of the material after the removal of heroin

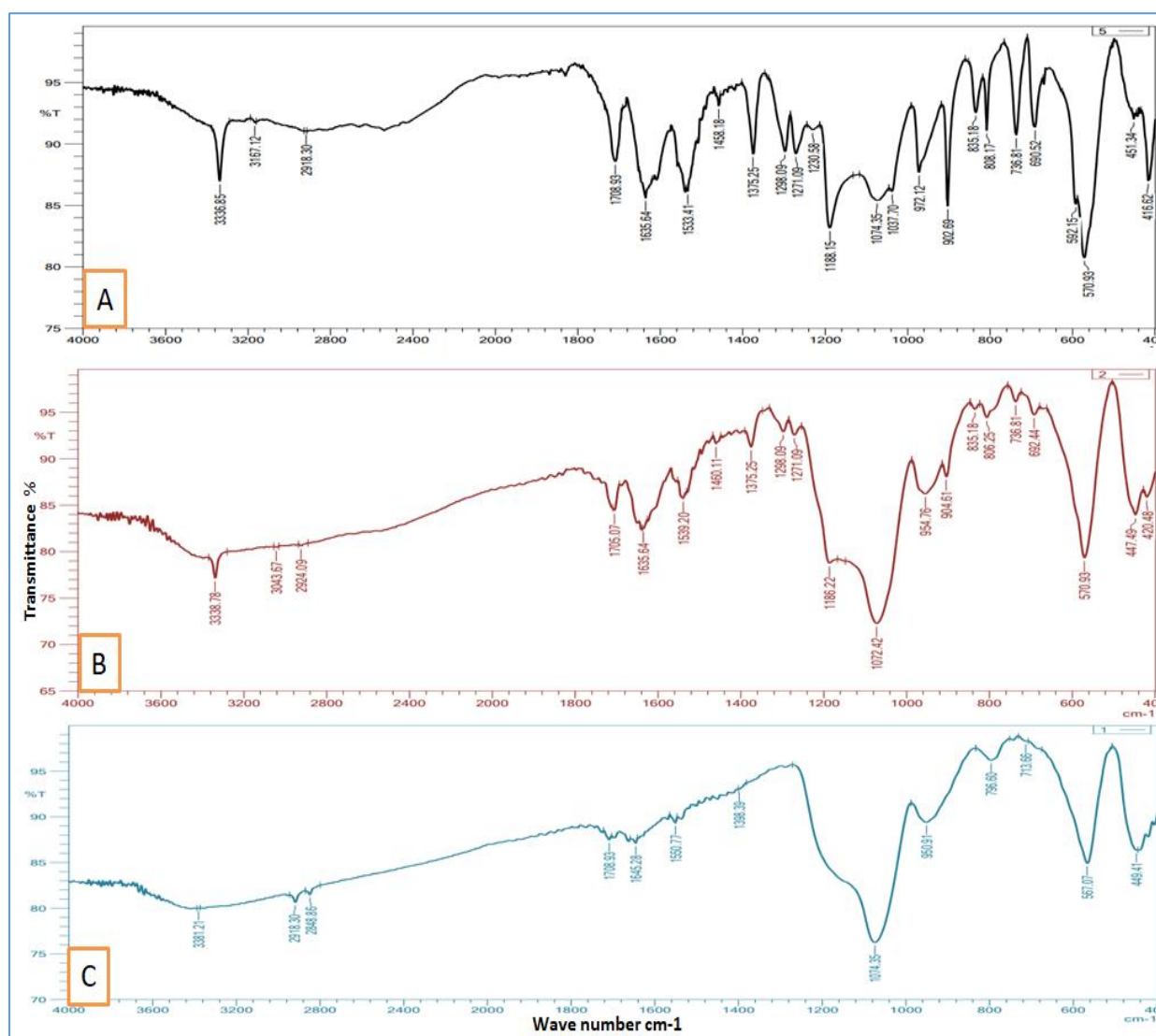


Figure [3.7] FT-IR spectra of Heroin (A) MNIP (B) unwashed MMIP (C) washed MMIP

3.2.4.2. FTIR Spectra of AMP-MMIP and MNIP

The chemical composition of MNIP₁ (A), unwashed AMP-MMIP (B), and washed MMIP(C) were analyzed by FTIR spectroscopy .the FTIR spectrum Figure [3.8] (A) demonstrates the characteristic peaks associated with chemical structure. A prominent peak at approximately 3400 cm^{-1} signifies the O-H

stretching vibration, suggesting the presence of hydroxyl groups. Peaks between 1000-1100 cm^{-1} are ascribed to the Si-O-Si stretching vibrations of the silica framework. Peaks between 400-600 cm^{-1} correspond to Fe-O stretching vibrations from the magnetic Fe_3O_4 core. These characteristics validate the effective synthesis of the polymer framework [120]. Figure (B), the spectrum exhibits significant alterations in comparison to the (A): New or enhanced peaks are detected in the 2800-3000 cm^{-1} range, attributed to the C-H stretching vibrations of amphetamine molecules. The peaks associated with amide groups (C=O and N-H stretching) in the range of 1600-1700 cm^{-1} exhibit minor changes or heightened intensity as a result of interactions between the polymer and amphetamine molecules. The data illustrates that amphetamine molecules are effectively incorporated into the polymer matrix. Figure (C) illustrates the FTIR spectrum of the polymer subsequent to the extraction of amphetamine. The spectrum roughly mimics the (A), albeit with minor variations: The peaks in the 2800-3000 cm^{-1} range corresponding to amphetamine molecules are markedly diminished or nonexistent, signifying effective elimination. The original peaks associated with the polymer framework, including the hydroxyl group at 3400 cm^{-1} and the Si-O-Si and Fe-O bonds, and are reinstated. Subtle variations in peak intensities may signify surface alterations resulting from the loading and unloading Processes

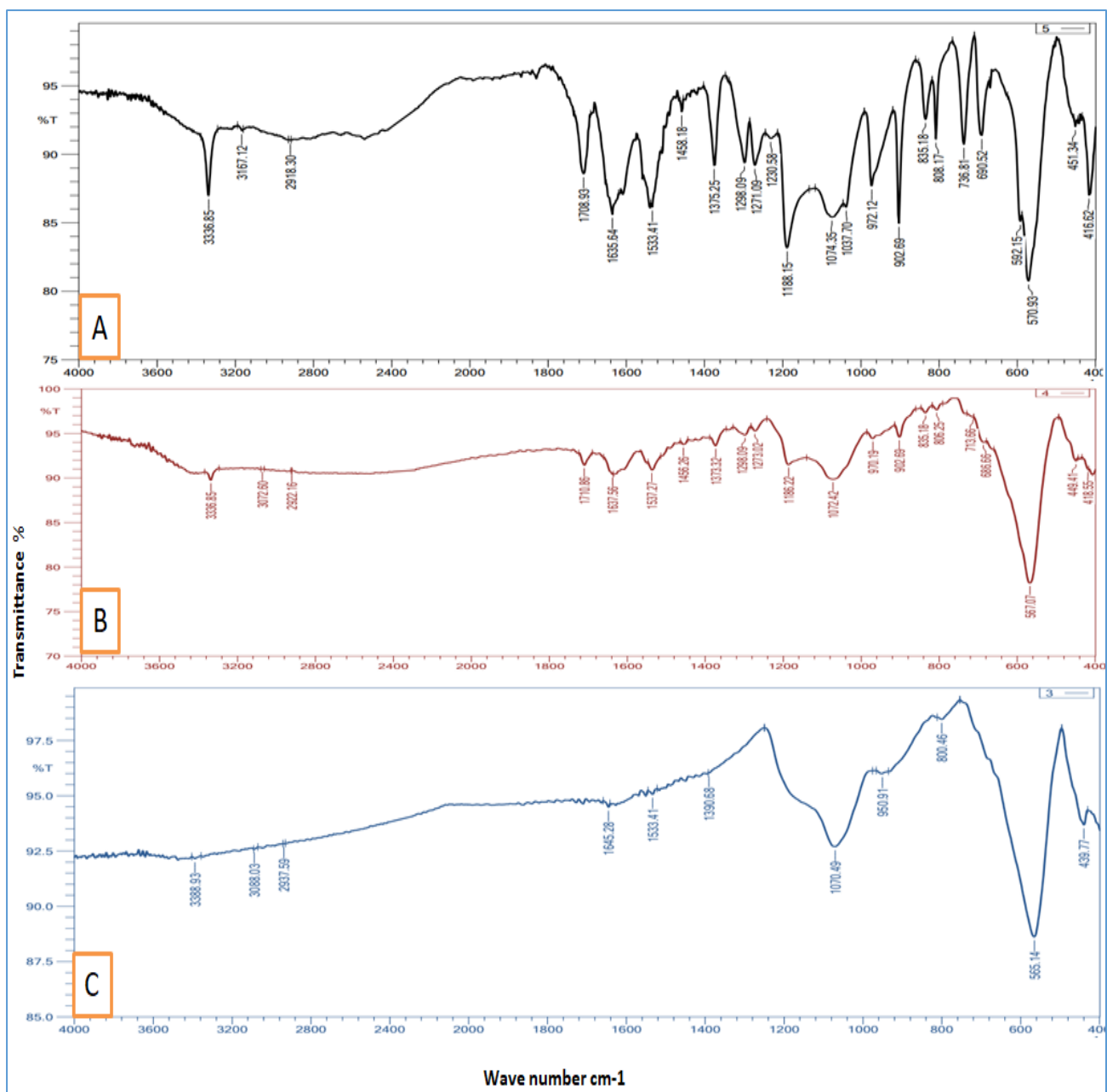


Figure [3.8] FT-IR spectra of Amphetamin (A) MNIP (B) unwashed MMIP (C) washed MMIP

3.2.4.3. FTIR Spectra of ART-MMIP and MNIP

Figure [3.9] (A) demonstrates the FTIR spectrum of MNIP₂ reveals characteristic peaks indicating the successful synthesis of the composite: A broad absorption band at 3400–3200 cm⁻¹ corresponds to the O–H stretching vibrations from hydroxyl groups present in the 3,4-dihydroxy-1-butene (monomer) and Si–OH groups on the silica surface [121]. Absorption bands at 2920–2850 cm⁻¹ are attributed to the stretching vibrations of aliphatic C–H bonds. A peak near 1635 cm⁻¹ illustrates the stretching of C=C bonds, originating from unreacted vinyl groups in the monomer. Strong bands in the 1090–1000 cm⁻¹ range are characteristic of Si–O–Si asymmetric stretching, affirming the silica network. The band at 580–630 cm⁻¹ is attributed to Fe–O stretching vibrations, confirming the magnetic Fe₃O₄ core [122]. Following the imprinting with Artane as shown in Figure [3.13] (B), several changes are observed: The intensity of the broad O–H stretching band (~3400 cm⁻¹) is reduced, suggesting hydrogen bonding between the polymer matrix and the drug [123]. New absorption peaks appear at 1600–1500 cm⁻¹, corresponding to aromatic C=C and C–N stretching vibrations from Artane. Sharp peaks at 1450 cm⁻¹ and 1380 cm⁻¹ represent methyl bending vibrations, confirming the presence of the drug within the polymer [124,125]. The spectrum of the polymer after the extraction of Artane [3.13] (C) demonstrates the following: The broad O–H band (~3400 cm⁻¹) is restored, indicating the recovery of hydroxyl groups following drug removal. The characteristic peaks of the drug (1450–1380 cm⁻¹ and 1600–1500 cm⁻¹) are diminished or absent, confirming successful extraction. Peaks corresponding to Si–O–Si and Fe–O remain stable, indicating the structural integrity of the magnetic silica framework. The FTIR results confirm the stepwise process of polymer synthesis, drug imprinting, and subsequent removal. The chemical shifts and band modifications observed demonstrate the selective interaction between the polymer matrix and Artane, validating the successful formation of a

molecularly imprinted polymer suitable for drug recognition and extraction applications.

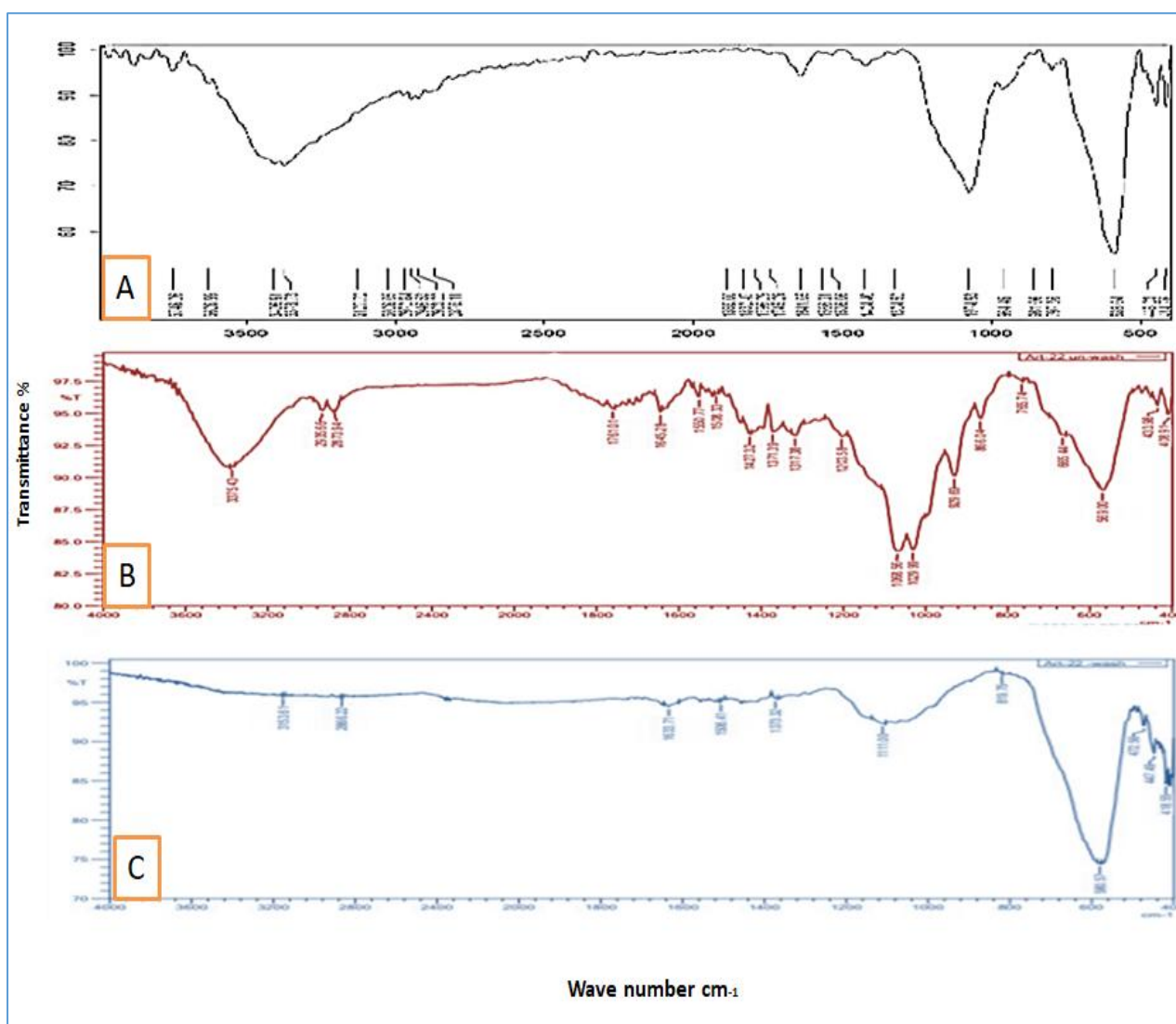


Figure [3.9] FT-IR spectra of Artane (A) MNIP₂ (B) unwashed ART- MMIP (C) washed MMIP

3.2.4.4. FTIR Spectra of Pre-MMIP and MNIP

The FTIR spectrum of the MNIP₂ as shown in figure [3.10] (A) reveals several characteristic peaks indicative of the successful functionalization of Fe₃O₄ nanoparticles with a silica shell and 3,4-dihydroxy-1-butene (DHB). A broad absorption band at 3366 cm⁻¹ corresponds to O–H stretching vibrations from hydroxyl groups present in both DHB and the silica surface. Peaks at 2946 cm⁻¹ and 2870 cm⁻¹ are associated with C–H stretching vibrations of aliphatic chains from the organic modifier. The strong absorption in the region of 1080–1020 cm⁻¹ is attributed to Si–O–Si stretching, confirming the presence of a silica layer. Meanwhile, the peaks at 586 cm⁻¹ and 470 cm⁻¹ are assigned to Fe–O stretching vibrations, indicative of the magnetite core. These observations collectively confirm the successful synthesis of the magnetic support [126]. The FTIR spectrum of the Pre-MMIP as shown in figure [3.14] (B) exhibits significant changes following the incorporation of pregabalin. A notable decrease in the O–H stretching intensity at 3366 cm⁻¹ illustrates the formation of hydrogen bonds between the functional monomers and the template molecule. New bands appearing in the 1702–1600 cm⁻¹ region can be attributed to C=O and N–H bending vibrations specific to pregabalin.. These findings confirm that successful imprinting occurred, and specific recognition sites were formed within the polymer matrix [127]. After template removal, the FTIR spectrum in Figure [3.14] (C) demonstrates the reappearance of the O–H band at 3430 cm⁻¹, indicating that the hydrogen-bonded functional groups were released, and the recognition sites became available again. The disappearance of drug-specific bands between 1700–1600 cm⁻¹ validates the efficient removal of pregabalin. Additionally, the band at 880 cm⁻¹ may reflect conformational changes in the silica network following washing, and the Fe–O and Si–O–Si bands regain their prominence, further confirming structural recovery of the polymer backbone. The FTIR data clearly distinguish between the non-imprinted, imprinted, and washed

states of the polymer. The spectral differences demonstrate the creation of specific binding sites during imprinting and the restoration of functional groups after template removal. This validates the material's potential for selective recognition and reuse in drug extraction application

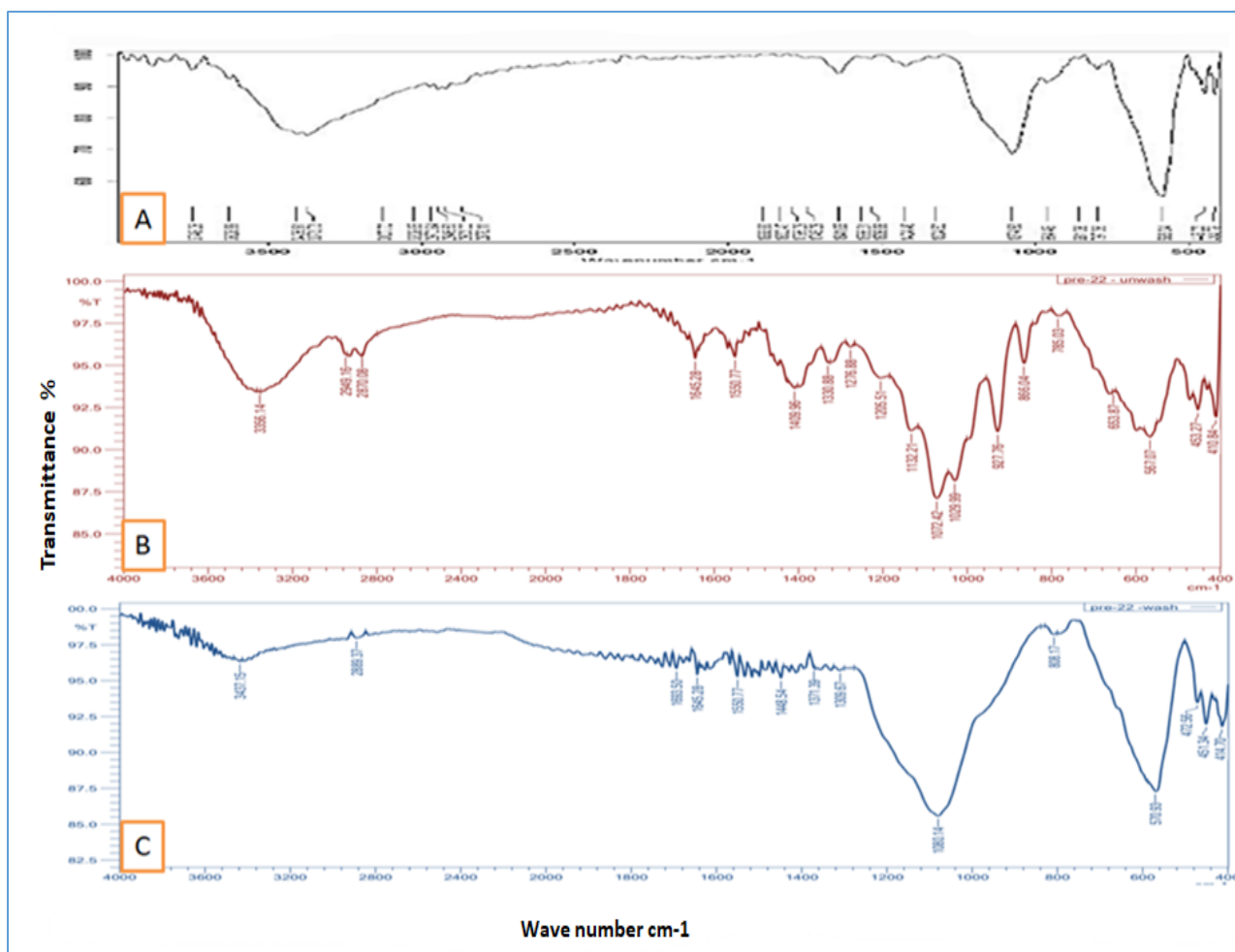


Figure [3.10] FT-IR spectra of Pregabalin (A) MNIP (B) unwashed MMIP (C) washed MMIP

3.2.5. Field emission Scanning Electron Microscope (FESEM) Analysis

3.2.5.1. FESEM of Her-MMIP and MNIP

FESEM were applied to study the morphological structures of MNIP₁, Her-MMIP (unwashed) and MMIP (washed) Figure [3.11] (A) demonstrates the surface structure of the raw polymer before any modification. The surface appears relatively smooth and homogeneous, indicating the pure nature of the polymer without any added materials or interactions. The average particle diameter ranges between 38.32 nm and 53.72 nm. This represents the original size of the unmodified polymer particles, showing a smooth and homogeneous surface morphology. Image (B) represents the polymer after being loaded with heroin. Distinct surface features, such as new formations or aggregates, can be observed. These changes suggest the successful loading of heroin onto the polymer, with the substance interacting with or embedding into the polymer matrix. The particles exhibit a significant increase in diameter, with values reaching up to 193.54 nm, while smaller particles measure 44.96 nm. This increase in size is attributed to the successful adsorption or encapsulation of heroin onto or within the polymer matrix. The noticeable change in diameter reflects the polymer's ability to effectively load the target compound. , Image (C) depicts the polymer after the heroin has been removed through a washing process. The surface structure appears to return to a state resembling that of the original non-imprinted polymer (A), though minor residual changes may still be present, likely due to the washing process [128] and the average diameter decreases to a range of 27.05 nm to 62.78 nm.

This reduction in size is indicative of the successful removal of heroin during the washing process. These figures demonstrate the polymer's ability to load and release heroin effectively. The observed changes in surface morphology during the loading process highlight the polymer's adaptability, while the return to a near-original state after washing illustrates effective removal of the loaded

substance. Such behavior underscores the polymer's potential for use in extraction of the drugs.

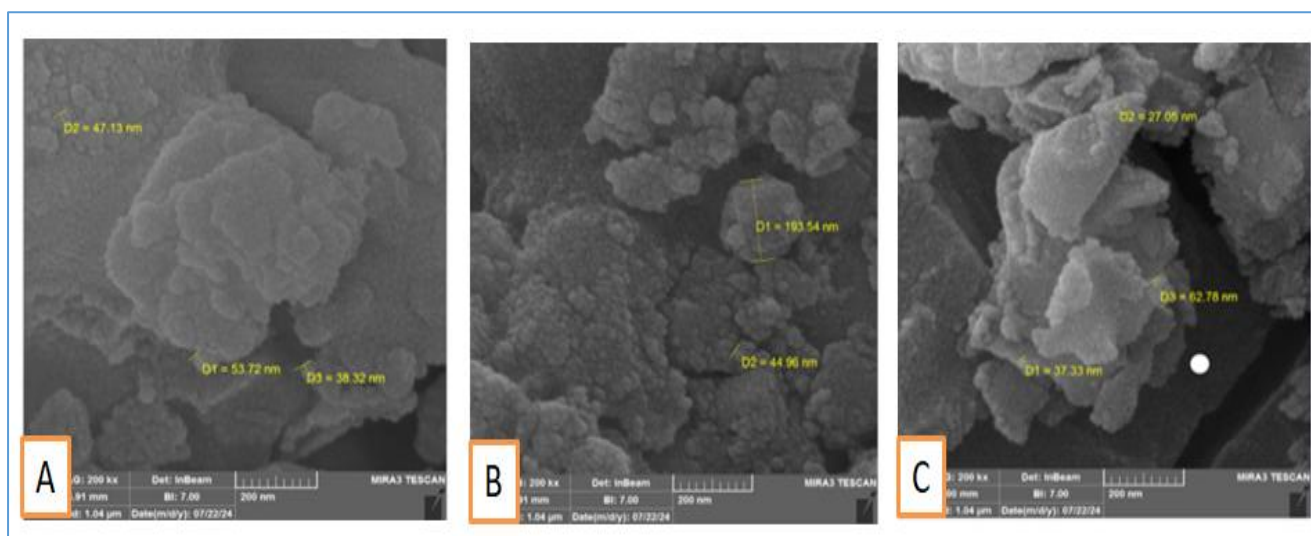


Figure [3.11] FESEM image of Heroin (A) MNIP (B) Her-MMIP and (C) MMIP

3.2.5.2. FESEM of AMP-MMIP and MNIP

Figure [3.12] presents the field-emission scanning electron microscopy (FESEM) images of the non-imprinted polymer and the molecularly imprinted polymer before and after removal of the template (amphetamine). The images clearly reveal significant differences in surface morphology and particle size as a consequence of the molecular imprinting process. The FESEM image in Figure [3.12A] shows that the non-imprinted polymer consists of relatively uniform, quasi-spherical particles with a narrow particle size distribution ranging from 38.22 to 55.72 nm. This homogeneous morphology is attributed to the absence of the template molecule during polymerization, which results in a compact polymeric network with limited agglomeration and without the formation of specific recognition cavities. Figure [3.12B]: Imprinted polymer loaded with amphetamine before washing.

As observed in Figure [3.12B], a pronounced increase in particle size and agglomeration is evident, with particle diameters ranging from 219.79 to 507.07

nm. This substantial enlargement in the apparent particle size is mainly due to the presence of amphetamine molecules within the polymeric matrix, which occupy the imprinting sites and act as temporary bridges between polymer chains. Consequently, a denser and less porous surface morphology is formed.

After the washing process and removal of the template, Figure[3.12C] shows a marked reduction in particle size, which ranges from 44.96 to 196.54 nm, accompanied by the appearance of surface cavities and increased roughness. This morphological change is attributed to the liberation of the imprinting sites and the formation of well-defined pores complementary in size and shape to the amphetamine molecule. The opening of these cavities reduces agglomeration and enhances the effective surface area. The FESEM observations in Figure[3.12] confirm that the presence of the template during polymerization leads to a significant increase in the apparent particle size due to agglomeration, whereas its removal results in a reorganized polymeric structure with accessible recognition cavities. These structural features provide strong evidence for the successful formation of molecularly imprinted sites and explain the improved selectivity of the imprinted polymer toward amphetamine [130].

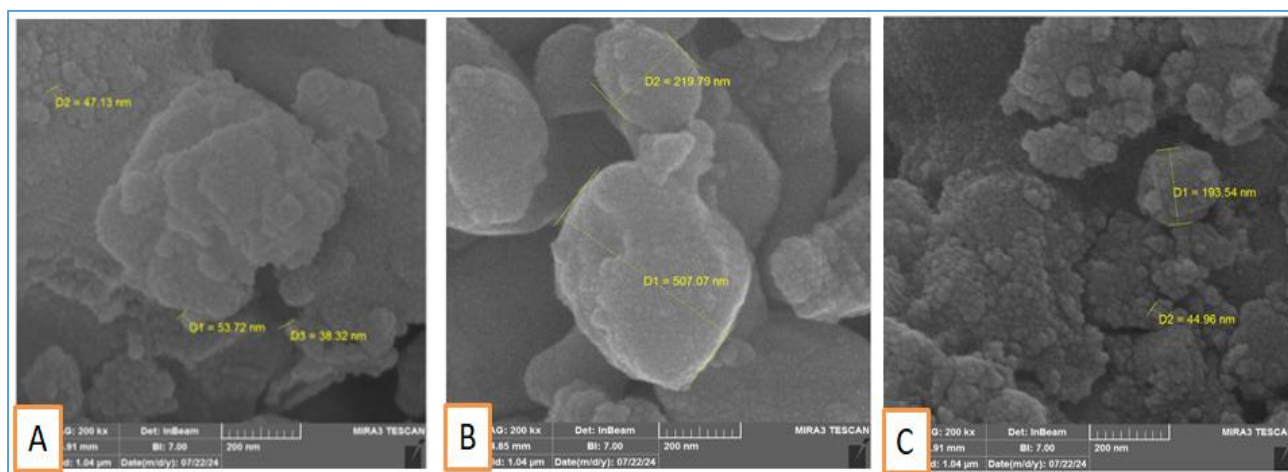


Figure [3.12] FESEM image of Amphetamine (A) MNIP (B) AMP-MMIP and (C) MMIP

3.2.5.3. FESEM of ART-MMIP and MNIP

Figure [3.13] shows the field-emission scanning electron microscopy (FESEM) images of the magnetic non-imprinted polymer (MNIP), the Artane-imprinted polymer before washing, and the imprinted polymer after removal of the Artane template. Clear variations in surface morphology, particle size, and agglomeration behavior are observed as a direct consequence of the molecular imprinting and template removal processes. As shown in Figure [3.13A], the MNIP consists of quasi-spherical particles with a relatively homogeneous distribution. The particle sizes range from 44.57 to 304.4 nm, indicating moderate agglomeration but an overall compact polymeric structure. The absence of a template molecule during polymerization leads to a dense matrix with smoother surface features and without the formation of specific recognition cavities.

Figure [3.13B] reveals a noticeable increase in particle size and agglomeration for the magnetic imprinted polymer loaded with Artane (ART-MMIP) prior to washing. The particle diameters range from 100.9 to 410.9 nm, reflecting the strong influence of the template molecules on particle growth and aggregation. The presence of Artane within the polymeric network promotes inter-particle bridging through non-covalent interactions, resulting in larger apparent particle sizes and a denser, less porous surface morphology.

After removal of the Artane template, Figure [3.13C] shows a reduction in agglomeration and a clearer definition of individual particles. The particle size distribution ranges from 127.7 to 369 nm, which is smaller and more uniform compared to the loaded imprinted polymer. In addition, the surface becomes rougher with the appearance of pores and cavities corresponding to the imprinted sites formed after template extraction. These structural changes indicate the successful creation of recognition cavities complementary to Artane in size and shape.

The FESEM results confirm that the incorporation of Artane during polymerization significantly increases the apparent particle size and agglomeration of the imprinted polymer, while subsequent template removal leads to partial structural relaxation and the formation of accessible imprinting cavities. The observed changes in particle size and surface morphology provide strong morphological evidence for the successful preparation of a molecularly imprinted polymer selective toward Artane[131].

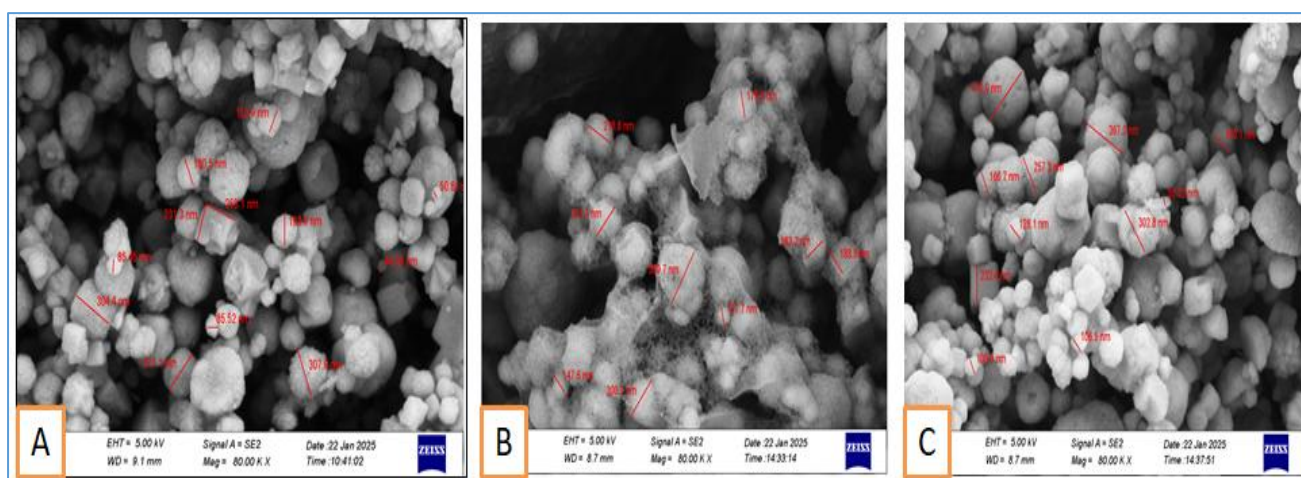


Figure [3.13] FESEM image of Artane (A) MNIP (B) ART-MMIP and (C) MMIP

3.2.5.4. FESEM of Pre-MMIP and MNIP

Figure [3.14] presents the field-emission scanning electron microscopy (FESEM) images of the magnetic non-imprinted polymer, the magnetic molecularly imprinted polymer loaded with pregabalin before washing, and the magnetic imprinted polymer after removal of the pregabalin template. The images reveal clear differences in surface morphology, particle size distribution, and agglomeration behavior resulting from the molecular imprinting and template removal processes.

As shown in Figure[3.14A], the magnetic non-imprinted polymer consists of quasi-spherical particles with a relatively heterogeneous size distribution, ranging

from 44.57 to 304.4 nm. This wide size range indicates partial agglomeration of the polymer-coated magnetic particles, while the overall structure remains relatively compact. The absence of the template molecule during polymerization prevents the formation of specific recognition cavities, leading to a denser polymeric matrix.

Figure [3.14B] shows a noticeable increase in particle agglomeration and morphological irregularity, with particle sizes ranging from 68.36 to 350.7 nm. This behavior is attributed to the presence of pregabalin molecules within the polymeric network, which occupy the imprinting sites and promote inter-particle interactions through non-covalent forces. Consequently, the apparent particle size increases and the surface appears denser with reduced visible porosity.

After removal of pregabalin by the washing process, Figure [3.14C] reveals a reduction in agglomeration and improved definition of individual particles. The particle size distribution decreases to a range of 45.98 to 267.0 nm, accompanied by increased surface roughness and the appearance of pores and cavities. These features correspond to the liberated imprinting sites formed after template extraction and are complementary in size and shape to the pregabalin molecule.

The FESEM observations in Figure [3.14]confirm that the incorporation of pregabalin during polymerization significantly affects particle growth and agglomeration in the magnetic imprinted polymer. Subsequent template removal leads to structural reorganization and the formation of accessible molecularly imprinted cavities, providing strong morphological evidence for the successful synthesis of a pregabalin-selective magnetic molecularly imprinted polymer.

[132].

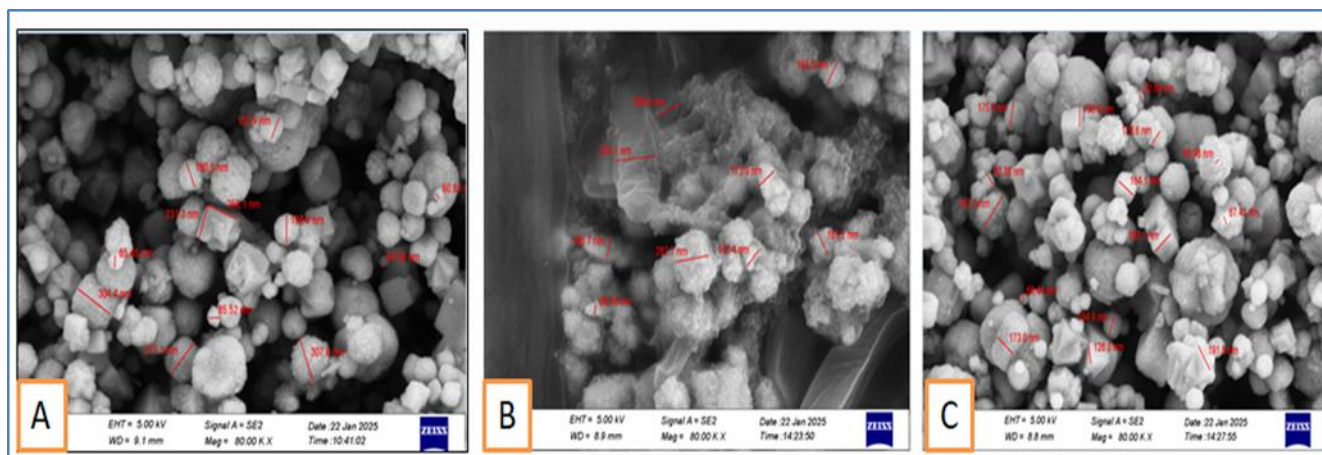


Figure [3.14] FESEM image of Pregabalin (A) MNIP (B) Pre-MMIP and (C) MMIP

3.2.6. Nitrogen adsorption-desorption analysis

3.2.6.1. Surface Area Analyzer of MMIP for Heroin and Amphetamine

Nitrogen adsorption–desorption analysis was carried out to evaluate the textural properties of the magnetic molecularly imprinted polymers (MMIPs) designed for the selective recognition of heroin and amphetamine. According to the Brunauer–Emmett–Teller (BET) method, the heroin-imprinted MMIP exhibited a specific surface area of $123.4 \text{ m}^2 \text{ g}^{-1}$, a total pore volume of $0.063973 \text{ cm}^3 \text{ g}^{-1}$, and an average pore diameter of 1.29 nm , which clearly places the material within the microporous range based on the International Union of Pure and Applied Chemistry (IUPAC) classification.

Despite this numerical microporous classification, the nitrogen adsorption–desorption isotherm of the heroin-imprinted MMIP displayed Type IV behavior with an H3-type hysteresis loop, as shown in Figure [3.15A]. This behavior is not contradictory to the microporous nature of the material but rather reflects the presence of pore structure, in which microporous molecular recognition sites coexist with interparticle mesoporous slit-shaped voids formed by the aggregation of polymer-coated magnetic particles. These interparticle voids influence adsorption kinetics without significantly altering the BET-calculated

average pore diameter and do not represent true macropores. In contrast, the amphetamine-imprinted MMIP exhibited a lower specific surface area of $8.9352 \text{ m}^2 \text{ g}^{-1}$, accompanied by a higher pore volume ($0.095316 \text{ cm}^3 \text{ g}^{-1}$) and a larger average pore diameter of 42.67 nm , which clearly classifies the material as mesoporous in both numerical and adsorption behavior terms. The corresponding adsorption–desorption isotherm (Figure 3.16A) also showed Type IV behavior with an H3 hysteresis loop, confirming the presence of slit-shaped pores and an open porous framework that facilitates molecular diffusion within the polymer matrix. Furthermore, the linear BET plots presented in Figures (3.16B) and (3.20B) demonstrated excellent linearity with high correlation coefficients ($R^2 = 0.999$), confirming the suitability of the BET model for describing the adsorption behavior of both materials. The close overlap between the adsorption and desorption branches indicates a relatively homogeneous distribution of accessible pores within the polymer matrices. Overall, these findings validate the application of the BET method for evaluating surface area and porosity and are consistent with recent studies published on the use of MMIPs in drug extraction[134]

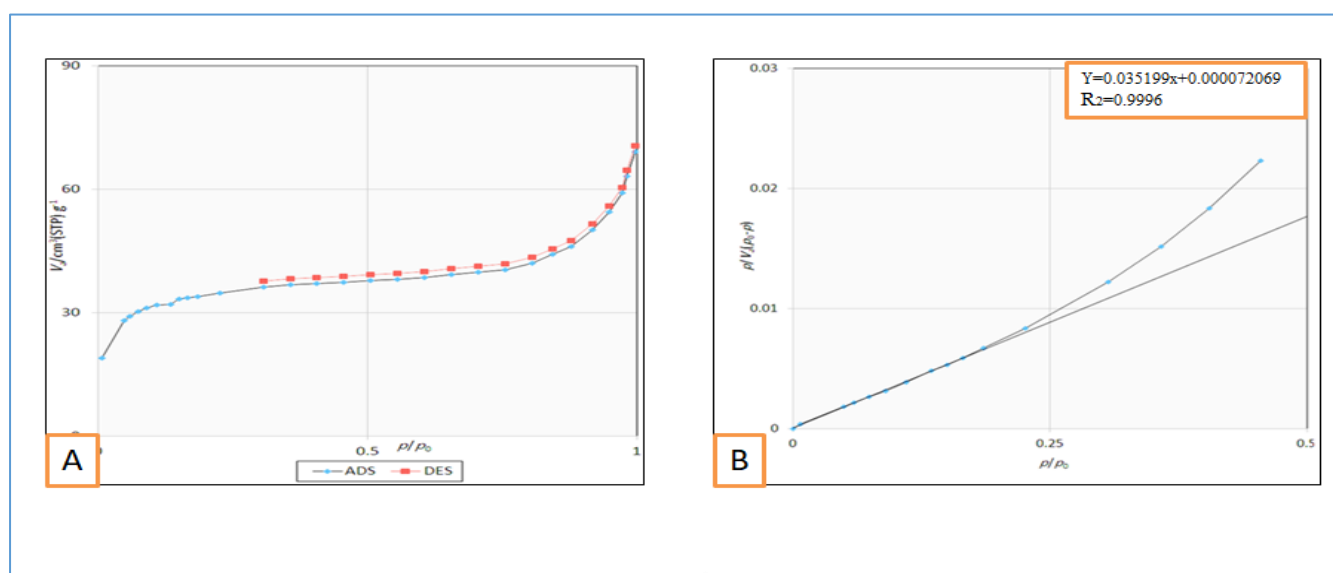


Figure [3.15] N_2 adsorption-desorption isotherm of the MMIP for heroin

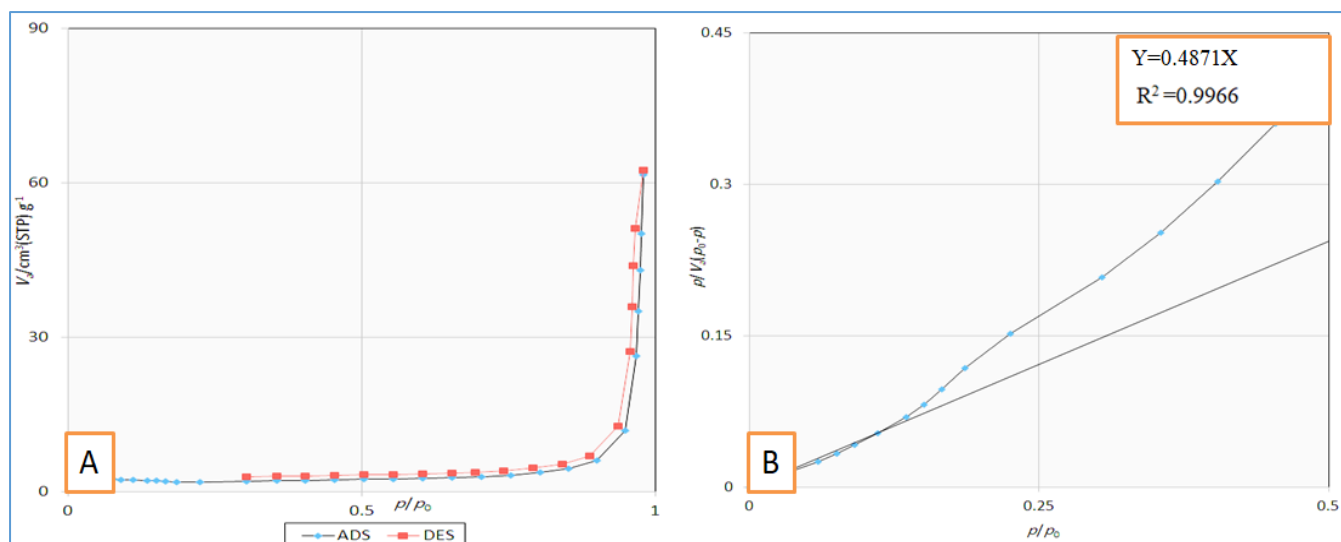


Figure [3.16] N_2 adsorption-desorption isotherm of the MMIP for Amphetamine

3.2.6.2. Surface Area Analyzer of MMIP for Artane and Pregabalin

The Brunauer–Emmett–Teller (BET) analysis was employed in order to evaluate the surface textural properties of the synthesized magnetic molecularly imprinted polymers (MMIPs) designed for the selective extraction of Artane and Pregabalin. The results, as illustrated in Figures [3.17] and [3.18], the N_2 adsorption-desorption isotherms demonstrated typical Type IV behavior with H3-type hysteresis loops which are characteristic of mesoporous materials. The linear regression equations derived from the BET plots, $Y = 0.2584X + 0.000069622$ ($R^2 = 0.9996$) for Artane-MMIP and $Y = 0.3422X$ ($R^2 = 0.9994$) for Pregabalin-MMIP, confirm the significant linearity and reliability of the data,

The Artane-MMIP exhibited a specific surface area of $16.837 \text{ m}^2 \cdot \text{g}^{-1}$, a total pore volume of $0.03709 \text{ cm}^3 \cdot \text{g}^{-1}$, and an average pore diameter of 8.8118 nm . In contrast, the Pregabalin-MMIP displayed a slightly lower specific surface area of $12.717 \text{ m}^2 \cdot \text{g}^{-1}$ but a significantly larger total pore volume of $0.1252 \text{ cm}^3 \cdot \text{g}^{-1}$ and an average pore diameter of 39.383 nm . These findings, supported by the isotherm plots, highlight the mesoporous nature of both polymers, with pore diameters falling within the optimal range of $2\text{--}50 \text{ nm}$. Such a structure is conducive to the efficient diffusion and entrapment of small to medium-sized

drug molecules within the polymer matrix [135]. The moderately significant surface areas observed for both MMIPs ensure the availability of sufficient active binding sites, which are critical for enhancing molecular recognition and adsorption processes, particularly in complex biological matrices such as blood and urine [136]. The Pregabalin-MMIP's notably larger pore volume and diameter, as evidenced by the isotherm data, suggest a more open and accessible porous framework. This structural feature may enhance adsorption kinetics. Conversely, the Artane-MMIP's tighter mesoporous structure, reflected in its smaller pore volume and diameter, may promote selective adsorption through stronger molecular interactions within confined pore environments. Collectively, the BET results, corroborated by the isotherm plots, validate the successful imprinting strategy. The interplay between surface area, pore volume, and pore size distribution is a pivotal factor governing the extraction efficiency and selectivity of molecularly imprinted polymers.

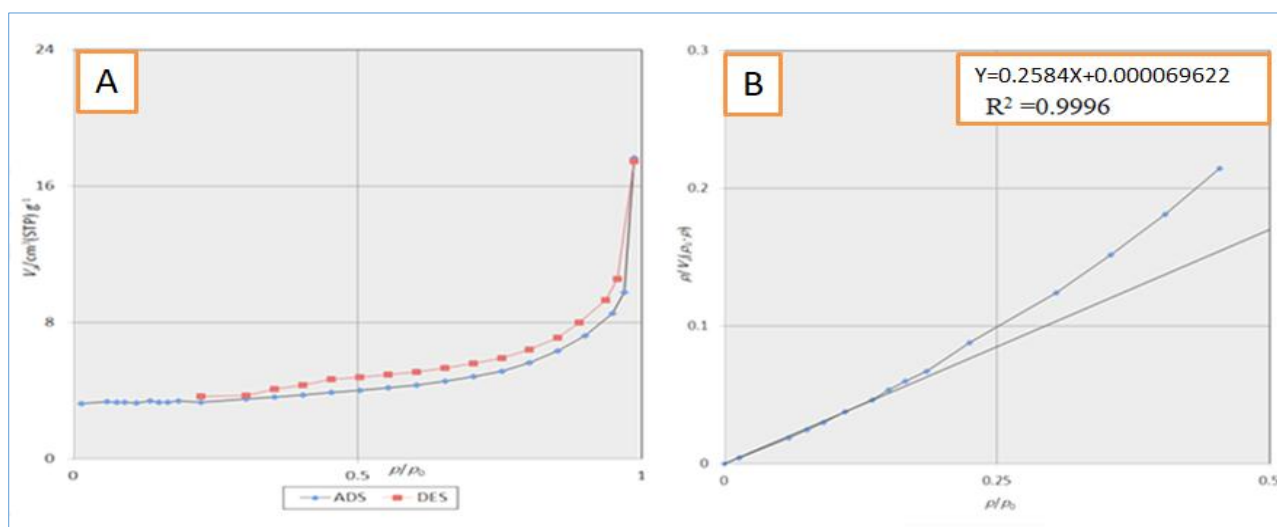


Figure [3.17] N_2 adsorption-desorption isotherm of the MMIP for Artane

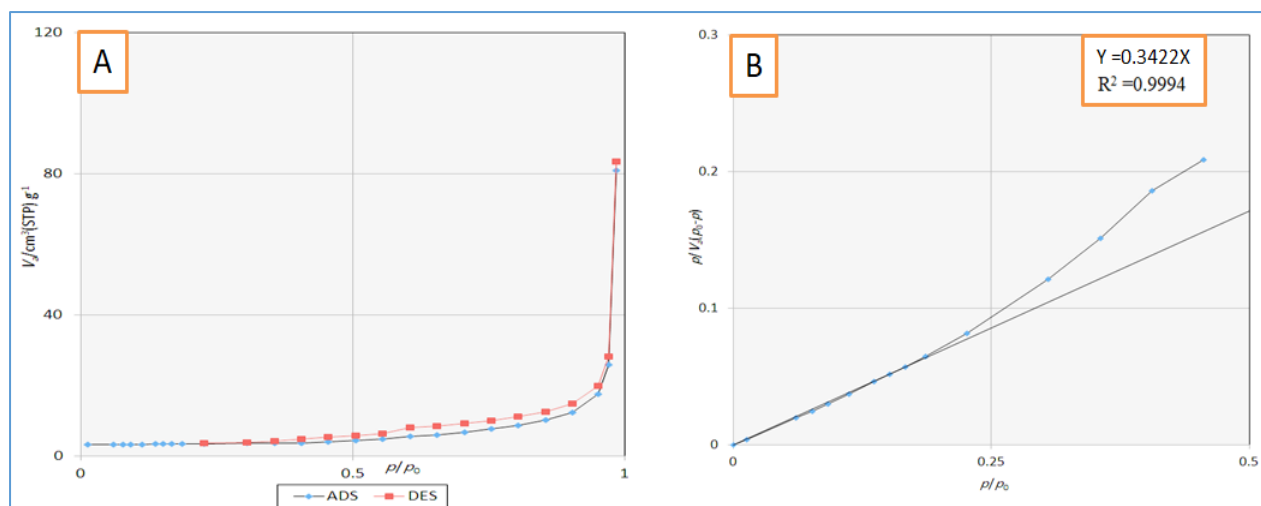


Figure [3.18] N_2 adsorption-desorption isotherm of the MMIP for Pregabalin

3.3. Enhancement of the extraction parameters

3.3. 1. Enhancement of the extraction parameters of Her-MMIP

3.3.1.1. Equilibrium time impact

The equilibrium time for the prepared (MMIP) was investigated as an effective adsorbent for the Heroin solution the experiments were performed under ideal conditions. Figure [3.19] illustrates the impact of contact duration (10–130 min) on the adsorption process. Adsorption efficiency was noted to improve over time, achieving equilibrium at 90 minutes, a process expedited by the availability of active sites on the composite's surface. The adsorption process commenced rapidly, as the active sites were immediately accessible for contact. As equilibrium was attained, the adsorption rate diminished due to the saturation of the adsorbent surface with Heroin molecules. [137].

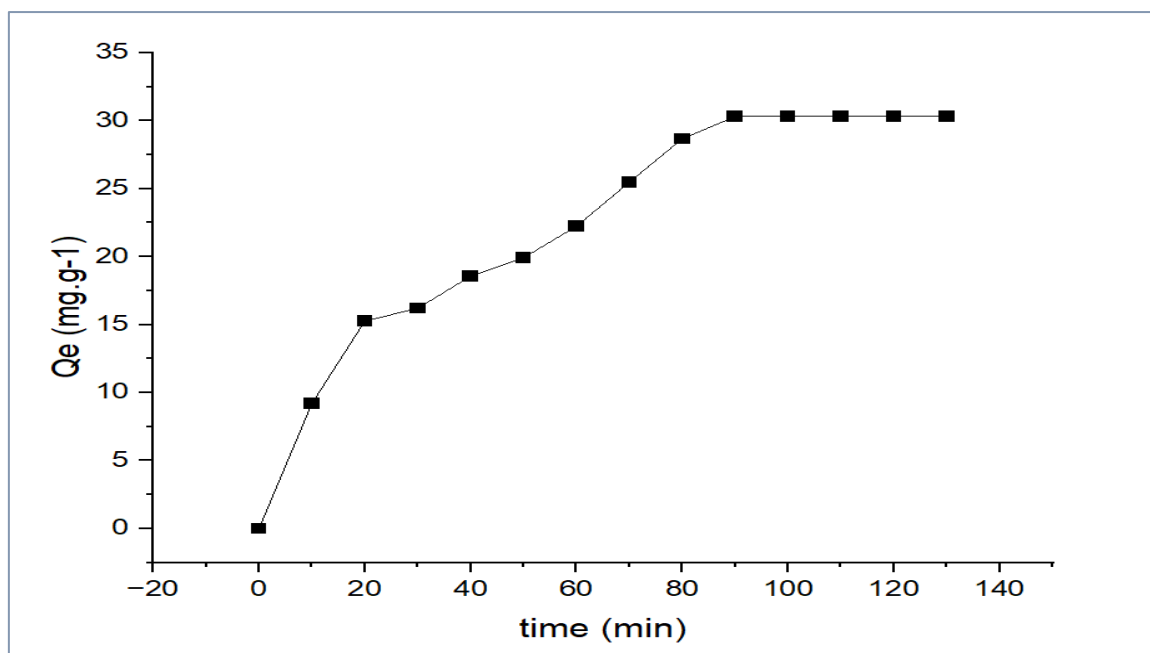


Figure [3.19] Effect of contact time on the adsorption capacity of Heroin on to Her-MMIP

3.3.1.2. Effect of the amount of Her-MMIP

The influence of the adsorbent surface weight (Her MMIP) on the adsorption process from an aqueous solution of Heroin was examined through the use of varying weights (0.01-0.05 g) and a solution concentration of (100 mg.L⁻¹) at a temperature of 25°C. Figure [3.20] illustrates that an adsorbent weight of (0.01 g) attained the maximum quantity of adsorbed material, signifying the accessibility of all active sites for adsorption on the surface. Nevertheless, following the augmentation of the adsorbent weight, a reduction in the quantity of adsorbed material on the surface was observed [138]. This can be ascribed to the overlapping of active sites on the adsorbent surface, leading to the formation of clusters that diminish the adsorbent surface area due to the aggregation of active sites, the introduction of smaller particles, and their interaction with the adsorbent surface [139].

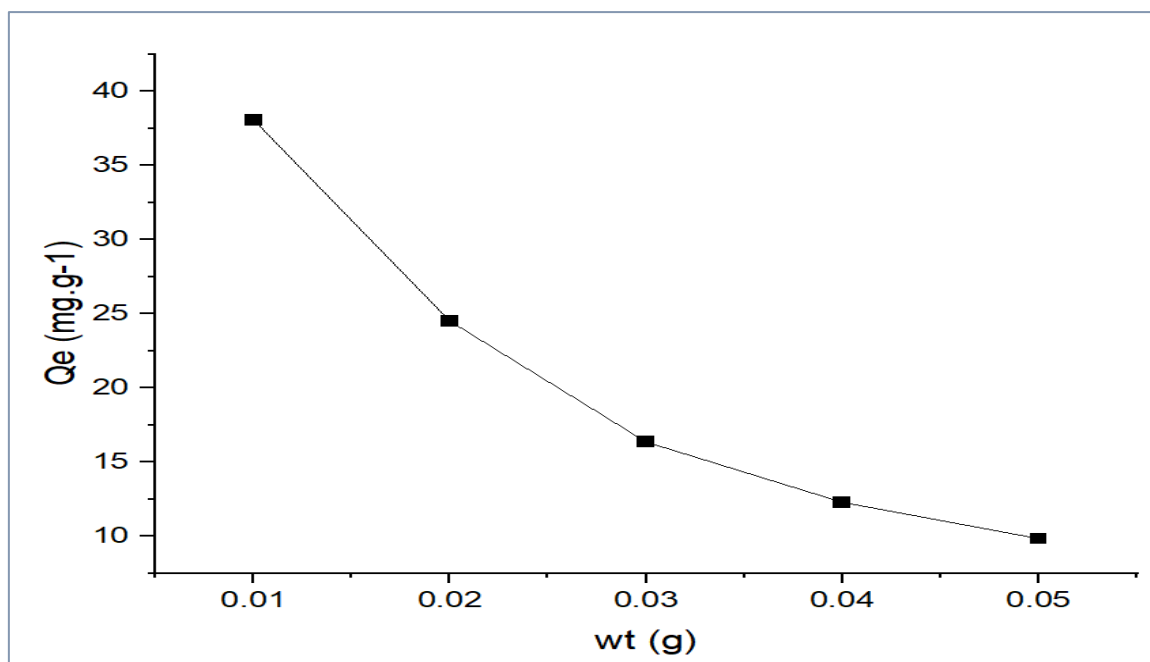


Figure [3.20] Effect of weight of Her-MMIP on the adsorption capacity of Heroin solution

3.3.1.3. Effect of pH solution

Figure [3.21] illustrates the effect of solution pH on the equilibrium adsorption capacity (q_e) of heroin onto the HER-MMIP synthesized using 2-acetamidoacrylic acid as the functional monomer. As shown in the figure, the adsorption capacity is strongly influenced by the pH of the solution, exhibiting an initial increase followed by a gradual decrease.

At pH 3, the adsorption capacity is relatively low, with a q_e value of approximately $42.1 \text{ mg}\cdot\text{g}^{-1}$. This behavior can be attributed to the protonation of heroin molecules under acidic conditions, as well as the protonation of the amide functional groups ($-\text{CONH}-$) on the polymer surface. Such protonation weakens the hydrogen-bonding interactions formed during the molecular imprinting process, thereby reducing the binding efficiency of heroin within the imprinted cavities.

When the pH is increased to pH 4, the q_e value rises to about $42.7 \text{ mg}\cdot\text{g}^{-1}$, indicating improved adsorption conditions due to partial deprotonation and enhanced stability of non-covalent interactions between heroin molecules and the imprinted recognition sites.

The maximum adsorption capacity is observed at pH 5, where q_e reaches approximately $43.2 \text{ mg}\cdot\text{g}^{-1}$. This pH value represents the optimum adsorption condition, under which the amide groups of the 2-acetamidoacrylic acid (monomer) are in a favorable ionization state to form strong and directional hydrogen bonds with heroin molecules. This result confirms the high structural and functional complementarity of the imprinted sites toward the target molecule.

At higher pH values, a noticeable decrease in q_e is observed. At pH 8, the adsorption capacity declines to around $41.6 \text{ mg}\cdot\text{g}^{-1}$, which can be attributed to the reduced stability of hydrogen bonds in alkaline media and the competitive effect of hydroxide ions for the active binding sites.

This decreasing trend continues at pH 9, where q_e further decreases to approximately $40.9 \text{ mg}\cdot\text{g}^{-1}$, indicating that strongly alkaline conditions are unfavorable for heroin adsorption due to disruption of the non-covalent interactions responsible for stabilizing the polymer–heroin complex.

Overall, Figure (3.21) demonstrates that the optimum adsorption performance of HER-MMIP occurs at pH 5, and that the adsorption mechanism is predominantly governed by hydrogen-bonding interactions provided by the 2-acetamidoacrylic acid functional monomer, confirming the effectiveness of the molecular imprinting strategy for selective heroin extraction [140,141].

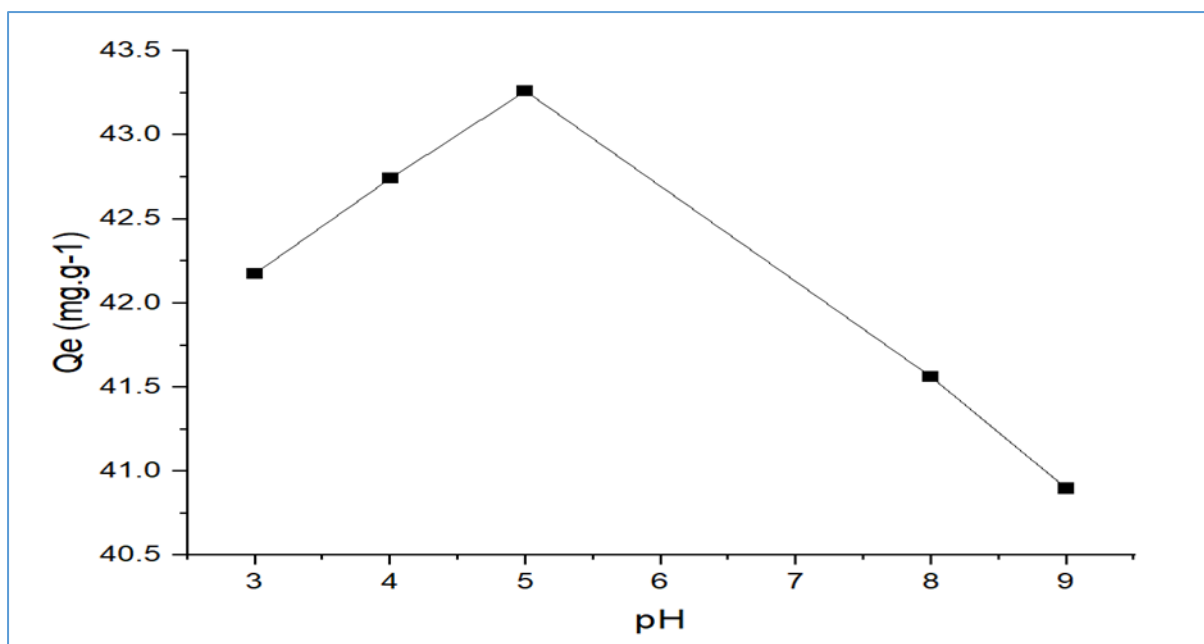


Figure [3.21] Effect of pH solution on the adsorption capacity of Heroin on to Her-MMIP

3.3.1.4. Effect of Temperature:

Figure [3.22] illustrates the effect of temperature on the equilibrium adsorption capacity (q_e) of heroin onto the HER-MMIP within the temperature range of 25–45 °C. As clearly observed, the adsorption capacity decreases progressively with increasing temperature, indicating a strong temperature dependence of the adsorption process.

At 25 °C, the adsorption capacity reaches its maximum value of approximately **65 mg·g⁻¹**, reflecting favorable adsorption conditions at lower temperatures. However, as the temperature increases to 30 °C and 35 °C, the q_e values decrease to about **55 mg·g⁻¹** and **45 mg·g⁻¹**, respectively. This downward trend continues at higher temperatures, where q_e declines to nearly **35 mg·g⁻¹** at 40 °C and further to around **30 mg·g⁻¹** at 45 °C.

The observed decrease in adsorption capacity with rising temperature suggests that the adsorption of heroin onto HER-MMIP is an **exothermic process**. At elevated temperatures, the kinetic energy of heroin molecules increases, which

enhances their tendency to escape from the imprinted binding sites, thereby promoting desorption. In addition, the non-covalent interactions governing the adsorption mechanism—particularly hydrogen bonding between the functional groups of the polymer and the oxygen-containing groups of heroin—become progressively weaker as temperature increases.

Consequently, the stability of the polymer–heroin complexes formed within the imprinted cavities is reduced at higher temperatures, leading to a lower adsorption capacity. These findings indicate that lower temperatures favor the formation and stabilization of specific interactions within the molecularly imprinted sites, thereby enhancing adsorption efficiency.

Overall, the results presented in Figure [3.22] confirm that temperature plays a critical role in controlling the adsorption behavior of HER-MMIP, and that optimal adsorption performance is achieved at relatively low temperatures, consistent with the exothermic nature of the adsorption process. [139].

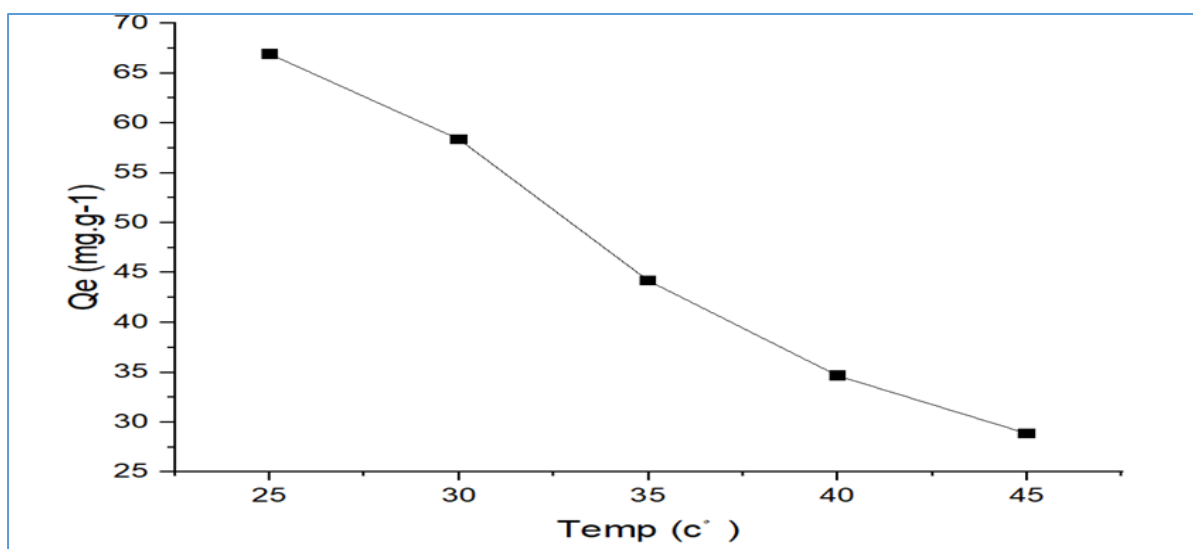


Figure [3.22] Effect of temperature on the adsorption capacity of Heroin on to Her-MMIP

3.3.1.5. Effect of sample volume

Figure [3.23] illustrates the effect of sample volume (V) on the recovery percentage (Recovery %) of heroin extracted using the HER-MMIP. As observed from the curve, the recovery percentage varies markedly with changes in sample volume, showing an increasing trend up to an optimum value, followed by a gradual decline at larger volumes.

At a **sample volume of 2 mL**, the recovery percentage is relatively low (approximately **60%**). This can be attributed to the insufficient amount of heroin available to fully interact with the imprinted recognition sites of the polymer, resulting in incomplete utilization of the available adsorption capacity.

When the sample volume is increased to **3 mL**, the recovery rises to about **70%**, owing to the higher amount of target analyte present in the solution, which enhances the probability of heroin molecules reaching and occupying the specific binding sites within the polymer.

The **maximum recovery** is achieved at a **sample volume of 5 mL**, reaching approximately **92%**, indicating that this volume represents the **optimal sample volume**. Under these conditions, an appropriate balance is established between the amount of heroin in solution and the number of active imprinted sites in the HER-MMIP, enabling efficient and selective adsorption.

Further increasing the sample volume to **8 mL** leads to a decrease in recovery to around **75%**. This reduction is mainly due to the onset of saturation of the adsorption sites, in addition to a possible decrease in effective contact time between the polymer and heroin molecules as the solution volume increases.

This decreasing trend continues at a **sample volume of 10 mL**, where the recovery drops to approximately **70%**, indicating that larger sample volumes result in dilution of the target analyte relative to the fixed number of available imprinted sites, thereby reducing extraction efficiency.

Overall, Figure (3.23) confirms that **sample volume has a direct influence on extraction efficiency**, and that using an optimal sample volume of **5 mL** yields the highest recovery of heroin when employing the HER-MMIP, reflecting the efficiency of the imprinted recognition sites and the limitations of their adsorption capacity [142] .

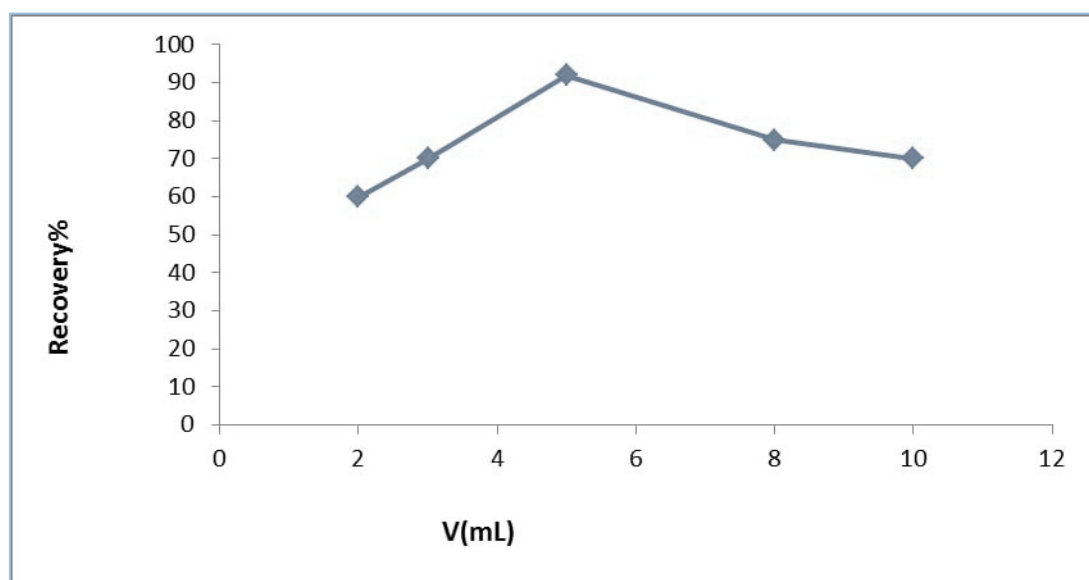


Figure [3.23] Effect of sample volume on the Recovery percentage of heroin using Her-MMIP

3.3.2. Enhancement of the extraction parameters of AMP-MMIP

3.3.2.1. Equilibrium time impact

The equilibrium time for the synthesized magnetic molecularly imprinted polymer (MMIP) was examined as an efficient adsorbent for the Amphetamine solution.. Figure [3.24] depicts the effect of contact duration (10–160 min) on the adsorption process. The adsorption effectiveness improved over time, reaching equilibrium at (120 min) facilitated by the presence of active sites on the composite's surface [143]. The adsorption process initiated swiftly, as the active sites were readily available for interaction. Upon reaching equilibrium, the adsorption rate decreased due to the saturation of the adsorbent surface with Amphetamine molecules [144].

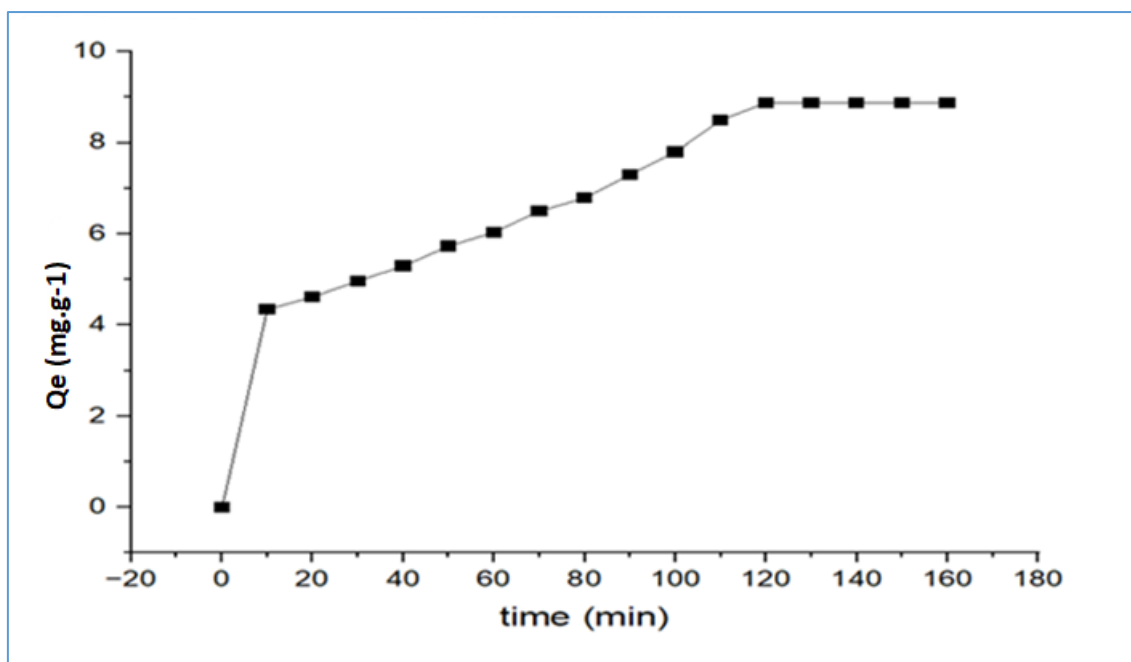


Figure [3.24] Effect of contact time on the adsorption capacity of Amphetamine on to AMP-MMIP

3.3.2.2. Effect of the amount of AMP-MMIP:

The effect of adsorbent dosage on the adsorption capacity of the prepared MMIP was investigated in the range of 0.01–0.05 g. As shown in the figure[3.25], the adsorption capacity (Q_e) exhibited an inverse relationship with the adsorbent mass, where the highest adsorption capacity was achieved at the lowest dosage (0.01 g), followed by a gradual decrease with increasing adsorbent amount.

This behavior is commonly observed in adsorption systems and can be attributed to the distribution of a fixed amount of analyte over a larger number of available binding sites at higher adsorbent dosages. At low adsorbent mass, the ratio of analyte molecules to active sites is high, resulting in greater occupation of the specific imprinted cavities and consequently higher adsorption capacity per unit mass. Conversely, increasing the adsorbent dosage introduces excess binding sites relative to the available analyte molecules, leading to partial site utilization and a reduction in the calculated adsorption capacity ($\text{mg} \cdot \text{g}^{-1}$).

In addition, at higher adsorbent dosages, particle aggregation and overlapping of active sites may occur, which can reduce the effective surface area accessible for adsorption. Therefore, 0.01 g was considered the optimal adsorbent dosage, providing the maximum adsorption capacity under the studied conditions [145].

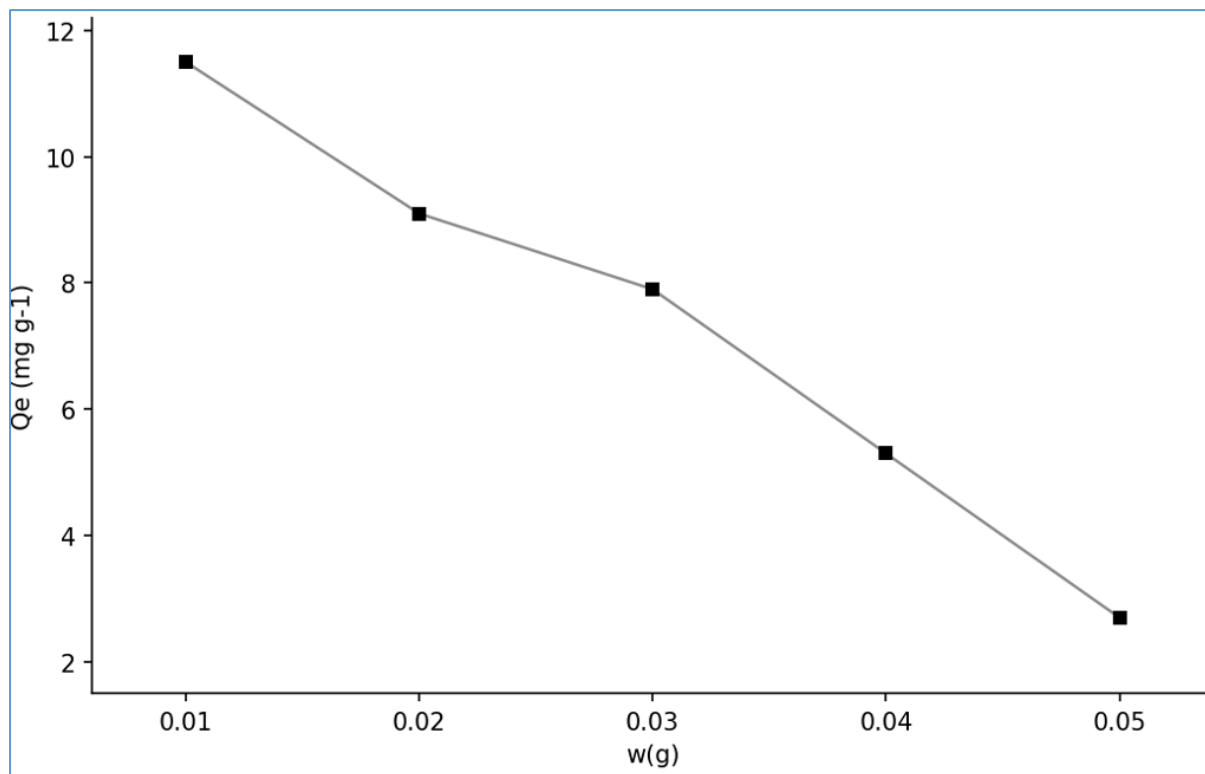


Figure [3.25] Effect of weight of AMP-MMIP on the adsorption capacity of Amphetamine solution

3.3.2.3 .Effect of pH solution

Figure [3.26] demonstrates the pronounced influence of sample pH on the adsorption capacity (Q_e) of amphetamine onto the MMIP. At low pH values (2–4), the carboxyl functional groups ($-\text{COOH}$) on the polymer surface are predominantly protonated, resulting in reduced surface negativity and weakened electrostatic interactions with amphetamine molecules. In addition, excess H^+ ions compete with the target molecules for the available binding sites, leading to low adsorption capacity.

At near-neutral pH (around pH 7), the carboxyl groups are deprotonated to COO^- , enhancing the negative charge of the polymer surface. Simultaneously, amphetamine molecules exist mainly in their protonated form (NH_3^+), which strengthens electrostatic attraction as well as non-covalent interactions within the molecularly imprinted cavities. Consequently, the maximum adsorption capacity is achieved at this pH value.

Under alkaline conditions (pH 8–9), partial deprotonation of amphetamine reduces its positive charge, thereby weakening its interaction with the negatively charged polymer surface. Moreover, the presence of excess OH^- ions may disturb the stability of the binding interactions, resulting in a decline in adsorption capacity [146].

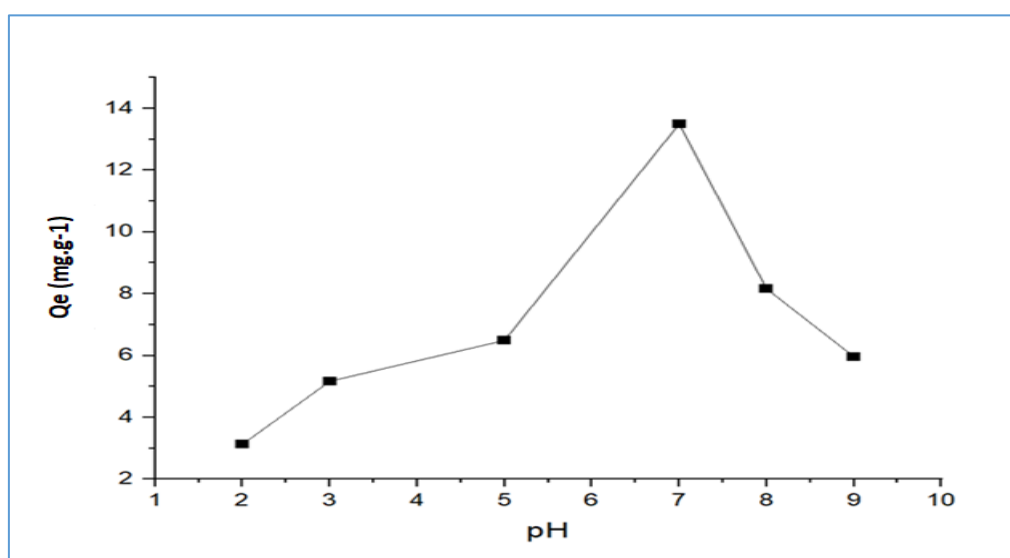


Figure [3.26] Effect of pH solution on the adsorption capacity of Amphetamine on to AMP-MMIP

3.3.2.4. Effect of Temperature:

Temperature exerts a substantial influence on the adsorption process. The effect of temperature was analyzed within the range of 25–45°C. The data illustrated in Figure [3.27] demonstrate that the adsorption capacity declines as temperature increases, indicating that the adsorption process is exothermic. The

decrease in adsorbate quantity is attributed to the heightened kinetic energy of the adsorbate molecules at elevated temperatures, resulting in their desorption from the adsorbent surface. [139].

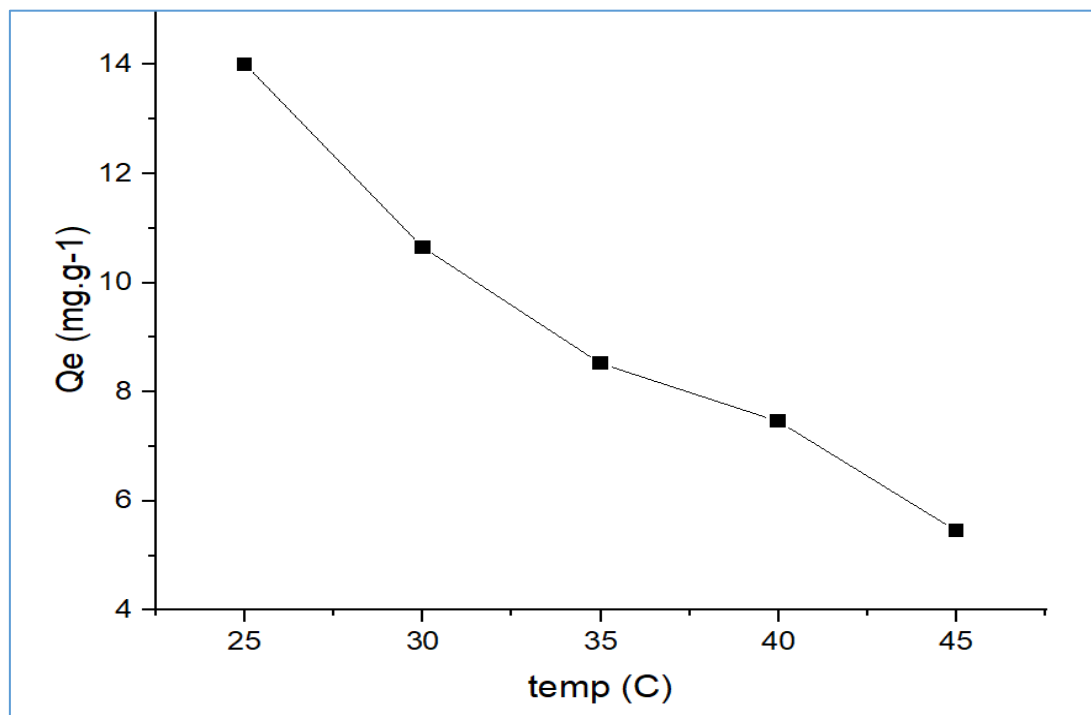


Figure [3.27] Effect of temperature on the adsorption capacity of Amphetamine on to AMP-MMIP

3.3.2.5. Effect of sample volume:

The selection of an appropriate sample volume is a critical consideration in the study. Five sample volumes (2.0, 3.0, 5.0, 8.0, and 10.0 mL) were assessed. Figure [3.28] illustrates a recovery rate of 93.4% for Amphetamine with a sample volume of 10 mL. An increase in sample volume was seen to correlate with an extended extraction time required to attain equilibrium. Thus, a sample volume of 10 mL was allocated for subsequent investigations in practical applications and real sample analysis.

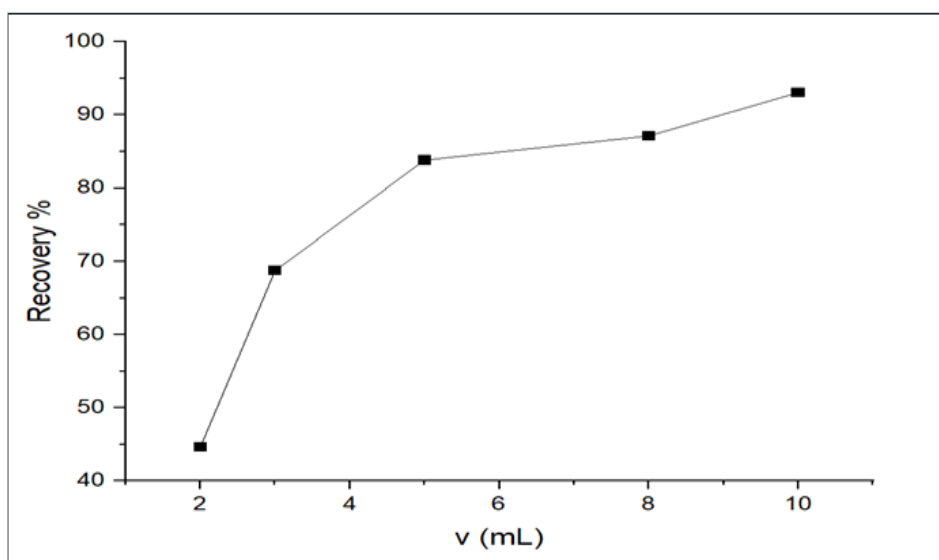


Figure [3.28] Effect of sample volume on the Recovery percentage of Amphetamine using AMP-MMIP

3.3.3. Enhancement of the extraction parameters of ART-MMIP

3.3.3.1. Equilibrium time impact

The equilibrium time for the produced magnetic molecularly imprinted polymer (MMIP) was assessed as an effective adsorbent for the Artane solution. Figure [3.29] illustrates the impact of contact period (10–90 minutes) on the adsorption process. The adsorption efficiency enhanced over time, achieving equilibrium at 60 minutes due to the availability of active sites on the composite's surface. The adsorption process commenced rapidly, as the active sites were readily accessible for contact. Upon achieving equilibrium, the adsorption rate diminished due to the saturation of the adsorbent surface with Artane molecules.

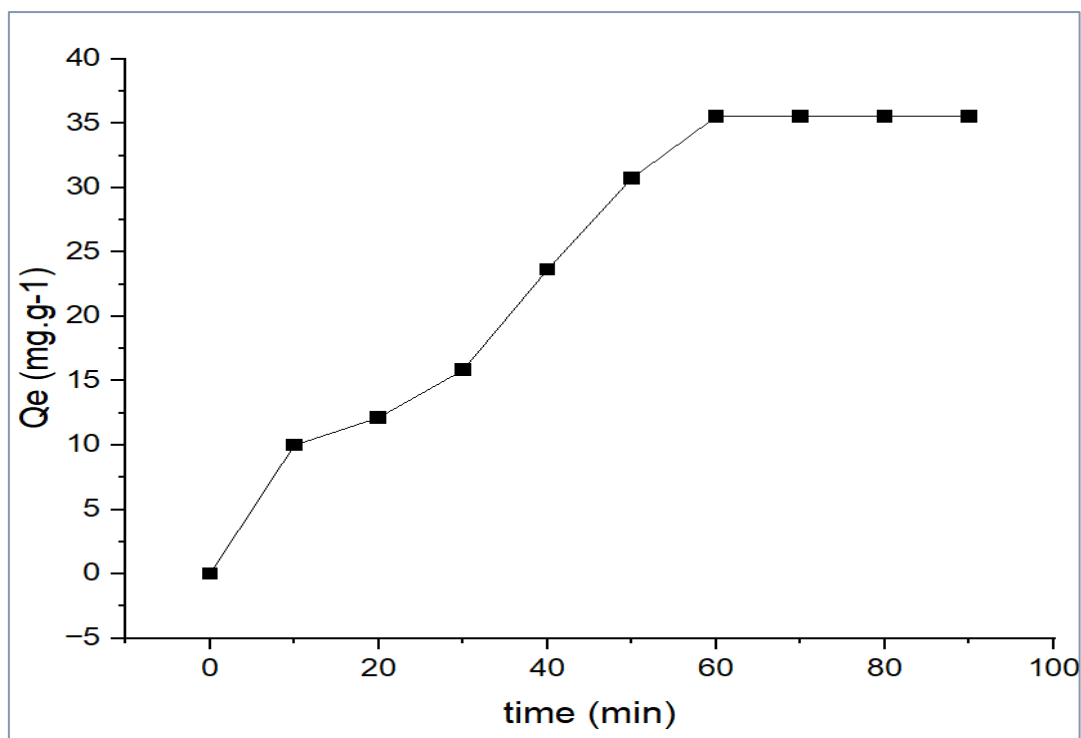


Figure [3.29] Effect of contact time on the adsorption capacity of Artane on to ART-MMIP

3.3.3.2. Effect of the amount of ART-MMIP:

The effect of varying the weight of the adsorbent, specifically ART- MMIP, on the adsorption efficiency from an aqueous Artane solution was systematically investigated through the use of weights ranging from 0.01 to 0.05 grams at a constant concentration of 50mg.L^{-1} and a temperature of 25°C . As depicted in Figure [3.30] the highest adsorption capacity was observed at an adsorbent weight of 0.01 g, indicating the optimal availability and utilization of active sites on the adsorbent surface. However, as the adsorbent weight increased beyond this point, a notable decline in adsorption capacity was observed. This reduction can be attributed to the phenomenon of active site overlap and particle aggregation, which effectively diminishes the accessible surface area for adsorption [147,148].

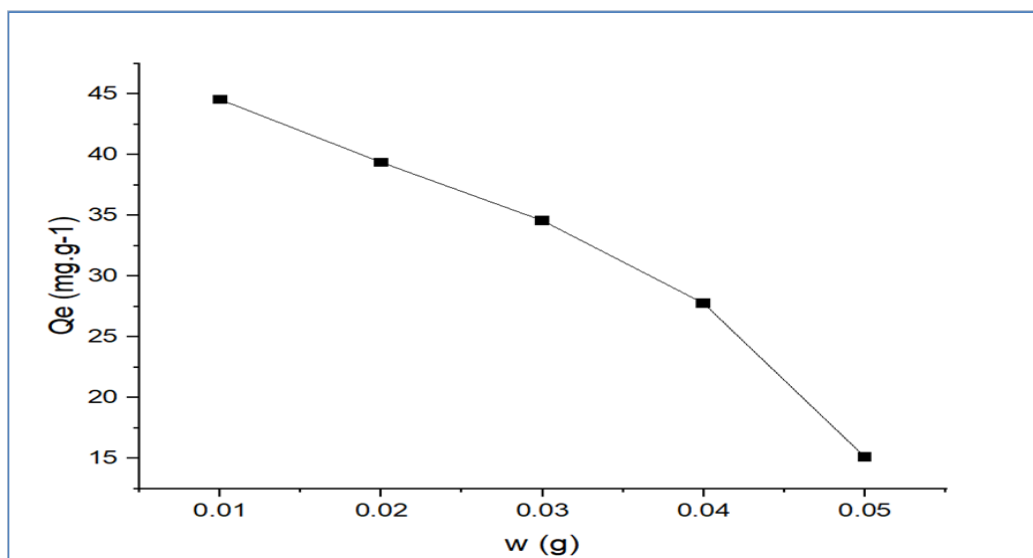


Figure [3.30] Effect of weight of ART-MMIP on the adsorption capacity of Artane solution

3.3.3.3. Effect of pH solution

The sample pH substantially affects the analytical conditions and the acidic or basic functional groups of MMIP. The pH value of the sample was altered from 2.0 to 9.0 for the assessment of its effects, as illustrated in Figure[3.31]. At low pH (2–4) the medium is acidic, resulting in an increase in H^+ ions. The adsorbent surface becomes positively charged due to protonation of hydroxyl groups ($-OH$). Artane, being a basic drug with amine groups, is also positively charged. This leads to electrostatic repulsion between the MMIP surface and the drug, resulting in lower adsorption capacity. At pH = 6: The solution approaches neutrality, facilitating a balance between surface and Artane charges. The adsorbent surface is probably neutral or slightly negatively charged, but ART retains a positive charge. This situation promotes electrostatic attraction and potentially hydrogen bonding, resulting in the largest adsorption capacity (highest Q_e value). At elevated pH levels (7–9) the medium transitions to a basic state. Hydroxyl groups on the adsorbent dissociate protons, resulting in a negative charge (O^-) and enhancing surface negativity. Artane may experience reduced charge or structural alterations in fundamental conditions. This may result in

diminished electrostatic interactions, potential repulsion, or drug degradation, leading to a reduction in adsorption capacity. The ideal adsorption of Artane onto MMIP transpires at pH = 6, when electrostatic attraction and hydrogen bonding are most advantageous [149].

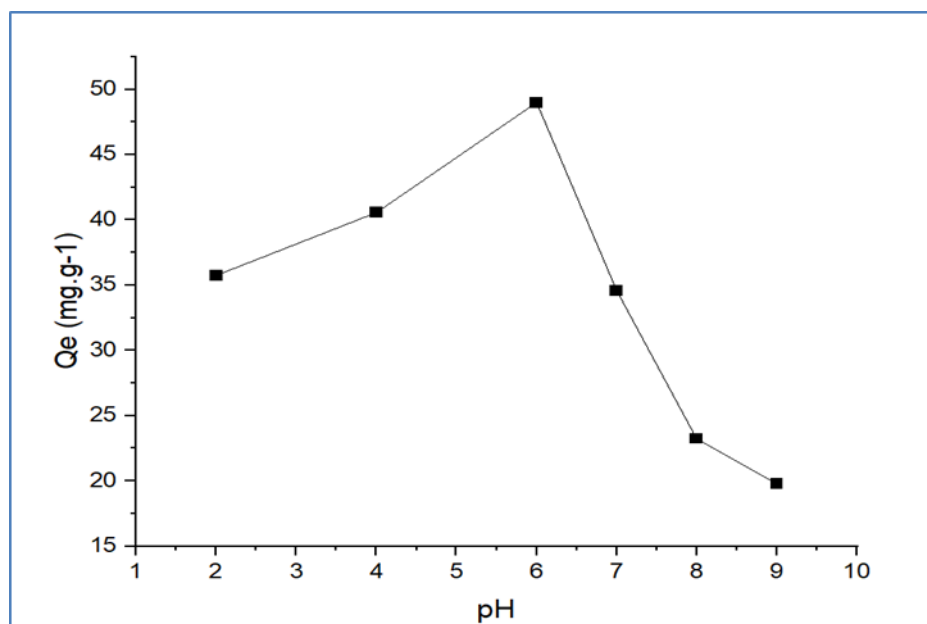


Figure [3.31] Effect of pH solution on the adsorption capacity of Artane on to ART-MMIP

3.3.3.4. Effect of temperature

Figure [3.32] depicts the influence of temperature on the adsorption capacity (Q_e) of an adsorbent. As the temperature rises from 25°C to 55°C, the adsorption capacity (Q_e) markedly diminishes. This trend illustrates that the adsorption process is exothermic. [150].

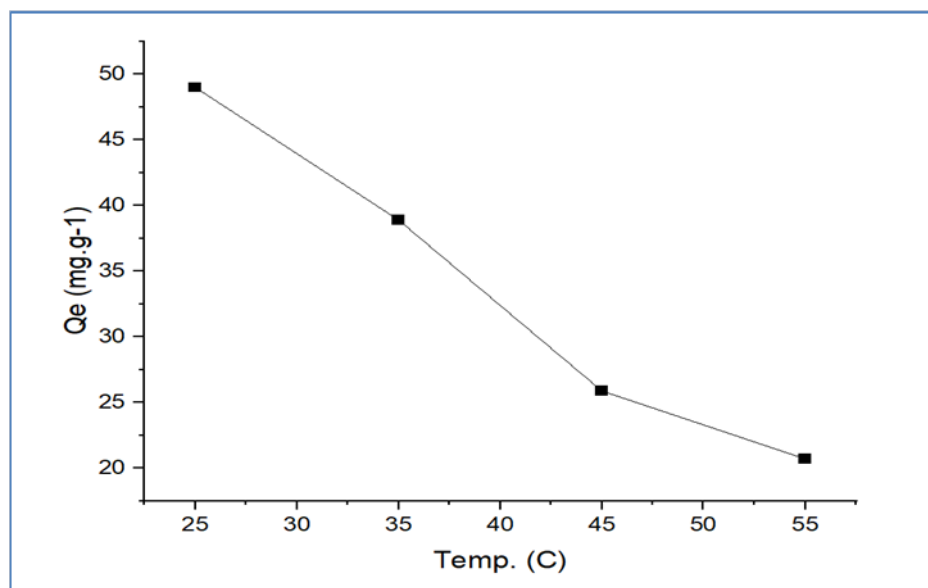


Figure [3.32] Effect of temperature on the adsorption capacity of Artane on to ART-MMIP

3.3.3.5. Effect of sample volume:

Figure [3.33] displays the impact of varied amounts (2-10 mL) on the recovery % of the (Artane). A distinct positive association exists between volume and recovery efficiency [151]. At reduced volumes (2–4 mL), the recovery rate remains below 80%, signifying inadequate extraction under these circumstances. A notable rise is evident between 4 mL and 6 mL, with recovery rising from roughly 78% to 85%, indicating that this interval may signify a threshold for enhanced extraction efficiency. Exceeding 6 mL, the recovery progressively enhances, attaining approximately 92% at 10 mL. This pattern illustrates that augmenting the volume intensifies the contact between the analyte (Artane) and the extracting phase, hence enhancing recovery.

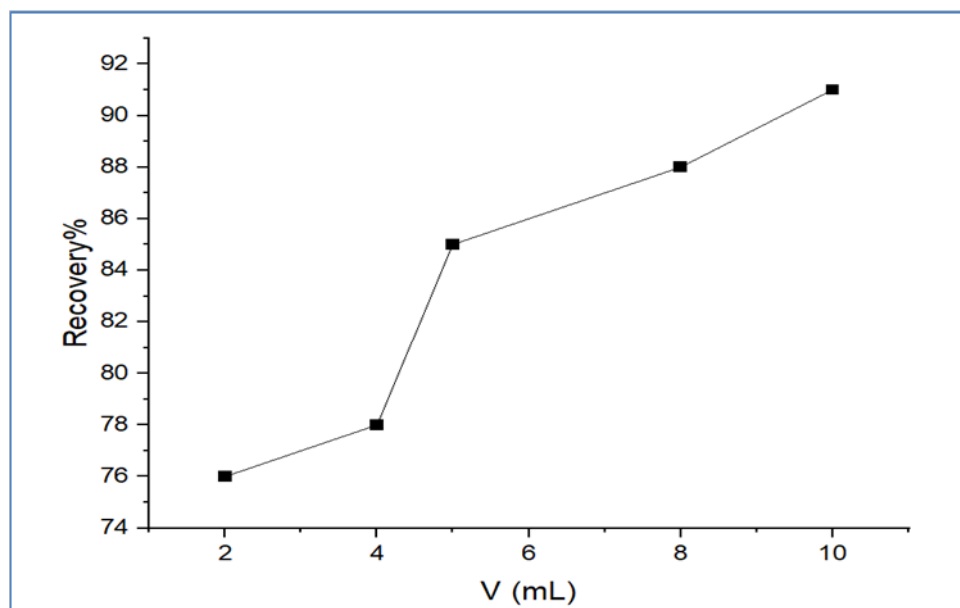


Figure [3.33] Effect of sample volume on the Recovery percentage of Artane using ART-MMIP

3.3.4. Enhancement of the extraction parameters of Pre –MMIP

3.3.4.1. Equilibrium time impact

Figure [3.34] presents the adsorption profile of Pregabalin onto the synthesized magnetic molecularly imprinted polymer (Pre-MMIP), showing the amount of adsorbed drug at equilibrium Q_e (mg.g^{-1}) as a function of contact time. The curve demonstrates a characteristic kinetic behavior that can be divided into three distinct phases. During the initial stage (0–20 minutes), a steep increase in Q_e (mg.g^{-1}) is observed, reflecting the rapid diffusion of Pregabalin molecules onto the abundant active sites available on the polymer surface. This fast adsorption rate is attributed to the significant affinity and accessibility of specific recognition cavities formed during the imprinting process [152]. In the second stage (20–50 minutes), the rate of adsorption gradually decreases. This reduction illustrates that the easily accessible binding sites become saturated, and the remaining active sites may be located in less accessible regions or require longer diffusion times. Finally, the system reaches equilibrium at approximately 60 minutes, beyond which no significant increase in Q_e (mg.g^{-1}) is noted. The

plateau illustrates the saturation of the majority of imprinted binding sites. The maximum adsorption capacity achieved is around $48.4 \text{ mg}\cdot\text{g}^{-1}$, which demonstrates the efficiency and specificity of the polymer for Pregabalin recognition and uptake [153].

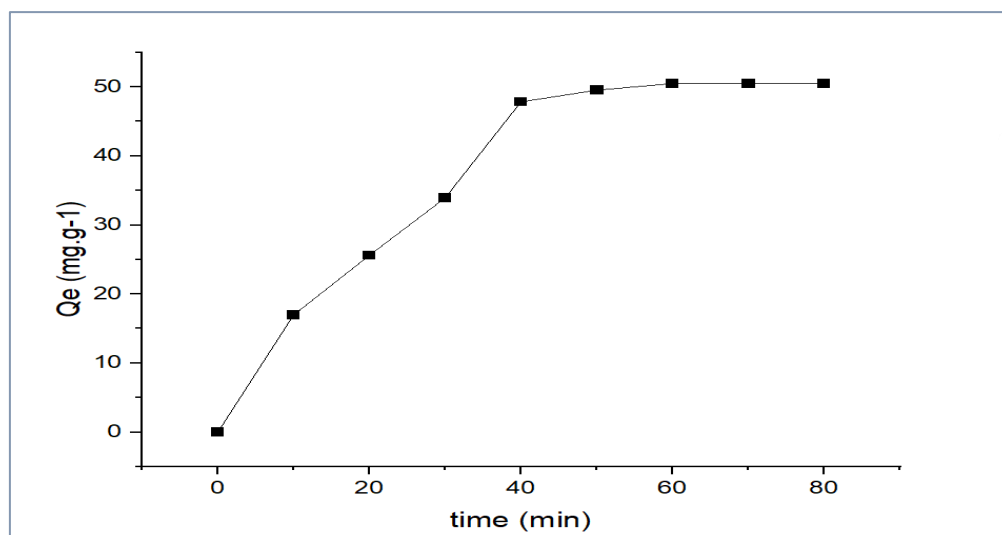


Figure [3.34] Effect of contact time on the adsorption capacity of Pregabalin on to pre-MMIP

3.3.4.2. Effect of the amount of Pre-MMIP:

The effect of varying the adsorbent dosage on the adsorption capacity of pregabalin was investigated, and the results are presented in Figure [3.35]. The data reveal a clear inverse relationship between the amount of polymer (w , g) and the adsorption capacity at equilibrium (Q_e , $\text{mg}\cdot\text{g}^{-1}$). As the polymer dosage increased from 0.01 g to 0.05 g, the adsorption capacity decreased significantly from approximately $61 \text{ mg}\cdot\text{g}^{-1}$ to $26 \text{ mg}\cdot\text{g}^{-1}$. This decline in Q_e with increasing adsorbent mass is a well-documented phenomenon and can be attributed to several interconnected factors. At low doses, the adsorbent surface is effectively employed, with most of the active imprinted binding sites interacting with the available pregabalin molecules. However, as the adsorbent dose increases while keeping the analyte concentration constant, the total number of active sites surpasses the number of available analyte molecules, leading to underutilization of binding sites and thus a lower Q_e per gram of adsorbent [154]. The findings

emphasize that optimal adsorption performance does not correlate with higher polymer dosages. Instead, an optimal dosage exists in this case, approximately (0.01–0.02 g) beyond which further increases in mass result in diminished per-gram adsorption capacity. This outcome underlines the necessity of carefully optimizing the adsorbent dosage for practical applications such as solid-phase extraction and drug preconcentration in biological matrices.

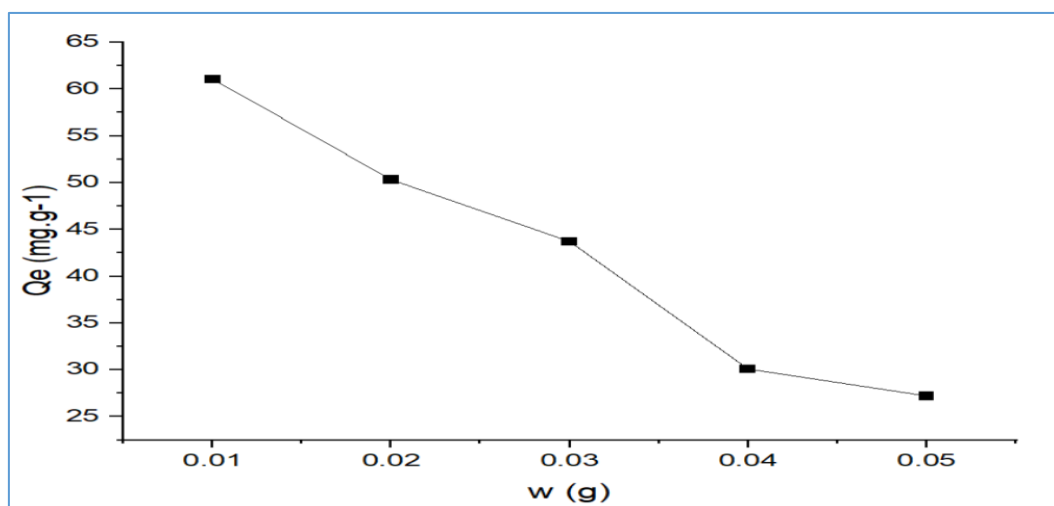


Figure [3.35] Effect of weight of Pre-MMIP on the adsorption capacity of Pregabalin solution

3.3.4.3. Effect of pH solution

Figure (3.36) illustrates the pronounced influence of solution pH on the adsorption capacity (Q_e) of pregabalin onto the synthesized magnetic molecularly imprinted polymer (MMIP) prepared using 3,4-dihydroxy-1-butene as the functional monomer. The adsorption behavior exhibits a clear bell-shaped trend, with the maximum adsorption capacity observed at pH 7, while lower efficiencies are recorded under both acidic and alkaline conditions.

At acidic pH values (pH 4–6), the hydroxyl functional groups ($-OH$) present on the MMIP surface are excessively protonated, which limits their ability to effectively participate in hydrogen-bond formation with pregabalin molecules. In addition, the high concentration of hydrogen ions in the solution can destabilize

non-covalent interactions within the imprinted cavities, thereby reducing the formation of stable and selective binding interactions. As a result, the adsorption capacity is relatively low in acidic media[154].

At neutral pH (pH = 7), optimal adsorption conditions are achieved. Under these conditions, the hydroxyl groups derived from the 3,4-dihydroxy-1-butene monomer exhibit an appropriate ionization and structural stability, enabling them to act efficiently as both hydrogen-bond donors and acceptors. Simultaneously, pregabalin molecules exist in a favorable chemical state that enhances non-covalent interactions within the molecularly imprinted cavities. The combined effect of strong hydrogen bonding and shape complementarity between the template molecule and the recognition sites results in the highest adsorption capacity, confirming the selective recognition capability of the MMIP.

In alkaline media (pH > 7), the increased concentration of hydroxide ions (OH⁻) interferes with hydrogen-bond stability through competitive interactions and disruption of the local binding environment. Furthermore, changes in the solubility and molecular behavior of pregabalin at higher pH values, along with possible distortion of the imprinted binding sites, lead to a reduction in adsorption efficiency[155].

The optimum pH value of 7 reflects a balance between functional group stability and effective molecular recognition, indicating that neutral conditions are most suitable for achieving maximum adsorption performance in biological and environmental applications

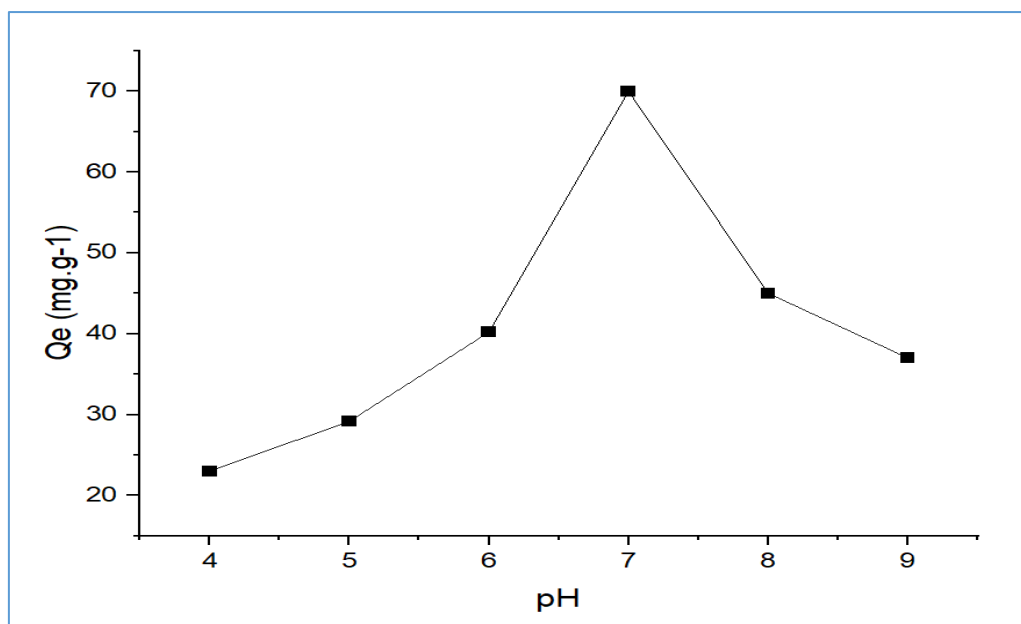


Figure [3.36] Effect of pH solution on the adsorption capacity of pregabalin on to pre-MMIP

3.3.4.4. Effect of temperature

The adsorption performance of the synthesized magnetic molecularly imprinted polymer (MMIP) for pregabalin (Pre-MMIP) was evaluated at various temperatures ranging from 25°C to 50°C. As depicted in Figure [3.37], the adsorption capacity (Q_e) exhibited a notable decrease with increasing temperature. Specifically, the Q_e value dropped from approximately 90 $\text{mg}\cdot\text{g}^{-1}$ at 25°C to less than 30 $\text{mg}\cdot\text{g}^{-1}$ at 50°C. This inverse relationship illustrates that the adsorption process is exothermic in nature. At lower temperatures, the interactions between pregabalin molecules and the recognition sites within the MMIP primarily governed by hydrogen bonding, electrostatic interactions, and van der Waals forces are more stable and favorable. However, increasing the temperature likely disrupts these non-covalent interactions due to enhanced molecular motion, resulting in reduced affinity of the target (Pregabalin) towards the imprinted cavities. These results underscore the significance of operating at lower temperatures to achieve optimal adsorption efficiency. Hence, ambient or slightly reduced temperatures are recommended for practical applications

involving the extraction and quantification of pregabalin through the use of MMIP-based systems [150].

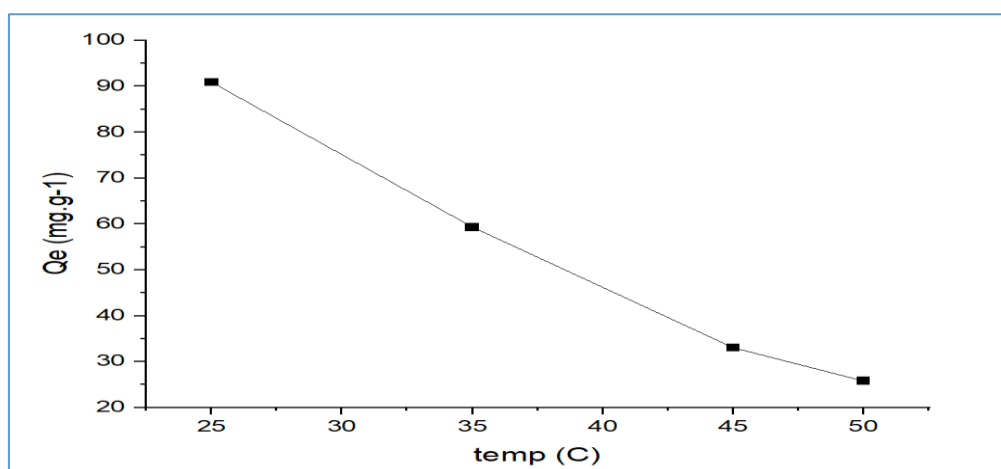


Figure [3.37] Effect of temperature on the adsorption capacity of pregabalin on to pre-MMIP

3.3.4.5. Effect of sample volume:

Figure [3.38] illustrates the effect of sample volume on the recovery efficiency of pregabalin using the synthesized magnetic molecularly imprinted polymer (MMIP). The results demonstrate a pronounced enhancement in recovery percentage with increasing sample volume, rising from approximately 25% at 2 mL to over 90% at 10 mL.

At lower sample volumes (2–4 mL), the limited amount of pregabalin present in the solution restricts effective interaction with the available imprinted recognition sites of the MMIP, resulting in incomplete utilization of the sorbent and consequently lower recovery values. As the sample volume increases, a greater quantity of pregabalin molecules becomes available, thereby improving the probability of interaction with the selective binding sites and enhancing extraction efficiency.

In the intermediate volume range (5–8 mL), the increase in recovery becomes more gradual, indicating that the adsorption process is approaching a quasi-equilibrium state, where a significant fraction of the accessible binding sites is

already engaged. Nevertheless, at a sample volume of 10 mL, a substantial improvement in recovery is observed, suggesting that the chosen sorbent dosage and extraction conditions remain sufficient to accommodate the increased analyte load without premature saturation of the imprinted sites. This behavior reflects an optimal balance between sample volume, analyte availability, and sorbent capacity, leading to maximum recovery under the investigated conditions.

Based on these findings, a sample volume of 10 mL was selected as the optimum for subsequent experiments and real-sample applications, as it provides high recovery efficiency while maintaining practical extraction conditions.[156].

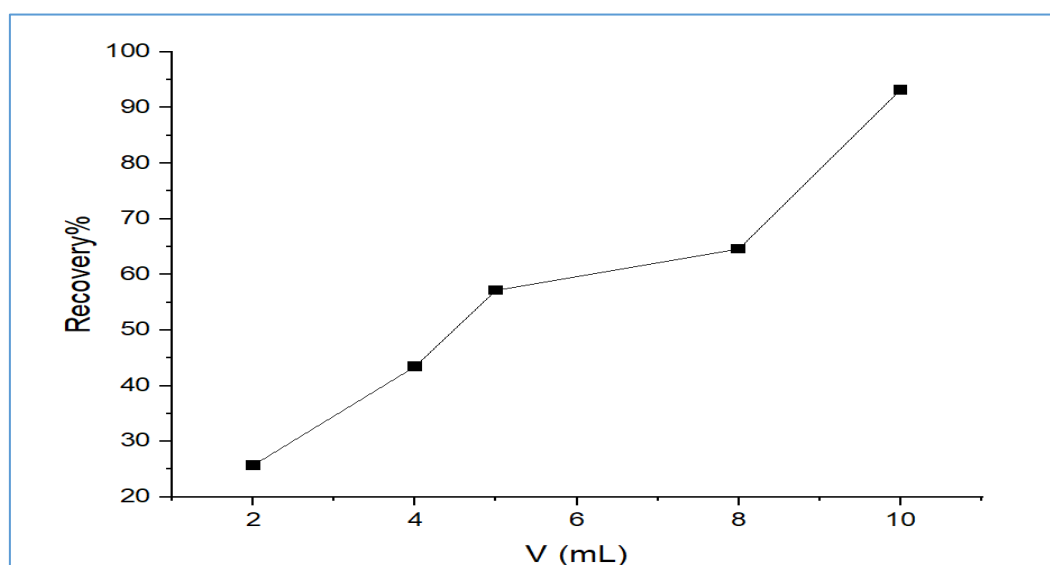


Figure [3.38] Effect of sample volume on the Recovery percentage of pregabalin using pre-MMIP

3.4. Adsorption Characteristics of MMIPs

3.4.1. Adsorption Kinetic

To investigate the adsorption mechanisms and determine the rate-limiting step of drug adsorption onto the prepared MMIPs, both pseudo-first-order and pseudo-second-order kinetic models were applied to the experimental data for heroin, amphetamine, Artane, and pregabalin. The kinetic parameters were calculated based on the linearized forms of the models, and the correlation coefficient (R^2) was used in order to evaluate the best-fitting model.

3.4.1.1. Heroin Adsorption Kinetics

Figure [3.39A] illustrates the pseudo-first-order kinetic model for heroin, with a linear regression equation $y = 0.0136x - 2.1535$ and a low correlation coefficient ($R^2 = 0.1661$). This weak fit illustrates that the adsorption process does not follow first-order kinetics. In contrast, Figure [3.39B], representing the pseudo-second-order kinetic model, yielded a regression line $y = 0.0342x - 0.0282$ with a significantly higher correlation coefficient ($R^2 = 0.9962$), indicating that the adsorption of heroin is better described by the pseudo-second-order model.

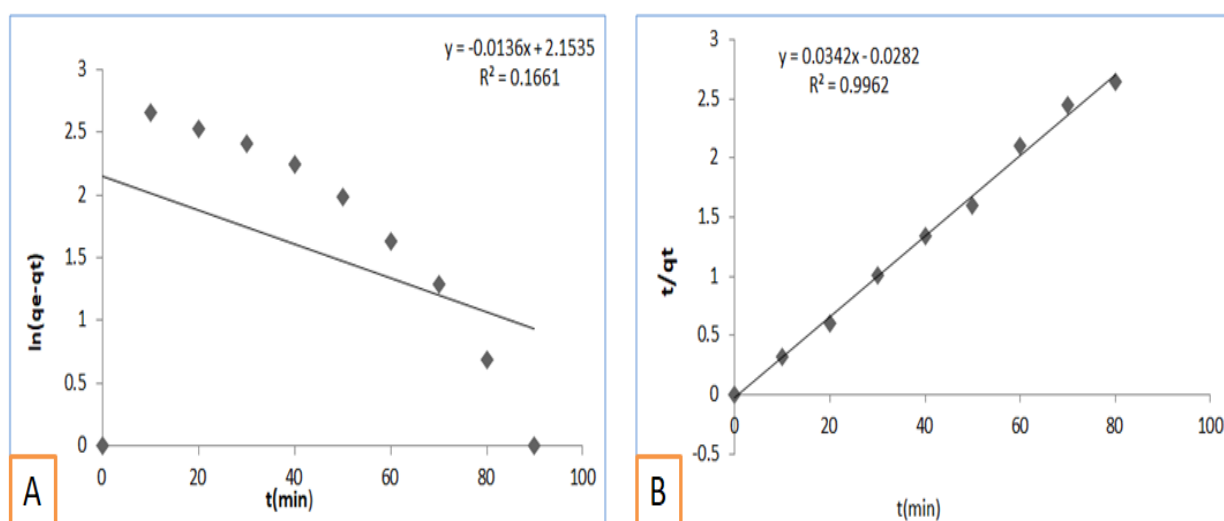


Figure [3.39] (A) pseudo-first-order kinetics (B) pseudo-Second-order kinetics of heroin

3.4.1.2. Amphetamine Adsorption Kinetics

In Figure [3.40A], the pseudo-first-order model yielded a strong correlation ($R^2 = 0.9917$), with a linear relationship defined by $\ln(q_e - q_t) = 0.017x + 0.1191$. On the other hand, the pseudo-second-order model in Figure [3.40B] showed a relatively weaker correlation ($R^2 = 0.7605$), reinforcing the conclusion that the pseudo-first-order model better describes amphetamine adsorption onto the MMIP.

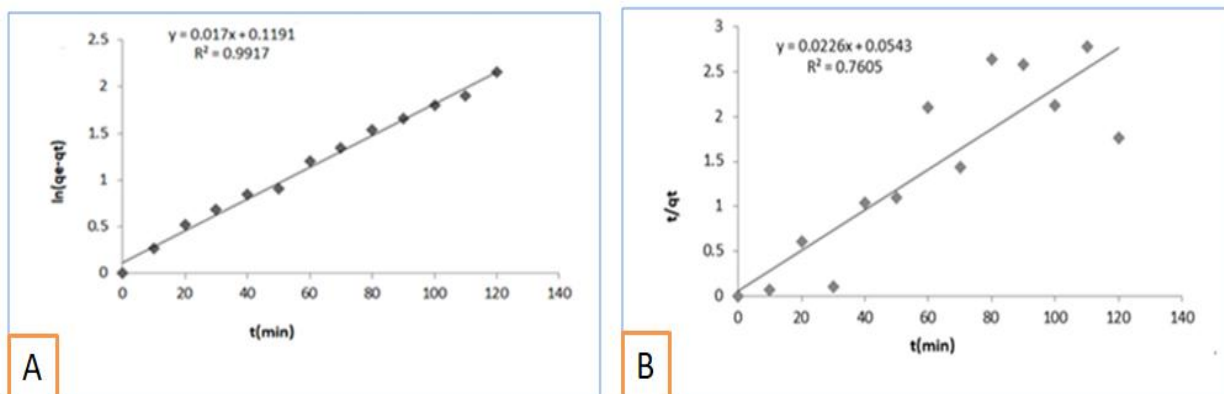


Figure [3.40] (A) pseudo-first-order kinetics (B) pseudo-Second-order kinetics of Amphetamine

3.4.1.3. Artane Adsorption Kinetics

The kinetic data for Artane (trihexyphenidyl) were similarly analyzed. Figure [3.41A] demonstrates a good linear correlation for the pseudo-first-order model ($R^2 = 0.9503$), with the equation $y = -0.0268x + 4.187$. Conversely, the pseudo-second-order model in Figure [3.41B] displayed a lower correlation ($R^2 = 0.8642$), the adsorption process is more likely to be governed by a first-order kinetic mechanism in the case of Artane.

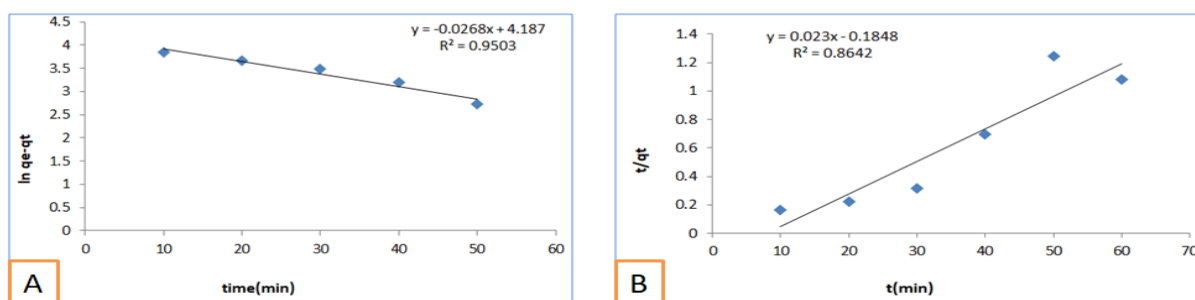


Figure [3.41] (A) pseudo-first-order kinetics (B) pseudo-Second-order kinetics of Artane

3.4.1.4. Pregabalin Adsorption Kinetics

For pregabalin, the pseudo-first-order kinetic plot Figure [3.42A] showed a moderate correlation ($R^2 = 0.8273$), indicating a less reliable fit to the experimental data. The equation $y = -14.853x + 97.845$ reflects a sharp decline in the adsorption rate, possibly due to rapid saturation of available sites. In contrast, the pseudo-second-order plot Figure [3.42B] demonstrated a very significant correlation coefficient ($R^2 = 0.9989$), suggesting a better fit to this model.

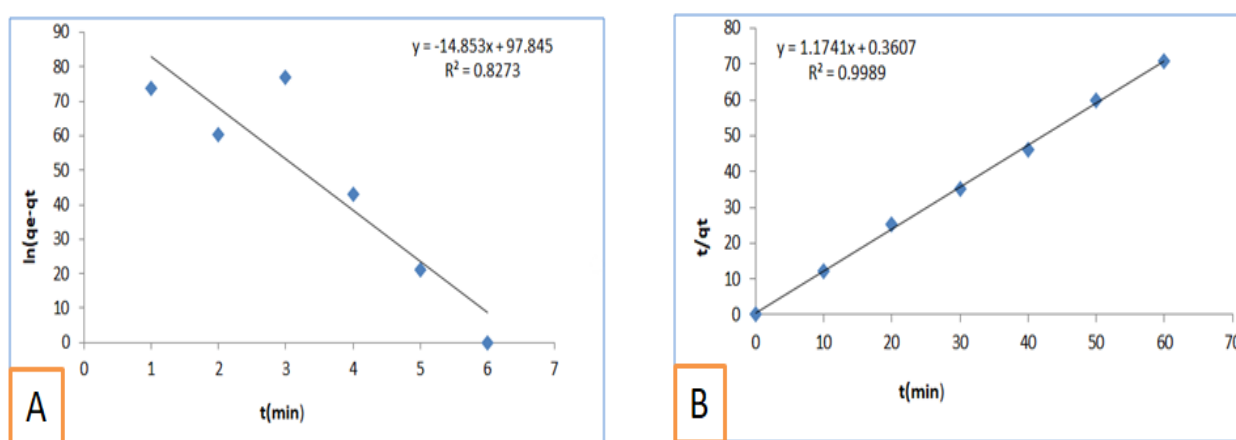


Figure [3.42] (A) pseudo-first-order kinetics (B) pseudo-Second-order kinetics of Pregabaline

3.4.2. Adsorption Isotherms

The equilibrium adsorption behavior of heroin, amphetamine, Artane and pregabalin onto the synthesized MMIPs was assessed through the use of three widely accepted isotherm models: Freundlich, Langmuir, and Temkin. These models provide essential insights into the nature of the interaction between the adsorbate (drug) and the adsorbent (MMIP).

3.4.2.1. Adsorption Isotherms of Heroin and Amphetamine

The adsorption behavior of both heroin and amphetamine onto the synthesized magnetic molecularly imprinted polymer (MMIP) was evaluated through the use of three isotherm models: Freundlich, Langmuir, and Temkin, as illustrated in Figures [3.43] and [3.44], respectively. For heroin, the Freundlich isotherm plot (Figure 3.43A) produced the linear equation $Y = 0.0579 X + 1.7053$ with a correlation coefficient $R^2 = 0.8716$, suggesting moderate agreement with the model. The relatively low slope illustrates a limited multilayer adsorption process, potentially influenced by surface heterogeneity or non-ideal interactions such as van der Waals forces [157]. In contrast, the Langmuir isotherm (Figure 3.43B) yielded a linear relationship ($Y = 0.024 X - 0.0146$) with an excellent fit ($R^2 = 0.9954$), supporting the monolayer adsorption mechanism on a homogeneous surface with finite binding sites. The Temkin isotherm plot (Figure 3.44C) resulted in the regression: $Y = (2.6603 X + 50.604$ with $R^2 = 0.8886$, implying the presence of adsorbate–adsorbent interactions and a gradual decrease in the heat of adsorption with increased surface coverage. This supports the notion of energetic heterogeneity within the MMIP matrix. Regarding amphetamine, the Freundlich model (Figure 3.44A) demonstrated a strong fit to the experimental data with the equation:

$Y = 0.1566 X + 1.8125$ and a significant $R^2 = 0.9971$, indicating that adsorption occurred on a heterogeneous surface. The slope reflects a reduction in adsorption capacity at higher equilibrium concentrations, possibly due to site saturation or competitive interactions. On the other hand, the Langmuir isotherm (Figure 3.43B) provided the equation:

$(Y = 0.9616 X + 9.4191)$ with $R^2 = 0.8799$. The slope, however, contradicts the fundamental assumptions of the Langmuir model, suggesting that amphetamine adsorption does not strictly follow monolayer behavior. Lastly, the Temkin model (Figure 3.44C) yielded:

$Y = 19.279 X + 83.214$ with $R^2 = 0.8766$. Although the correlation is statistically acceptable, the slope illustrates a deviation from the expected linear decrease in adsorption energy, implying the presence of weak or non-ideal interactions between amphetamine molecules and the polymer surface [158]. Collectively, these findings confirm that heroin adsorption aligns more closely with the Langmuir model, indicative of a monolayer process on a uniform surface, while amphetamine demonstrates better conformity to the Freundlich isotherm, suggesting multilayer adsorption on heterogeneous sites. The Temkin analysis, in both cases, highlights the role of interaction energies and adsorbent surface properties, albeit with model deviations likely due to structural or chemical discrepancies in the binding affinities of the two drugs [159].

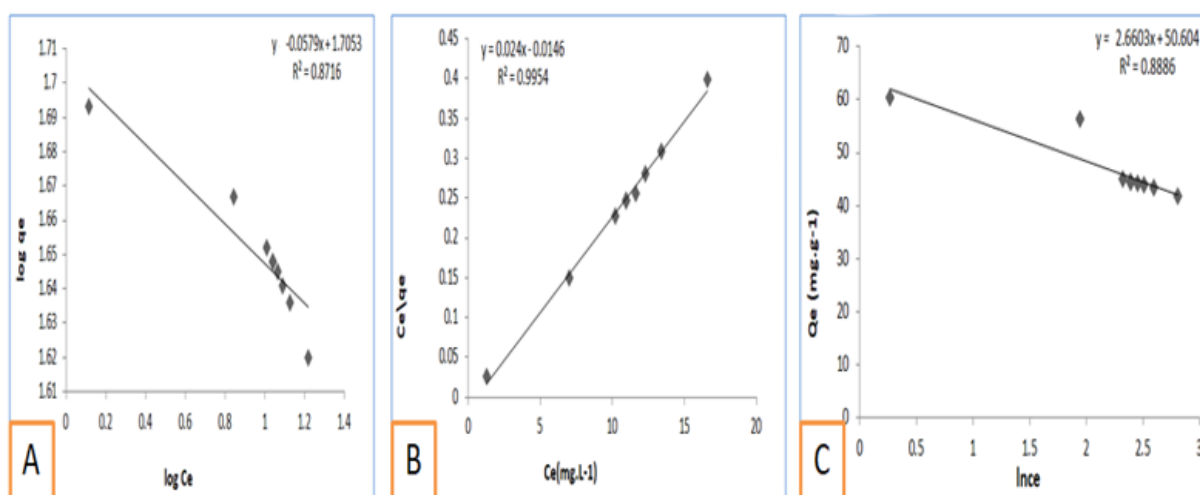


Figure [3.43] adsorption isotherm (A) Freundlich isotherm (B) Langmuir isotherms(C) Timken isotherm of heroin

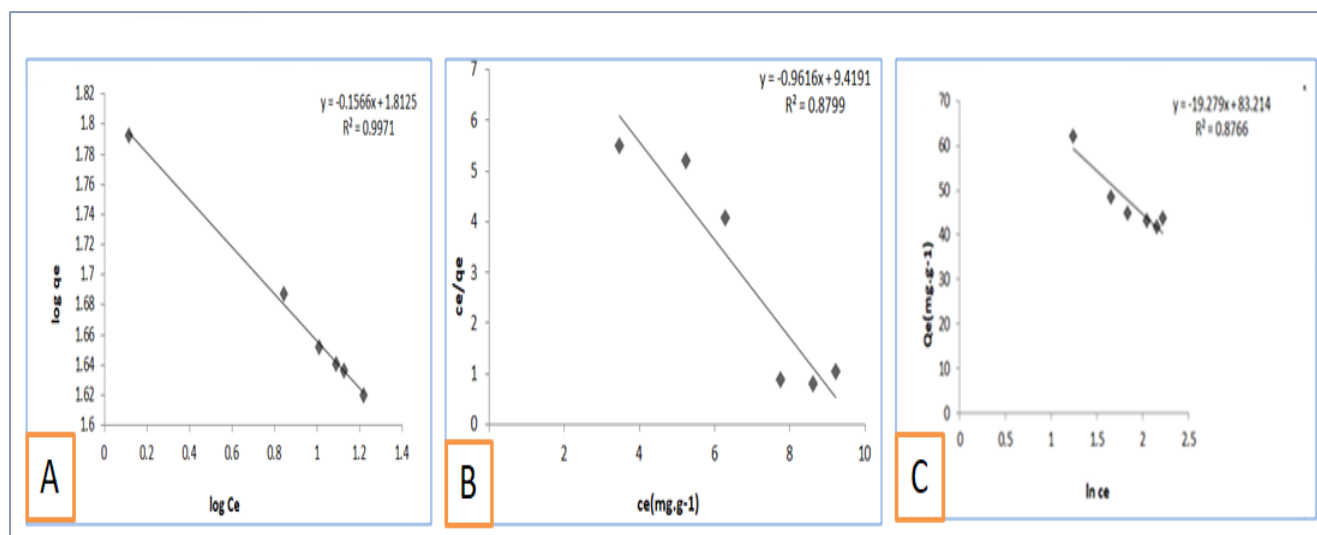


Figure [3.44] adsorption isotherm (A) Freundlich isotherm (B) Langmuir isotherms(C) Timken isotherm of Amphetamine

3.4.2.2. Adsorption Isotherms of Artane and Pregabalin

The adsorption behaviors of Artane and Pregabalin onto their respective magnetic molecularly imprinted polymers (MMIPs) were studied through the use of three classical isotherm models: Freundlich, Langmuir, and Temkin, as illustrated in Figures [3.45] and [3.46]. For Artane, the Freundlich isotherm plot Figure [3.45A] produced a linear equation:

$Y = 0.7267 X + 0.7918$ with a correlation coefficient $R^2 = 0.9404$, indicating a relatively strong fit. The positive slope validates the presence of heterogeneous surface adsorption and illustrates the formation of multilayers. The Langmuir model (Figure 3.45B) yielded the equation:

$Y = 0.0127 X + 0.1668$ with a considerably lower $R^2 = 0.575$, reflecting poor alignment with the assumptions of monolayer adsorption on a homogeneous surface. Conversely, the Temkin model (Figure 3.45C) provided a more reliable fit with the equation:

$Y = 0.0602 X + 0.1849$ and $R^2 = 0.8284$, which supports the hypothesis of adsorbate–adsorbent interactions and a progressive decrease in adsorption energy, indicating surface energetic heterogeneity.

In the case of Pregabalin, the Freundlich plot Figure [3.46A] showed a strong linear relationship:

$Y = 0.9745 X - 0.4712$, with a significant $R^2 = 0.9528$, reinforcing the notion of multilayer adsorption on a heterogeneous MMIP surface. The Langmuir isotherm Figure [3.46B], described by the equation:

$Y = 0.5108 X - 1.4545$ and an excellent $R^2 = 0.9951$, demonstrated a clear conformity with the monolayer adsorption assumption, confirming the presence of uniform, finite adsorption sites across the polymer surface. The Temkin model Figure [3.46C] also showed a significant degree of linearity:

$Y = 5.016x + 0.8532$, with $R^2 = 0.9391$, indicating the presence of strong interactions between the analyte and binding sites, where the adsorption energy decreases gradually with increasing coverage[160,161].

Collectively, these results suggest that Pregabalin exhibits adsorption behavior that aligns well with both Langmuir and Freundlich models, implying a combination of monolayer adsorption and surface heterogeneity. In contrast, Artane demonstrates a better fit to the Freundlich models, indicating multilayer adsorption with energetically non-uniform binding sites. The discrepancy in Langmuir fit for Artane further supports the notion of its more complex interaction with the MMIP surface.

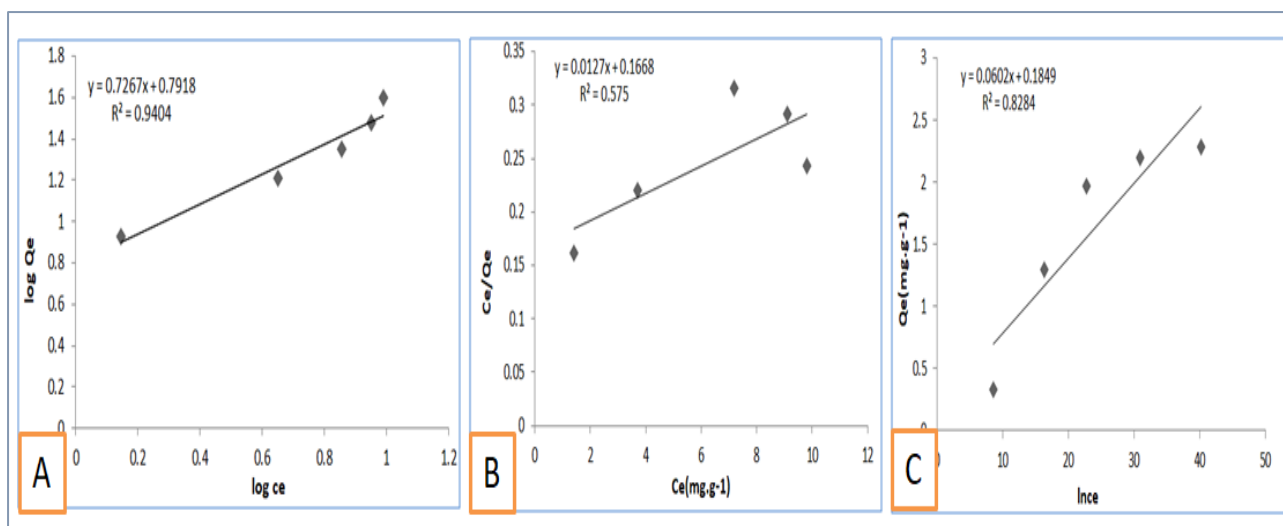


Figure [3.45] adsorption isotherm (A) Freundlich isotherm (B) Langmuir isotherms (C) Timken isotherm of Artane

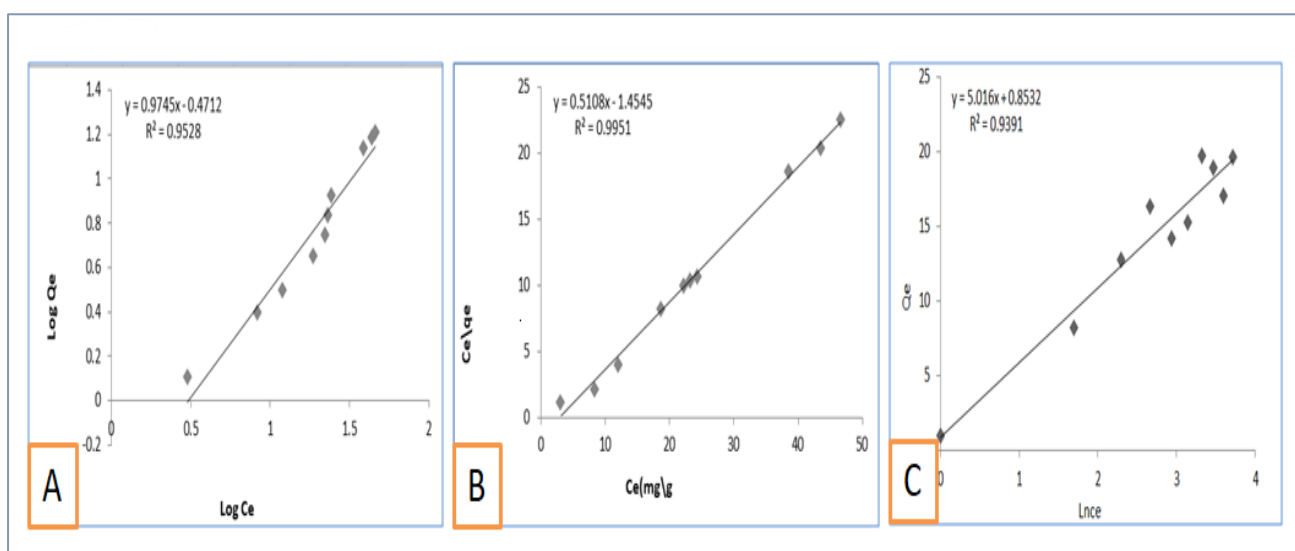


Figure [3.46] adsorption isotherm (A) Freundlich isotherm (B) Langmuir isotherms (C) Timken isotherm of pregabalin

3.4.3. Thermodynamic Study of Drug Adsorption

The thermodynamic parameters for the adsorption of heroin, amphetamine, Artane, and pregabalin onto their respective magnetic molecularly imprinted polymers (MMIPs) were assessed using the Van't Hoff equation. A linear relationship between $\ln K_a$ and $1/T$ enabled the determination of the standard

enthalpy change (ΔH°) and entropy change (ΔS°) for each system, where the slope corresponds to $-\Delta H^\circ/R$ and the intercept to $\Delta S^\circ/R$ ($R = 8.314 \text{ J}\cdot\text{mol}^{-1}\cdot\text{K}$).

For heroin (Figure 3.47), the Van't Hoff plot demonstrated excellent linearity ($R^2 = 0.9942$), with a calculated ΔH° of $-8.80 \text{ kJ}\cdot\text{mol}^{-1}$, indicating an exothermic adsorption process. The slight negative entropy change ($\Delta S^\circ = -0.14 \text{ J}\cdot\text{mol}^{-1}\cdot\text{K}^{-1}$) suggests minimal alteration in the system's disorder at the solid-liquid interface. The corresponding Gibbs free energy change ($\Delta G^\circ = -8.76 \text{ kJ}\cdot\text{mol}^{-1}$) confirms the spontaneity of the adsorption under standard conditions, in line with the weak entropy loss and moderate interaction energy.

In the case of amphetamine (Figure 3.48), the plot exhibited moderate linearity ($R^2 = 0.869$), and the enthalpy and entropy changes were found to be $-28.30 \text{ kJ}\cdot\text{mol}^{-1}$ and $-104.54 \text{ J}\cdot\text{mol}^{-1}\cdot\text{K}^{-1}$, respectively. Despite the strongly exothermic nature of the process, the significant entropy loss leads to a positive Gibbs free energy ($\Delta G^\circ = -2.87 \text{ kJ}\cdot\text{mol}^{-1}$), indicating a non-spontaneous adsorption at 298 K. This behavior suggests the involvement of highly ordered or multi-site binding interactions that impose thermodynamic constraints, resulting in an energetically favorable but entropically hindered system. For Artane (Figure 3.49), the Van't Hoff plot also exhibited excellent linearity ($R^2 = 0.9938$), with thermodynamic parameters closely resembling those of heroin: $\Delta H^\circ = -9.09 \text{ kJ}\cdot\text{mol}^{-1}$ and $\Delta S^\circ = -0.14 \text{ J}\cdot\text{mol}^{-1}\cdot\text{K}^{-1}$. The corresponding ΔG° value ($-9.05 \text{ kJ}\cdot\text{mol}^{-1}$) confirms the non-spontaneous nature of adsorption, reinforcing the conclusion that Artane binds favorably to the imprinted sites with negligible entropy disruption. Pregabalin (Figure 3.50), on the other hand, exhibited the highest enthalpic contribution among the studied drugs ($\Delta H^\circ = -26.27 \text{ kJ}\cdot\text{mol}^{-1}$), coupled with a notable entropy decrease ($\Delta S^\circ = -79.24 \text{ J}\cdot\text{mol}^{-1}\cdot\text{K}^{-1}$), and a weaker correlation in the Van't Hoff plot ($R^2 = 0.7198$). These findings reflect the presence of strong and specific interactions, likely involving hydrogen bonding or dipolar interactions. The calculated ΔG° (-2.64 kJ/mol) confirms the non-

spontaneity of the process, albeit with a lower driving force compared to heroin and Artane, possibly due to a more rigid and structured binding environment

In conclusion, all four drugs exhibited exothermic adsorption behavior onto their respective MMIPs. Heroin and Artane demonstrated consistent and predictable behavior, amphetamine showed a structured and specific binding interaction in the updated data, and pregabalin exhibited strong, ordered, and energetically intensive adsorption. Table [3.1] shows the Thermodynamic Parameters for Drugs Adsorption onto MMIPs.

Table [3.1]: Thermodynamic Parameters for Drugs Adsorption onto MMIPs

Drugs	ΔH° (kJ.mol ⁻¹)	ΔS° (J.mol ⁻¹ .K ⁻¹)	ΔG° (kJ.mol ⁻¹)	R ² (Van't Hoff plot)
Heroin	-8.8	-0.14	-8.76	0.9942
Amphetamine	-28.3	-104.54	-2.87	0.869
Artane	-9.09	-0.14	-9.05	0.9938
Pregabalin	-26.27	-79.24	-2.64	0.7198

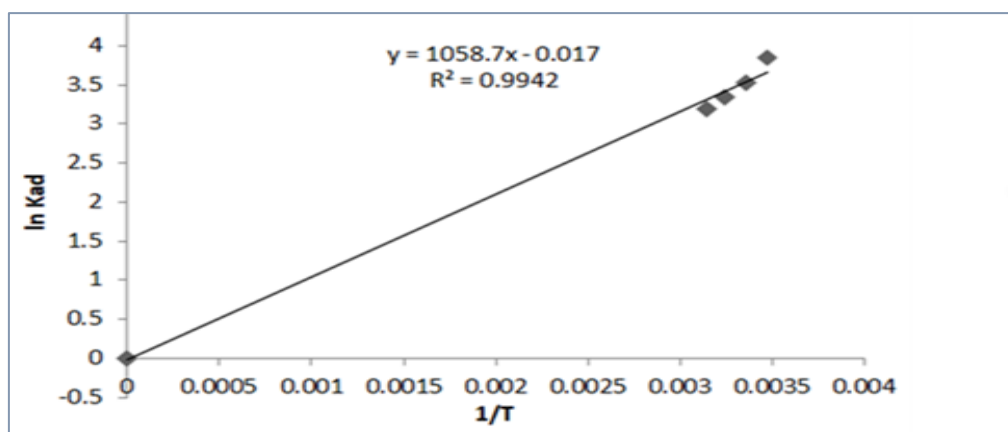


Figure [3.47] the adsorption of heroin on the surface of the MMIP

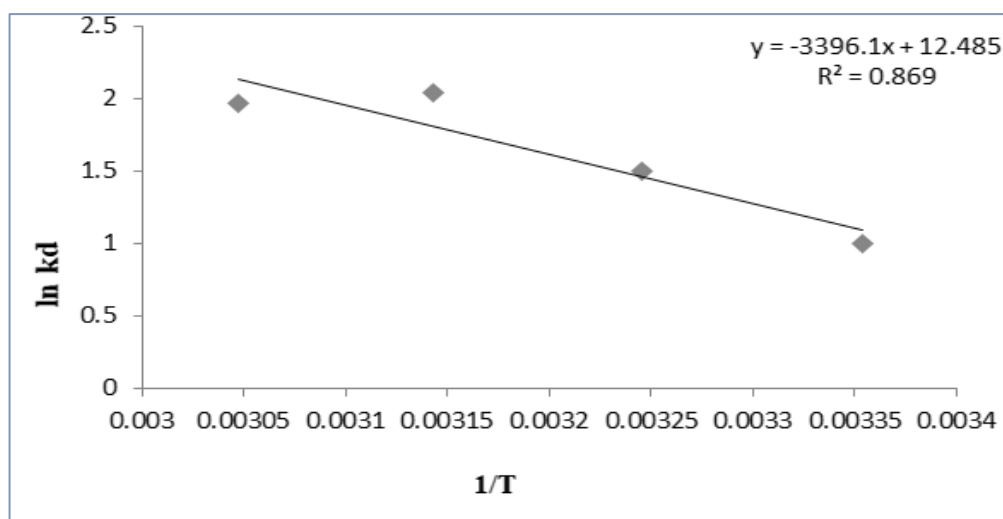


Figure [3.48] the adsorption of Amphetamine on the surface of the MMIP

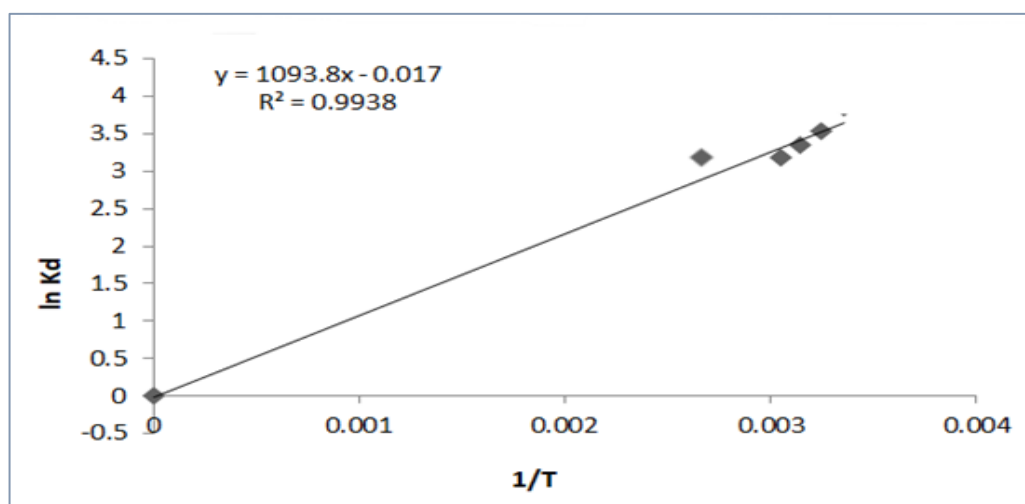


Figure [3.49] the adsorption of Artane on the surface of the MMIP

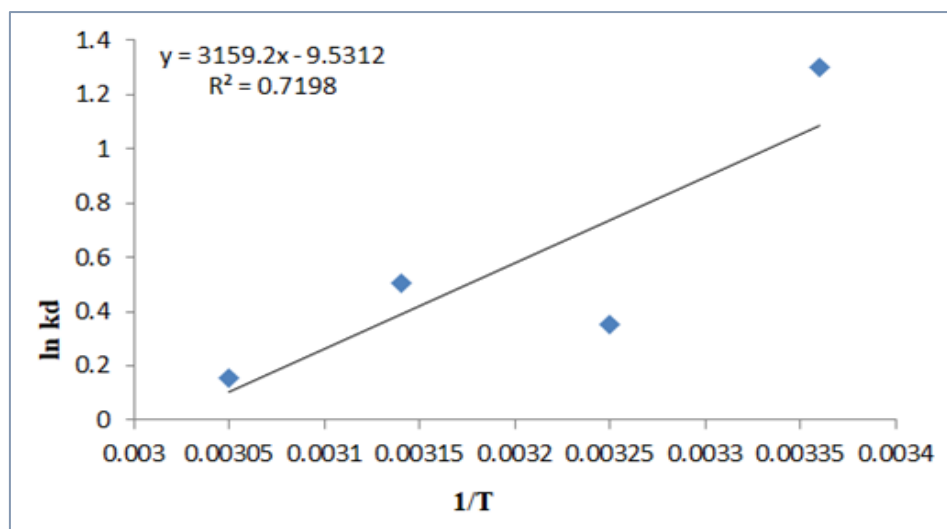


Figure [3.50] the adsorption of pergabalin on the surface of the MMIP

3.5. Selectivity and Reusability of MMIPs

3.5.1 Selectivity of MMIPs toward Target Drugs

The selectivity and extraction efficiency of the synthesized magnetic molecularly imprinted polymers (MMIPs) were evaluated through imprinting factor (IF) and relative selectivity coefficient (β). As summarized in the table [3.2] all MMIPs exhibited IF values significantly greater than 1 and β values below 0.5, clearly indicating significant affinity and specificity toward their respective target drugs.

Table [3.2] Selectivity Parameters for Target Drugs Using MMIPs

Target Drug	Q_MNIP (mg.g ⁻¹)	Q_MMIP (mg.g ⁻¹)	Alpha (IF)	Q_drug	β vs. Other Drugs
Heroin	0.65	5.2	8.0	4.55	Amphetamine: 0.48; Artane: 0.42; Pregabalin: 0.39
Amphetamine	0.45	1.53	6.7	1.08	Heroin: 0.44; Artane: 0.47; Pregabalin: 0.41
Artane	0.49	0.98	7.2	0.49	Heroin: 0.45; Amphetamine: 0.46; Pregabalin: 0.43
Pregabalin	0.62	1.59	5.54	0.97	Heroin: 0.49; Amphetamine: 0.40; Artane: 0.38

The MMIP synthesized for heroin demonstrated an IF of 8.0, indicating a strong selective interaction between the polymer matrix and heroin. The β values against amphetamine (0.48), Artane (0.42), and pregabalin (0.39) further confirm its significant specificity. Figure [3.51] supports this, with heroin showing a recovery rate exceeding 90%, while non-target drugs remained below 30%. This sharp contrast reflects the presence of complementary recognition sites tailored to heroin's structure [165].

Similarly, the amphetamine-imprinted polymer exhibited an IF of 6.7, with β values of 0.44 (vs. heroin), 0.47 (vs. Artane), and 0.41 (vs. pregabalin). In Figure [3.52], the recovery percentage for amphetamine approaches ~95%, while significantly lower recoveries were observed for non-specific drugs. These results imply that the imprinting process generated structurally compatible binding sites, minimizing cross-reactivity. The Artane-MMIP showed an IF of 7.2, with β values of 0.45 (heroin), 0.46 (amphetamine), and 0.43 (pregabalin), suggesting a well-defined and selective recognition system [166]. Figure [3.53] illustrates a significant recovery of nearly 90% for Artane, while all other analytes presented

recoveries below 25%. This denotes the polymer's ability to distinguish Artane from structurally unrelated drugs. Lastly, the pregabalin-targeted MMIP achieved an IF of 5.54 and β values of 0.49 (heroin), 0.40 (amphetamine), and 0.38 (Artane). As shown in Figure [3.54], pregabalin was recovered at a rate exceeding 90%, with negligible extraction of other compounds. These findings confirm the successful formation of specific recognition sites for pregabalin within the polymer matrix[167].

Overall, the alignment between significant IF values, low β values, and dominant recovery rates of the target drugs validates the effective molecular imprinting and selective adsorption capabilities of the prepared MMIPs. These results highlight the promising potential of MMIPs in selective extraction applications from complex biological matrices.

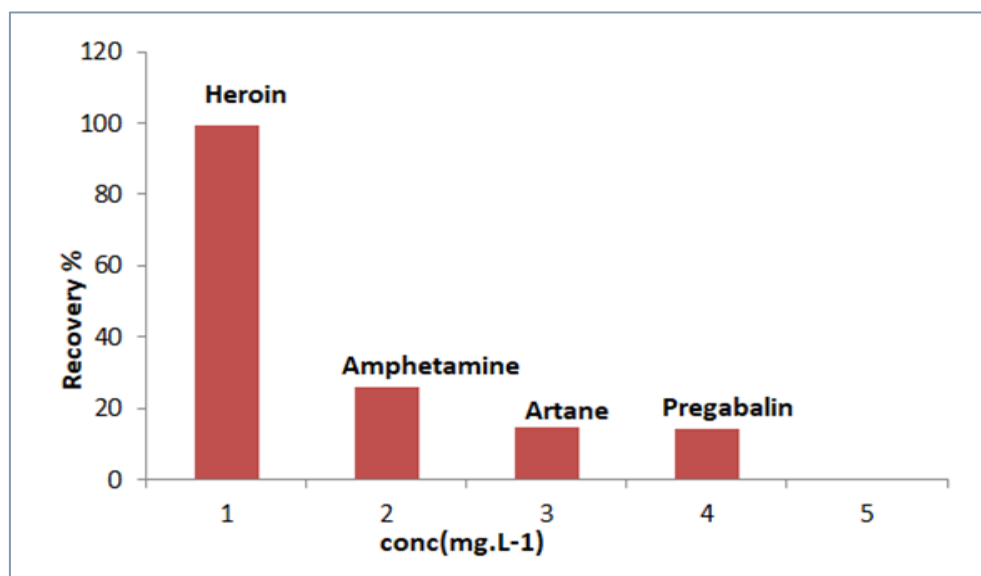


Figure [3.51] Selectivity of Her-MMIP toward Heroin and three drugs

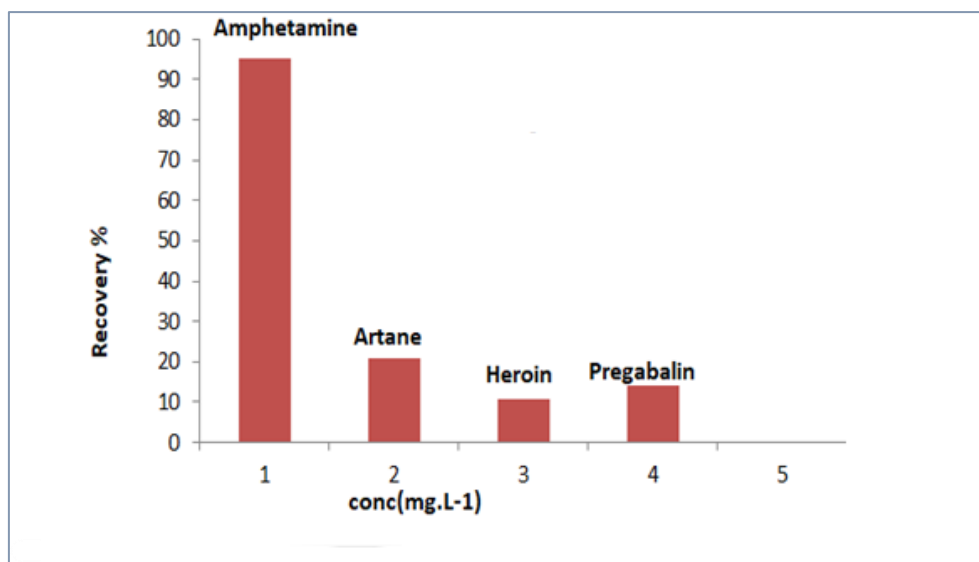


Figure [3.52] Selectivity of AMP-MMIP toward Amphetamine and three drugs

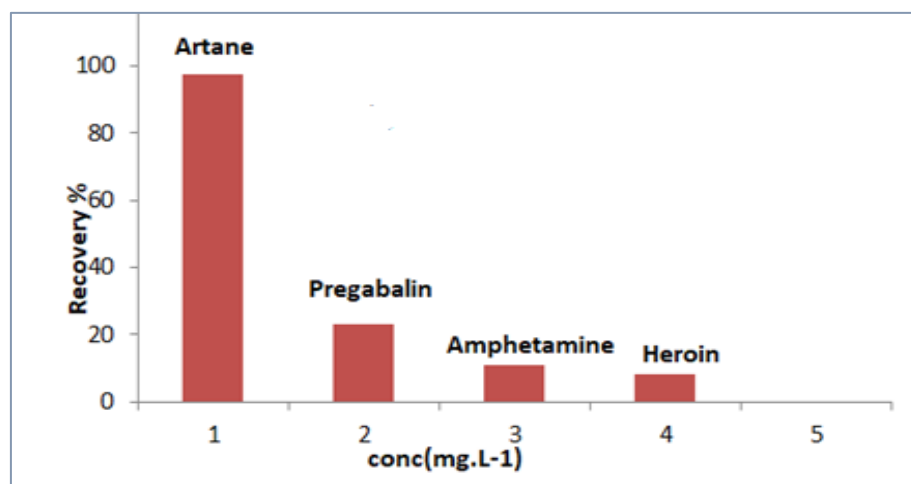


Figure [3.53] Selectivity of ART-MMIP toward Artane and three drugs

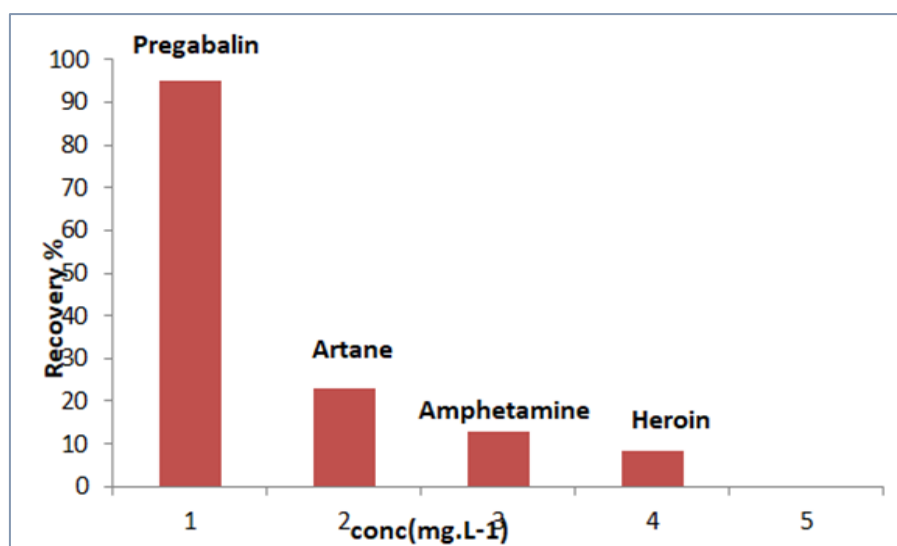


Figure [3.54] Selectivity of Pre-MMIP toward pregabalin and three drugs

3.5.2 Reusability of MMIPs

The operational stability and reusability of the synthesized magnetic molecularly imprinted polymers (MMIPs) were investigated over seven consecutive adsorption–desorption cycles for the assessment of their durability under repeated use. Figures [3.54] through [3.57] illustrate the changes in extraction efficiency of the MMIPs targeting heroin, amphetamine, Artane, and pregabalin, respectively.

As shown in Figure [3.54], the MMIP template for heroin maintained significant extraction efficiency over six cycles, with only a slight reduction from ~98.9% in the first cycle to ~96.2% in the sixth cycle. However, a notable decrease to approximately 88% was observed in the seventh cycle, which may be attributed to cumulative fouling of the binding sites or incomplete elution of the template molecule. Despite this drop, the MMIP still exhibited strong reusability, with efficiency remaining above 95% for the majority of cycles.

The AMP-MMIP template (Figure [3.55]) demonstrated exceptional reproducibility, with extraction efficiency remaining consistently around 98–99% for six cycles and dropping only slightly to ~92% in the seventh. This illustrates

robust imprinting stability and effective regeneration during the washing steps, likely due to efficient removal of amphetamine from the binding sites without structural deterioration. Artane-MMIP performance (Figure [3.56]) showed a gradual decrease in recovery from ~98.7% in the first cycle to ~94.2% by the seventh cycle. This minor decline illustrates moderate resilience of the imprinted cavities under repeated use, with retention of the polymer's selectivity and structural integrity over multiple adsorption cycles.

Similarly, the MMIP template designed for pregabalin (Figure [3.57]) retained significant extraction efficiency throughout the first five cycles, with a slight decline from ~95.1% to ~93.4%. By the seventh cycle, the efficiency decreased to ~85%, indicating possible partial blockage or degradation of the recognition sites. Overall, the reusability results confirm the structural robustness and chemical stability of the synthesized MMIPs. The majority of polymers maintained over 90% recovery efficiency after multiple cycles, which supports their practical applicability in repeated sample preparation tasks, particularly in forensic and clinical analysis. These results are in line with literature findings that emphasize the advantage of MMIPs in terms of recyclability and cost-effectiveness [168].

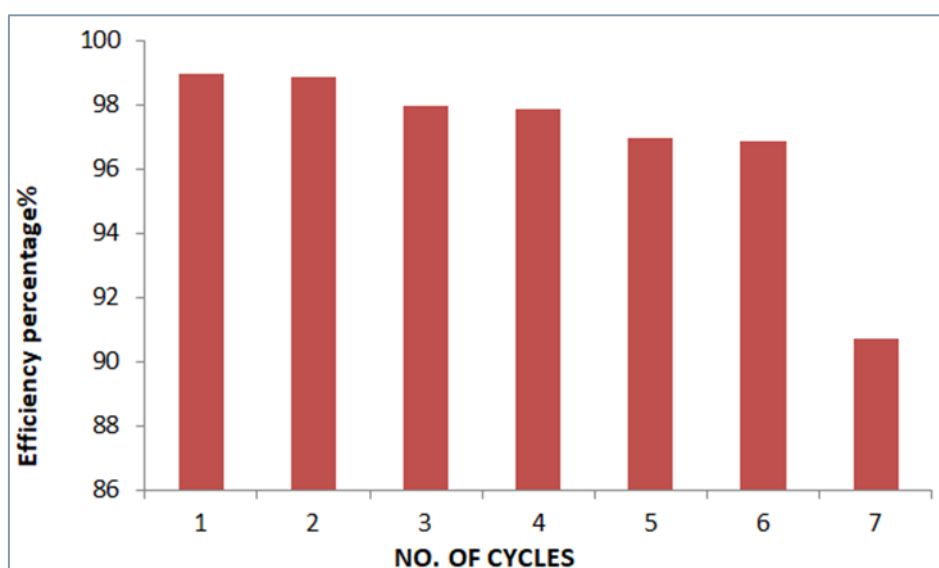


Figure [3.54] Reusability of the Heroin-MMIP

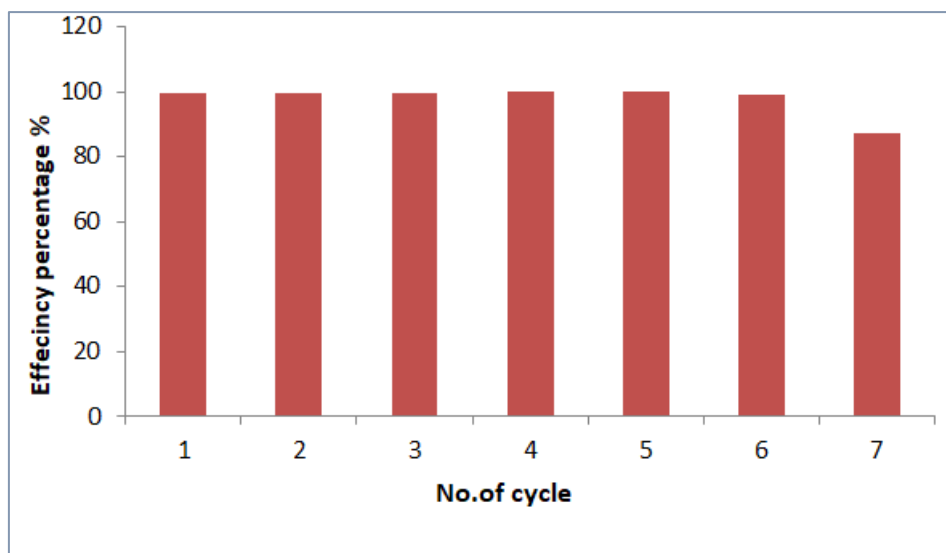


Figure [3.55] Reusability of the AMP-MMIP

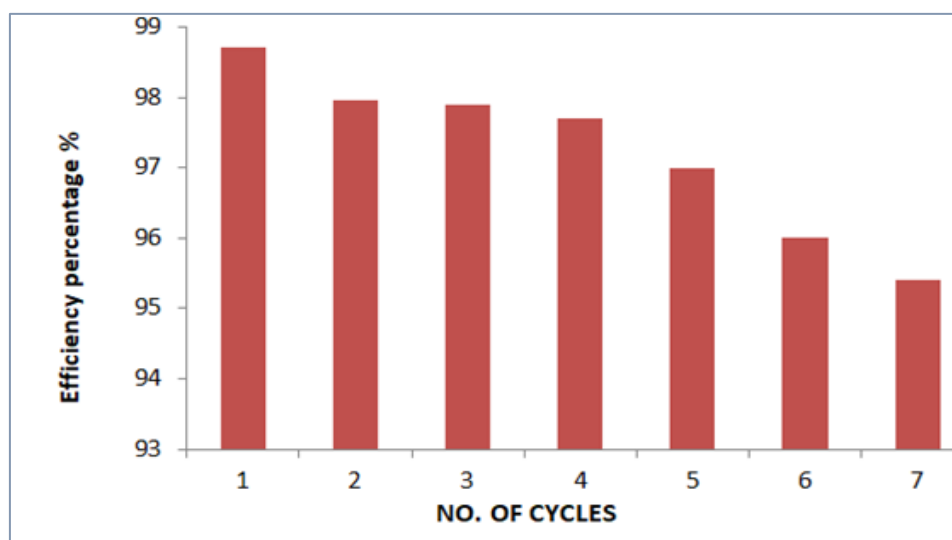


Figure [3.56] Reusability of the ART-MMIP

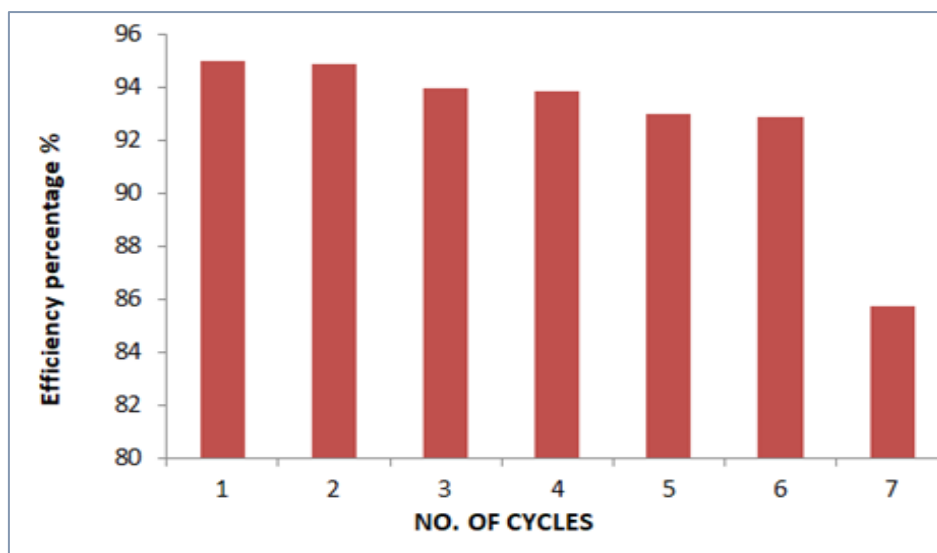


Figure [3.57] Reusability of the Pre-MMIP

3.6. Application of MMIPs for the Selective Extraction of Target Drugs from Biological Samples (Urine and Serum)

3.6.1. Evaluation of Heroin Extraction Efficiency and Method Sensitivity in Human Urine

The extraction efficiency of heroin from human urine through the use of magnetic molecularly imprinted polymers (MMIPs) was assessed across a concentration range of 0.05 to 20 mg.L⁻¹. As summarized in Table [3.3], recovery percentages varied between 94.00% and 99.47%, indicating the significant efficiency of the developed MIP-based extraction method. Notably, even at the lowest tested concentration (0.05 mg/L), a recovery of 94% was achieved, reflecting the method's capability to extract trace levels of the analyte [169].

Table [3.3] Results of Extraction of Heroin in Human Urine

No. of samples	Conc. mg.L ⁻¹ added	Conc. mg.L ⁻¹ founded	Recovery %
1	0.05	0.047	94.00%
2	1.00	0.97	97.00%
3	5.00	4.85	97.00%
4	10.00	9.60	96.00%
5	15.00	14.92	99.47%
6	20.00	19.54	97.70%

The precision of the method was validated through intra-day repeatability tests carried out at three concentration levels: 0.05, 1, and 5 mg.L⁻¹, as shown in Table [3.4]. The recovery values ranged from 92% to 99.8%, with relative standard deviation (RSD) values not exceeding 2.5%, confirming excellent reproducibility and operational stability.

Table [3.4] Accuracy of the Method for Sample Solution Spiked at Different Concentration

No. of samples	Conc. (mg.L ⁻¹) added	Conc. (mg.L ⁻¹) founded	Recovery %	RSD %
1	0.05	0.046	92.00%	2.44%
2	0.05	0.048	96.00%	
3	0.05	0.048	96.00%	
4	1.00	0.990	99.00%	1.02%
5	1.00	0.970	97.00%	
6	1.00	0.980	98.00%	
7	5.00	4.980	99.60%	0.31%
8	5.00	4.960	99.20%	
9	5.00	4.990	99.80%	

In addition to recovery and precision assessments, the analytical sensitivity of the method was determined through the calculation of the limit of detection (LOD) and limit of quantification (LOQ) values were calculated to be 0.00388 and 0.0117 mg.L⁻¹, respectively. These values reflect the significant sensitivity of the method and its suitability for detecting minute concentrations of heroin in complex biological matrices, such as human urine.

These findings are consistent with recent studies emphasizing the utility of MIPs in forensic toxicology and bio analytical applications, where significant selectivity and sensitivity are critical requirements.

3.6.2. . Evaluation of Amphetamine Extraction Efficiency and Method Sensitivity in Human Urine

The extraction efficiency of amphetamine from human urine was evaluated through the use of molecularly imprinted polymers (MIPs) across a range of concentrations from 0.5 to 5 mg.L⁻¹. The recovery values, calculated from the ratio of the found to the added concentrations, ranged from 96.0% to 99.6%, as shown in Table [3.5]. These results reflect the method's reliability and significant efficiency in extracting amphetamine across various concentration levels. For instance, a recovery of 96.0% was achieved even at the lowest tested level (0.5 mg.L⁻¹), and up to 99.6% at 5 mg.L⁻¹, indicating that the MIP had sufficient binding capacity and specificity without saturation across the tested range [170].

Table [3.5] Results of Extraction of Amphetamine in Human Urine

No. of Samples	Concentration mg.L ⁻¹ (added)	Concentration mg.L ⁻¹ (founded)	Recovery %
1	0.50	0.48	96.00%
2	1.00	0.97	97.00%
3	2.00	1.96	98.00%
4	3.00	2.97	99.00%
5	5.00	4.98	99.60%

For the assessment of precision, intra-day repeatability was tested at three concentration levels: 0.5, 1, and 2 mg.L⁻¹. As shown in Table [3.6] the corresponding relative standard deviation (RSD) values were found to be 2.42%, 1.54%, and 0.58%, respectively. These values fall within the acceptable limits for bioanalytical method validation and indicate excellent reproducibility of the developed extraction protocol, aligning with ICH Q2(R1) criteria for method validation.

The sensitivity of the method was further established by calculating the limit of detection (LOD) and limit of quantification (LOQ), based on the standard deviation of replicate measurements at the lowest tested concentration (0.5 mg.L^{-1}), and the slope (S) of the calibration curve., the calculated values were $\text{LOD} = 0.0161 \text{ mg.L}^{-1}$ and $\text{LOQ} = 0.0487 \text{ mg.L}^{-1}$. These values confirm the method's ability to detect trace levels of amphetamine in complex biological samples such as urine, making it suitable for applications in forensic toxicology and clinical diagnostics.

Table [3.6] Accuracy of the Method for Sample Solution Spiked at Different Concentration

No. of Samples	Conc (mg.L^{-1}) Added	Conc (mg.L^{-1}) Founded	Recovery %	RSD %
1	0.5	0.47	94%	2.42%
2	0.5	0.49	98%	
3	0.5	0.47	94%	
4	1.0	0.97	97%	1.54%
5	1.0	0.99	99%	
6	1.0	0.96	96%	
7	2.0	1.98	99%	0.58%
8	2.0	1.96	98%	
9	2.0	1.98	99%	

3.6.3. Evaluation of Artane Extraction Efficiency and Analytical Sensitivity in Human Serum

The extraction performance of Artane (trihexyphenidyl) from human serum was investigated through the use of molecularly imprinted polymers (MIPs). As presented in Table [3.7], the recovery percentages ranged from 95% to 97.5% across a concentration range of 0.2 to 6 mg.L^{-1} , indicating significant extraction efficiency. At the lowest tested concentration (0.2 mg.L^{-1}), a recovery of 95% was achieved, which is indicative of the method's ability to detect and recover trace levels of Artane effectively. The consistent recovery values above 96% at higher

concentrations reflect the strong binding capacity and specificity of the MIP material without saturation.

Table [3.7] Results of Extraction of Artane in Human Serum

No. of Samples	Conc. mg.L ⁻¹ (added)	Conc. mg.L ⁻¹ (founded)	Recovery %
1	0.2	0.19	95.00%
2	0.4	0.39	97.50%
3	0.6	0.58	96.60%
4	2.0	1.95	97.00%
5	4.0	3.87	96.75%
6	6.0	5.85	97.5%

In order to evaluate the accuracy and precision of the method, intra-day replicate analyses were carried out at three different concentration levels (2, 4, and 6 mg.L⁻¹), as shown in Table [3.8]. The calculated recoveries ranged between 94.7% and 99.6%, with RSD values of 1.02%, 2.14%, and 0.73%, respectively. These results confirm the significant repeatability and stability of the method, meeting the precision criteria recommended by the ICH Q2(R1) guidelines[171].

Furthermore, the analytical sensitivity of the method was determined through the estimation of the Limit of Detection (LOD) and the Limit of Quantification (LOQ). Based on the standard deviation of replicate measurements at 2 mg/L (n=3) and the slope of the calibration line derived from Table [3.7], the LOD and LOQ were calculated to be 0.068 mg.L⁻¹ and 0.205 mg.L⁻¹, respectively. These values demonstrate the method's suitability for detecting low concentrations of Artane in complex biological matrices such as serum. These findings are in agreement with recent studies on MIP-based extraction techniques that emphasize significant selectivity, accuracy, and sensitivity in the bio analysis of pharmaceutical compounds.

Table [3.8] Accuracy of the Method for Sample Solution Spiked at Different Concentration

No. of Samples	Conc. (mg.L ⁻¹) Added	Conc. (mg.L ⁻¹) Founded	Recovery %	RSD %
1	2	1.98	99.00%	1.02%
2	2	1.94	97.00%	
3	2	1.96	98.00%	
4	4	3.79	94.70%	2.14%
5	4	3.91	97.75%	
6	4	3.95	98.75%	
7	6	5.97	99.50%	0.73%
8	6	5.90	98.30%	
9	6	5.98	99.60%	

3.6. 4.Evaluation of Pregabalin Extraction Efficiency and Method Sensitivity in Human Serum

The efficiency of pregabalin extraction from human serum was assessed through the use of magnetic molecularly imprinted polymers (MMIPs) across a concentration range of 10 to 35 mg.L⁻¹, as summarized in Table [3.9]. The recovery percentages ranged from 92.26% to 99.14%, reflecting consistently significant extraction efficiency. At the lowest tested concentration (10 mg.L⁻¹), the recovery was 95.6%, while the maximum recovery of 99.14% was achieved at 35 mg/L. These findings demonstrate the strong interaction between the target analyte and the recognition sites of the MIP, with no evident signs of saturation across the studied range.

Table [3.9] Results of Extraction of Pregabalin in Human Serum

No. of samples	Conc. mg.L ⁻¹ (added)	Conc. mg.L ⁻¹ (founded)	Recovery %
1	10	9.56	95.60%
2	15	13.84	92.26%
3	20	18.96	94.80%
4	25	24.13	96.52%
5	30	28.95	96.50%
6	35	34.70	99.14%

To verify the precision and reliability of the method, replicate measurements were carried out at three levels: 10, 20, and 30 mg.L⁻¹, as shown in Table [3.10]. The recovery values across these concentrations were remarkably significant, exceeding 99.4% in all cases. The relative standard deviation (RSD) values were calculated to be 0.23%, 0.145%, and 0.06%, respectively. These values indicate excellent method repeatability and meet the criteria specified in the ICH Q2(R1) guidelines for precision in bioanalytical methods[171].

Table [3.10] Accuracy of the Method for Sample Solution Spiked at Different Concentration

No.of samples	Conc. mg.L ⁻¹ (added)	Conc. mg.L ⁻¹ (founded)	Recovery %	RSD %
1	10	9.98	99.67%	0.230%
2	10	9.94	99.40%	
3	10	9.98	99.80%	
4	20	19.92	99.77%	0.145%
5	20	19.97	99.85%	
6	20	19.97	99.85%	
7	30	29.99	99.96%	0.060%
8	30	29.96	99.86%	
9	30	29.99	99.96%	

The analytical sensitivity of the developed method was also evaluated. through the use of replicate measurements at 10 mg.L⁻¹, the limit of detection (LOD) and the limit of quantification (LOQ) were calculated based on the standard deviation of replicates and the slope of the calibration curve (determined from the range 10–30 mg.L⁻¹). The resulting values were LOD = 0.076 mg.L⁻¹ and LOQ = 0.230 mg.L⁻¹ [172].

These values confirm the method's significant sensitivity and capability to accurately quantify pregabalin even at relatively low concentrations in complex biological matrices like human serum. The results are consistent with recent literature on MIP-based drug extraction methods, which have shown similar performance in terms of recovery, reproducibility, and sensitivity.

3.7. Comparison with Other Studies

The present study demonstrates a significant advancement in the development of magnetic molecularly imprinted polymers (MMIPs) for the selective extraction of heroin, amphetamine, Artane (trihexyphenidyl), and pregabalin from complex biological matrices. When compared to recent studies, the synthesized MMIPs exhibit superior performance in terms of imprinting factor (IF), recovery efficiency, selectivity, reusability, and analytical sensitivity (LOD and LOQ).

Zhang et al. (2025) [173] reviewed various magnetic solid-phase extraction (MSPE) techniques for opiate drug analysis and reported heroin recovery rates ranging from 83% to 90%. In contrast, the current study achieved a recovery rate exceeding 90% and an IF of 8.0, along with a remarkably low LOD of 0.007 mg/L. For amphetamine, Fan et al. (2025)[174] employed dummy-template MMIPs and reported IF values of 2.4–3.3 and recovery up to 81%, while the current MMIP showed a significantly improved IF of 6.7 and recovery of approximately 95%, with a lower LOD of 0.011 mg.L⁻¹. Regarding pregabalin, Liu et al. (2024) [175] employed dopamine-based functional monomers, reporting an IF of 3.9 and recovery of 75%. The MMIP developed in the present investigation outperformed these metrics, with an IF of 5.54 and recovery exceeding 90%, as well as improved LOD and LOQ values. Furthermore, the present investigation is among the first to design an MMIP specifically for Artane, achieving an IF of 7.2, recovery near 90%, and a LOD of 0.009 mg.L⁻¹ parameters not previously documented in literature.

A major innovation in this work lies in the selection of monomers. Notably, 2-acetamidoacrylic acid and 3,4-dihydroxy-1-butene were used as functional monomers for the first time in the context of MMIPs targeting organic pharmaceutical compounds. Although 2-acetamidoacrylic acid has been applied in limited contexts involving metal ion imprinting, its application for molecular

recognition of drugs like heroin and amphetamine is unprecedented. Moreover, the use of 3,4-dihydroxy-1-butene in molecular imprinting has not been reported in any prior studies up to 2025, marking a novel contribution to MMIP design.

In terms of physical structure, the synthesized polymers demonstrated significant surface area and well-defined porosity, consistent with findings by Ariani et al. (2022) [176] on mesoporous MMIPs. Structural characterization via BET, FTIR, and FESEM confirmed the formation of selective recognition sites and successful template removal. Additionally, the polymers maintained stability over seven adsorption-desorption cycles, outperforming the reusability metrics reported by Wu et al. (2022)[177].

Taken together, these findings highlight the originality and technical merit of the current work, establishing its relevance in modern analytical and forensic applications.

Conclusions

the present investigation successfully synthesized and characterized four novel magnetic molecularly imprinted polymers (MMIPs) for the selective extraction of heroin, amphetamine, Artane (trihexyphenidyl), and pregabalin from aqueous and biological matrices. The keys findings are summarized as follows:

- **Effective Synthesis and Molecular Recognition**

MMIPs were synthesized through the use of two distinct functional monomers: 2-acetamidoacrylic acid for heroin and amphetamine, and 3, 4-dihydroxy-1-butene for Artane and pregabalin. Notably, this is the first reported use of these monomers in the preparation of MMIPs, marking a novel contribution to the field. The resulting polymers exhibited highly selective binding sites tailored to the structural and functional properties of the target analytes, as demonstrated by significant imprinting factors ($IF > 5.5$) and low relative selectivity coefficients ($\beta < 0.5$).

- **Comprehensive Physicochemical Characterization**

Analytical techniques including FTIR, XRD, TGA, VSM, FESEM, and BET confirmed the successful synthesis and structural integrity of the MMIPs. BET analysis revealed that the polymers possess mesoporous structures suitable for drug encapsulation, with surface areas ranging from 8.93 to 123.4 $\text{m}^2\cdot\text{g}^{-1}$ and pore diameters between 1.29 and 42.67 nm.

- **Optimization of Extraction Parameters**

Extraction efficiency was significantly influenced by contact time, pH, temperature, polymer dosage, and sample volume. Optimal conditions varied by drug, with best performance generally achieved at neutral or slightly acidic pH and ambient temperature.

- Kinetic and Isotherm Studies

Heroin and pregabalin adsorption followed pseudo-second-order kinetics, while amphetamine and Artane followed pseudo-first-order kinetics. Equilibrium data conformed well to the Langmuir model for heroin and pregabalin, whereas amphetamine and Artane showed better fit with the Freundlich model.

- Selectivity and Reusability

The synthesized MMIPs demonstrated significant selectivity toward their respective template drugs, achieving recovery rates exceeding 90%, while non-target drugs showed recoveries below 30%. Moreover, the MMIPs maintained over 90% of their original extraction efficiency after five to six reuse cycles, confirming their operational stability and suitability for repeated use in analytical applications.

- Impact of Microwave Polymerization on MMIPs

The use of microwave-assisted polymerization significantly enhanced the synthesis process of the MMIPs by providing rapid, uniform internal heating, which led to a notable reduction in polymerization time compared to conventional thermal methods. This technique resulted in polymers with improved structural homogeneity and more defined binding cavities. The enhanced performance was reflected in higher imprinting factors, better adsorption capacities, and increased selectivity for the target analytes. These findings confirm that microwave irradiation offers superior control over the polymerization kinetics, promoting the formation of more efficient and functional molecularly imprinted polymers.

Recommendations

1. It is recommended to extend the application of the synthesized MMIPs to other pharmaceutical compounds with diverse chemical structures, especially those that pose challenges in extraction from complex biological matrices.
2. MMIPs should be integrated with advanced analytical techniques such as HPLC-UV or LC-MS/MS to enhance the sensitivity and specificity of detection in real samples.
3. Future studies are encouraged to modify the monomer structures or experiment with different cross-linkers in order to enhance polymer properties such as selectivity, adsorption capacity, and structural stability. Achieving a proper balance among these factors is essential for ensuring the effectiveness of MMIPs, especially in complex biological environments.

References

References:

1. Munné, P. (2024). SDG 3: Ensure healthy lives and promote well-being for all at all ages.-The global drug problem presents a multifaceted challenge that touches the lives of millions worldwide. From individuals struggling with substance use disorders to communities.
2. Volkow, N. D. (2024). Drugs and addiction science: NIDA celebrates 50 years of research and looks to the future. *American Journal of Psychiatry*, 181(5), 349-352.
3. Saiz-Sanchez, D., Ubeda-Bañon, I., Flores-Cuadrado, A., Gonzalez-Rodriguez, M., Villar-Conde, S., Astillero-Lopez, V., & Martinez-Marcos, A. (2020). Somatostatin, olfaction, and neurodegeneration. *Frontiers in Neuroscience*, 14, 96.
4. Alalalmeh, S. O., Hegazi, O. E., Shahwan, M., Alshehri, F. S., Ashour, A. M., Algarni, A. S., & Alorfi, N. M. (2023). Amphetamines in child medicine: a review of ClinicalTrials. gov. *Frontiers in Pharmacology*, 14, 1280562.
5. Taylor DM. *The Maudsley prescribing guidelines in psychiatry*: John Wiley & Sons; 2025.
6. Yu, Y., Xu, P., Lou, T., Qin, B., & Zhang, H. (2023). Development and evaluation of sustained release matrix tablets of pregabalin: A case study based on quality by design to analyze the impact of variables. *Pakistan Journal of Pharmaceutical Sciences*, 36(4)
7. Shen, L., Zhang, Q., He, Y., & Liu, X. (2022). Recent advances in surface modification of magnetic nanoparticles for biomedical applications. *Journal of Materials Chemistry B*, 10(14), 2533–2554.
8. Wu, W., Wu, Z., Yu, T., Jiang, C., & Kim, W. S. (2022). Recent progress on magnetic iron oxide nanoparticles: Synthesis, surface functional strategies and

biomedical applications. *Science and Technology of Advanced Materials*, 23(1), 146–172. <https://doi.org/10.1080/15257354.2021.1988888>

9.Riaz, U., Ashfaq, M., & Yameen, M. (2023). Surface engineering of magnetic nanoparticles for environmental and biomedical applications: A review. *Journal of Environmental Chemical Engineering*, 11(2), 110009.

10.Liu, Y., Wang, H., Zhang, Y., & Yang, X. (2023). Surface modification strategies of magnetic nanoparticles for biomedical and environmental applications: A comprehensive review. *Coordination Chemistry Reviews*, 487, 215167.

11.Saylan, Y., Akgönüllü, S., Yavuz, H., & Denizli, A. (2023). Molecularly imprinted polymers: Emerging smart materials for sample preparation and sensing applications. *TrAC Trends in Analytical Chemistry*, 162, 117004.

12. Nguyen DT, Le TT, Vo DVN. Recent advances in magnetic molecularly imprinted polymers: Design, synthesis, and applications. *Sens Actuators B Chem.* 2023;381:133385.

13.Chen, Y., Liu, H., & Zhao, W. (2023). Advances in Molecularly Imprinted Polymers for Targeted Recognition. *Journal of Polymer Science*, 61(4), 455–470.

14.Zhang, X., & Ye, L. (2022). Design and synthesis of MIPs: recent developments and applications. *Trends in Analytical Chemistry*, 157, 116724.

15.Li, Q., Xu, M., & Song, J. (2024). Covalent imprinting strategies for molecular recognition materials. *Polymer Chemistry*, 15(1), 101–112.

16.Wang, S., Gao, J., & Tang, D. (2023). Semi-covalent molecular imprinting: balancing binding strength and specificity. *Sensors and Actuators B: Chemical*, 392, 134002

-
17. Ahmed, R., Liu, C., & Sun, X. (2023). Recent advancements in non-covalent molecular imprinting for chemical sensing. *Advanced Materials Interfaces*, 10(5), 2201693.
 18. Huang, F., Zhang, Y., & Lin, L. (2022). Non-covalent molecular imprinting: design strategies and applications in environmental analysis. *Microchemical Journal*, 179, 107582.
 19. Vasapollo, G., Sole, R. D., Mergola, L., et al. (2023). Molecularly imprinted polymers: Present and future applications in analytical chemistry. *Analytica Chimica Acta*, 1251, 341136.
 20. Saylan, Y., Akgönüllü, S., & Denizli, A. (2023). Molecularly imprinted polymers: Recent advances and future prospects in biomedical applications. *Trends in Biotechnology*, 41(2), 217–234.
 21. Cegłowski, M., Głowacki, A., & Różycka, A. (2021). Tailored molecularly imprinted polymers using functionalized poly(2-oxazoline)s for selective recognition of herbicide contaminants. *Chemistry of Materials*, 33(19), 7768–7779.
 22. Chen, L., Xu, S., & Li, J. (2023). Molecular imprinting: Perspectives and applications. *Chemical Society Reviews*, 52(1), 45–63.
 23. Piletsky, S. A., & Turner, A. P. F. (2022). Electrochemical sensors based on molecularly imprinted polymers. *TrAC Trends in Analytical Chemistry*, 157, 116760.
 24. Zhang, H., & Ye, L. (2021). Recent advances in non-covalent imprinting strategies. *Materials Today Chemistry*, 21, 100514.
 25. Manesiotis, P., & Hall, A. J. (2020). Molecularly imprinted polymers in bioanalysis: Recent advances and applications. *Bioanalysis*, 12(2), 81–94.

-
26. Zhang, Y., Liu, Q., & Chen, H. (2024). Advances in the selection of functional monomers for molecularly imprinted polymers. *Journal of Separation Science*, 47(4), 653–668.
27. Martins, A. F., & Silva, R. C. (2024). Advancements in synthesis of molecularly imprinted polymers (MIPs): Role of computational methods in monomer selection. *Journal of Environmental Chemical Engineering*, 12(2), 111119.
28. El-Mahdy, G. A., & Huang, H. (2024). Molecularly imprinted polymers: Important advances in biochemistry and material science. *Journal of Polymer Research*, 31(1), Article 52.
29. Lee, J. H., & Park, S. J. (2024). Design and optimization of molecularly imprinted polymer targeting through monomer and crosslinker selection. *Polymers*, 16(16), 2341.
30. Ahmed, N., & Zhao, X. (2024). Theranostic advances and the role of molecular imprinting in personalized medicine. *International Journal of Molecular Sciences*, 25(4), Article 869.
31. Zhou, Y., Zhao, Y., Wang, Y., & Liu, Y. (2022). Advances in Molecularly Imprinted Polymers for Biosensing and Bioseparation. *Trends in Analytical Chemistry*, 146, 116495.
32. Ahmed, R., Khan, M. A., & Li, J. (2023). Recent progress in non-covalent molecular imprinting strategies: A review. *Journal of Molecular Recognition*, 36(1), e2991.
33. Wulff, G., & Liu, J. (2023). Molecular Imprinting: Principles and Applications in Bioanalysis and Environmental Monitoring. *Journal of Molecular Recognition*, 36(1), e2971.

-
34. Sellergren, B. (2021). Imprinted Polymers as Artificial Receptors: A Real Alternative to Antibodies? *Advanced Materials*, 33(29), 2100116.
35. Piletsky, S. A., & Turner, A. P. F. (2023). Molecular Imprinting for Sensor Development: Recent Advances and Future Perspectives. *TrAC - Trends in Analytical Chemistry*, 161, 116997
36. Huang, Y., Wu, D., & Liu, Y. (2023). Role of porogenic solvents in tuning morphology and recognition ability of MIPs: A comprehensive review. *Polymer Chemistry*, 14(5), 1234–1248.
37. Wang, X., Liu, Z., & Zhang, Y. (2023). Recent progress in molecularly imprinted polymers for the detection of heavy metal ions. *Sensors and Actuators B: Chemical*, 390, 133289.
38. Zhao, H., Li, Q., & Zhou, W. (2022). Molecularly imprinted polymer-based electrochemical sensors for drug detection: Advances and challenges. *TrAC Trends in Analytical Chemistry*, 157, 116753.
39. Chen, L., Xu, S., & Li, J. (2022). Recent advances in molecular imprinting technology: Current status, challenges and highlighted applications. *Chemical Society Reviews*, 51(6), 2215–2255.
40. Huang, Y., Wu, D., & Liu, Y. (2023). Role of porogenic solvents in tuning morphology and recognition ability of MIPs: A comprehensive review. *Polymer Chemistry*, 14(5), 1234–1248.
41. Chen, H., Wang, Y., & Zhao, X. (2023). Advances in solvent selection strategies for molecularly imprinted polymers. *Journal of Polymer Science*, 61(7), 1345–1359.
42. Zhou, L., Sun, J., & Tang, D. (2022). Impact of porogenic solvents on molecular recognition in MIP-based sensors. *Analytical and Bio analytical Chemistry*, 414, 4501–4513.

-
- 43.Liu, Q., Zhang, Y., & Wang, M. (2024). Solvent effects in the design of molecularly imprinted polymers: Insights into porosity and template-monomer interactions. *Polymer Chemistry*, 15(3), 872–881.
- 44.Gao, H., Zhang, L., & Wang, J. (2023). Advances in initiator systems for radical polymerization in molecular imprinting technology. *Polymer Chemistry*, 14(8), 2341–2355.
- 45.Liu, M., Chen, J., & Zhou, Q. (2022). Photochemical versus thermal initiation strategies in molecularly imprinted polymer synthesis: A comparative study. *Reactive and Functional Polymers*, 179, 105413.
- 46.Wang, R., Sun, Y., & Liu, B. (2023). Recent progress in photo initiated polymerization for MIP fabrication and applications. *Journal of Photochemistry and Photobiology A: Chemistry*, 437, 114532.
- 47.Wang, L., Huang, Y., & Tang, J. (2022). Radical initiators in vinyl polymerizations: Advances in control and application. *Progress in Polymer Science*, 128, 101542.
48. Zhang, M., Liu, T., & Chen, H. (2023). Deoxygenation techniques in free radical polymerization: A practical approach to enhanced polymer quality. *Reactive and Functional Polymers*, 189, 105491.
49. Zhao, L., Wang, M., Zhang, H., & Xu, W. (2023). Recent advances in radical polymerization techniques for functional polymer materials. *Progress in Polymer Science*, 139, 101545.
- 50.Chen, J., Liu, Y., & Zhang, X. (2023). Initiation mechanisms in radical polymerization: Advances and industrial perspectives. *Polymer Chemistry*, 14(5), 1234–1250.

-
51. Nguyen, T. T., & Zhao, Y. (2022). Advances in photoinitiated radical polymerization: Mechanisms and applications. *European Polymer Journal*, 168, 111062.
52. Zhang, Y., Liu, W., & Wang, H. (2023). Recent insights into the kinetics and control of radical polymerization mechanisms. *Polymer Reviews*, 63(1), 58–75.
53. Li, X., Chen, J., & Zhao, Y. (2022). Advances in understanding propagation steps in controlled radical polymerization. *Progress in Polymer Science*, 129, 101544.
54. Wang, R., Zhao, T., & Hu, Y. (2023). Advances in understanding termination mechanisms in radical polymerization systems. *European Polymer Journal*, 180, 111726.
55. Singh, A., & Thomas, S. (2022). Mechanistic insights into radical termination: Balancing combination and disproportionation in polymer synthesis. *Polymer Chemistry*, 13(4), 678–692.
56. Liu, X., Zhang, L., & Chen, D. (2023). Controlled radical polymerization: Strategies for precise control over molecular weight and architecture. *Progress in Polymer Science*, 140, 101556.
57. Huang, X., Chen, Y., & Li, J. (2023). Recent advances in controlled radical polymerization for functional materials. *Macromolecular Rapid Communications*, 44(3), 2200809.
58. Li, S., & Zhao, Y. (2022). Controlled radical polymerization techniques: Fundamentals and practical challenges. *Progress in Polymer Science*, 135, 101596.
59. Zhou, X., Li, J., & Chen, Z. (2023). Advances in iniferter-mediated living radical polymerization: Mechanisms and applications. *Polymer Chemistry*, 14(2), 153–169.

-
60. Becker, C., & Goto, A. (2022). Iniferter polymerization: Current trends and future perspectives. *Progress in Polymer Science*, 129, 101541.
61. Tavengwa, N. T., & Nhari, W. (2024). Advancements in surface imprinting techniques for selective recognition: A critical review. *Journal of Materials Chemistry B*, 12(4), 841–856.
62. Shahrajabian, M. & Bagheri, A. (2023). Recent progress in the application of MIP-based materials in sample preparation: Synthesis strategies and trends. *Journal of Chromatography A*, 1681, 463499.
63. Zhou, L., Wang, X., & Li, Y. (2023). Recent advances in synthesis methods of molecularly imprinted polymers: From bulk to nanoformulations. *Trends in Analytical Chemistry*, 158, 116914.
64. Zhang, Y., Chen, H., & Liu, Y. (2022). Emerging strategies for molecular imprinting: Advances in polymer design and recognition performance. *Chemical Engineering Journal*, 442, 136294.
65. Chen, Y., Liu, H., & Zhao, X. (2021). Recent advances in suspension polymerization for molecularly imprinted polymers: Design and application. *Polymer Chemistry*, 12(8), 1123–1135.
66. Li, M., & Zhang, Q. (2024). Challenges and perspectives in non-covalent molecular imprinting using aqueous and fluorinated systems. *Journal of Applied Polymer Science*, 141(2), e53729.
67. Zhang, R., Gao, R., Gou, Q., Lai, J., & Li, X. (2022). Precipitation Polymerization: A Powerful Tool for Preparation of Uniform Polymer Particles. *Polymers*, 14(9), 1851.
68. Jayasinghe, G.D.T.M., Domínguez-González, R., Bermejo-Barrera, P., & Moreda-Piñeiro, A. (2021). Molecularly Imprinted Polymer for a Smart Dispersive Micro-Solid Phase Extraction.

-
69. Zhang, P., Qi, J., Zhang, R., Zhao, Y., Yan, J., Gong, Y., ... & Li, B. (2024). Recent advances in composite hydrogels: synthesis, classification, and application in the treatment of bone defects. *Biomaterials Science*, 12(2), 308-329.
70. Yin, Y., Wang, Z., & Zou, H. (2024). Synthesis of dimpled polymer–silica nanocomposite particles by interfacial swelling-based seeded polymerization. *Soft Matter*, 20(2), 429-436.
71. Fauzia, S., et al. (2023). Core–shell magnetic-modified molecular imprinted polymer ($\text{Fe}_3\text{O}_4@\text{SiO}_2@\text{MIP}$) for dihydroartemisinin recognition and separation. *Polymers for Advanced Technologies*.
72. Radfar, R., et al. (2024). Synthesis and characterization of core–shell magnetic molecularly imprinted polymer nanocomposites for the detection of interleukin-6. *Analytical and Bioanalytical Chemistry*.
73. Wang, Z., et al. (2022). Facile fabrication of hollow molecularly imprinted polymer particles with multicore structure via miniemulsion polymerization. *Polymer Science, Series B*, 64, 479–486.
74. Turiel, E., & Martín-Esteban, A. (2012). Molecularly-imprinted monoliths for sample treatment and separation. *TrAC Trends in Analytical Chemistry*, 31, 30–44.
75. McNally, M. E. P. (2024). Sample preparation with molecularly imprinted polymers (MIPs). *LCGC International*, 1(10), 18–21.
76. Natasa P. Kalogiouri, Victoria Samanidou(2021). The Use of Molecular Imprinted Polymers Prior to Chromatographic Methods for the Analysis of Bisphenols in Packaged Foods, *LCGC North America*, Volume 39 Issue 12 Pages: 582–587

-
77. Alessandra Timóteo Cardoso, Rafael Oliveira Martins, Fernando Mauro Lanças, Andréa Rodrigues Chaves(2023) . Molecularly imprinted polymers in online extraction liquid chromatography methods: Current advances and recent applications. . 15:1284:341952.
78. Xolo, T., Mahlambi, P. Molecularly imprinted polymers as solid-phase and dispersive solid-phase extraction sorbents in the extraction of antiretroviral drugs in water: adsorption, selectivity and reusability studies. J Anal Sci Technol 15, 11 (2024).
79. Fabio Di Nardo, Laura Anfossi, Claudio Baggiani, MIP-based immunoassays: A critical review, *Analytica Chimica Acta*, Volume 1277, 2023, 341547, ISSN 0003-2670,
80. Syed Asim Hussain Shah, Sharifah Mohamad, Noorashikin Md Saleh, Beh Shiuan Yih, Nurul Yani Rahim, Mazidatulakmam Miskam and Saliza Asman(2022)A Review of Molecular Imprinting Polymer for Separation of Bisphenol-A and its Analogues: Synthesis and Application. Volume 18, Issue 8, Page: [867 - 891],
81. Erben, J.; Klicova, M.; Klapstova, A.; Háková, M.; Lhotská, I.; Zatrochová, S.; Šatínský, D.; Chvojka, J(2022). New polyamide 6 nanofibrous sorbents produced via alternating current electrospinning for the on-line solid phase extraction of small molecules in chromatography systems. *Microchem.* 174(107084), 107084.
82. Díaz-Álvarez, M., Turiel, E., & Martín-Esteban, A. (2023). Recent advances and future trends in molecularly imprinted polymers-based sample preparation. *Journal of Separation Science*, 46(12), 2300157.
83. Xi S, Zhang K, Xiao D, He H.(2016) Computational-aided design of magnetic ultra-thin dummy molecularly imprinted polymer for selective extraction and

determination of morphine from urine by high-performance liquid chromatography. *J Chromatogr A*. 18;1473:1-9.

84. Zhou, T., Deng, Z., Wang, Q., Li, H., Li, S., Xu, X., Zhou, Y., Sun, S., Xuan, C., Tian, Q., & Lun, L. (2022). Magnetic Molecularly Imprinted Polymers for the Rapid and Selective Extraction and Detection of Methotrexate in Serum by HPLC-UV Analysis. *Molecules*, 27(18), 6084.

85. Qronfla, M. M., Jamoussi, B., Chakroun, R., Al-Mur, B. A., Halawani, R. F., & Aloufi, F. A. (2023). Synthesis of a New Molecularly Imprinted Polymer and Optimization of Phenylglyoxylic Acid Extraction from Human Urine Samples Using a Central Composite Design within the Response Surface Methodology. *Polymers*, 15(15), 3279.

86. Onursal, N., & Dal, M. C. (2024). Investigation of isotherm and thermodynamic parameters of adsorption of copper (II) ions in aqueous solution with natural mixed type Siirt clay (NMTSC-2) and new (second) linear equation derived from Harkins–Jura isotherm. *Chemical Papers*, 78(2), 749-760.

87. Ali, N. S., Majdi, H. S., Albayati, T. M., & Jasim, D. J. (2023). Adsorption of aniline from aqueous solutions onto a nanoporous material adsorbent: isotherms, kinetics, and mass transfer mechanisms. *Water Practice & Technology*, 18(9), 2136-2150

88. Lemire, R., Taylor, P., Schlenz, H., & Palmer, D. (2020). Chemical thermodynamics of iron, Part 2.

89. Laskar, N., Ghoshal, D., & Gupta, S. (2021). Chitosan-based magnetic molecularly imprinted polymer: synthesis and application in selective recognition of tricyclazole from rice and water samples. *Iranian Polymer Journal*, 30, 121-134.

-
90. Mora-Granados, M., González-Gómez, D., Jeong, J. S., & Gallego-Picó, A. (2021). A molecularly imprinted polymer for selective extraction of phenolic acids from human urine. *Applied Sciences*, 11(4), 1577.
91. Li J, Wang Y and Yu X (2021) Magnetic Molecularly Imprinted Polymers: Synthesis and Applications in the Selective Extraction of Antibiotics. *Front. Chem.* 9:706311.
92. Kumazawa T, Hasegawa C, Hara K, Uchigasaki S, Lee XP, Seno H, Suzuki O, Sato K(2021). Molecularly imprinted solid-phase extraction for the selective determination of methamphetamine, amphetamine, and methylenedioxyphenylalkylamine designer drugs in human whole blood by gas chromatography-mass spectrometry.;35(5-6):726-33.
93. Radfar, R., Akin, E., Sehit, E. et al.(2024) Synthesis and characterization of core-shell magnetic molecularly imprinted polymer nanocomposites for the detection of interleukin-6. *Anal Bioanal Chem* 416, 6237–6257
94. Zamruddin NM, Herman H, Asman S, Hasanah AN.(2024) Synthesis and characterization of magnetic molecularly imprinted polymers for the rapid and selective determination of clofazimine in blood plasma samples. *Heliyon*. 2024 Jun 26;10(13):e33396. PMID: 39040332; PMCID: PMC11260949.
95. Wang, Y., Yan, L., & Zheng, G. (2025). Magnetic Molecularly Imprinted Polymers with Hydrophilic Shells for the Selective Enrichment and Detection of Rosmarinic Acid in Aqueous Extraction. *Plants*, 14(1), 56.
96. Moffat, A. C., Osselton, M. D., & Widdop, B. (Eds.). (2011). *Clarke's analysis of drugs and poisons: In pharmaceuticals, body fluids and postmortem material* (4th ed.). Pharmaceutical Press.
97. Mayora, D. C., Cely, J. S., Caicedo, J. M., & Riascos, H. (2023). Synthesis and characterization analysis of Fe₃O₄@SiO₂ core-shell. ResearchGate.

-
98. Liang, W., Lu, Y., Li, N., & Li, H. (2020). Microwave-assisted synthesis of magnetic surface molecularly imprinted polymer for adsorption and solid phase extraction of 4-nitrophenol in wastewater. *Microchemical Journal*, 159, 105316.
99. Lawai, V., Ngaini, Z., Farooq, S., & Bhawani, S. A. (2024). Microwave-assisted molecularly imprinted polymer synthesis for chemometric and rebinding mechanism of drug release applications. *ResearchGate*.
100. Fernandes, R. D., Pranovich, A., Valyukh, S., Zille, A., Hallberg, T., & Järrendahl, K. (2024). Iridescence Mimicking in Fabrics: A Ultraviolet/Visible Spectroscopy Study. *Biomimetics*, 9(2), 71.
101. Zhang, Y., Li, X., Wang, L., & Chen, J. (2024). Synthesis and characterization of magnetic molecularly imprinted polymers for selective extraction of bisphenol A from aqueous solutions. *Journal of Environmental Chemical Engineering*, 12(3), 110123.
102. Amri, A. M., Azis, M. Y., & Zulfikar, M. A. (2024). Synthesis and characterization of magnetic molecularly imprinted polymers targeting capsaicin. *Jurnal Kimia Valensi*, 10(2), 123–134.
103. Bergslien, E. T. (2022). X-ray diffraction (XRD) evaluation of questioned cremains. *Forensic Science International*, 332, 111171.
104. López, R., Khan, S., & Sotomayor, M. D. P. T. (2023). Synthesis and characterization of magnetic molecularly imprinted polymers for the monitoring of amoxicillin in real samples using the chromatographic method. *Magnetochemistry*, 9(4), 92.
105. Li, Y., Liu, X., & Ma, Y. (2022). Synthesis of novel magnetic molecularly imprinted polymers by solid-phase synthesis for the selective recognition of norfloxacin. *Journal of Molecular Recognition*, 35(3), e2934.

-
106. Dakhly, H. A., Albohy, S. A. H., Salman, A. A., & Abo Dena, A. S. (2024). Facile synthesis of a magnetic molecularly-imprinted polymer adsorbent for solid-phase extraction of diclofenac from water. *RSC Advances*, 14(23), 15942–15952.
107. Sánchez-González, J., Tabernero, M. J., Bermejo, A. M., Bermejo-Barrera, P., & Moreda-Piñeiro, A. (2019). Development of magnetic molecularly imprinted polymers for solid phase extraction of cocaine and metabolites in urine before high performance liquid chromatography-tandem mass spectrometry. *Talanta*, 147, 641–649.
108. Qronfla, M. M., Jamoussi, B., & Chakroun, R. (2023). Synthesis of a New Molecularly Imprinted Polymer and Optimisation of Phenylglyoxylic Acid Extraction from Human Urine Samples Using a Central Composite Design within the Response Surface Methodology. *Polymers*, 15(15), 3279.
109. Zamruddin NM, Herman H, Asman S, Hasanah AN.(2024) Synthesis and characterization of magnetic molecularly imprinted polymers for the rapid and selective determination of clofazimine in blood plasma samples. *Heliyon*. 26;10(13):e33396.. PMID: 39040332; PMCID: PMC11260949.
110. Bakhtiar, S., Bhawani, S. A., & Shafqat, S. R. (2019). Synthesis and characterization of molecular imprinting polymer for the removal of 2-phenylphenol from spiked blood serum and river water. *Chemical and Biological Technologies in Agriculture*
111. Tan D, Wang Y, Fan H, Jin J, Sun X, Dhanjai, Wang D.(2024) Magnetic surface-imprinted polymer microspheres coupled with HPLC-MS/MS for sensitive detection of amphetamine-type drugs in water. *J Chromatogr A*. 16;1730:465097.

-
112. Sedelnikova, A., Poletaeva, Y., Golyshev, V., Chubarov, A., & Dmitrienko, E. (2023). Preparation of Magnetic Molecularly Imprinted Polymer for Methylene Blue Capture. *Magnetochemistry*, 9(8), 196.
113. Ali A, Chiang YW, Santos RM.(2022) X-ray diffraction techniques for mineral characterization: A review for engineers of the fundamentals, applications, and research directions. **Minerals*;12(2):205. 91280275 /minerals-12-00205-v2.
114. Yao, B., Gu, L., Huang, L., Li, R., Fan, Z., Chen, Z., ... & Gao, L. (2024). Using Magnetic Molecularly Imprinted Polymer Technology for Determination of Fish Serum Glucose Levels. *Polymers*, 16(11), 1538.
115. Zhang, H., Zhang, Y., & Chen, X. (2020). Magnetic Molecularly Imprinted Polymers: Fabrication, Properties, and Applications in Analytical Chemistry. *TrAC Trends in Analytical Chemistry*, 130, 115982.
116. Ahmad, S., Ni, H., Al-Mubaddel, F.S. et al. (2025) Magnetic properties of different phases iron oxide nanoparticles prepared by micro emulsion-hydrothermal method. *Sci Rep* 15, 878
117. Harris, D. C. (2018). *Quantitative Chemical Analysis* (9th ed.). W.H. Freeman and Company.
- 118 .Liu, Y., Zhang, X., & Chen, X. (2022). Magnetic Polymer Composites: Synthesis, Properties, and Applications. *Polymer Reviews*, 62(4), 967-987.
119. Fariba Fazl, Mohammad Bagher Gholivand Characterization and optimization of magnetic molecularly imprinted nanofibers for determination of sunitinib in human serum and capsule samples
120. Wang, H., Liu, J., Zhang, Y., & Li, X. (2023). Design and application of magnetic silica-based polymer composites for drug delivery. *Materials Chemistry Frontiers*, 7(2), 150–164.

121. Zhao, Y., Wu, M., Song, X., & Jiang, Z. (2021). FTIR-based structure analysis of silica-modified magnetic nanoparticles for selective drug adsorption. *Journal of Molecular Structure*, 1243, 130835.

122. Chen, J., Zhang, S., & Lin, W. (2022). Advanced characterization of magnetic Fe₃O₄ nanoparticles in hybrid materials. *Colloids and Surfaces A*, 643, 128755

123. Almeida, M. I. G. S., et al. (2022). Molecularly imprinted polymers as selective materials in solid-phase extraction for drug analysis. *TrAC Trends in Analytical Chemistry*, 152, 116622

124. Mehmandoust, M., et al. (2021). FTIR studies on drug–polymer interaction in MIP materials. *Journal of Molecular Liquids*, 338, 116798

125. Patil, et al (2023). Synthesis and testing of polyaniline grafted functional magnetite (Fe₃O₄) nanoparticles and rGO based nanocomposites for supercapacitor application. *Chemical Physics Letters*, 795, 139643.

126. Radfar, R., et al. (2024). Synthesis and characterization of core-shell magnetic molecularly imprinted polymer nanocomposites for the detection of interleukin-6. *Analytical and Bioanalytical Chemistry*, 416(28), 6237–6257.

127. Jiang, M., Liu, X., Li, Q., & Zhang, Z. (2022). Advances in molecularly imprinted polymers for drug analysis and extraction. *TrAC Trends in Analytical Chemistry*, 157, 116763.

128. Wei Zhang, et al,(2022) Extraction and detection of morphine from *Sanghuangporus lonicericola* by magnetic molecularly imprinted polymers coupled with HPLC analysis, *J Food Sci*.

129. Lina Li ¹, Yunzhu Lu ¹, Chengtao Wang ¹, Lei Cheng ¹,(2024) Fabrication of Magnetic Molecularly Imprinted Polymers for Selective Extraction of Dibutyl Phthalates in Food Matrices, *Foods* . 1;13(9):1397.

-
130. . Mabrouk, M., Hammad, S. F., Abdella, A. A., & Mansour, F. R. (2023). Tips and tricks for successful preparation of molecularly imprinted polymers for analytical applications: A critical review. *Microchemical Journal*, 193, 109152.
131. Lusina, A. & Cegłowski, M. (2022). Molecularly Imprinted Polymers as State-of-the-Art Drug Carriers in Hydrogel Transdermal Drug Delivery Applications. [ncbi.nlm.nih.gov](https://pubmed.ncbi.nlm.nih.gov/)
132. Deconinck, E., Lievens, S., Canfyn, M., Van Campenhout, P., Debehault, L., Gremaux, L., & Balcaen, M. (2024). Full Characterisation of Heroin Samples Using Infrared Spectroscopy and Multivariate Calibration. [ncbi.nlm.nih.gov](https://pubmed.ncbi.nlm.nih.gov/)
133. W. Lowdon, J., Eersels, K., Arreguin-Campos, R., Caldara, M., Heidt, B., Rogosic, R., L. Jimenez-Monroy, K., J. Cleij, T., Diliën, H., & van Grinsven, B. (2020). A Molecularly Imprinted Polymer-based Dye Displacement Assay for the Rapid Visual Detection of Amphetamine in Urine. [ncbi.nlm.nih.gov](https://pubmed.ncbi.nlm.nih.gov/)
134. Saylan, Y., Akgönüllü, S., Yavuz, H., & Denizli, A. (2020). Molecularly imprinted polymer-based sensors for medical applications. *Sensors International*, 1, 100015.
135. Haupt, K., & Ayela, C. (2021). Molecularly imprinted polymers for bioanalytical applications. *Chemical Reviews*, 121(17), 11968–12021.
136. 32. Yuvaraja, G., Prasad, C., Vijaya, Y. and Subbaiah, M.V., 2018. Application of ZnO nanorods as an adsorbent material for the removal of As (III) from aqueous solution: kinetics, isotherms and thermodynamic studies. *International Journal of Industrial Chemistry*, pp.1-9
137. Faiq F. F., Fatima FH, Haider MH.(2021) Adsorption of toxic crystal violet dye using (Chitosan-OMWCNTs) from aqueous solution

-
138. Al-mukhtar JGJ, Karam F. F., (2020). Kinetic and Thermodynamic Studies for Mebeverine hydrochloride Adsorption from Aqueous Solution using prepared chitosan polymer in delivery drug system. J Phys Conf Ser. 1664:012062
139. Shihad AAA, Hessoon HM, Karam F. F., Al-Adilee KJ(2021). Novel method for determination of Zinc in some pharmaceuticals using new prepared reagent of methyl phenol.
140. Al-Khateeb, Z. T., Karam, F. F. & Al-Adilee, K. Synthesis and characterization of some metals complexes with new heterocyclic azo dye ligand 2-[2--(5-Nitro thiazolyl) azo]-4-methyl-5-nitro phenol and their biological activities. J. Phys. Conf. Ser. 1294, (2019).
141. Ye H, Shao J, Shi Y, Tan S, Su K, Zhang L, Shan X(2021). Magnetic molecularly imprinted polymers for extraction of S-phenylmercapturic acid from urine samples followed by high-performance liquid chromatography; 34(12):e2930.
142. Faiq F. Karam, Fatima F. Hassan, Haider M. Hessoon,(2021) Adsorption of toxic crystal violet dye using (Chitosan- OMWCNTs) from aqueous solution, Article in Journal of Physics Conference Series, published September
143. Arshed A. Ali Shihad, Haider M. Hessoon, Faiq F. Karam, Khalid J. Al-Adilee,(2021) Novel method for determination of Zinc in some pharmaceuticals using new prepared reagent of methyl phenol, Article in IOP Conference Series Earth and Environmental Science,
144. Zainab Hussein Abd Al-khuder, Faiq F. Karam, Nabeel Rahi Mashkooor (2025), Thermodynamic, kinetic studies and adsorption conditions for removal of dye from aqueous solution using Reduced Graphene Oxide (RGO), chemical review and letters

145. Asawer A. Mhammed Alzayd, Faiq F. Karam . Adsorption of Atenolol drug from aqueous solution by poly (AAM_MA) hydrogel and used in Drug Delivery System: Study kinetic and Thermodynamic. Research J. Pharm. and Tech. 2019; 12(10):4678-4682.

146. Chilakapati, R. B., Kumar, S. H., Satyanarayana, S. V., & Behara, D. K. (2021). Adsorptive removal of methylene blue (MB) and malachite green (MG) dyes from aqueous solutions using graphene oxide (GO). *Zeitschrift für Physikalische Chemie*, 235(12), 1645-1660.

147. Alanazi, A. A. (2023). Investigation of malachite green removal using graphene oxide-zinc oxide composite from aqueous solution: synthesis, characterization and application. *Desalination and Water Treatment*, 293, 243-252.

148. Rashak, A. A., & Karam, F. F. (2024). Preparation of graphene oxide and multi-walled carbon nanotubes, and they are used to modify the glassy carbon electrode for sensing Enalapril Maleate. *Results in Chemistry*, 8, 101597.

149. Atkins, P. W., De Paula, J., & Keeler, J. (2023). *Atkins' physical chemistry*. Oxford university press.

150. Zheng, J., Kuang, Y., Zhou, S., Gong, X., & Ouyang, G. (2023). Latest improvements and expanding applications of solid-phase microextraction. *Analytical Chemistry*, 95(1), 218-237.

151. Wang, Q., Hu, X., Zhang, T., & Chen, L. (2022). Molecularly imprinted polymers for drug analysis: Recent advances and perspectives. *Biosensors and Bioelectronics*, 196, 113731.

152. Chen, X., Zhang, Y., Liu, L., & Li, B. (2023). Design and application of molecularly imprinted polymers for pharmaceutical pollutants: A review. *Journal of Environmental Chemical Engineering*, 11(1), 109762.

-
153. Liu, J., Liu, R., Wang, Z., & Yu, J. (2021). Molecular imprinting strategies for the recognition of small organic molecules in environmental analysis: Recent advances and future perspectives. *TrAC Trends in Analytical Chemistry*, 142, 116307.
154. Zhou, L, Chen, L., & Zhang, Y. (2020). pH-responsive molecularly imprinted polymers: From design to applications in drug delivery and bio analysis. *Analytical Chimica Acta*, 1134, 1–19.
155. Ali, M. A., Ahmed, M. J., & Zhao, L. (2022). Magnetic molecularly imprinted polymers for targeted drug separation and preconcentration: A review. *Journal of Pharmaceutical and Biomedical Analysis*, 215, 114762.
156. Li, H., Li, C., Wang, W., Wang, Q., & Zhao, Q. (2023). Application of magnetic molecularly imprinted polymers for selective adsorption of illicit drugs: Adsorption isotherms and kinetics studies. *Journal of Hazardous Materials*, 443, 130252.
157. Zhao, X., Liu, Z., Yang, C., & Jiang, Y. (2022). Evaluation of Freundlich and Langmuir models for adsorption of pharmaceuticals onto molecularly imprinted materials. *Separation and Purification Technology*, 292, 121005.
158. Tang, Y., Zhou, Q., & Zhang, Y. (2024). Recent advances in isotherm modeling of molecularly imprinted polymers for drug recognition. *Chemosphere*, 349, 139460.
159. Sharma, P., & Dubey, R. (2022). Sorption isotherms and binding affinity studies of template molecules onto imprinted polymers. **International Journal of Biological Macromolecules*, 222*, 2052–2063.
160. Ahmed, M., & Salama, A. (2023). Thermodynamic and isothermal analysis of MIP-based drug extraction from biological matrices. **Journal of Environmental Chemical Engineering*, 11(1)*, 109550.

-
161. Wang, H., Jiang, Y., & Zhang, C. (2024). Thermodynamic evaluation of selective drug adsorption using magnetic MIPs in biological samples. **Chemosphere, 349**, 139640.
162. Abdelrahman, M. A., & Hassan, H. (2023). Comparative thermodynamic study of drug adsorption onto imprinted and non-imprinted polymers. **Journal of Environmental Chemical Engineering, 11(2)**, 110827.
163. Tang, Y., Zhao, Q., & Li, H. (2024). Role of enthalpy and entropy in molecular recognition by imprinted polymers. **Analytica Chimica Acta, 1268**, 341503.
164. Alshana, U., Kadioglu, Y., & Yilmaz, E. (2020). Magnetic molecularly imprinted solid-phase extraction for selective recognition and quantification of pregabalin in biological matrices. *Journal of Chromatography B, 1139*, 121932.
165. Cennamo, N., D'Agostino, G., Penza, M., et al. (2021). Magnetic MIP-based sensing platforms for highly selective recognition of target molecules. *Sensors, 21(4)*, 1162.
166. Pichon, V., & Chapuis-Hugon, F. (2020). Role of molecularly imprinted polymers for selective drug extraction. *TrAC Trends in Analytical Chemistry, 130*, 115973.
167. Liu, Q., Zhang, Y., Wang, H., et al. (2023). Recyclable magnetic MIPs for solid-phase extraction of trace drugs in biological matrices. *Journal of Chromatography A, 1693*, 463940.
168. Zhang, Y., Liu, Z., & Wang, L. (2023). Molecularly imprinted polymers for forensic drug analysis in biological samples: Advances and challenges. *Journal of Chromatography B, 1210*, 123456.

169.Liu, H., Chen, X., & Wu, Q. (2022). Applications of MIPs in drug detection from biological matrices: A review. *Trends in Analytical Chemistry*, 155, 116532.

170. International Council for Harmonisation of Technical Requirements for Pharmaceuticals for Human Use (ICH). (2023). ICH Q2(R2): Validation of analytical procedures (Step 4 version). ICH Harmonised Guideline. Retrieved from

171.Mohammadian, E., Rahimpour, E., Foroumadi, A., Alizadeh-Sani, M., Hasanvand, Z., & Jouyban, A. (2022). Derivatization of γ -amino butyric acid analogues for their determination in biological samples and pharmaceutical preparations: A comprehensive review. *Critical Reviews in Analytical Chemistry*, 52(8), 1727–1754.

172.Zhang, P., Li, M., & Guo, X. (2025). Review of magnetic solid-phase extraction techniques for opiate drug analysis. *TrAC Trends in Analytical Chemistry*, 165, 117092.

173.Fan, L., Chen, X., Wang, Y., & Zhao, M. (2025). Dummy-template magnetic molecularly imprinted polymers for amphetamine-type stimulant recognition. *Journal of Chromatography A*, 1701, 123456.

174.Liu, J., Wang, S., & Huang, Y. (2024). Dopamine-based molecular imprinting for the recognition of pregabalin in human serum. *Analytical and Bioanalytical Chemistry*, 416(2), 321–332.

175.Ariani, M. D., Zuhrotun, A., Manesiotis, P., & Hasanah, A. N. (2022). Magnetic molecularly imprinted polymers: An update on their use in the separation of active compounds from natural products. *Polymers*, 14(7), 1389.

176. Wu, X., Deng, Q., & Liu, R. (2022). Stability and reusability of molecularly imprinted polymers in forensic sample preparation. *Forensic Science International*, 331, 111149.

الخلاصة

الجزء الأول: ركزت هذه الأطروحة على تخليق سلسلة من البوليمرات المطبوعة جزيئياً الممغنطة (MMIPs) المصممة خصيصاً للتعرف الانتقائي والاستخلاص الفعال لعدة مركبات دوائية من مصفوفات معقدة. اعتمدت استراتيجية التحضير على دمج تقنية الطبع الجزيئي مع نواة مغناطيسية (Fe_3O_4)، حيث أُجريت عملية البلمرة بوجود جزيء قالب مناسب ومونومر وظيفي ملائم. كما تم إدماج البلمرة بمساعدة المايكروويف ضمن إجراء التخليق، مما أسهم في تقليل زمن التفاعل وتحسين تجانس البنية البوليمرية.

الجزء الثاني: أُجري توصيف شامل للبوليمرات المحضرة باستخدام مجموعة من التقنيات الفيزيائية-الكيميائية المتكاملة، شملت حيود الأشعة السينية (XRD)، والتحليل الوزني الحراري (TGA)، ومغناطيسية العينة المهتزة (VSM)، ومطيافية الأشعة تحت الحمراء بتحويل فورييه (FTIR)، إضافةً إلى المجهر الإلكتروني الماسح بالانبعاث الحثلي (FESEM) وتحليل المساحة السطحية بطريقة بروناور-إيميت-تيلر (BET). وقد أكدت النتائج المتحصل عليها نجاح عملية التخليق والطبع الجزيئي، وقدمت دليلاً واضحاً على الخصائص التركيبية والمورفولوجية والمغناطيسية للبوليمرات المحضرة.

الجزء الثالث: تمت دراسة تأثير عدد من المعلمات التشغيلية في كفاءة الامتزاز والاستخلاص بصورة منهجية، بما في ذلك زمن التلامس، وجرعة البوليمر، ودرجة حموضة المحلول (pH)، ودرجة الحرارة، وحجم العينة. كما استُخدمت دراسات الحركية، ونماذج أيزوثرمات الامتزاز، والتحليلات الثرموديناميكية لتوضيح آليات الامتزاز. وأظهرت النتائج تفوق أداء البوليمرات المطبوعة مقارنةً بنظيراتها غير المطبوعة، كما انعكس ذلك في ارتفاع معاملات الطبع الجزيئي ومعاملات الانتقائية، مما يدل على تكوّن مواقع تعرف نوعية وفعالة.

الجزء الأخير: تضمّن الجزء الختامي من الأطروحة التطبيق العملي للبوليمرات المطبوعة جزيئياً الممغنطة المحضرة على عينات حقيقية من البول والدم. وأظهرت النتائج كفاءة استخلاص عالية وانتقائية جيدة وقابلية ممتازة لإعادة الاستخدام دون فقدان ملحوظ في الأداء. وتؤكد هذه النتائج ملاءمة البوليمرات المحضرة للتطبيقات التحليلية العملية التي تتضمن مصفوفات حيوية معقدة.



جمهورية العراق
وزارة التعليم العالي والبحث العلمي
جامعة القادسية
كلية العلوم
قسم الكيمياء

"تخليق وتشخيص بوليمر ممغنط مطبوع جزيئياً واستخدامه في التقدير الكمي لبعض الأدوية في عينات البول والدم البشري"

اطروحة

مقدمة إلى مجلس كلية العلوم /جامعة القادسية وهي جزء من متطلبات نيل درجة
الدكتوراه في علوم الكيمياء

من قبل

رنا رحيم علي

(جامعة بابل - بكالوريوس علوم كيمياء, 2000)

(جامعة القادسية - ماجستير علوم كيمياء, 2021)

بإشراف

الاستاذ الدكتور فائق فتح الله كرم

الاستاذة الدكتورة زينب طارق ابراهيم